UNIVERSITY OF CALIFORNIA, SAN DIEGO

Systems Biology of the Cardiac Hypoxia Response in *Drosophila*

A Dissertation submitted in partial satisfaction of the Requirements for the degree
Doctor of Philosophy

in

Bioengineering

by

Jacob Daniel Feala

Committee in charge:

Professor Andrew D. McCulloch, Chair
Professor Giovanni Paternostro, Co-Chair
Professor Gabriel Haddad
Professor Trey Ideker
Professor Jeffrey H. Omens
Professor Bernhard O. Palsson

2008

The Dissertation of Jacob Daniel Feala is approved, and it is acceptable in quality and form for publication on microfilm:

_____

_____

_____

_____

_____

Co-Chair

_____

Chair

University of California, San Diego

2008

To Mom and Dad …

Das Sein is ewig; denn Gesetze
Bewahren die lebend'gen Schätze,
Aus welchen sich das All geschmückt.

[Being is eternal; for laws there are
To conserve the treasures of life,
On which the Universe draws for beauty]

- Goethe

TABLE OF CONTENTS

Signature Page……. iii

Dedication……. iv

Epigraph…….. v

Table of Contents……... vi

List of Figures…….. xiii

List of Tables……. xvi

Preface……... xvii

Acknowledgements…….. xx

Vita……. xxiii

Abstract……. xxiv

Chapter I – Introduction……..……..1

I.1 Overview of the Dissertation……1

I.2 Background……..4

I.2.1 Hypoxia in cardiac myocytes……..5

I.2.2 Systems biology……..12

I.2.3 Drosophila as a model for systems analysis of cardiac hypoxia…….15

I.3 Cardiac phenotype screen……...18

I.3.1 Automated cardiac phenotyping technology……...18

I.3.2 Screening cardiac hypoxia phenotypes……...19

I.4 NMR metabolomics……21

I.5 Metabolic models……..23

I.5.1 Reconstructing Drosophila metabolism ……...23

I.5.2 Simulating hypoxic metabolism……24

I.5.3 Refining with phenotype data……26
I.6 Iteration and detailed follow-up……26
I.7 Discussion……27
References……30

Chapter II – Discovering Regulators of the Drosophila Cardiac Hypoxia Response Using Automated Phenotyping Technology……40

Abstract……40
II.1 Introduction……41
II.2 Screening the cardiac hypoxia response……42
II.3 Hypoxia tolerance in Drosophila……44
II.4 Automation Methods……45
II.4.1 Automated measurement overview……45
II.4.2 Anesthetize……47
II.4.3 Mounting……48
II.4.4 Detection algorithms……50
II.4.5 M-mode acquisition……54
II.4.6 Parallelization……55
II.4.7 Automated analysis……55
II.4.8 User Interface ……56
II.5 Results……57
II.5.1 Speed and accuracy of heart measurements……57
II.5.2 Characterization of the wild-type response to mild cardiac hypoxia……60
II.5.3 Positive controls: oxygen-sensitive mutations……61
II.6 Discussion……64

II.6.1 Designing a large-scale genetic screen……..64
II.6.2 Incorporating a phenotype screen into a systems approach……65
II.6.3 Constraint-based metabolic modeling……..66
II.7 Summary……68
References……69

Chapter III – Flexibility in energy metabolism supports hypoxia tolerance in Drosophila flight muscle: metabolomic and computational systems analysis……72

Abstract……72
III.1 Introduction……..73
III.2 Materials and Methods……75
III.2.1 Fly preparation……..75
III.2.2 Hypoxia experiments……75
III.2.3 NMR spectroscopy and data analysis……77
III.2.4 Global metabolite profiles under hypoxia……..78
III.2.5 Statistical analysis……80
III.2.6 Building the reconstruction……81
III.2.7 Constraint-based modeling……..82
III.2.8 Hypoxia simulation……83
III.2.9 Model Validation……84
III.3 Results and Discussion……..86
III.3.1 Global metabolite profiles under hypoxia……..86
III.3.2 Reconstruction and expansion of Drosophila metabolic network……..88
III.3.3 Hypoxia simulation……89
III.3.4 Simplified simulations of hypoxia metabolism ……..96

III.3.5 Lactate dehydrogenase mutant……101
III.4 Summary……106
Acknowledgements……107
References……107

Chapter IV – Metabolomic and flux-balance analysis of aging and hypoxia tolerance in Drosophila muscle tissue……111

Abstract……111
IV.1 Introduction……112
IV.2 Materials and Methods……116
IV.2.1 Fly preparation……116
IV.2.2 Hypoxia experiments.. ……116
IV.2.3 Heart rate measurement……117
IV.2.4 Whole body recovery……118
IV.2.5 NMR preparation……118
IV.2.6 NMR spectroscopy and data analysis ……119
IV.2.7 Standards and scaling factors for metabolite concentrations……119
IV.2.8 ATP assay……120
IV.2.9 Glycogen and Trehalose assay……121
IV.2.10 Statistical analysis……122
IV.2.11 Expanding the metabolic network reconstruction……122
IV.2.12 Flux-balance analysis……123
IV.3 Results……125
IV.3.1 Post-hypoxic recovery of physiological function……125
IV.3.2 Metabolite Assays……128

IV.3.2.1 Glycogen, glucose and trehalose……..128
IV.3.2.2 1H NMR metabolomics……129
IV.3.3 Metabolic reconstruction……135
IV.3.4 Flux-balance analysis……139
IV.4 Discussion……..146
Acknowledgements……..150
References……151

Chapter V – Metabolic profiling and computational modeling of Drosophila metabolism following adaptation to chronic hypoxia……..155

Abstract……..155
V.1 Introduction……..156
V.2 Materials and Methods……..158
V.3 Results and Discussion……158
V.2.1 Normalization……159
V.2.2 Raw concentration profiles……..160
V.2.3 Principal component analysis……160
V.2.4 Flux-balance analysis……..165
V.2.5 Incorporating gene expression profiles……172
V.3 Summary..……...173
References……176

Chapter VI – Conclusions and future directions……177

VI.1 Summary of results……..177

Chapter I……..177
Chapter II……..178
Chapter III……178
Chapter IV……179
Chapter V……..179
VI.2 Limitations……..180
VI.2.1 Genetic background……..180
VI.2.2 Hypoxia stimuli ……181
VI.2.3 Heart measurements……..181
VI.2.4 Metabolomics……...182
VI.2.5 Metabolic reconstruction and modeling……183
VI.3 Future directions……184
VI.3.1 Transgenic UAS-RNAi libraries……184
VI.3.2 Biochemical validation……185
VI.3.3 Precision oxygen control……186
VI.3.4 Automated fly mounting……..187
VI.3.5 Feature-based image analysis……..187
VI.3.6 13C isotopomer-based fluxomics……..188
VI.3.7 Automated reconstruction……..189
VI.3.8 Advanced constraint-based analysis……190
VI.3.9 Integrating signaling networks ……..190
Conclusion……..194
References……195

Appendix A – Automated heart measurement technical details……..……197

A.1 Overview……..……..197

A.2 Measurement protocol……..198

A.2.1 Baseline measurement and hypoxia stimulus……..198

A.2.2 Recovery measurement……....199

A.2.3 End of experiment……...200

A.3 Hardware……200

A.4 Automation code……202

A.4.1 Overview……202

A.4.2 Script “run.py”……203

A.4.3 Script “threads.py”……203

A.4.4 Script “detect.py”……...204

A.4.5 Script “measure.py”……..……204

A.4.6 Script “mmode.py”……204

A.4.7 Script “fly.py”……..205

Appendix B – Characterization of the Drosophila heart to mild acute hypoxia…....206

Appendix C – Reactions in the Drosophila metabolic reconstruction……212

LIST OF FIGURES

Figure I.1: The systems approach to studying cardiac hypoxia……..……..7

Figure I.2: Automated cardiac phenotyping methods……..……20

Figure I.3: Time course of hypoxia tolerance in flies and mammals……..21

Figure II.1: Automation overview……...……47

Figure II.2: Triboelectrical series……..48

Figure II.3: Detection algorithms……..51

Figure II.4: Discard edges of the fly image……53

Figure II.5: User interfaces……..58

Figure II.6: The tps1 gene has altered phenotype in mild hypoxia……..62

Figure II.7: The tps1 gene has altered phenotype in mild hypoxia……..63

Figure III.1: Hypoxic NMR spectra……..78

Figure III.2: Metabolites affected by hypoxia……87

Figure III.3: Pathways of ATP generation during hypoxia……..91

Figure III.4: Flux-balance analysis of Drosophila central metabolism……..94

Figure III.5: Simulating classical anaerobic metabolism……..……97

Figure III.6: Using the model to find alanine transaminase compartment.....99

Figure III.7: Characteristics of hypoxic acetate production……..100

Figure III.8: Simulation of all anaerobic pathways……..101

Figure III.9: Simulation of lactate dehydrogenase mutant……102

Figure III.10: Metabolic effects of lactate dehydrogenase mutant.……....103

Figure III.11: Physiological effects of lactate dehydrogenase mutant……....104

Figure IV.1: Recovery of function after hypoxia in young and old flies.……....126

Figure IV.2: ATP in hypoxia and recovery in young and old flies……..127

Figure IV.3: Substrates during hypoxia and recovery in aging flies ……..130

Figure IV.4: Principal component analysis of the metabolomics data……132

Figure IV.5: Thorax gene expression mapped to KEGG enzymes……..138

Figure IV.6: Fluxes calculated from NMR and flux-balance analysis.……141

Figure IV.7: Flux map comparing recovery fluxes in young and old flies……...144

Figure V.1: Summary of ^{1}H NMR metabolomics experiments..……159

Figure V.2: Raw metabolic profiles for selected compounds……161

Figure V.3: Principal component analysis of all metabolic profiles……..163

Figure V.4: Efficiency of oxygen utilization adapted versus naïve flies ..……..167

Figure V.5: Key metabolite fluxes in adapted versus naïve flies……..168

Figure V.6: Key enzyme activity in adapted versus naïve flies……170

Figure V.7: Pathway regulation in adapted flies……172

Figure V.8: Gene expression in adapted flies……175

Figure VI.1: Tissue-specific expression of RNAi using GAL4/UAS system……...186

Figure VI.2: Integrating the model with interaction networks……...192

Figure VI.3: Interacting “neighbors” of the metabolic model……....193

Figure A.1: Automated anesthesia and mounting overview……..201

Figure A.2: Circuit and hardware schematic……202

Figure B.1: Acute hypoxia response over temperatures……207

Figure B.2: Acute hypoxia response over oxygen concentrations……...208

Figure B.3: Heart rate and regularity for wild-type strains and a mutant……210

LIST OF TABLES

Table III.1 – Approximation of fluxes from NMR data……..……...86

Table IV.1 – Comparison of Drosophila models……..……...136

Table IV.2 – Averages of key fluxes in the simulations…..……...143

PREFACE

In Kurt Vonnegut's book *Cat's Cradle*, the infamous Dr. Felix Hoenikker says that any scientist who can't explain to an eight-year-old what he is doing is a charlatan. Of course in reality it would be impossible to truly understand all of the details of a project without years of scientific education, but reducing the essence of research into simplest terms is nevertheless a good exercise. If I were to try to explain my current research to an eight-year-old, I might begin by relating the parable of the three blind men who try to learn the nature of an elephant. The men are led to the leg, trunk, and tusk of the elephant, respectively, and then are allowed to touch the animal. After a thorough examination, the men separately conclude that an elephant is like a tree, a snake, and a sword. The moral of the story is that "though each was partly in the right … all were in the wrong." Similarly, biologists (usually highly specialized in one field) know quite a bit about how cells work within one specific realm, but so far they have been less successful in bringing this vast knowledge together to understand the cellular system as a cohesive whole. I hope to be part of a growing field of researchers who are devising methods that allow us to back up and see the whole "elephant" at the expense of glossing over a few wrinkles.

For as long as I can remember, I have always been in awe of the organized complexity of life's machinery. The study of biology is an enormous fractal landscape – there is intricate detail at every scale. There is no one functional level from which you can see the whole picture, since the details within one layer depend on all the others, from biochemical interactions to evolutionary pressures. Scientists have long recognized the need for integrating models across multiple scales and on a system-wide scope, but only recently have the experimental and computational tools become

available for doing this. "Systems biology," the term for integrating and modeling genome-wide networks and data, has enormous potential for understanding biological systems within the cell.

I learned about systems biology in my search for graduate schools, and the more I read, the more the concept resonated with me. Up until graduate school I had been interested in all of my studies and enjoyed the winding path classes and research had taken me, but I had not really acquired a true passion for any of it. However, some extracurricular reading late in college had turned me onto new scientific lines of thinking that acknowledge the intractable complexity of systems such as the cell, the brain, or the economy, yet recognize organizational and functional similarities among these systems as well as unpredictable but deterministic origins for their behavior. I couldn't yet wrap my brain around these ideas or imagine how they could be applied to practical biomedicine, but I was fascinated nevertheless, and the spark had been planted.

I found out that the University of California, San Diego had one of the few Bioengineering programs with a concentration in systems biology. Upon entering UCSD I had the luck of being placed on a project that would provide an easy springboard to this type of research – the design of a high-throughput physiological measurement system. My primary adviser, Dr. Andrew McCulloch, was an expert in computational modeling at all scales, and my co-adviser on the project, Dr. Giovanni Paternostro, was eager to apply systems modeling to his research on cardiac aging in *Drosophila*. In addition, I was surrounded by the influential leaders in genome-scale systems biology, and had the chance to learn from them directly in a series of courses in the subject.

What I learned from these classes was that gaps in our understanding of global cellular coordination are being addressed by new technology that measures all cellular components at once, new techniques to integrate these components and their interactions, and new computer models to quantitatively analyze their function. In Chapter 1 I will introduce a few of these ideas in my introduction to the field of systems biology.

This field is not simply the merging of sciences. It is a different way of practicing biology (regardless of whether it is truly “new” or not), and systems biology has become the first and only subject that I have felt truly passionate about. I believe that the future of biology and medicine will be dramatically altered by innovations stemming directly from this approach, and if in later life I can play even a minor role in this revolution, I will be satisfied.

Sweeping comments aside, this is a dissertation rather than a high-level commentary, and as such is thick with the details of putting the systems approach into practice in an important biological context – cardiac hypoxia – via bioinstrumentation, bioinformatics, metabolomics, and computer modeling. Although the first chapter will outline the “big picture,” these overall goals all but disappear in the technical details of some of the later chapters. However, it should be kept in the reader's mind, as it was kept in my mind, that all of the time and effort described here was spent in pursuit of this ideal of a true genome-wide systems model of cellular function, a goal obviously much larger than this thesis managed to accomplish, but one which science will no doubt approach within our lifetimes.

ACKNOWLEDGEMENTS

Chapter I, in part, is adapted from a review that originally appeared in Progress in Biophysics and Molecular Biology, volume 96, issues 1-3, pages 209-25, published August, 2008. The dissertation author was the primary author of this paper, which was co-authored by Drs. Laurence Coquin, Giovanni Paternostro, and Andrew D. McCulloch.

Chapter 2, in part, is adapted from an article that originally appeared in the Annals of the New York Academy of the Sciences, volume 1123, pages 169-177, published March, 2008. The dissertation author was the primary investigator and author of this paper, which was co-authored by Drs. Jeffrey H. Omens, Giovanni Paternostro, and Andrew D. McCulloch.

Chapter 3, in part, is adapted from an article that originally appeared in Molecular Systems Biology , volume 3, article number 99, published April 2007. The dissertation author was the primary investigator and author of this paper, which was co-authored by Drs. Laurence Coquin, Andrew D. McCulloch, and Giovanni Paternostro.

Chapter 4, in full, has been submitted for publication of the material as it may appear in Molecular Systems Biology. The dissertation author and the first author (Laurence Coquin) were the primary investigators and contributed equally to this paper. Co-authors were Drs. Andrew D. McCulloch and Giovanni Paternostro

Over the course of my graduate experience I have been indebted to a number of people. First and foremost, my advisers, Drs. McCulloch and Paternostro, have

been so good to me – inspirational, flexible, supportive, and fantastic overall. Thanks to my labmates for all their advice and help, especially Adam Wright, who would drop everything he was doing (even if it was an intense experiment or an intense Sudoku) in order to help me solve whatever problem I was having building something or writing Matlab scripts. Thanks to Darlene Hunt for helpful discussions about microarrays and immunohistochemistry, and to Stuart Cambell for great conversations about the project in general. Amy Hsieh provided me with candy and undergrads. Eleanore Hewitt has been an indispensable resource on just about everything in our lab and all over campus. Christine Miller never seemed to mind when I waltzed in her office, unannounced, with silly questions I could have answered by checking the school website. Sarah Healy, Jeff Saucerman, Bob Mills, and Peter Costandi all gave me invaluable survival skills for UCSD, our lab, and the PhD in general. Jen Marciniak was nice enough to let me pat her head to relieve stress. John Gallagher was always good for a laugh, a weird T-shirt, and a ride to lunch off campus in his sweet ride. Adam Feist acted as my SimPheny guru, ate his lunch twice as fast as me, made up fly-themed nicknames for me and forced me to watch him buy fruit every Tuesday at the Farmers' Market. Geoff von Maltzahn took me under his wing and taught me foosball in the grad student lounge, but not before winning nearly a hundred dollars from me in friendly wagers.

I have also had a number of undergrads helping me with various aspects of the project. Tanya Ee did much of the legwork for making sure our GAL4 drivers in Chapter VI were working right, Francis Le built the hypoxia chambers, Wen Wai Yim built the slide "sandwich assemblies" in Chapter II, Rachel Nguyen ran the whole-body recovery assays in Chapter IV, Polly Huang helped with the NMR preparation in

Chapter III, and Omer Tal worked on wall detection algorithms mentioned in Chapter VI. Also, many volunteers helped me maintain the stocks and test the heart measurement system, including Maggie Kuo, Daniel Han, Heather Griffith, Mandana Farhadieh, Gian-carlo Parico, Iwen Wu and several others that I apologize if I missed.

And thank you to everybody for not complaining too much about the flies in your coffee.

VITA

2003 Bachelor of Science, Biomedical Engineering, Bachelor of Science, Electrical Engineering, Certificate in Business, University of Wisconsin-Madison

2008 Doctor of Philosophy, Bioengineering, University of California, San Diego

PUBLICATIONS

Feala JD, Omens JH, Paternostro G, McCulloch AD (2008) Discovering regulators of the Drosophila cardiac hypoxia response using automated phenotyping technology. *Annals NY Acad Sci* 1123:169-77

Feala JD, Coquin L, Paternostro G, McCulloch AD (2008) Integrating metabolomics and phenomics with systems models of cardiac hypoxia. *Prog Biophys Mol Biol* 96(1-3):209-25

Feala JD, Coquin L, McCulloch AD, Paternostro G (2007) Flexibility in energy metabolism supports hypoxia tolerance in Drosophila flight muscle: metabolomic and computational systems analysis. *Mol Syst Biol* 3: 99

FIELDS OF STUDY

Major Field: Bioengineering – Studies in Systems Biology
Professors Andrew McCulloch, Giovanni Paternostro, Bernhard Palsson, and Trey Ideker

Major Field: Medicine
Professors Jeffrey Omens and Gabriel Haddad

ABSTRACT OF THE DISSERTATION

Systems Biology of the Cardiac Hypoxia Response in *Drosophila*

by

Jacob Daniel Feala

Doctor of Philosophy in Bioengineering

University of California, San Diego, 2008

Professor Andrew D. McCulloch, Chair

Professor Giovanni Paternostro, Co-Chair

Drosophila is an emerging model for studying genetic influences on heart function, and has also been found to be highly tolerant to hypoxia. Strategies for controlling metabolism in the hypoxic adult fly heart may give clues to new therapies for myocardial ischemia in humans, however, the mechanisms of their hypoxic

metabolic regulation are not well known. We adopt a systems biology approach to discover important hypoxia-tolerance strategies in ATP-generating metabolism in *Drosophila* heart.

First, we built automation technology for rapidly screening the *in vivo* cardiac hypoxia response in adult flies, and proved its speed by characterizing the wild type over a range of conditions. The assay detected loss-of-function phenotypes in known hypoxia-sensitive mutants.

Next we used ^{1}H NMR metabolomics to discover the major anaerobic end products (lactate, alanine, and acetate), which we built into a genome-wide reconstruction of central metabolism. We fit metabolomic data to the model and used it to examine the benefits of these pathways under hypoxia. The model was then used to predict the effects of a lactate dehydrogenase (LDH) mutant, which were supported by metabolomic, heart phenotype, and whole-body assays on an LDH mutant strain.

The model was further refined with gene expression data and used with metabolomic profiling to study the effects of age on the hypoxia response. Recovery of heart rate, whole-body activity, and ATP concentration was delayed in older flies. After fitting the model to metabolomic data for young and old flies, flux-balance analysis pointed to impaired mitochondrial recovery, with excess pyruvate converted to acetate, as the major source of differences between the age groups. Gene expression and the literature on *Drosophila* aging supported these conclusions.

This approach was repeated for a strain of flies that had been experimentally selected to survive chronic hypoxia. Flux-balance modeling suggested that adapted flies may better divert pyruvate flux through pyruvate dehydrogenase rather than

pyruvate carboxylase in order to better tolerate acute hypoxia. Gene expression data from microarrays helped support this finding.

The dissertation offers clues to hypoxia tolerance in flies, generating hypotheses for further research, and also provides a technology platform for a systematic perturbation analysis.

Chapter I –

Introduction

I.1 Overview of the Dissertation

Ischemic heart disease is the leading cause of death worldwide (Murray & Lopez, 1997). At the cellular level, impairments in heart function are caused by necrosis and apoptosis following occluded blood supply, or ischemia. Ischemia impedes the uptake and washout of nutrients, but its most important component is the severely restricted oxygen supply, or hypoxia. Although many genes and pathways are known to be involved in cellular damage and defenses in the face of ischemic and hypoxic insult, the molecular basis for injury versus resistance to hypoxia is not well understood.

While cellular hypoxia has long been an area of intense research, only recently have studies attempted to use genome-scale, discovery-based strategies. Global snapshots of the transcriptome, proteome, and metabolome have provided a first introduction to the wide array of cellular changes that take place under hypoxic conditions. New methods for modeling and visualizing high-throughput data in the context of interaction networks can help filter these large datasets to produce new insights and hypotheses. The broad nature of the cellular hypoxia response, involving multiple pathways across all three major levels of cellular information processing

(metabolic, protein signaling, and transcriptional), makes it an interesting paradigm for applying these new techniques.

This dissertation introduces a systems biology approach for studying metabolic regulation during acute hypoxia in heart and muscle tissue, using Drosophila as a model organism. Although there are clear anatomical and physiological differences between mammalian and fly heart, multiple genetic similarities exist which make the fruit fly an interesting model for hypoxia research. Flies are extremely resistant to hypoxic stress, which presents the opportunity for discovering novel protective strategies as well as basic shared mechanisms.

Central to the systems biology approach is the integration of genome-scale datasets. **Chapter II** (adapted from (Feala et al., 2008b)) describes the development and validation of new automation technology with the potential to generate a new genome-scale dataset, by screening *in vivo* hypoxia responses in the fly heart for large numbers of genetic perturbations. **Chapter III** (adapted from (Feala et al., 2007)) details how we combined the annotated *Drosophila* genome (Adams et al., 2000), an online database of enzymes and pathways (Ogata et al., 1999), and the legacy of *Drosophila* biochemistry data from the literature to build an *in silico* reconstruction of all metabolic pathways active in *Drosophila* myocytes. In **Chapter IV** (reproduced in full from (Coquin et al., 2008) *in revision*) we incorporate adult thorax microarray data into the reconstruction, refining the network to better represent enzymes expressed in muscle tissue.

The other important concepts in systems biology are quantitative modeling, perturbation analysis, and iterative refinement of these networks. In **Chapter III** we used NMR spectroscopy to gather metabolic profiles of the thorax during hypoxia (the

thorax is mostly composed of flight muscle), which suggested new pathways to add to the model. Then we simulated metabolic fluxes during hypoxia in a flux-balance model of the network reconstruction, first by constraining the model to data from the NMR and then in a series of simple pathway-by-pathway demonstrations. We use the results of the simulations to hypothesize mechanisms for hypoxia tolerance, assign an important reaction to its correct cellular compartment, and predict the effects of a specific enzyme perturbation. At the end of the chapter we use our new measurement technology and an assay of whole-body activity to test the prediction on a knock-out strain for this enzyme.

In **Chapters IV and V** we apply our flux-balance modeling approach to two separate but complementary systems. Chapter IV examines the degradation of hypoxia tolerance by aging, while Chapter V studies a population of flies that has had its tolerance to hypoxia improved by many generations of experimental selection. In both studies, metabolic profiles are gathered under various oxygen conditions and fitted to the model as flux constraints. Simulations are then used to support physiological observations of hypoxic resistance or sensitivity using quantitative measures of metabolic performance. Finally, for each system we point to specific mechanisms in the model that may account for the metabolic differences, and support our hypotheses for regulatory control with existing gene expression data.

Finally, **Chapter VI** discusses preliminary results and next steps for incorporating a heart phenotype screen and protein interaction networks to construct a network model of metabolic regulation, specific for genes that are essential to the hypoxia response in the heart. Chapter VI also addresses some of the limitations of

the model and our approach, and then summarizes the major scientific conclusions and engineering accomplishments.

The remainder of **Chapter I** (adapted from (Feala et al., 2008a)) will provide background and an introduction to the theory of our approach.

I.2 Background

The ultimate goal of this research is development of a genome-wide, data-driven model that includes all genes, enzymes, metabolites, and regulatory proteins that are involved in hypoxia defenses. It is advantageous to decide *a priori* the necessary level of detail and the corresponding modeling strategy. Our aim was to model metabolism at the level of enzyme fluxes. Although it is a daunting task to build complete representations of these networks, factors that define the problem of interest, such as cell type (cardiac myocyte), time window (acute), and the specific context (hypoxia) help to narrow the number of players.

Although *Drosophila* has many advantages as a model organism for genetics of the heart and hypoxia tolerance (detailed later), the small size of the fruit fly also presents a major limitation in that it is difficult to extract enough myocardial tissue for biochemical experimentation. Without biochemical data for *Drosophila* myocardium, we are forced to take more indirect steps to model metabolism in the fly heart. For this reason, we choose to develop a metabolic model of flight muscle – for which much biochemical data is available both in the literature and our own lab – as a reasonable first approximation. We can then use microscope-based methods for measuring fly heart function *in-vivo* to study the effect of enzyme mutations on heart phenotypes under stress, and adapt the model to reflect essential pathways in the

cardiac myocyte. Figure I.1 shows an overview of these steps, illustrating the biological level and tissue specificity of each data source available for our model.

I.2.1 Hypoxia in cardiac myocytes

Ischemia (the obstruction of blood flow) and reperfusion injury (tissue damage from the sudden reperfusion of the blood supply) are the causes of cell death in acute myocardial infarction (Opie, 1991). In the heart, both the incidence and mortality of ischemic events worsen with age (Bonow et al., 1996). Currently the only treatment is to restore oxygen-rich blood as soon as possible, either by mechanical (angioplasty) or chemical (thrombolytic) means. Thus there is a need for preventative measures to improve tolerance to ischemia-reperfusion injury in high-risk patients.

Ischemia obstructs three major functions of circulation: oxygen supply, nutrient supply, and the washout of byproduct or waste metabolites. Hypoxia-reoxygenation is the major cellular insult during ischemia-reperfusion, but depleted metabolite supply and washout also play an important role in cellular damage. Hypoxia alone, for example when environmental oxygen is lowered, is thus different from ischemia in that blood flow is uninterrupted and therefore metabolites are free to circulate. However, the level of hypoxic insult during ischemia is much more severe than that normally caused by environmental changes seen by humans (e.g. at high altitudes) and can also cause some metabolite (e.g. acid) buildup even within an unobstructed blood supply. Additionally, in the experiments described in this thesis, the 4-hour severe hypoxia stimulus actually causes the fly heart to stop (see Chapter II) and therefore the stress is assumed to resemble ischemia in that circulation is impaired and metabolites are able to accumulate. Thus the following background on hypoxia

covers cellular damages caused by metabolite accumulation as well as in hypoxia alone.

The exact mechanism whereby reversible hypoxic tissue damage finally evolves into irreversible damage and cell death is still controversial (Opie, 1998b)**,** but is likely to involve both necrotic and apoptotic mechanisms, stemming from the hypoxic event itself as well as metabolic stresses introduced during reperfusion. Reduced O_2 inhibits mitochondrial pathways that produce ATP, which supplies energy to the contractile machinery of the heart. In mammalian heart there is a limit to which the cell can downregulate ATP demand, since the organ must continue to pump for the body to survive. Therefore metabolic pathways that supply ATP are a major target for regulation in cardiac hypoxia.

The heart is able to flexibly use a variety of substrates for energy depending on physiological condition (i.e. starvation, ischemia, exercise) and substrate availability (Kodde et al., 2007). Under normal conditions, fatty acid oxidation accounts for the majority of ATP production, with glucose and lactate contributing smaller amounts (Opie, 1998b). Importantly for this thesis, the heart also has enzymes for utilizing many other substrate pathways including acetate and amino acids, although these contribute very little to overall metabolism. Some evidence does suggest that transamination of pyruvate to amino acids may have a role in ischemia resistance in the mammalian heart (Julia et al., 1990; Taegtmeyer et al., 1977). However, the major metabolic effect of hypoxia is that the cell undergoes a major shift toward anaerobic glycolysis, inhibiting oxidation of pyruvate and fatty acids and relying instead on extracellular glucose and intracellular glycogen.

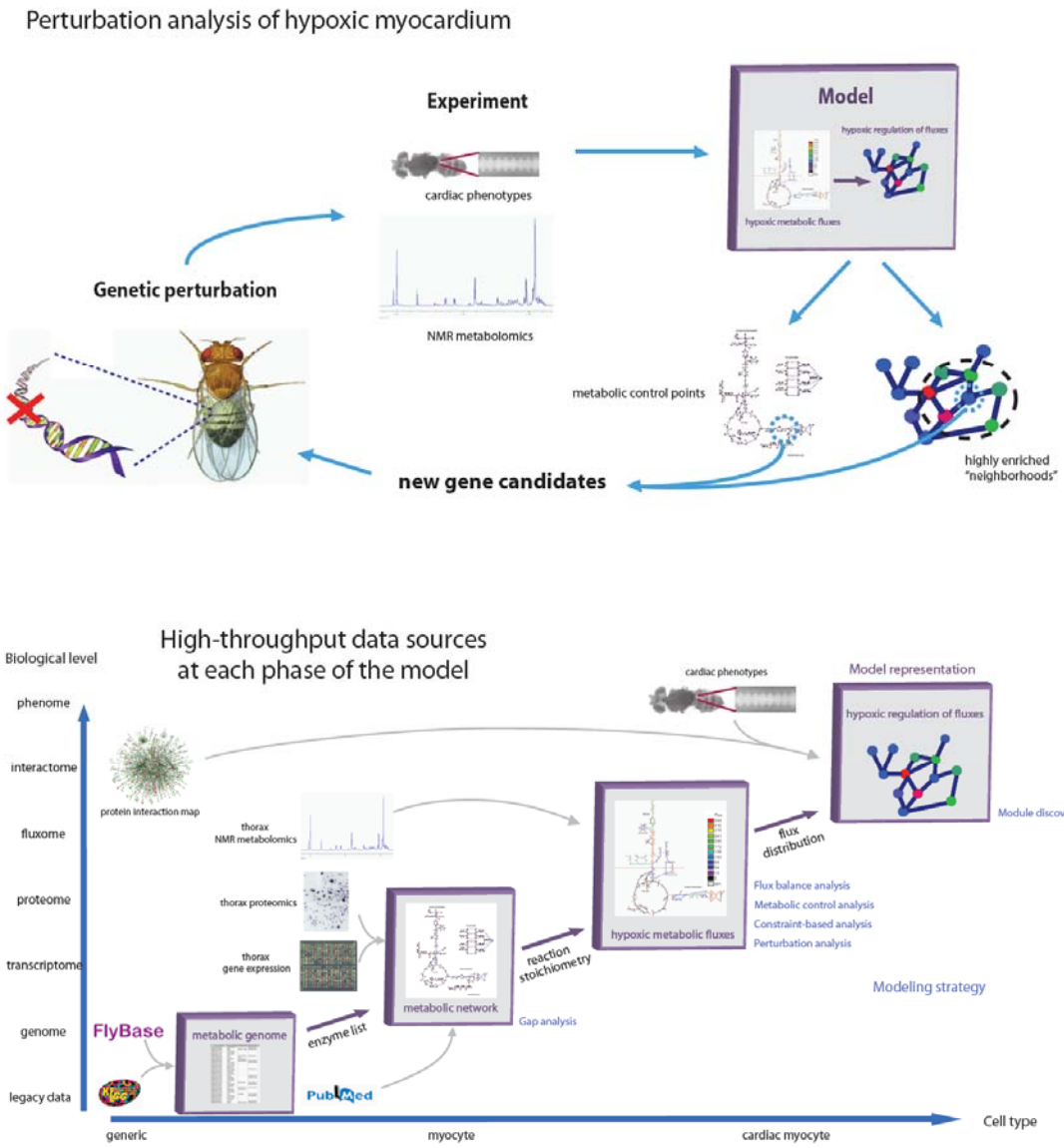

Figure I.1: TOP: Overview of the systems approach to studying cardiac hypoxia. In each iteration, candidate genes for regulation of the hypoxia response are hypothesized by the constraint-based and network models and then validated by experiment.

BOTTOM: Initial construction of the model can incorporate several genome-wide datasets of varying cell-type specificity and at different levels in the biological hierarchy.

As respiration slows, pyruvate uptake into the mitochondria is decreased, and the majority is instead converted into lactate. This is the classic fermentation pathway, whereby lactate dehydrogenase (LDH) consumes the end products of glycolysis (2 pyruvate, 2 protons, and 2 NADH) and replenishes one NAD+ for the pathway to continue to function (Lehninger et al., 2000). The net reaction of anaerobic glycolysis is then

1 glucose -> 2 ATP + 2 lactate

It is well-known that the use of this pathway results in acidosis (for example in exercising muscle), but a common misconception is that acidosis is caused by the production of “lactic acid.” On the contrary, the LDH reaction actually consumes protons, and it is the ATP hydrolysis reaction – carried out by the cellular machinery – that produces the imbalance of protons. Under normal conditions, pyruvate is completely oxidized in the mitochondria, where oxidative phosphorylation consumes the balance of NADH and protons from glycolysis and ATP hydrolysis. When cellular respiration slows, glycolysis is decoupled from oxidative phosphorylation, and one proton accumulates for each pyruvate diverted from the mitochondria and converted to lactate (Ingwall, 2002). See Robergs et. al. (2004) for a review on the biochemistry of metabolic acidosis and a discussion of the “lactic acid” misconception.

The primary metabolic effect of hypoxia is that the cell is forced to depend on anaerobic glycolysis for ATP, though glycolytic ATP production is only a fraction of mitochondrial output, and acidosis occurs as mitochondrial consumption of protons slows. In transition, some additional ATP is made available by release from buffers such as creatine phosphate and the conversion of ADP to ATP by adenylate kinase

(Ingwall, 2002), but when these sources are exhausted, ATP concentration (more precisely, ATP:AMP ratio (Fell, 1997)) begins to drop.

The loss of ATP and increased acidosis may cause damage by a number of mechanisms. Ion pumps are inhibited by depletion of ATP, which causes decreased uptake of calcium by the sarcoplasmic reticulum and reduced extrusion of intracellular Na^+ and from the cell via the Na^+/H^+ and Na^+/Ca^{2+} exchangers (Steenbergen et al., 1987). Ion accumulation can increase osmotic pressure and excess Ca^{2+} can damage mitochondria (Jennings et al., 1986; Opie, 1998a). Contractile machinery and metabolic enzymes are negatively regulated by acidosis (Opie, 1998b), and contractile forces are reduced. Hypoxia and acidosis together may also activate apoptosis pathways that hypoxia alone does not (Graham et al., 2004).

Paradoxically, even more cellular damage can occur upon reperfusion, due to the influx of oxygen that inactive oxidative pathways and damaged mitochondria cannot immediately metabolize (Ambrosio et al., 1987). The rise in cellular oxygen produces reactive oxygen species (ROS) which can damage proteins and DNA and initiate apoptosis (Solaini & Harris, 2005; Yellon & Downey, 2003).

All cells have intrinsic defenses to maintain homeostasis during oxygen fluctuations. The transcriptional, signaling, and metabolic pathways that carry out adaptation to hypoxia are far-reaching and complex, and yet are so highly orchestrated that they can be modeled as a single functional unit (Hochachka & Somero, 2002). The response can be separated into two timescales, the early and late response. The early response is characterized by the immediate shift to anaerobic metabolism, as well as signaling cascades that act to decrease ATP demand throughout the cell (e.g. by decreasing protein translation). The metabolic

“master switch,” AMP-activated protein kinase (AMPK), senses decreases in the ATP:AMP ratio and triggers increased carbohydrate metabolism (Pan & Hardie, 2002). AMPK upregulates glycolysis during ischemia by upregulating glucose transporters and stimulating glycolytic enzymes, then increases fatty acid oxidation during reperfusion by activating specific control enzymes (Arad et al., 2007; Sambandam & Lopaschuk, 2003). Membrane ion pumps are also regulated by AMPK in an effort to maintain pH and energy balance in the hypoxic cell. The late response to hypoxia involves a transcriptional cascade, triggered by hypoxia-inducible factor HIF-1α, as the cell differentiates into a hypoxia-tolerant phenotype (Hochachka & Somero, 2002; Semenza, 2001). The full range of AMPK and HIF targets and their roles in health and disease are not completely understood.

Researchers have long desired to enhance survival in the hypoxic cell, but attempts to engineer better defenses have proven difficult. Some success has come from single molecule interventions in ischemia, either by overexpressing a gene (Du et al., 2006), or triggering a signalling pathway (Hataishi et al., 2006), but in general these strategies are difficult without a system-wide understanding. For example, in glycolysis we know that an attempt to reduce acidosis by decreasing lactate production (without increasing mitochondrial respiration) would do more harm than good because of the role of LDH in proton consumption and symport. We must first understand natural hypoxia defense systems and how they are regulated before we can improve on them.

In fact, the best strategy discovered so far for ischemia resistance is an adaptive mechanism that is already intrinsic to the mammalian heart. Ischemic preconditioning is an increased resistance brought on by inducing multiple short, mild

ischemic insults hours to days before the major ischemic event. The actual protective mechanisms of preconditioning have still not been worked out completely, even after years of research, but the signalling cascades involve many of the intrinsic hypoxia defense pathways mentioned above (Yellon & Downey, 2003). In addition, evidence has been accumulating for the involvement of nitric oxide signaling in innate hypoxia defenses and the preconditioning response (Jones & Bolli, 2006). The mitochondria have been implicated as the primary end effectors of preconditioning protection, with the opening of ATP-regulated potassium channels (K_{ATP}) playing a major role via a number of theorized mechanisms including anti-apoptotic prevention of the mitochondrial permeability transition (Murphy & Steenbergen, 2007; Yellon & Downey, 2003). Though drugs are being developed to trigger endogenous pathways for ischemic preconditioning (Budas et al., 2007; Yellon & Downey, 2003), these have not yet achieved common use in the clinic.

Another strategy for engineering hypoxia protection is to look in other species for novel tolerance mechanisms that can be transferred to humans. Many organisms are able to tolerate severe hypoxia for hours at a time with full recovery. It has been suggested that one way that hypoxia tolerant organisms prevent the dangerous imbalances caused by hypoxia is through rapid and global regulation of metabolism (Hochachka, 1980; Hochachka, 2003). These organisms use a wide variety of anaerobic pathways besides fermentation to lactate, and it is thought that these exotic pathways carry their own specific benefits for ATP generation, pH maintenance, redox potential (NADH/NAD+), and supply of metabolic intermediates (Murphy & Steenbergen, 2007). Though these alternative anaerobic pathways may have potential for enhancing hypoxia tolerance in humans, the precise role of each of

these pathways within the larger, tightly integrated metabolic network must be fully understood before such a translational attempt is made.

I.2.2 Systems biology

We have much to gain from using engineering systems analyses to study complex networks of interactions in the cell. Most complex biological phenomena are emergent properties of the system, i.e. behaviors not predictable from a detailed knowledge of the parts. Quantitative models can help to predict and explain these emergent properties. Although this concept has existed for decades among computational biologists, the recent emergence of systems biology into the mainstream has indisputably been driven by the appearance of large high-throughput datasets, and the reliance on computer models to integrate and decipher them.

One view of the systems approach, emulated in the framework described here, involves the following sequence of steps adapted from (Ideker et al., 2001):

- Gather high-throughput data to define all the components involved under the context of interest,
- Reconstruct integrated cellular networks into an *in-silico* model,
- Systematically perturb and monitor the components,
- Reconcile the experimentally observed responses with those predicted by the model,
- Design and perform new perturbation experiments to distinguish between competing model hypotheses.

The first step in this approach is high-throughput collection of biological data. High-throughput studies have examined the response to myocardial ischemia at the level of transcriptome (Onody et al., 2003; Sehl et al., 2000; Simkhovich et al., 2003;

Stanton et al., 2000), metabolome (Sabatine et al., 2005), and proteome (Cuong et al., 2006; De Celle et al., 2005; Sakai et al., 2003; White et al., 2005), providing a useful – albeit noisy and incomplete – sketch of the cellular milieu in response to hypoxia (or hypoxia-reoxygenation) stimulus. These datasets provide global snapshots of molecular components, but by themselves say little about function. In multicellular organisms especially, several layers of complexity are added to the system between the cell and organ levels. Phenotype measurements, quantifying the effect on the system as a whole when a component is perturbed, bridge the molecular and functional levels. The "phenome" is the set of quantitative measurements of phenotypic function under a specific physiological context, for gene perturbations covering the entire genome – i.e. a directed genetic screen. Quantitative genomic phenotype information can be integrated with molecular-level data to add an extra layer of biological context.

The second step in the systems biology paradigm is to map global intracellular networks, since cellular components are highly interconnected beyond the traditional view of isolated pathways (Barabasi & Oltvai, 2004). It has been shown that in some intracellular systems, the topology of the network is more important for determining function than the kinetic parameters of individual interactions (Albert & Othmer, 2003; Urbanczik & Wagner, 2005). Although researchers have long used cartoon networks and systems models to describe specific cellular pathways, genome-wide network reconstructions have recently been made possible by new bioinformatics tools (Karp et al., 2002), high-throughput measurement of protein interactions (Giot et al., 2003; Ito et al., 2001; Li et al., 2004; Uetz et al., 2000), and large-scale efforts of manual interaction mapping (Reguly et al., 2006). Manually curated genome-scale metabolic reconstructions have been built for a number of model organisms including bacteria

(Reed et al., 2003), yeast (Duarte et al., 2004), mice (Sheikh et al., 2005), and humans (Duarte et al., 2007), but not yet for *Drosophila melanogaster*.

The third new idea in this approach is the predictive modeling of these networks. Researchers have built a number of kinetic models of smaller systems (Le Novere et al., 2006), which can be interfaced with each other in a modular fashion using common standards such as Systems Biology Markup Language (SBML) (Hucka et al., 2003) or Cell Markup Language (CellML) (Lloyd et al., 2004). However, modeling the detailed dynamics of biological systems generally requires a large set of kinetic parameters, which would be impractical to obtain for a genome-wide network. Several recent studies have used statistical models and integration of heterogeneous datatypes to infer function from large biological networks without relying on computationally intensive, parameter-dependent systems of differential equations (Han et al., 2004; Ideker et al., 2002; Walhout et al., 2002). For metabolic reconstructions in particular, the *constraint-based method* is a useful way to quantitatively analyze genome-wide networks without large numbers of kinetic parameters. Using the assumption of steady state, this method uncovers the space of all possible enzyme flux distributions under the set of physiochemical limitations imposed on the system (Palsson, 2000; Papin et al., 2003). A number of quantitative analyses have been developed to explore the biological consequences of this solution space (Price et al., 2004). *Flux-balance analysis,* the most commonly used technique, predicts an optimum flux distribution given the constraints and an objective for the system (for example, growth rate or ATP production) (Ibarra et al., 2002; Kauffman et al., 2003). Using these methods, computer simulations of microorganisms can approximate fluxes and growth rates seen *in-vivo* (Duarte et al., 2004; Edwards et al., 2001).

The last steps of the systems approach describe iterative refinement to the model using the results of perturbation analysis. From this point of view, data-driven or 'inductive' reasoning is complementary to hypothesis-driven or 'deductive' reasoning, and for large, complex systems iterative modeling may be the best way to generate testable hypotheses (Kell & Oliver, 2004). This general framework has seen much success in studying the single-cell organisms *E. coli* and *S. cerevisae*, as well as the multicellular eukaryotes *C. elegans* and *Drosophila melanogaster*, and shows promise as a tool for analyzing more complex organisms.

I.2.3 Drosophila as a model for systems analysis of cardiac hypoxia

Fruit flies have received increasing interest as a model for cardiac research (Bier & Bodmer, 2004; McCulloch & Paternostro, 2005; Serluca & Fishman, 2006). *Drosophila* has a tube-like heart and a simple circulatory system, which, when combined with its legacy of genetic research, makes the fly an attractive organism for studying genetic influences of cardiac function. With its genome sequence currently in its fourth revision (Adams et al., 2000; FlyBase, 2003), the fruit fly has one of the best characterized genomes of multicellular organisms. Flies can be reared and manipulated with minimal equipment and care, and their fecundity and ease of genetic manipulation have made them a popular subject for genetic screens. The Berkeley Drosophila Genome Project has provided a public resource of *Drosophila* P-element insertions, covering over 40% of the genome (Bellen et al., 2004).

Genomic similarities between flies and humans suggest that *Drosophila* genes found to influence cardiac function are likely to have a human counterpart. About half of *Drosophila* protein sequences are homologous to mammalian proteins (Adams et al., 2000), and in a survey of 287 humans disease genes across several physiological

categories, *Drosophila* was found to have a homolog for 62%, including all 6 cardiac disease genes examined (Fortini et al., 2000). Aside from “disease genes”, flies and mammals share many other genes underlying basic mechanisms of heart development and function. The identification of the homeobox transcription factor *tinman*, essential for heart vessel formation in flies (Bodmer & Venkatesh, 1998), prompted the cloning of homologues (Nkx2-5/Csx) which regulate cardiac development in mice (Ikeda et al., 2002; Lints et al., 1993). Although flies, unlike mammals, do not use sodium channels to create cardiac action potentials (Gu & Singh, 1995; Johnson et al., 1998), the fly pacemaker nevertheless relies on several conserved calcium and potassium channels. One important example is *ether-a-go-go*, which is similar in sequence and function to the human HERG potassium channel which has been implicated in long QT syndrome, a potentially fatal cardiac arrhythmia (Curran et al., 1995; Warmke & Ganetzky, 1994). Mutations in the *Drosophila* version of sarco-endoplasmic reticulum calcium ATPase (SERCA), a membrane pump important for maintaining calcium homeostasis in mammalian hearts, alters heart rate and rhythm in flies (Sanyal et al., 2006).

Fruit flies have also been used as a model organism for hypoxia research. Their innate tolerance to anoxia, being able to recover completely from up to 4 hours without oxygen (Haddad et al., 1997), has sparked recent efforts to understand the molecular basis for this tolerance. The presence of the disaccharide trehalose increases anoxia tolerance in flies, probably by protecting against protein desiccation and aggregation (Chen et al., 2002), and its protective effects were extended to human cells by transfecting the *Drosophila* trehalose synthase enzyme (Chen et al., 2003). A mutagenesis screen for anoxia sensitivity discovered the *hypnos* genes (Haddad et al., 1997), one of which was later identified as pre-mRNA adenosine

deaminase (dADAR), which edits the mRNA sequences of a number of ion channels and is expressed mainly in neurons (Ma et al., 2001).

It is likely that a core set of genes for defending cells against oxygen fluctuations also evolved early and has been conserved in evolution from flies to humans (O'Farrell, 2001). For example, hypoxia inducible factor HIF-1, the metabolic "master switch" AMP-activated protein kinase, and nitric oxide signaling all coordinate hypoxia adaptation in mammalian heart (Jones & Bolli, 2006; Kido et al., 2005; Pan & Hardie, 2002), and are all present and functional in flies (Lavista-Llanos et al., 2002; Pan & Hardie, 2002; Wingrove & O'Farrell, 1999). However, it is not known whether these hypoxia tolerance mechanisms are active in fly myocardial tissue specifically.

The fly has been a subject for applying novel systems biology approaches (Albert & Othmer, 2003; Stuart et al., 2006). RNA interference has been used in genome-wide screens for cell viability and for more specific phenotypes relating to developmental signaling pathways in flies (Boutros et al., 2004; Friedman & Perrimon, 2006), and the potential advantages of using transgenic RNAi libraries in this project are discussed in the Future Directions section of Chapter VI. Large-scale transcriptional profiling studies have been performed (Arbeitman et al., 2002; Furlong et al., 2001) and the resulting gene expression data were used to construct networks of co-expressed genes (Stuart et al., 2003). Importantly, a genome-scale *Drosophila* protein interaction map (Giot et al., 2003), generated using the yeast two-hybrid technique, can be used as a scaffold with which to reconstruct cellular networks.

I.3 Cardiac phenotype screen

One strategy for discovering the complete set of genes influencing cardiac adaptation to hypoxia is to systematically knock out each gene and measure the hypoxic heart phenotype. Of the organisms with publicly available mutant libraries of DNA-level perturbations, only *Drosophila* has a heart, offering the possibility of a genetic screen of function in the heart organ.

I.3.1 Automated cardiac phenotyping technology

Directed, systematic screens have several advantages over random mutagenesis: every gene can be screened, influential genes are instantly identified without follow-up sequencing, and phenotypes can be quantified for all genes rather than the top scoring 'hits' (Carpenter & Sabatini, 2004). However, as opposed to mutagenesis screens which can have arbitrary duration and scope, a systematic genome-wide screen is, by definition, not complete until each gene perturbation has been examined. New technology has made this daunting task conceptually feasible. When mounted on a transparent surface with its wings spread, the fly heart is easily visible from the dorsal side by a light microscope. Taking advantage of this property, we and others previously developed optical imaging methods for rapid measurement of cardiac function in adult flies (Choma et al., 2006; Paternostro et al., 2001; Wolf et al., 2006). Although these methods are computer-aided for faster throughput, none are fast enough to screen the approximately 14,000 *Drosophila* genes within a reasonable timeframe.

We recently developed new automation for rapid *in-vivo* measurement and analysis of the cardiac hypoxia response in adult flies, improving the speed of previous methods and reducing human error from repeated experiments. Automation

increases the throughput at several bottlenecks including anesthetization and mounting, locating each fly heart under the microscope, environmental control and hypoxia stimulus, and gathering M-mode representations of each heart tube. The M-mode is a two-dimensional time-space representation of cardiac contraction from image intensities measured along a line perpendicular to the heart. Image analysis algorithms can automatically extract functional information such as heart rate and diameter from the raw M-mode image. An overview of the system is displayed in Figure I.2.

I.3.2 Screening cardiac hypoxia phenotypes

Before initiating a screen for cardiac hypoxia tolerance, the endpoint must be defined. In their genetic screen, Haddad et. al. (1997) characterized the whole-body response, administering total anoxia for 5 minutes and measuring the time to recover to a prone body position as the endpoint for distinguishing hypoxia-sensitive mutations. Studies of cardioprotection in mammals use five physiological endpoints: infarct size, myocardial stunning, recovery of mechanical function, arrhythmias, and electrocardiographic changes (Yellon & Downey, 2003). Although infarct size and electrocardiograms are difficult to obtain in flies, our imaging-based system can approximately measure the other three end points. This technology is able to measure real-time heart rhythms – and potentially wall motion – under hypoxic stress; therefore stunning, mechanical recovery, and post-hypoxic arrhythmias are three measures of function in the hypoxic heart that can be adapted for rapid screening in *Drosophila*. For example, flies undergo a change in heart rate resembling myocardial stunning in mammals, and dilation of the fly heart tube during hypoxia mirrors changes in contractility.

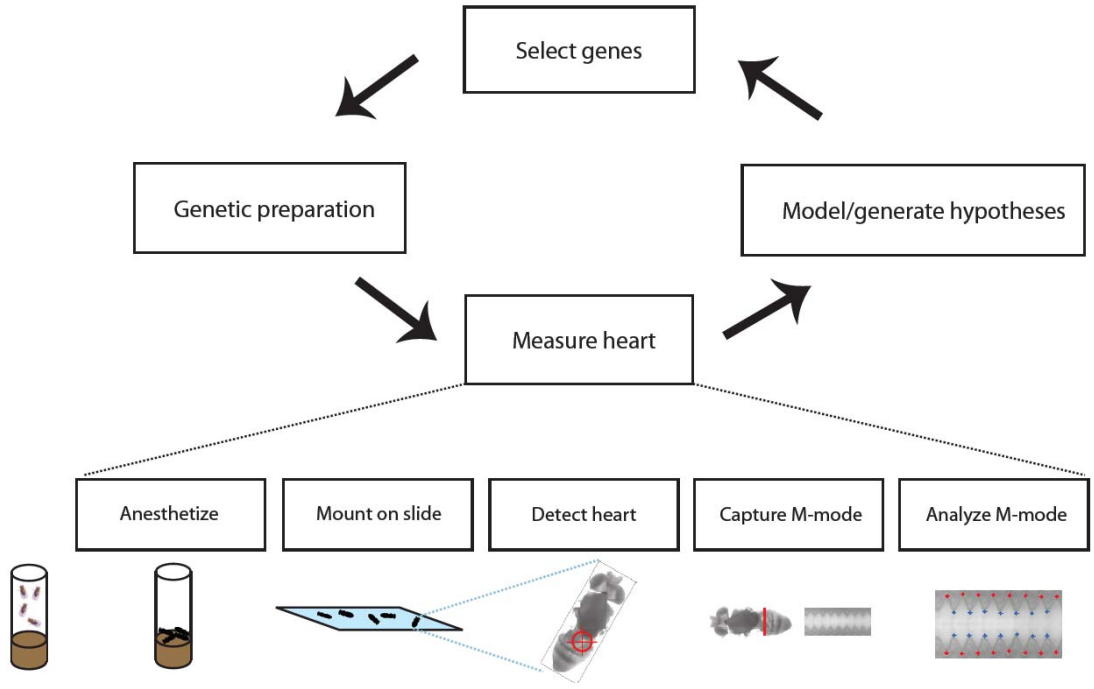

Figure I.2: Automated cardiac phenotyping methods. A computer-controlled system anesthetizes flies and mounts them on a microscope slide, then uses image process algorithms to find and measure the heart of each fly under controlled hypoxia stimulus.

The time course of phenotypic effects of hypoxia in adult flies and mammalian hearts, compared in Figure I.3, suggests a possible range of hypoxia durations that may expose physiological differences in a genetic screen. Before starting the mutant screen, automated methods can help to systematically characterize wild-type cardiac phenotypes under hypoxic stresses of varying durations and magnitudes. The screen can identify loss of hypoxia tolerance for any reason by a gene deletion, but

integration of phenotype data into the molecular network, described later, can then help to generate hypotheses for specific metabolic mechanisms.

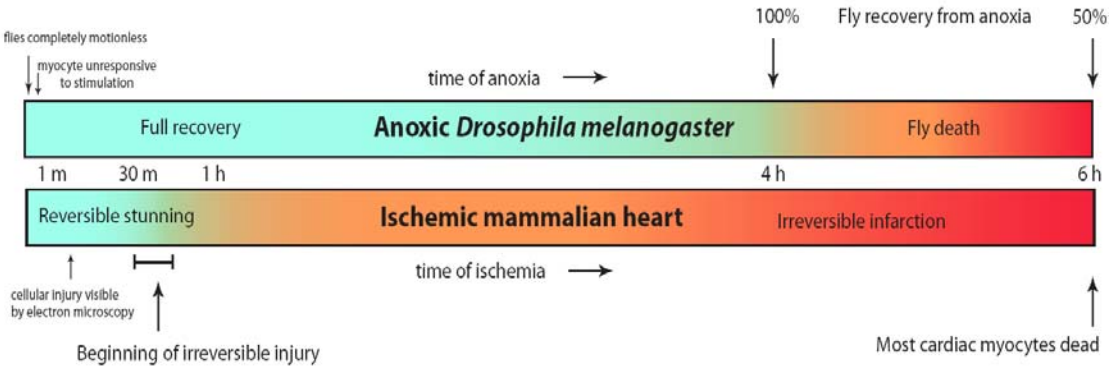

Figure I.3: Time-course of hypoxia tolerance in flies and mammalian heart. Flies can survive up to 4 hours of total anoxia, whereas heart cells begin to die from coronary occlusion in under an hour.

I.4 NMR metabolomics

Metabolomics is the comprehensive study of endogenous metabolites with the goal of understanding their role in systems biology. *Fluxomics* is the direct measurement of global metabolite fluxes, usually by using metabolomic methods to track molecules labeled with an isotope such as carbon-13. Two of the most common approaches for profiling metabolites and their changes are nuclear magnetic resonance (NMR) spectroscopy and mass spectrometry (MS) (Goodacre et al., 2004; Nicholson et al., 2002; Watkins & German, 2002; Whitfield et al., 2004). These techniques have been used to study isolated metabolites for decades and, because of the greatly increased sensitivity of modern methods and instrumentation, in the last

few years have been able to provide more comprehensive metabolic profiles. Recent advances in magnet field strength and probe technology (Keun et al., 2002a) have expanded the capability of NMR spectroscopy as a metabolomics tool. Some metabolites can be measured with both NMR and mass spectrometry but others are best measured by only one of these techniques - for example carbohydrates do not ionize well and for them it is preferable to use NMR. NMR results generally provide more accurate quantitative measurements (Keun et al., 2002b).

Metabolic profiling is central to a strategy for modeling adaptation to hypoxia in flies because metabolite fluxes are, at the molecular level, the main phenotypic endpoint for adaptation to hypoxia by signaling networks. Due to the low sensitivity of NMR methods and the difficulty in harvesting heart tissue in the fly, it is difficult to obtain large enough samples of *Drosophila* myocardium for NMR spectroscopy. Flight muscle, which takes up most of the mass of the thorax, can perhaps provide a reasonable substitute. Most of the literature on fruit fly biochemistry focuses on flight muscle and its metabolic adaptation for flight, therefore reconstruction of the fly metabolism is easier for flight muscle tissue. The biochemistry of *Drosophila* heart is not known, but flight muscle is similar to cardiac muscle in other organisms in that it has very high aerobic requirements during exercise and is well supplied with oxygen. One major drawback of flight muscle as an approximation to heart metabolism is that in many insects such as bees and blowflies it is thought to rely on carbohydrates as the major substrate (Gilmour, 1961; Suarez et al., 2005), whereas the heart uses both carbohydrates and fatty acids under normal operation (Opie, 1998a).

Our lab used ^{1}H NMR spectroscopy as a starting point for understanding the pathways involved in adaptation to hypoxia in *Drosophila* flight muscle. Our results

showed that lactate, alanine, and acetate concentrations increase over 4 hours of hypoxia, suggesting that *Drosophila* coordinates glycolysis with three pathways of pyruvate metabolism in order to cope with hypoxia (Feala et al., 2007). However, concentration measurements only provide a snapshot in time of the integral of all fluxes into and out of a metabolite pool. Another problem with these data is that the relatively low sensitivity of NMR spectroscopy prevents intermediate metabolites from being quantified, which would better identify specific pathways. Isotopomer-based fluxomics, discussed in Chapter VI – Future Directions, are discussed as a potential solution to these problems.

NMR spectroscopy is limited by difficulties including the necessity of water suppression. Certain metabolites, such as the important substrates trehalose, glycogen and fatty acids, need to be assayed by other methods due to limitations in detection by NMR.

I.5 Metabolic models

I.5.1 Reconstructing Drosophila metabolism

The number of published metabolic reconstructions continues to grow every year. Although the majority of available models are for microbes, reconstructions of more complex organisms and subsystems are becoming more common. For example, curated models of the human cardiac mitochondria, human red blood cell, generic mouse metabolism, mouse cardiomyocyte, and draft multicellular human reconstruction have been made publicly available (Duarte et al., 2007; Morel et al., 2006; Palsson et al., 1989; Sheikh et al., 2005; Vo et al., 2004).

Our lab completed a draft *in-silico* reconstruction of ATP-generating metabolism in *Drosophila* flight muscle to study metabolic adaptation to hypoxia (Feala et al., 2007). The model is curated, meaning that all reactions in the reconstruction are balanced and individually inspected by a search of the literature and databases before inclusion into the model. Also, all reactions are compartmentalized (cytosol or mitochondria) and balanced for conservation of elements and charge. Reed et. al (2006) reviews the reconstruction process in detail.

High-throughput data measured in controlled studies can be used to suggest the existence or absence of enzymes when refining for a specific cell type or condition. Transcriptomics data are available for fly thorax (Girardot et al., 2006), and fly mitochondria have been examined by proteomics methods (Alonso et al., 2005). Although these techniques are likely to miss mRNA and proteins present in low concentrations, many enzymes can be found in these gene and protein lists, which can refine the model to better represent the muscle cell type. Tissue specificity of a metabolic reconstruction can be improved using a list of genes and proteins discovered in high-throughput assays of individual cell types and organelles (Vo et al., 2004). In Chapter IV we use a microarray dataset from adult thorax to refine the metabolic reconstruction.

I.5.2 Simulating hypoxic metabolism

In hypoxia, the overall reduction in energy production is thought to be less important to cardiac dysfunction than the loss of metabolite balance within the system (Ingwall, 2002). One major advantage of a mathematical model is that conservation of mass is enforced; therefore all elements and charges are balanced within the system, including electron transport, cofactor concentration, and protons (pH). Thus,

the complicated problems of balancing redox potential and accounting for ATP and proton production are solved intrinsically during simulation. Flux-balance analysis (FBA) on the network reconstruction can quantitatively model these relationships in a large metabolic network. See (Schilling et al., 2000), (Papin et al., 2003) and (Kauffman et al., 2003) for a review of the mathematics involved in flux-balance analysis.

FBA requires an "objective function" to maximize in order to select an optimum set of steady-state fluxes from the solution space. In both heart and flight muscle, the objective of metabolism is primarily to provide ATP to the energy-consuming myosin cross-bridges and ion pumps. The result of FBA is the distribution of fluxes that maximize the objective function under the imposed constraints. The main type of constraint commonly used in these models is restricted metabolite influx and efflux rates. Fluxes measured experimentally, whether by isotopomer labeling or by linear approximation of the rate of metabolite accumulation, can be integrated into the metabolic model as upper and lower bounds on reaction rates, following the example of Vo and Palsson (2006). Fitting to measured fluxes results in a model experimentally refined to represent the specific tissue and context of interest, in our case hypoxic flight muscle, reducing the degrees of freedom of the solution.

Our metabolic model helped us to understand how the three pyruvate pathways, hypothesized from the ^{1}H NMR data, might stabilize pH and redox potential while maximizing ATP production under low oxygen . Anaerobic pathways for generating these end products were hypothesized, and the corresponding reactions were linked to existing *Drosophila* genes and built into the model. In order to isolate the effects of hypoxia, we used FBA under varying O_2 uptake to find the

network states which maximize ATP production under changes in oxygen availability. Simulations suggested that the flexibility of pyruvate metabolism provided by these three pathways might provide extra tolerance to hypoxia by increasing the ratio of H^+ produced per ATP generated while simultaneously reducing the amount of carbohydrate fuel required per ATP.

I.5.3 Refining with phenotype data

Cardiac phenotypes of enzyme mutants can also provide some limited information about reactions in cardiomyocyte metabolism. Systematic perturbation analysis – measurements of cardiac phenotypes for all available enzyme mutations – can be compared with the results of an *in-silico* deletion analysis. For example, if a mutation produces a significant decrease in hypoxia tolerance and simulations show a decrease in ATP during hypoxia, the enzyme is likely to be an essential component of heart metabolism and should be included in the cardiomyocyte network. The methods developed in Chapter II

I.6 Iteration and detailed follow-up

Systems analysis of the cardiac hypoxia response generates hypotheses for essential pathways and proteins that can be easily tested using mutants or biochemical methods. For example, our lab used metabolomics and modeling to predict pathways for the anaerobic production of acetate and alanine under hypoxic conditions. This is being tested with repeated application of our high-throughput techniques, gathering metabolomic profiles and cardiac phenotypes of mutants in these pathways.

Hypoxia sensitive mutants can be further verified by more detailed experimental methods, for example by producing transgenic flies for temporal control

of gene expression, using cardiac-specific promoters can be used for tissue specificity. In this way, molecular biology has a complementary role in coarse-grained systems analyses, because any results from the model are only hypotheses until they are validated by standard techniques. Valid results can be entered back into the model, improving its accuracy for future simulations.

I.7 Discussion

Our systems analysis of the hypoxia response in ATP-producing pathways in *Drosophila* flight muscle provided insights and hypotheses for molecular mechanisms contributing to their remarkable hypoxia tolerance. The other half of the anaerobic shift, down-regulation of ATP-consuming pathways, was not modeled but plays a crucial role in survival during hypoxia. Therefore our current efforts are only a first step in this framework for developing a global model that represents both ATP supply and demand, with a greater relevance to the heart.

In order to extend this approach to cardiac myocytes, both the model and its underlying data must be expanded to represent global regulation of metabolism in the heart. The most logical step would be to use high-throughput data specific for *Drosophila* cardiac myocytes, adding microarray and proteomic data from the fly heart to complement our cardiac phenotype measurements of enzymatic mutants. However, this approach is limited by the difficulty of obtaining large amounts of fly myocardial tissue.

Chapter VI discusses future applications for the network modeling approached discussed in this dissertation. Our experimentally validated, global model of hypoxic metabolism could be studied further using flux-balance analysis and other constraint-based techniques. To expand the model to encompass possible signaling networks

acting on enzymes, it is possible to integrate a protein interaction network (from online interaction databases) and measure cardiac phenotypes for all close neighbors to enzymes in the metabolic model (preliminary results in this direction are shown in Chapter VI). Although the dense interaction network cannot be functionally simulated in the same way as the metabolic model, statistical methods can be used to discover highly connected modules enriched with large phenotype changes.

Efforts to bring data and models together under the context of acute cardiac hypoxia could be replicated for other systems of interest, possibly using some of the data or networks mentioned here. Conversely, it would be possible for future work on *Drosophila* cardiac hypoxia to use this integrated model as a framework with which to incorporate and interpret further models or experiments. A major goal for systems biology is to provide scaffolds for storing and integrating the overwhelming data both in the existing literature and in new high-throughput experiments. For example, our network incorporates the *Drosophila* annotated genome with decades of literature on fly metabolism as well as our newly gathered metabolomic and phenotype data.

We have taken a discovery-based approach to find system-wide properties of the cardiac hypoxia response, integrating “top-down” (phenotype) and “bottom-up” (molecular) data. Network models are a way of bridging the gap across these functional scales. The incorporation of genome-wide data provides a coarse-grained view of the system, complementary to a more detailed biochemical and molecular biology approach. By ensuring that all important components are accounted for, a global modeling approach is an unbiased way to focus future, more detailed efforts on the most important parts of the system.

Acknowledgements

Chapter I, in part, is adapted from a review that originally appeared in Progress in Biophysics and Molecular Biology, volume 96, issues 1-3, pages 209-25, published August, 2008. The dissertation author was the primary author of this paper, which was co-authored by Drs. Laurence Coquin, Giovanni Paternostro, and Andrew D. McCulloch.

References

Adams MD, Celniker SE, Holt RA, Evans CA, Gocayne JD, Amanatides PG, Scherer SE, Li PW, Hoskins RA, Galle RF, George RA, Lewis SE, Richards S, Ashburner M, Henderson SN, Sutton GG, Wortman JR, Yandell MD, Zhang Q, Chen LX, et al. (2000) The genome sequence of Drosophila melanogaster. *Science* **287:** 2185-2195.

Albert R, Othmer HG (2003) The topology of the regulatory interactions predicts the expression pattern of the segment polarity genes in Drosophila melanogaster. *J Theor Biol* **223:** 1-18.

Alonso J, Rodriguez JM, Baena-Lopez LA, Santaren JF (2005) Characterization of the Drosophila melanogaster mitochondrial proteome. *J Proteome Res* **4:** 1636-1645.

Ambrosio G, Weisfeldt ML, Jacobus WE, Flaherty JT (1987) Evidence for a reversible oxygen radical-mediated component of reperfusion injury: reduction by recombinant human superoxide dismutase administered at the time of reflow. *Circulation* **75:** 282-291.

Arad M, Seidman CE, Seidman JG (2007) AMP-activated protein kinase in the heart: role during health and disease. *Circ Res* **100:** 474-488.

Arbeitman MN, Furlong EE, Imam F, Johnson E, Null BH, Baker BS, Krasnow MA, Scott MP, Davis RW, White KP (2002) Gene expression during the life cycle of Drosophila melanogaster. *Science* **297:** 2270-2275.

Barabasi AL, Oltvai ZN (2004) Network biology: understanding the cell's functional organization. *Nat Rev Genet* **5:** 101-113.

Bellen HJ, Levis RW, Liao G, He Y, Carlson JW, Tsang G, Evans-Holm M, Hiesinger PR, Schulze KL, Rubin GM, Hoskins RA, Spradling AC (2004) The BDGP gene disruption project: single transposon insertions associated with 40% of Drosophila genes. *Genetics* **167:** 761-781.

Bier E, Bodmer R (2004) Drosophila, an emerging model for cardiac disease. *Gene* **342:** 1-11.

Bodmer R, Venkatesh TV (1998) Heart development in Drosophila and vertebrates: conservation of molecular mechanisms. *Dev Genet* **22:** 181-186.

Bonow RO, Bohannon N, Hazzard W (1996) Risk stratification in coronary artery disease and special populations. *Am J Med* **101:** 4A17S-22S; discussion 22S-24S.

Boutros M, Kiger AA, Armknecht S, Kerr K, Hild M, Koch B, Haas SA, Paro R, Perrimon N (2004) Genome-wide RNAi analysis of growth and viability in Drosophila cells. *Science* **303:** 832-835.

Budas GR, Churchill EN, Mochly-Rosen D (2007) Cardioprotective mechanisms of PKC isozyme-selective activators and inhibitors in the treatment of ischemia-reperfusion injury. *Pharmacol Res*.

Carpenter AE, Sabatini DM (2004) Systematic genome-wide screens of gene function. *Nat Rev Genet* **5:** 11-22.

Chen Q, Behar KL, Xu T, Fan C, Haddad GG (2003) Expression of Drosophila trehalose-phosphate synthase in HEK-293 cells increases hypoxia tolerance. *J Biol Chem* **278:** 49113-49118.

Chen Q, Ma E, Behar KL, Xu T, Haddad GG (2002) Role of trehalose phosphate synthase in anoxia tolerance and development in Drosophila melanogaster. *J Biol Chem* **277:** 3274-3279.

Choma MA, Izatt SD, Wessells RJ, Bodmer R, Izatt JA (2006) Images in cardiovascular medicine: in vivo imaging of the adult Drosophila melanogaster heart with real-time optical coherence tomography. *Circulation* **114:** e35-36.

Coquin L, Feala JF, A.M. M, G. P (2008) Metabolomic and flux-balance analysis of aging and hypoxia tolerance in Drosophila muscle tissue. *Mol Cell Biol*.

Cuong DV, Kim N, Youm JB, Joo H, Warda M, Lee JW, Park WS, Kim T, Kang S, Kim H, Han J (2006) Nitric oxide-cGMP-protein kinase G signaling pathway induces anoxic preconditioning through activation of ATP-sensitive K+ channels in rat hearts. *Am J Physiol Heart Circ Physiol* **290:** H1808-1817.

Curran ME, Splawski I, Timothy KW, Vincent GM, Green ED, Keating MT (1995) A molecular basis for cardiac arrhythmia: HERG mutations cause long QT syndrome. *Cell* **80:** 795-803.

De Celle T, Vanrobaeys F, Lijnen P, Blankesteijn WM, Heeneman S, Van Beeumen J, Devreese B, Smits JF, Janssen BJ (2005) Alterations in mouse cardiac proteome after in vivo myocardial infarction: permanent ischaemia versus ischaemia-reperfusion. *Exp Physiol* **90:** 593-606.

Du Q, Jovanovic S, Clelland A, Sukhodub A, Budas G, Phelan K, Murray-Tait V, Malone L, Jovanovic A (2006) Overexpression of SUR2A generates a cardiac phenotype resistant to ischemia. *Faseb J* **20:** 1131-1141.

Duarte NC, Becker SA, Jamshidi N, Thiele I, Mo ML, Vo TD, Srivas R, Palsson BO (2007) Global reconstruction of the human metabolic network based on genomic and bibliomic data. *Proc Natl Acad Sci U S A* **104:** 1777-1782.

Duarte NC, Herrgard MJ, Palsson BO (2004) Reconstruction and validation of Saccharomyces cerevisiae iND750, a fully compartmentalized genome-scale metabolic model. *Genome Res* **14:** 1298-1309.

Edwards JS, Ibarra RU, Palsson BO (2001) In silico predictions of Escherichia coli metabolic capabilities are consistent with experimental data. *Nat Biotechnol* **19:** 125-130.

Feala JD, Coquin L, McCulloch AD, Paternostro G (2007) Flexibility in energy metabolism supports hypoxia tolerance in Drosophila flight muscle: metabolomic and computational systems analysis. *Mol Syst Biol* **3:** 99.

Feala JD, Coquin L, Paternostro G, McCulloch AD (2008a) Integrating metabolomics and phenomics with systems models of cardiac hypoxia. *Prog Biophys Mol Biol* **96:** 209-225.

Feala JD, Omens JH, Paternostro G, McCulloch AD (2008b) Discovering regulators of the Drosophila cardiac hypoxia response using automated phenotyping technology. *Ann N Y Acad Sci* **1123:** 169-177.

Fell D (1997) *Understanding the control of metabolism*. Portland Press ;
Distributed by Ashgate Pub. Co. in North America, London ; Miami
Brookfield, VT.

FlyBase (2003) The FlyBase database of the Drosophila genome projects and community literature. *Nucleic Acids Res* **31:** 172-175.

Fortini ME, Skupski MP, Boguski MS, Hariharan IK (2000) A survey of human disease gene counterparts in the Drosophila genome. *J Cell Biol* **150:** F23-30.

Friedman A, Perrimon N (2006) A functional RNAi screen for regulators of receptor tyrosine kinase and ERK signalling. *Nature* **444:** 230-234.

Furlong EE, Andersen EC, Null B, White KP, Scott MP (2001) Patterns of gene expression during Drosophila mesoderm development. *Science* **293:** 1629-1633.

Gilmour D (1961) *The biochemistry of insects*. Academic Press, New York,.

Giot L, Bader JS, Brouwer C, Chaudhuri A, Kuang B, Li Y, Hao YL, Ooi CE, Godwin B, Vitols E, Vijayadamodar G, Pochart P, Machineni H, Welsh M, Kong Y, Zerhusen B, Malcolm R, Varrone Z, Collis A, Minto M, et al. (2003) A protein interaction map of Drosophila melanogaster. *Science* **302:** 1727-1736.

Girardot F, Lasbleiz C, Monnier V, Tricoire H (2006) Specific age-related signatures in Drosophila body parts transcriptome. *BMC Genomics* **7:** 69.

Goodacre R, Vaidyanathan S, Dunn WB, Harrigan GG, Kell DB (2004) Metabolomics by numbers: acquiring and understanding global metabolite data. *Trends Biotechnol* **22:** 245-252.

Graham RM, Frazier DP, Thompson JW, Haliko S, Li H, Wasserlauf BJ, Spiga MG, Bishopric NH, Webster KA (2004) A unique pathway of cardiac myocyte death caused by hypoxia-acidosis. *J Exp Biol* **207:** 3189-3200.

Gu GG, Singh S (1995) Pharmacological analysis of heartbeat in Drosophila. *J Neurobiol* **28:** 269-280.

Haddad GG, Wyman RJ, Mohsenin A, Sun Y, Krishnan SN (1997) Behavioral and Electrophysiologic Responses of Drosophila melanogaster to Prolonged Periods of Anoxia. *J Insect Physiol* **43:** 203-210.

Han JD, Bertin N, Hao T, Goldberg DS, Berriz GF, Zhang LV, Dupuy D, Walhout AJ, Cusick ME, Roth FP, Vidal M (2004) Evidence for dynamically organized modularity in the yeast protein-protein interaction network. *Nature* **430:** 88-93.

Hataishi R, Rodrigues AC, Neilan TG, Morgan JG, Buys E, Shiva S, Tambouret R, Jassal DS, Raher MJ, Furutani E, Ichinose F, Gladwin MT, Rosenzweig A, Zapol WM, Picard MH, Bloch KD, Scherrer-Crosbie M (2006) Inhaled nitric oxide decreases infarction size and improves left ventricular function in a murine model of myocardial ischemia-reperfusion injury. *Am J Physiol Heart Circ Physiol* **291:** H379-384.

Hochachka PW (1980) *Living without oxygen : closed and open systems in hypoxia tolerance*. Harvard Univ. Press, Cambridge.

Hochachka PW (2003) Intracellular convection, homeostasis and metabolic regulation. *J Exp Biol* **206:** 2001-2009.

Hochachka PW, Somero GN (2002) *Biochemical adaptation : mechanism and process in physiological evolution*. Oxford University Press, New York.

Hucka M, Finney A, Sauro HM, Bolouri H, Doyle JC, Kitano H, Arkin AP, Bornstein BJ, Bray D, Cornish-Bowden A, Cuellar AA, Dronov S, Gilles ED, Ginkel M, Gor V, Goryanin, II, Hedley WJ, Hodgman TC, Hofmeyr JH, Hunter PJ, et al. (2003) The systems biology markup language (SBML): a medium for representation and exchange of biochemical network models. *Bioinformatics* **19:** 524-531.

Ibarra RU, Edwards JS, Palsson BO (2002) Escherichia coli K-12 undergoes adaptive evolution to achieve in silico predicted optimal growth. *Nature* **420:** 186-189.

Ideker T, Galitski T, Hood L (2001) A new approach to decoding life: systems biology. *Annu Rev Genomics Hum Genet* **2:** 343-372.

Ideker T, Ozier O, Schwikowski B, Siegel AF (2002) Discovering regulatory and signalling circuits in molecular interaction networks. *Bioinformatics* **18 Suppl 1:** S233-240.

Ikeda Y, Hiroi Y, Hosoda T, Utsunomiya T, Matsuo S, Ito T, Inoue J, Sumiyoshi T, Takano H, Nagai R, Komuro I (2002) Novel point mutation in the cardiac transcription factor CSX/NKX2.5 associated with congenital heart disease. *Circ J* **66:** 561-563.

Ingwall J (2002) *ATP and the Heart*. Kluwer Academic Publishers, Boston, London.

Irie H, Krukenkamp IB, Brinkmann JF, Gaudette GR, Saltman AE, Jou W, Glatz JF, Abumrad NA, Ibrahimi A (2003) Myocardial recovery from ischemia is impaired in CD36-null mice and restored by myocyte CD36 expression or medium-chain fatty acids. *Proc Natl Acad Sci U S A* **100:** 6819-6824.

Ito T, Chiba T, Ozawa R, Yoshida M, Hattori M, Sakaki Y (2001) A comprehensive two-hybrid analysis to explore the yeast protein interactome. *Proc Natl Acad Sci U S A* **98:** 4569-4574.

Jennings RB, Reimer KA, Steenbergen C (1986) Myocardial ischemia revisited. The osmolar load, membrane damage, and reperfusion. *J Mol Cell Cardiol* **18:** 769-780.

Johnson E, Ringo J, Bray N, Dowse H (1998) Genetic and pharmacological identification of ion channels central to the Drosophila cardiac pacemaker. *J Neurogenet* **12:** 1-24.

Jones SP, Bolli R (2006) The ubiquitous role of nitric oxide in cardioprotection. *J Mol Cell Cardiol* **40:** 16-23.

Julia P, Young HH, Buckberg GD, Kofsky ER, Bugyi HI (1990) Studies of myocardial protection in the immature heart. II. Evidence for importance of amino acid metabolism in tolerance to ischemia. *J Thorac Cardiovasc Surg* **100:** 888-895.

Karp PD, Paley S, Romero P (2002) The Pathway Tools software. *Bioinformatics* **18 Suppl 1:** S225-232.

Kauffman KJ, Prakash P, Edwards JS (2003) Advances in flux balance analysis. *Curr Opin Biotechnol* **14:** 491-496.

Kell DB, Oliver SG (2004) Here is the evidence, now what is the hypothesis? The complementary roles of inductive and hypothesis-driven science in the post-genomic era. *Bioessays* **26:** 99-105.

Keun HC, Beckonert O, Griffin JL, Richter C, Moskau D, Lindon JC, Nicholson JK (2002a) Cryogenic probe 13C NMR spectroscopy of urine for metabonomic studies. *Anal Chem* **74:** 4588-4593.

Keun HC, Ebbels TM, Antti H, Bollard ME, Beckonert O, Schlotterbeck G, Senn H, Niederhauser U, Holmes E, Lindon JC, Nicholson JK (2002b) Analytical reproducibility in (1)H NMR-based metabonomic urinalysis. *Chem Res Toxicol* **15:** 1380-1386.

Kido M, Du L, Sullivan CC, Li X, Deutsch R, Jamieson SW, Thistlethwaite PA (2005) Hypoxia-inducible factor 1-alpha reduces infarction and attenuates progression of cardiac dysfunction after myocardial infarction in the mouse. *J Am Coll Cardiol* **46:** 2116-2124.

Kodde IF, van der Stok J, Smolenski RT, de Jong JW (2007) Metabolic and genetic regulation of cardiac energy substrate preference. *Comp Biochem Physiol A Mol Integr Physiol* **146:** 26-39.

Kolar F, Ostadal B (2004) Molecular mechanisms of cardiac protection by adaptation to chronic hypoxia. *Physiol Res* **53 Suppl 1:** S3-13.

Lavista-Llanos S, Centanin L, Irisarri M, Russo DM, Gleadle JM, Bocca SN, Muzzopappa M, Ratcliffe PJ, Wappner P (2002) Control of the hypoxic response in Drosophila melanogaster by the basic helix-loop-helix PAS protein similar. *Mol Cell Biol* **22:** 6842-6853.

Le Novere N, Bornstein B, Broicher A, Courtot M, Donizelli M, Dharuri H, Li L, Sauro H, Schilstra M, Shapiro B, Snoep JL, Hucka M (2006) BioModels Database: a free, centralized database of curated, published, quantitative kinetic models of biochemical and cellular systems. *Nucleic Acids Res* **34:** D689-691.

Lehninger AL, Nelson DL, Cox MM (2000) *Lehninger principles of biochemistry*. Worth Publishers, New York.

Li S, Armstrong CM, Bertin N, Ge H, Milstein S, Boxem M, Vidalain PO, Han JD, Chesneau A, Hao T, Goldberg DS, Li N, Martinez M, Rual JF, Lamesch P, Xu L, Tewari M, Wong SL, Zhang LV, Berriz GF, et al. (2004) A map of the interactome network of the metazoan C. elegans. *Science* **303:** 540-543.

Lints TJ, Parsons LM, Hartley L, Lyons I, Harvey RP (1993) Nkx-2.5: a novel murine homeobox gene expressed in early heart progenitor cells and their myogenic descendants. *Development* **119:** 419-431.

Lloyd CM, Halstead MD, Nielsen PF (2004) CellML: its future, present and past. *Prog Biophys Mol Biol* **85:** 433-450.

Ma E, Gu XQ, Wu X, Xu T, Haddad GG (2001) Mutation in pre-mRNA adenosine deaminase markedly attenuates neuronal tolerance to O2 deprivation in Drosophila melanogaster. *J Clin Invest* **107:** 685-693.

McCulloch AD, Paternostro G (2005) Cardiac systems biology. *Ann N Y Acad Sci* **1047:** 283-295.

Morel S, Milano G, Ludunge KM, Corno AF, Samaja M, Fleury S, Bonny C, Kappenberger L, von Segesser LK, Vassalli G (2006) Brief reoxygenation episodes during chronic hypoxia enhance posthypoxic recovery of LV function : Role of mitogen-activated protein kinase signaling pathways. *Basic Res Cardiol* **101:** 336-345.

Murphy E, Steenbergen C (2007) Preconditioning: the mitochondrial connection. *Annu Rev Physiol* **69:** 51-67.

Murray CJ, Lopez AD (1997) Alternative projections of mortality and disability by cause 1990-2020: Global Burden of Disease Study. *Lancet* **349:** 1498-1504.

Nicholson JK, Connelly J, Lindon JC, Holmes E (2002) Metabonomics: a platform for studying drug toxicity and gene function. *Nat Rev Drug Discov* **1:** 153-161.

O'Farrell PH (2001) Conserved responses to oxygen deprivation. *J Clin Invest* **107:** 671-674.

Ogata H, Goto S, Sato K, Fujibuchi W, Bono H, Kanehisa M (1999) KEGG: Kyoto Encyclopedia of Genes and Genomes. *Nucleic Acids Res* **27:** 29-34.

Onody A, Zvara A, Hackler L, Jr., Vigh L, Ferdinandy P, Puskas LG (2003) Effect of classic preconditioning on the gene expression pattern of rat hearts: a DNA microarray study. *FEBS Lett* **536:** 35-40.

Opie L (1998a) *The Heart*. Raven Press, New York.

Opie LH (1991) *The heart : physiology and metabolism*. Raven Press, New York.

Opie LH (1998b) *The heart : physiology, from cell to circulation*. Lippincott-Raven, Philadelphia.

Palsson B (2000) The challenges of in silico biology. *Nat Biotechnol* **18:** 1147-1150.

Palsson BO, Narang A, Joshi A (1989) Computer model of human erythrocyte metabolism. *Prog Clin Biol Res* **319:** 133-150; discussion 151-134.

Pan DA, Hardie DG (2002) A homologue of AMP-activated protein kinase in Drosophila melanogaster is sensitive to AMP and is activated by ATP depletion. *Biochem J* **367:** 179-186.

Papin JA, Price ND, Wiback SJ, Fell DA, Palsson BO (2003) Metabolic pathways in the post-genome era. *Trends Biochem Sci* **28:** 250-258.

Paternostro G, Vignola C, Bartsch DU, Omens JH, McCulloch AD, Reed JC (2001) Age-associated cardiac dysfunction in Drosophila melanogaster. *Circ Res* **88:** 1053-1058.

Price ND, Reed JL, Palsson BO (2004) Genome-scale models of microbial cells: evaluating the consequences of constraints. *Nat Rev Microbiol* **2:** 886-897.

Reed JL, Famili I, Thiele I, Palsson BO (2006) Towards multidimensional genome annotation. *Nat Rev Genet* **7:** 130-141.

Reed JL, Vo TD, Schilling CH, Palsson BO (2003) An expanded genome-scale model of Escherichia coli K-12 (iJR904 GSM/GPR). *Genome Biol* **4:** R54.

Reguly T, Breitkreutz A, Boucher L, Breitkreutz BJ, Hon GC, Myers CL, Parsons A, Friesen H, Oughtred R, Tong A, Stark C, Ho Y, Botstein D, Andrews B, Boone C, Troyanskya OG, Ideker T, Dolinski K, Batada NN, Tyers M (2006) Comprehensive curation and analysis of global interaction networks in Saccharomyces cerevisiae. *J Biol* **5:** 11.

Robergs RA, Ghiasvand F, Parker D (2004) Biochemistry of exercise-induced metabolic acidosis. *Am J Physiol Regul Integr Comp Physiol* **287:** R502-516.

Sabatine MS, Liu E, Morrow DA, Heller E, McCarroll R, Wiegand R, Berriz GF, Roth FP, Gerszten RE (2005) Metabolomic identification of novel biomarkers of myocardial ischemia. *Circulation* **112:** 3868-3875.

Sakai J, Ishikawa H, Kojima S, Satoh H, Yamamoto S, Kanaoka M (2003) Proteomic analysis of rat heart in ischemia and ischemia-reperfusion using fluorescence two-dimensional difference gel electrophoresis. *Proteomics* **3:** 1318-1324.

Sambandam N, Lopaschuk GD (2003) AMP-activated protein kinase (AMPK) control of fatty acid and glucose metabolism in the ischemic heart. *Prog Lipid Res* **42:** 238-256.

Sanyal S, Jennings T, Dowse H, Ramaswami M (2006) Conditional mutations in SERCA, the Sarco-endoplasmic reticulum Ca(2+)-ATPase, alter heart rate and rhythmicity in Drosophila. *J Comp Physiol [B]* **176:** 253-263.

Schilling CH, Letscher D, Palsson BO (2000) Theory for the systemic definition of metabolic pathways and their use in interpreting metabolic function from a pathway-oriented perspective. *J Theor Biol* **203:** 229-248.

Sehl PD, Tai JT, Hillan KJ, Brown LA, Goddard A, Yang R, Jin H, Lowe DG (2000) Application of cDNA microarrays in determining molecular phenotype in cardiac growth, development, and response to injury. *Circulation* **101:** 1990-1999.

Semenza GL (2001) Hypoxia-inducible factor 1: oxygen homeostasis and disease pathophysiology. *Trends Mol Med* **7:** 345-350.

Serluca FC, Fishman MC (2006) Big, bad hearts: from flies to man. *Proc Natl Acad Sci U S A* **103:** 3947-3948.

Sheikh K, Forster J, Nielsen LK (2005) Modeling hybridoma cell metabolism using a generic genome-scale metabolic model of Mus musculus. *Biotechnol Prog* **21:** 112-121.

Simkhovich BZ, Marjoram P, Poizat C, Kedes L, Kloner RA (2003) Brief episode of ischemia activates protective genetic program in rat heart: a gene chip study. *Cardiovasc Res* **59:** 450-459.

Solaini G, Harris DA (2005) Biochemical dysfunction in heart mitochondria exposed to ischaemia and reperfusion. *Biochem J* **390:** 377-394.

Stanton LW, Garrard LJ, Damm D, Garrick BL, Lam A, Kapoun AM, Zheng Q, Protter AA, Schreiner GF, White RT (2000) Altered patterns of gene expression in response to myocardial infarction. *Circ Res* **86:** 939-945.

Steenbergen C, Murphy E, Levy L, London RE (1987) Elevation in cytosolic free calcium concentration early in myocardial ischemia in perfused rat heart. *Circ Res* **60:** 700-707.

Stuart JM, Segal E, Koller D, Kim SK (2003) A gene-coexpression network for global discovery of conserved genetic modules. *Science* **302:** 249-255.

Stuart LM, Boulais J, Charriere GM, Hennessy EJ, Brunet S, Jutras I, Goyette G, Rondeau C, Letarte S, Huang H, Ye P, Morales F, Kocks C, Bader JS, Desjardins M, Ezekowitz RA (2006) A systems biology analysis of the Drosophila phagosome. *Nature*.

Suarez RK, Darveau CA, Welch KC, Jr., O'Brien DM, Roubik DW, Hochachka PW (2005) Energy metabolism in orchid bee flight muscles: carbohydrate fuels all. *J Exp Biol* **208:** 3573-3579.

Taegtmeyer H, Peterson MB, Ragavan VV, Ferguson AG, Lesch M (1977) De novo alanine synthesis in isolated oxygen-deprived rabbit myocardium. *J Biol Chem* **252:** 5010-5018.

Uetz P, Giot L, Cagney G, Mansfield TA, Judson RS, Knight JR, Lockshon D, Narayan V, Srinivasan M, Pochart P, Qureshi-Emili A, Li Y, Godwin B, Conover D, Kalbfleisch T, Vijayadamodar G, Yang M, Johnston M, Fields S, Rothberg JM (2000) A comprehensive analysis of protein-protein interactions in Saccharomyces cerevisiae. *Nature* **403:** 623-627.

Urbanczik R, Wagner C (2005) Functional stoichiometric analysis of metabolic networks. *Bioinformatics* **21:** 4176-4180.

Vo TD, Greenberg HJ, Palsson BO (2004) Reconstruction and functional characterization of the human mitochondrial metabolic network based on proteomic and biochemical data. *J Biol Chem* **279:** 39532-39540.

Walhout AJ, Reboul J, Shtanko O, Bertin N, Vaglio P, Ge H, Lee H, Doucette-Stamm L, Gunsalus KC, Schetter AJ, Morton DG, Kemphues KJ, Reinke V, Kim SK, Piano F, Vidal M (2002) Integrating interactome, phenome, and transcriptome mapping data for the C. elegans germline. *Curr Biol* **12:** 1952-1958.

Warmke JW, Ganetzky B (1994) A family of potassium channel genes related to eag in Drosophila and mammals. *Proc Natl Acad Sci U S A* **91:** 3438-3442.

Watkins SM, German JB (2002) Metabolomics and biochemical profiling in drug discovery and development. *Curr Opin Mol Ther* **4:** 224-228.

White MY, Cordwell SJ, McCarron HC, Prasan AM, Craft G, Hambly BD, Jeremy RW (2005) Proteomics of ischemia/reperfusion injury in rabbit myocardium reveals alterations to proteins of essential functional systems. *Proteomics* **5:** 1395-1410.

Whitfield PD, German AJ, Noble PJ (2004) Metabolomics: an emerging post-genomic tool for nutrition. *Br J Nutr* **92:** 549-555.

Wingrove JA, O'Farrell PH (1999) Nitric oxide contributes to behavioral, cellular, and developmental responses to low oxygen in Drosophila. *Cell* **98:** 105-114.

Wolf MJ, Amrein H, Izatt JA, Choma MA, Reedy MC, Rockman HA (2006) Drosophila as a model for the identification of genes causing adult human heart disease. *Proc Natl Acad Sci U S A* **103:** 1394-1399.

Yellon DM, Downey JM (2003) Preconditioning the myocardium: from cellular physiology to clinical cardiology. *Physiol Rev* **83:** 1113-1151.

Chapter II –

Discovering Regulators of the *Drosophila* Cardiac Hypoxia Response Using Automated Phenotyping Technology

Abstract

Necrosis and apoptosis during acute myocardial infarction result in part from the inability of hypoxic cardiac myocytes to match ATP supply and demand. In contrast, hypoxia tolerant organisms such as Drosophila can rapidly regulate cellular metabolism to survive large oxygen fluctuations. A genetic screen of fly heart function during acute hypoxia can be an unbiased way to discover essential enzymes and novel signaling proteins involved in this response. We have developed a prototype to show proof of concept for a genome-scale screen, using computer automation to rapidly gather in-vivo hypoxic heart data in adult Drosophila. Our system automatically anesthetizes flies for mounting on a slide, and then locates the heart organ of each fly. The system then applies a hypoxia stimulus, acquires time-space (M-mode) images of the heart walls, and analyzes heart rate and rhythm. The assay can gather rapid, highly controlled measurements, and was able to detect phenotype differences in two known hypoxia-sensitive mutations used as positive controls – trehalose phosphate synthase, a metabolic enzyme, and guanylyl cyclase, a signaling enzyme in the nitric oxide pathway. We discuss the possible applications

of a genome-wide cardiac phenotype dataset in systems biology analyses of hypoxic metabolism, using genome-scale interaction networks and constraint-based metabolic models.

II.1 Introduction

The fruitfly is gaining interest as a model organism for heart research not only for the ease of its handling and short life cycle, as compared to vertebrate models, but also because its well known genome and the array of available genetic tools allows for a genomic and systems biology approach. In contrast with the mouse, which takes months to develop new genetic knockout strains, and with the zebrafish, which is a relatively new model organism, *Drosophila* has a genome that is both well-understood and easy to manipulate. With its sequence currently in its 4th revision (Adams et al., 2000), the fly has one of the best characterized genomes of multicellular organisms. Several publicly available libraries provide strains of single-gene disruptions via deletion, P-element insertion (Spradling et al., 1999), or transgenic RNA interference (Dietzl et al., 2007). In particular, transgenic RNAi libraries make it possible to use the binary GAL4/UAS expression system to cause tissue-specific gene inactivation any time during the fly's lifespan, providing the ability to measure the effects of gene perturbations that would cause lethality in early development or in other cell types.

Flies are a favorite for performing forward genetic screens, but so far there has not been a large-scale attempt to screen mutants for heart function. New technology for rapid *in-vivo* measurement of adult fly hearts would allow researchers to reverse screen the *Drosophila* genome for novel genetic influences on cardiovascular function. Several systems do exist for measuring rate and contraction

of the fly heart based on video microsocopy (Ocorr et al., 2007; Paternostro et al., 2001) or optical coherence tomography (Choma et al., 2006; Wolf et al., 2006). However, the current methods require many steps of labor-intensive manual preparation and data analysis. In order to fully capitalize on the advantages offered by using *Drosophila* as a model (size, fecundity, life cycle, genetic libraries), we have improved on these techniques by automating as many of the steps in the heart measurement process as possible. With computer automation, the fatigue and human error that comes with repeated measurements can be minimized, if not eliminated. Our prototype system can be used for a smaller-scale genetic screen and also serves as proof of the concept that a genome-wide screen would be feasible with parallel implementation and further engineering efforts.

II.2 Screening the cardiac hypoxia response

A genetic screen of heart function only has translational benefit under specific biological or environmental contexts such as adaptation to stress or disease states. We have chosen to focus on adaptation to acute hypoxia, but in theory our measurement system could be useful for screening the cardiac effects of drugs, chemicals, aging, environmental stimuli, or most other contexts of interest.

Hypoxia-reoxygenation injury is thought to be the primary cause of cell death in myocardial infarction (MI) (Opie, 1991). Currently the only treatment for acute MI is to restore blood flow as soon as possible, either by mechanical (angioplasty) or chemical (thrombolytic) means. No treatments are currently available for increasing the tolerance of cardiac tissue to hypoxic stress, though some potential lies in drugs

that trigger endogenous pathways for ischemic preconditioning (Budas et al., 2007; Yellon & Downey, 2003).

In animals, all cells have intrinsic metabolic and signaling mechanisms for adapting to acute hypoxia. In the ischemic mammalian heart, reduced oxidative metabolism causes a decrease in ATP, which stimulates anaerobic glycolysis, i.e. fermentation of glucose to lactate, through allosteric stimulation of key enzymes (Opie, 1991). Protein kinases also play a regulatory role in this anaerobic shift, stimulating the breakdown of glycogen into glucose and also regulating pyruvate dehydrogenase (PDH) to alter the flux through the citrate cycle (Opie, 1991).

Since oxygen fluctuations can manifest in countless ways over the life of a cell, it is likely that the genetic and metabolic core of the cellular hypoxia response evolves very early and is tightly conserved from flies to humans (O'Farrell, 2001). For example, hypoxia-inducible factor (HIF-1), AMP-activated protein kinase (AMPK), and nitric oxide (NO) are important mediators of the hypoxia response in both mammals (Hardie et al., 2003; Semenza, 2001) and flies (Lavista-Llanos et al., 2002; Pan & Hardie, 2002). However, the total cellular response is far-reaching and complex, causing an array of changes in metabolic, signaling, and transcriptional networks (Hochachka & Somero, 2002), and this system-wide orchestration of cellular hypoxia defenses is not well understood. A screen for hypoxia-sensitive responses during cardiac hypoxia would provide a starting point by gathering the list of genes involved.

II.3 Hypoxia tolerance in Drosophila

Fruitflies, like many invertebrates, are extremely tolerant to oxygen fluctuations, surviving total anoxia for 4-6 hours with full recovery (Haddad et al., 1997b). It is thought that this remarkable tolerance stems from the ability to achieve system-wide matching of metabolic supply and demand, especially ATP (Hochachka, 1980). The genetic basis for hypoxia tolerance in flies has begun to be explored: the *Drosophila* gene coding for the enzyme trehalose phosphate synthase increases hypoxia tolerance when overexpressed in flies (Chen et al., 2002) and when transfected into human cells (Chen et al., 2003), which lack the gene. The nitric oxide pathway, known to be important for hypoxia sensing and response in mammalian heart (Jones & Bolli, 2006; Schulz et al., 2004), was found to mediate cellular and behavioral responses to hypoxia in fly larvae (Wingrove & O'Farrell, 1999). A genetic screen for hypoxia tolerance (Haddad et al., 1997a) discovered that dADAR, an mRNA editor acting on ion channel transcripts (Ma et al., 2001), sensitizes the fly to hypoxia when mutated.

Although Drosophila flight muscle metabolism has been well studied, energy metabolism in the fly heart remains mostly unknown, partly due to the difficulty of accessing the small heart organ. In flight muscle, carbohydrates are the main source of fuel, and ATP is generated through aerobic glycolysis even during maximum exercise. Under anaerobic conditions, we found that flight muscle produces not only lactate (as in mammalian skeletal and cardiac muscle), but also comparably large amounts of alanine and acetate (Feala et al., 2007) (see Chapter III). It is not known whether the fly heart oxidizes fatty acids and lactate under normal conditions, as mammals do, and we also do not know whether the anaerobic fly heart produces all

three end products (lactate, alanine, and acetate) that flight muscle does. Measuring the heart phenotype for targeted perturbations of these enzymes will show which pathways of cardiac metabolism are essential for hypoxia tolerance.

As Drosophila becomes an established model organism for studying cardiac hypoxia, there is much to be learned about its metabolism under normal and anaerobic conditions. Targeted gene perturbations can be used with *in-vivo* measurement of heart function to test hypotheses for essential pathways and regulators of anaerobic metabolism. Beyond the enzymes and genes of central metabolism, a genome-scale screen of the cardiac hypoxia response in flies may be an unbiased way to uncover unique heart-specific hypoxia response genes that give flies their extraordinary tolerance.

We have characterized the acute hypoxia response under various conditions (temperature, age, oxygen levels) in adult *Drosophila*, both to demonstrate the ability of our new technology to rapidly gather and analyze fly heart data and also to understand limitations and optimize controllable parameters for a future genetic screen. Next we describe our automation technology and some characteristic results, and then discuss the possible applications of a 'genomic phenotype' dataset in a systems approach to studying hypoxic myocardium.

II.4 Automation Methods

II.4.1 Automated measurement overview

Customized software, written in the Python programming language was implemented to automate mounting flies on the slide, locating the moving hearts, and

measuring heart parameters. The automated measurement process consists of the following steps (Figure II.1A) :

- Anesthetize flies
- *Deposit on slide (optional)*
- Refine fly position (manual)
- Locate flies
- Detect heart
- Position M-mode line
- Capture time-space M-mode image
- Detect beats in M-modes

Upon insertion of the vials into the system, flies are automatically anesthetized with vaporized triethylamine and then manually mounted on microscope slides. A robotic stage then manipulates the slide following a series of image processing algorithms in order to locate and focus on the heart tube of each fly under the microscope. The computer then uses the video feed to construct a time-space (M-mode) representation of a line of pixels across the heart during baseline, optionally during a hypoxia stimulus, and then during recovery from hypoxia. A microscope-mounted incubator and a temperature controller (REX-C10, RKC Instrument Inc.) maintain the slide at a user-defined temperature during the duration of the experiment. The slide is removed and replaced, and the process is repeated. Software code and circuit diagrams can be found in Appendix A: Automated heart measurement technical details.

-

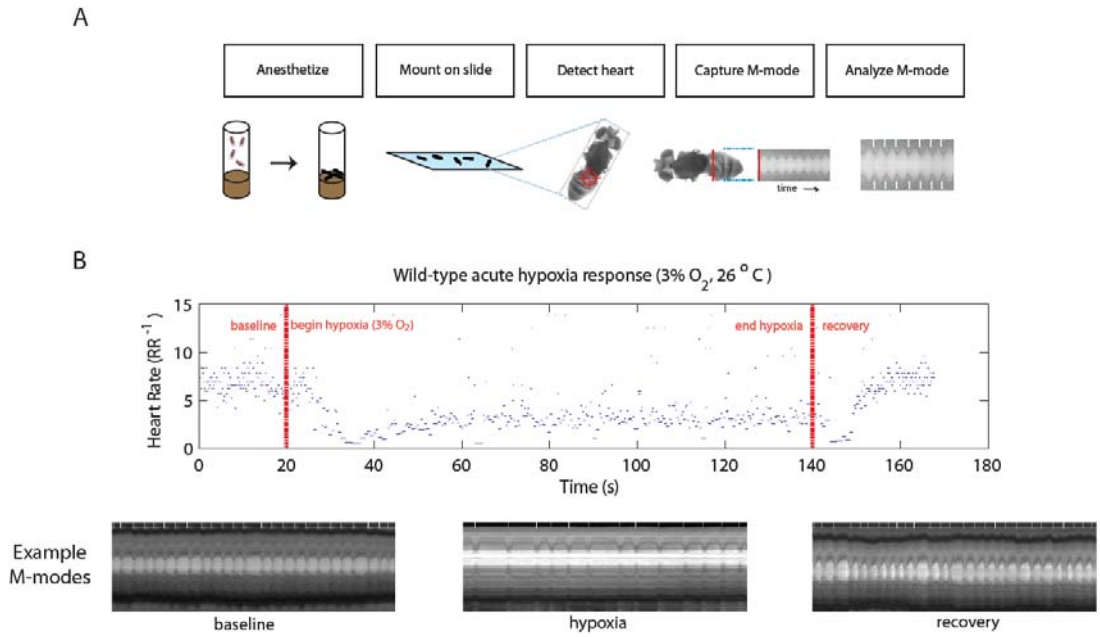

Figure II.1: Automation overview.

A) The computer-controlled system anesthetizes flies, deposits them on a microscope slide, and detects and focuses the heart for acquisition of a time-space M-mode image of wall contractions.

B) Typical M-mode images and heart rates for baseline, 120-second hypoxia stimulus, and recovery in the wild-type fly.

II.4.2 Anesthetize

Flies must be anesthetized and mounted on a microscope slide before imaging. This process is automated by computer-controlled activation of a number of electrically actuated pinch valves (#98302-06, Cole-Parmer Instrument Co.) within a network of tubes connected to anesthetic and a vacuum pump. Vacuum pressure is used to bubble liquid triethylamine anesthesia (FlyNap, Carolina Biological) and send the vapor into the sealed chamber containing the fly vial. The vacuum line is

opened and closed several times during anesthetization, alternately drawing FlyNap into the chamber and allowing time for the flies to absorb the vapors.

II.4.3 Mounting

Microscope images of the heart tube have the best quality when the flies are mounted on their backs with the wings spread out of the field of view. This precise positioning of flies is the most challenging step to automate; however, this step is greatly aided by using plastic slides, specifically polyvinyl chloride (PVC). The advantage of using plastic slides stems from the discovery that the wings of the fruit fly are strongly attracted to static electric charge.

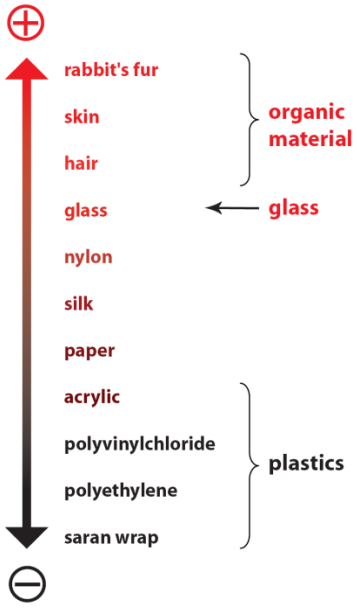

Figure II.2: The triboelectric series. Organic outer layers (hair, fur, skin) are repelled by glass and attracted to plastics. The attraction of plastic slides to the fly wings obviates the need for adhesives.

The triboelectric series compares the ability of materials to accept and retain static charges (Adams, 1987). Figure II.2 shows the position of some sample materials on the triboelectric spectrum. Organic outer materials such as hair, fur, and skin appear on the strongly positive end of the spectrum, while plastic materials tend to have a strong affinity for negative charge. Glass appears near the same end of the spectrum as organic materials, suggesting that plastic slides would perform better than standard glass slides at holding the wings. Polyvinylchloride (PVC) plastic microscope slides are available as an alternative to glass slides, and – as predicted by the triboelectric series – retain a negative charge that attracts the wings. Though the flies must be manually positioned on the slide using tweezers, this is made easier by the electrostatic attraction, and obviates the need for any adhesives such as double-sided tape or gels used previously.

Under long-term or severe hypoxia, flies undergo reflexive body movement (described in II.6 Discussion, and again in more detail in Appendix B: Characterization of the Drosophila heart to mild acute hypoxia). Therefore, these experiments necessitate an extra step to restrict movement. We developed a “sandwich” assembly consisting of the plastic slide, a thin strip of material with precise depth at the top and bottom edges of the slide, and an unfrosted glass slide laid on top. Divider strips are adhered to glass slides after flies are mounted normally on the plastic slides, then the entire assembly is set on an acrylic frame for stability and held together with custom aluminum clasps. To allow a pipeline of experiments to be run, many sets of frames, clasps, and divider strips were machined to fit standard plastic and glass slides (diagrams and specifications can be found in Appendix A).

From this point, the computer uses the mechanical stage and microscope video feed to automatically find the heart tubes and gather measurements.

II.4.4 Detection algorithms

Flies are located by systematically scanning the slide for dark areas. The stark contrast between the bright white of an empty field of view and the dark image of the fly allows the use of a simple threshold algorithm.

The measurement automation software is designed with multiple threads to speed the process of scanning the slide for flies. Rather than scanning point-by-point, the stage sweeps across the entire length of the slide, as the camera continuously gathers images in a separate processing thread. The resulting sequence of images is downsampled in order to minimize overlap, aligned at the edges, and reconstructed into an image of the entire slide, as in Figure II.3A. Pixels within the slide image are subjected to a grayscale threshold, and dark spots in the resulting binary image are clustered. The centroid of each cluster is calculated, mapped to stage coordinates, and saved as the location of the fly.

Once the fly has been detected, the next step is to find and focus on the heart organ. The center position of the fly and the direction of its orientation on the slide are valuable information for finding the heart, as well as drawing the perpendicular M-mode line. The program uses heuristic rules to move the stage along the outer edges of the fly (Figure II.3B), excluding the wings which are not seen at this light intensity and focus length. The orientation of the fly can be calculated from the coordinates of the fly outline using singular value decomposition (SVD). The orientation of the long axis of the fly is approximated by the first component vector of the SVD, and the M-mode line is drawn in the direction of the second vector, perpendicular to the heart tube. The centroid of these coordinates usually falls very close to the position of the heart. These values are saved for future use.

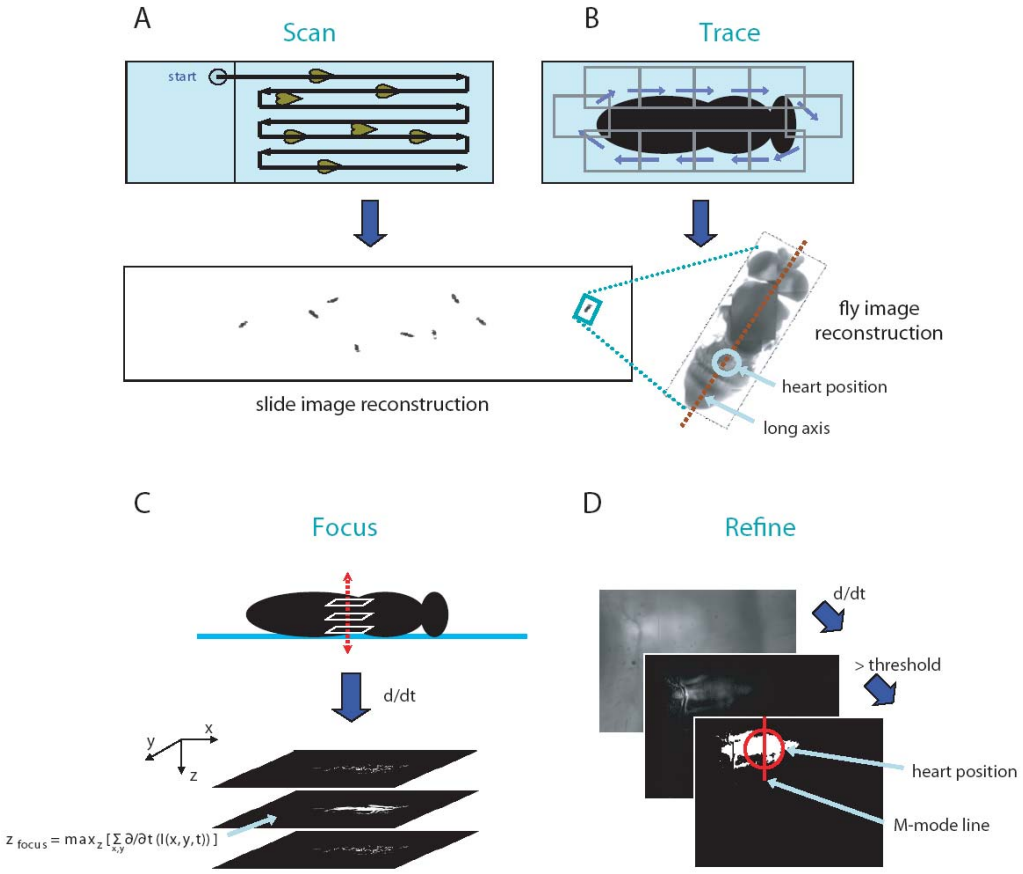

Figure II.3: Detection algorithms overview

- **A) Threaded software allows the stage to sweep the slide while the camera continuously captures frames, which are then reconstructed into a composite image of the slide.**
- **B) Heuristic rules direct the stage around the outer edges of each fly, then find the orientation and centroid.**
- **C) To autofocus, frames are captured as the z-axis is swept, similarly to (A), then motion is calculated at each position.**
- **D) The heart is centered under the M-mode lines by moving to the center of accumulated motion within the frame.**

Since the heart is generally the only moving part of the anesthetized fly, motion detection algorithms can be used to find and focus it with good accuracy. Calculating the accumulated frame-to-frame difference is a simple way to emphasize

the moving part of an image, and this technique is used repeatedly in the next steps for finding and focusing on the heart. A time-consecutive sequence of N frames F_0 to F_N is recorded and stored. A new image *M* is constructed that accumulates the absolute frame-to-frame variation for each pixel *j*, calculating differences in every third frame in order to capture more movement with less computation. Mathematically, this computation can be represented

$$M[j] = \sum_n |F_n[j]-F_{n-2}[j]| \qquad (1)$$

The resulting image is scaled to limit values to within the grayscale range of 0 to 255. This image then represents maximal variation for a single pixel as white and no variation as black.

A pre-processing step is applied before the program attempts to detect the position of the heart. Since the contrast between the dark fly image and the bright white of the empty slide is so large, the edge of the fly has the largest pixel gradient. This presents a problem in the above motion detection algorithm, since slight movements of the fly will result in a disproportionately large pixel variation along the edges. To combat this, the steps that follow are applied only to the part of the image close to the long axis of the fly, de-emphasizing the edges of the fly. This step is implemented by multiplying the accumulated motion image by a unit Gaussian curve oriented along the short axis and centered on the long axis of the fly (Figure II.4)

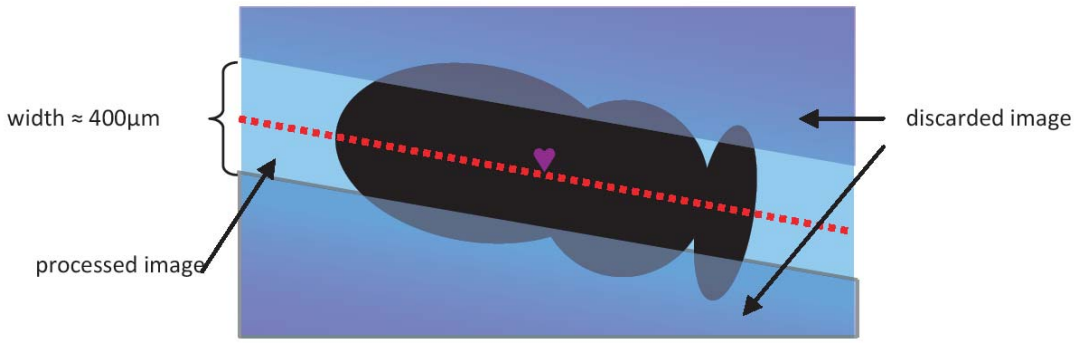

Figure II.4: Image processing is limited to a range near the center of the fly, along the long axis.

Although the heart tube is usually very near the centroid of the image, this position is fine-tuned by using the accumulated motion algorithm to detect movement in the frame containing the centroid, as well as in one frame in either direction along the long axis of the fly. Total movement is calculated by simply summing the *j* pixel values in the accumulated motion image *M*. The slide is moved to the frame with the greatest accumulated movement out of the three, which is usually the view containing the heart.

$$\text{Heart frame} = \text{argmax}_k(\sum_j M_k[j]) \qquad (2)$$

An autofocus algorithm searches for the focus length that captures the most heart movement, using the motion detection algorithm. As with the initial scanning of the slide in the x direction, a multi-threaded program enables the focus length *z* to be swept over a wide range as the camera continuously grabs frames. The focus length at which the frame has the most motion is saved as the focus length of the heart (Figure II.3C).

$$\text{Heart focus} = \text{argmax}_z(\sum_j M_z[j]) \qquad (3)$$

At this point the heart is somewhere within the microscope view, in focus, and the M-mode image is almost ready to be captured. The next challenge is to pinpoint the location of the heart within the frame. The M-mode line can then be drawn at this point, in the direction perpendicular to the long axis of the fly (calculated previously by SVD). To pinpoint the location of the heart, the program again generates the accumulated motion image *M* of the current view. The pulsatile heart is expected to be the region of this image with the greatest intensity. Using this expectation and the upper bound of the size of the heart tube, a variable threshold can be used to approximate the position of the heart within the frame. Thresholds are applied to the grayscale image at a series of pixel values, from 0 (black) to 255 (white), where 0 indicates zero change in that pixel over time. At each of these steps, a bounding box is drawn around all pixels above the threshold intensity. The area of the box naturally decreases with the increasing threshold, and the process is terminated when this area is smaller or equal to the expected size of the heart. The center of this bounding box is a consistently accurate estimate of the heart position. This concept is illustrated in Figure II.3D.

II.4.5 M-mode acquisition

Once the camera is centered on the heart, a virtual line is drawn in the center of the frame, perpendicular to the long axis of the fly. A time-space image, or M-mode, is created, which captures the variation of this line of pixels in time. Both the heart rate and variations in wall diameter can be derived from the M-mode image. Since the motion of the heart is represented as a 2-D image rather than a movie, thousands of M-modes can be saved with minimal disk space requirements. This

allows further analysis of the images to be done “offline,” after the flies have gone through the scanning process. Figure II.1B depicts M-mode images of the fly heart organ during baseline, hypoxia, and recovery from a short stimulus.

For each fly on the slide, the M-mode is recorded for 20 seconds of baseline, a user-controlled duration of hypoxia and recovery. The M-mode is broken into 2-second images and saved to disk, along with a snapshot of the heart frame and an image of the entire fly reconstructed from frames acquired during the tracing algorithm.

II.4.6 Parallelization

In addition to its utility in the slide scanning algorithm, the multi-threaded nature of the program also allows the user to anesthetize a new batch of flies as the current batch is being measured. This reduces bottlenecks in the measurement process and results in the automated detection and measurement becoming the rate-limiting process. Further opportunities for pipelining may be possible in the future because of the separate threads of operation.

II.4.7 Automated analysis

Heart rate and rhythm can easily be extracted from the M-mode representations using image processing algorithms. When dilated the heart tube is translucent and appears much brighter through the microscope than in the contracted state, therefore the average brightness of pixels in the M-mode line follows the contractions of the heart. The M-mode is reduced to a one-dimensional intensity signal by averaging the columns of the image. Full 2D M-modes are also saved for future application of heart wall detection algorithms.

Beat detection is more accurate than spectral analysis in analyzing the heart rate in hypoxic flies. As shown in the Results, the heart rate slows dramatically under severely hypoxic conditions, which often causes peaks in the spectrum to be masked by low-frequency noise. Also, the heart rhythm is variable during the hypoxic response, resulting in broad or scattered peaks that are difficult to detect and quantify. To overcome these problems, we adapted a beat detection algorithm to locate contractions within the intensity signal.

Rather than using the standard beat detection designed for electrocardiogram signals, we adapted an algorithm developed for detecting heartbeats from blood pressure waves (Aboy et al., 2005), which have slower upstrokes resembling the M-mode intensity signal. One-dimensional intensity signals are bandpass filtered (3^{rd} order Butterworth, fc = 1 Hz, 40 Hz) and the derivative is calculated by the 3-point central difference method. An exponentially decaying threshold is then applied to the derivative signal, with empirically derived high and low limits. Peaks in the original signal closest to suprathreshold peaks in the derivative are marked as beats, and then another filter discards beats occurring within the minimum cycle length from another beat. Appendix A contains the analysis code as well as an evaluation of the algorithm's accuracy.

II.4.8 User Interface

A graphical user interface (GUI) provides the user with full control and monitoring of the process. The GUI allows the user to view intermediate steps of the detection algorithms, and buttons for manual control of the stage allow corrections to be made if the heart is not detected or focused correctly. Clicking on the microscope window centers the M-mode line on the selected pixel, allowing small adjustments to

be made during detection and measurement. In addition to the current camera view, the GUI displays the last 2 seconds of M-mode acquisition so that the user can monitor the raw data, as well as oxygen concentration of the gas mixture.

A separate GUI, written in Matlab, allows fast inspection and analysis of large amounts of M-mode data. This interface allows the user to discard poor data from badly positioned flies, and (blinded to the identity of the fly stock) mark beats missed by the analysis algorithm. Also, we built in the capability for displaying the results of heart wall detection and manual marking of systolic and diastolic wall positions in the M-mode images. This leaves our platform open to future work designing image processing to automatically trace heart walls and calculate fractional shortening, a valuable addition to the analysis of heart rate and rhythm presented here.

II.5 Results

II.5.1 Speed and accuracy of heart measurements

Automation often involves a tradeoff between speed and accuracy. Our work adds automation to all steps of the measurement process, including anesthetization, mounting, detecting the heart, measurement, and analysis. The increased speed of experiments and decreased reliance on the experimenter results in lower yield, accuracy, and data quality, which we quantify in this section.

Figure II.5 (facing page): User interfaces

A) Measurement GUI. Most steps can be performed manually or automatically within the GUI.
B) The analysis GUI allows the user to evaluate image quality and results of the detection algorithm

A

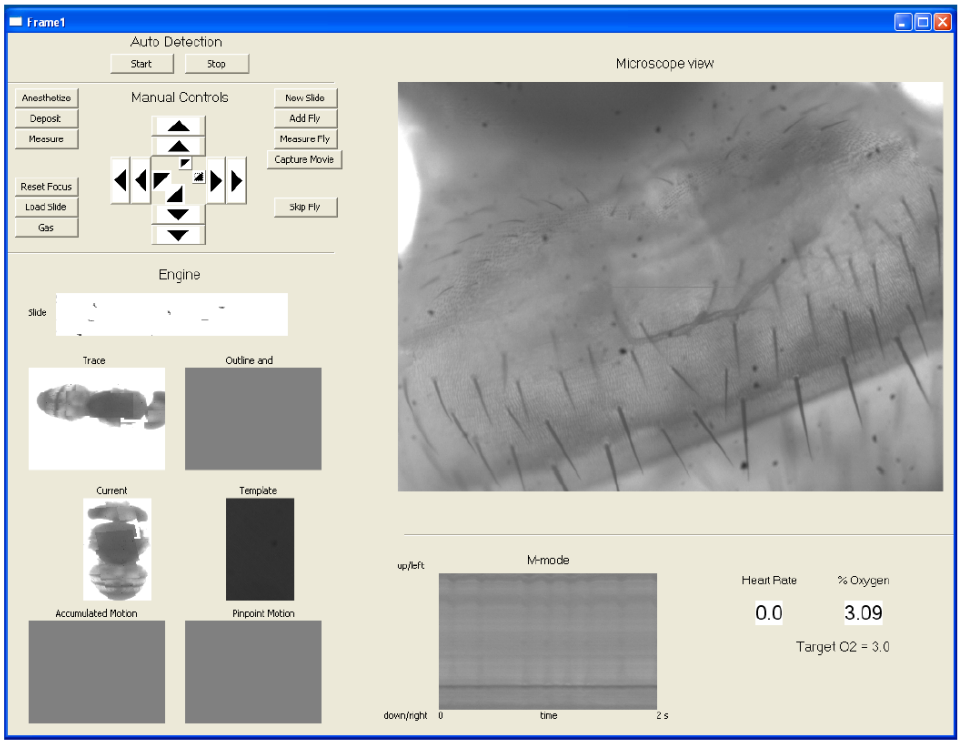
Frame1
Auto Detection
Start
Stop
Microscope view
Anesthetize
Deposit
Measure
Manual Controls
New Slide
Add Fly
Measure Fly
Capture Movie
Reset Focus
Load Slide
Gas
Skip Fly
Engine
Slide
Trace
Outline and
Current
Template
Accumulated Motion
Pinpoint Motion
M-mode
up/left
down/right
0
time
2 s
Heart Rate
% Oxygen
0.0
3.09
Target O2 = 3.0

B

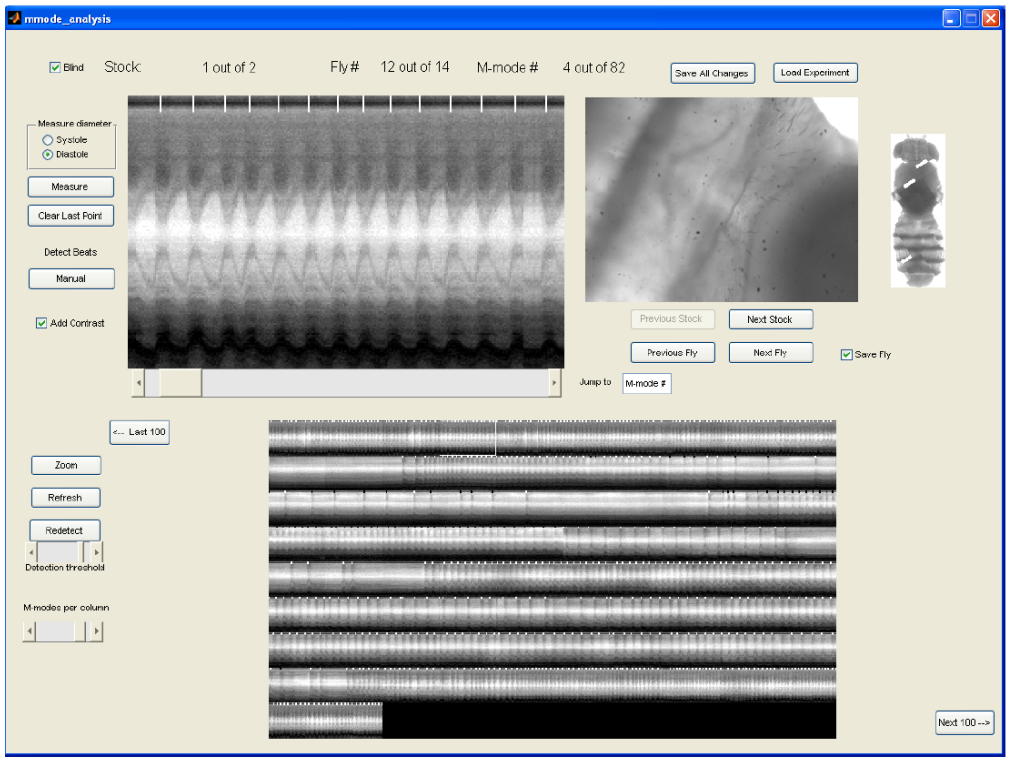
mmode_analysis
Blind
Stock:
1 out of 2
Fly #
12 out of 14
M-mode #
4 out of 82
Save All Changes
Load Experiment
Measure diameter
Systole
Diastole
Measure
Clear Last Point
Detect Beats
Manual
Add Contrast
Previous Stock
Next Stock
Previous Fly
Next Fly
Save Fly
Jump to
M-mode #
<-- Last 100
Zoom
Refresh
Redetect
Detection threshold
M-modes per column
Next 100 -->

The initial scanning of the slide takes a constant amount of time (155 seconds) independent of the number of flies in the batch. Detecting and focusing on the heart takes 28 seconds per fly, which amounts to a total detection time of 155+28*20 = 715 seconds for a batch of 20 flies per slide. Total measurement time for each slide (155 + 28*N + T*N) is dependent on both the number of flies N and the experimental duration T.

Performance of the analysis algorithm is crucial for post-processing of the large amounts of data produced by our system. The accuracy of the beat detection algorithm was tested against a truth table of 400 manually annotated 2-second M-modes from baseline, mild hypoxia, and recovery. A successful detection was counted when the algorithm's beat index came within 3 samples (sample rate = 125 Hz) of the manually marked beat. In these conditions, beat detection performed with 98% sensitivity and 94% specificity at the optimal threshold chosen from the ROC (receiver-operating characteristic) curve of the detection algorithm (see Appendix A).

When analysis algorithms were applied to images from severe hypoxia and recovery, poor image quality caused a large drop in beat detection accuracy. Errors were corrected in post-processing by manually marking beats using the analysis GUI, with the user blinded to the identity of the fly stocks. The necessity of additional manual post-processing in the severe hypoxia protocol limits the throughput, but Chapter VI lists potential ways to improve the detection algorithms in the future.

II.5.2 Characterization of the wild-type response to mild cardiac hypoxia

Our automation allows the highly controlled measurement of hypoxic heartbeats for 25 to 50 flies per hour, depending on the measurement duration. When nitrogen-oxygen mixtures of less than about 10% O2 are passed over the fly,

the heart rate instantly declines, then partially recovers and maintains a reduced rate. Restoration of atmospheric oxygen causes transient slowing, then a recovery to baseline. Figure II.1B shows example M-modes and heart rate for a single measurement.

To demonstrate the rapid acquisition of heart measurements, we used our automation technology to characterize the effect of acute hypoxia on heart rate (HR) and regularity of rhythm in the Oregon-R wild-type fly for different oxygen percentages, temperatures, ages, sex, and wild-type strains. See Appendix B for an extensive characterization of the mild hypoxia response.

II.5.3 Positive controls: oxygen-sensitive mutations

The literature describes some known hypoxia-sensitive *Drosophila* genes (Chen et al., 2002; Ma et al., 2001; Wingrove & O'Farrell, 1999) linked to a variety of biological functions. We tested mutants of three of these genes as positive controls for detecting hypoxia sensitivity with our system: *dADAR*, *tps1* and *for*, with respective roles in sugar metabolism, nitric oxide signaling, and mRNA editing. All three P-element strains were measured using the mild hypoxia protocol (3% for 2 minutes), and *dADAR* and *for* were measured under severe hypoxia (recovery from 4 hours at 0.5% O_2).

Under mild hypoxia only the *tps1* mutant showed small changes in heart rate from wild type. While this difference was statistically significant by one-way ANOVA, the reduction in heart rate was less than 1 beat per second (Figure II.6). This level of hypoxic stress was not sufficient to induce phenotypic differences for the other two mutants.

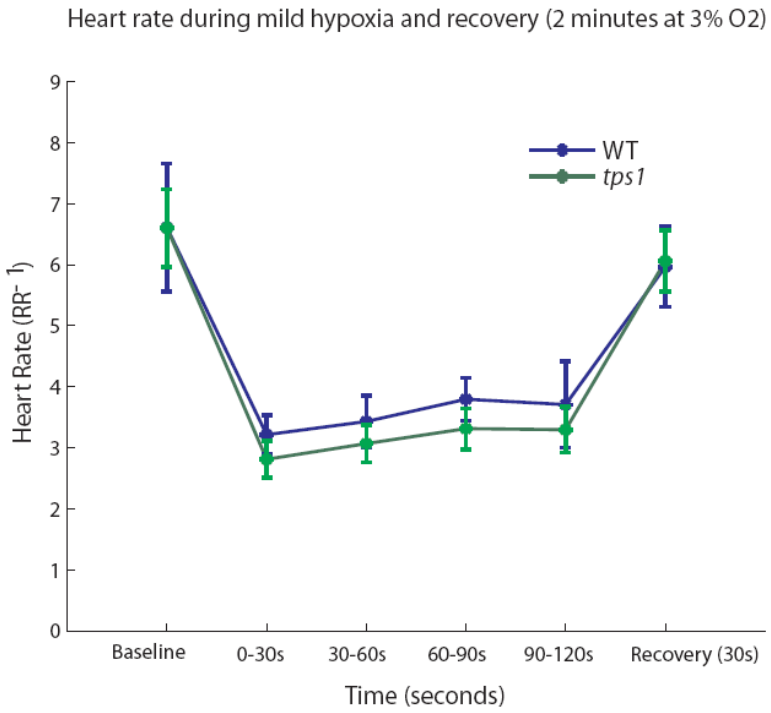

Figure II.6: Mutation of the *tps1* gene, trehalose phosphate synthase, had a slight but significant slowing of heart rate during mild hypoxia stimulus. Heart rate is calculated as the inverse of binned beat-to-beat (RR) intervals.

Our severe hypoxia protocol (recovery from 4 hours at 0.5%) showed a degraded hypoxia response in P-element mutations of the *for* locus (Figure II.7). This locus contains the *dg2* gene for guanylyl cyclase, which catalyzes the formation of cGMP, a second messenger in the hypoxia-responsive nitric oxide signaling pathway. Wingrove and O'Farrell (1999) demonstrated that allelic differences in this gene change the nitric-oxide mediated behavioral response to hypoxia, and our results suggest that the influence of this pathway extends the adult heart organ. In the mammalian heart nitric oxide has recently been identified as a fundamentally important cardioprotective agent, mediating cellular defenses against ischemia and reperfusion (Jones & Bolli, 2006).

Although the *dADAR* mutant was discovered for its delayed whole body recovery following 4 hours of anoxia (Haddad et al., 1997b), the *dADAR* heart did not respond differently from wild type after 4 hours at 0.5% oxygen. This may be due to the small difference in oxygen but more likely is due to the fact that the mRNA editor acts primarily on mRNA of sodium channels, which are not present in the fly pacemaker (Johnson et al., 1998). When testing the severe hypoxia protocol, the *tps1* stock had contamination problems and was not measured.

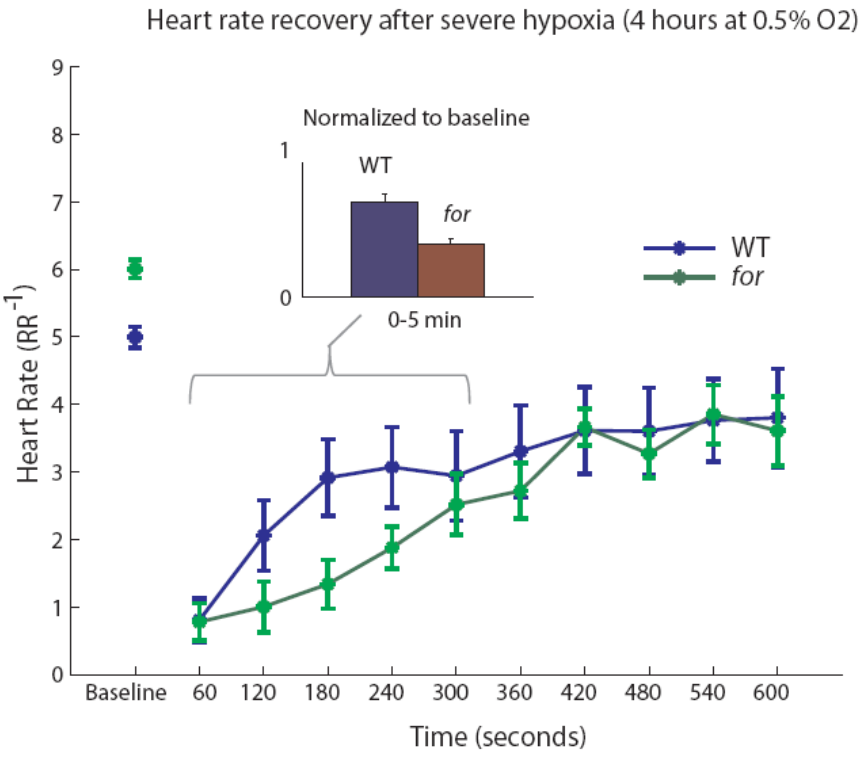

Figure II.7: Mutation of the *for* gene, important for nitric oxide signaling, showed delayed recovery from severe hypoxia.

II.6 Discussion

We have developed automation for rapid *in-vivo* measurement and analysis of heart phenotypes in adult *Drosophila*, and demonstrated the proof of concept by characterizing the wild-type hypoxia response for a wide range of parameters. One major limitation that we discovered was that at oxygen levels below 3% (which we refer to as “mild hypoxia”), measurements became difficult due to reflexive movement of the body and wings. To overcome this problem, we developed an additional “severe hypoxia” protocol, which physically restricts fly movement and measures only the recovery after 4 hours of 0.5% oxygen. Although both protocols were able to induce an altered cardiac phenotype in a hypoxia-sensitive mutant, the effect was much more pronounced for severe hypoxia. Beat detection algorithms performed accurately for M-mode images of mild hypoxia, but had to be supplemented by manual inspection for severe hypoxia data.

II.6.1 Designing a large-scale genetic screen

The goal of large-scale directed screening affects all aspects of the assay, including fly culturing, experimental setup and data analysis. The ideal measurement is fast, scalable and well-controlled not only for the measurements themselves but across all of these aspects.

As mentioned above, severe hypoxia was able to bring about greater phenotypic differences in a genetic mutation than mild hypoxia. This protocol limits the throughput, however, adding a 4-hour delay to apply the hypoxia stimulus and additional time to analyze the poor quality M-mode images. Also, a measurement pipeline requires separate components to induce hypoxia while other groups are

being measured for baseline and recovery. In the future it is feasible to improve the analysis algorithms and add a hypoxia chamber to the system, so this version of the assay is most suitable for a screen.

The genetic background of the flies must also be taken into account in designing a screen, since background strain had a surprising effect on the heart even in mild hypoxia. The *yw* strain had an irregular heartbeat as compared to Oregon-R flies (Appendix B). Heart phenotypes of all F1 crosses performed better than inbred stocks, reflecting global genetic improvement from outcrossing that could mask the effect of individual mutations. These results imply that careful attention must be paid to the genetic background when performing a screen. In the Bloomington Stock Collection, the P-element insertions have been generated in a variety of wild-type backgrounds such as *yw*, ry^{506}, *y*, and *w*. Mutant strains must therefore be out-crossed to isolate the effects of the gene of interest from the detrimental effects of inbreeding, but this adds a minimum of 10 days to the breeding cycle and doubles the labor of rearing the flies.

The most promising solution for the problem of noisy genetic backgrounds is the possibility of screening transgenic RNAi libraries. These recently developed resources offer both an isogenetic background and the opportunity for tissue- and temporal specificity when used with the GAL4/UAS system. Though it would still require a cross to be performed for each stock, this might be the most reliable method. Chapter VI discusses this option in further detail.

II.6.2 Incorporating a phenotype screen into a systems approach

Although gathering heart data from 2,500 mutant *Drosophila* strains would no doubt uncover a handful of novel and interesting genes, the fraction of the genome

covered by a screen of that size would be small. Flies have approximately 14,000 identified genes, so even at full-time operation the proposed screen would cover less than one-fifth of the genome per year. Until the methods can be improved further or implemented in parallel, it may be worthwhile to consider strategies for a targeted screen rather than randomly sampling the genome. We previously presented a network-based strategy for ranking genes more likely to affect lifespan (Ferrarini et al., 2005).

Similarly, it may be possible to build a ranked list of candidate hypoxia-responsive genes based on genome-wide networks. Since the primary effects of oxygen deprivation are metabolic (decreased ATP production, shift in redox potential, pH and ion imbalance), a list of candidates could be generated using our constraint-based network model of hypoxic metabolic regulation described in later chapters.

II.6.3 Constraint-based metabolic modeling

A goal of systems biology research is to invent new techniques for integrating different types of high-throughput data into functional network models which can be simulated to generate testable hypotheses. The constraint-based method is currently the most popular and successful method for modeling genome-wide metabolic networks (Price et al., 2004), although most *in-silico* metabolic reconstructions on which constraint-based techniques can be applied have focused on single-cell microbes. However, reconstructions have been performed for the red blood cell (Jamshidi et al., 2001), mouse cardiomyocyte (Sheikh et al., 2005), and more recently a multicellular human metabolic network was completed (Duarte et al., 2007). In Chapters III through V we expand and validate our model of central ATP-generating metabolism in *Drosophila* muscle cells using microarrays and metabolomic data.

These genome-wide reconstructions are usually curated manually, starting from a high-throughput dataset such as the annotated genome and/or proteomics data for the cell type of interest and referring to the literature to confirm putative reactions and enzymes. This method ensures that models start with a complete "parts list" for the system, a cornerstone of the systems biology paradigm (Ideker et al., 2001). Iterations of high-throughput experimentation and computer simulation are then used to generate and test predictions to progressively increase the accuracy of the model. A genome-wide phenotype screen is a very useful dataset for earlier stages of refinement, since the loss of function of particular enzyme gene disruptions identifies the essential reactions to be included in the model. The goal is to create a metabolic model that contains all reactions important to hypoxia tolerance in the fly heart, and a genetic screen of cardiac hypoxia will let us identify reactions that manifest at the phenotype level (the "top down" view), which molecular data and modeling can help explain mechanistically (from the "bottom up").

The quantitative nature of our screening method fits well with systems models. Flux-balance simulations of metabolism provide steady-state flux values for all enzymes in the system when optimizing for some objective such as ATP production (Kauffman et al., 2003; Palsson, 2006; Stephanopoulos, 1999). These intra-system flux values allow the model to be directly validated against fluxomics data derived from metabolomics methods, such as mass spectrometry and NMR spectroscopy (as we have done with the *Drosophila* model (Feala et al., 2007)). Although some assumptions must be made, it is also possible to compare quantitative phenotype values to the ability of the model to meet its objectives. For example, the hypoxic heart rate for a certain mutation can be compared against simulated metabolic fluxes, as we will show for measurements and simulations of a lactate dehydrogenase

deletion in Chapter III. When performed with a large number of genes in the future, these comparisons may provide a coarse-grained quantitative view of system operation that goes beyond the “all-or-none” results of a qualitative screen.

II.7 Summary

Our system for rapid measurement of cardiac hypoxia phenotypes has the potential to measure hundreds of fly stocks per year, which is of the order of magnitude required for a genome-wide screen. Though valuable on its own, such a screen also has the potential to be integrated into systems analyses, for example with computer simulations of metabolism or in protein interaction networks, as a complementary “top-down” dataset. The complexity and scope of the myocardial response to acute hypoxia suggests the benefit of studying this system at the genome scale. A reverse genetic screen of cardiac hypoxia phenotypes is the first step toward identifying and quantifying all of the important components involved.

Acknowledgements

Chapter 2, in part, is adapted from an article that originally appeared in the Annals of the New York Academy of the Sciences, volume 1123, pages 169-177, published March, 2008. The dissertation author was the primary investigator and author of this paper, which was co-authored by Drs. Jeffrey H. Omens, Giovanni Paternostro, and Andrew D. McCulloch.

References

Aboy M, McNames J, Thong T, Tsunami D, Ellenby MS, Goldstein B (2005) An automatic beat detection algorithm for pressure signals. *IEEE Trans Biomed Eng* **52:** 1662-1670.

Adams CK (1987) *Nature's electricity*. Tab Books, Blue Ridge Summit, PA.

Adams MD, Celniker SE, Holt RA, Evans CA, Gocayne JD, Amanatides PG, Scherer SE, Li PW, Hoskins RA, Galle RF, George RA, Lewis SE, Richards S, Ashburner M, Henderson SN, Sutton GG, Wortman JR, Yandell MD, Zhang Q, Chen LX, et al. (2000) The genome sequence of Drosophila melanogaster. *Science* **287:** 2185-2195.

Budas GR, Churchill EN, Mochly-Rosen D (2007) Cardioprotective mechanisms of PKC isozyme-selective activators and inhibitors in the treatment of ischemia-reperfusion injury. *Pharmacol Res*.

Chen Q, Behar KL, Xu T, Fan C, Haddad GG (2003) Expression of Drosophila trehalose-phosphate synthase in HEK-293 cells increases hypoxia tolerance. *J Biol Chem* **278:** 49113-49118.

Chen Q, Ma E, Behar KL, Xu T, Haddad GG (2002) Role of trehalose phosphate synthase in anoxia tolerance and development in Drosophila melanogaster. *J Biol Chem* **277:** 3274-3279.

Choma MA, Izatt SD, Wessells RJ, Bodmer R, Izatt JA (2006) Images in cardiovascular medicine: in vivo imaging of the adult Drosophila melanogaster heart with real-time optical coherence tomography. *Circulation* **114:** e35-36.

Dietzl G, Chen D, Schnorrer F, Su KC, Barinova Y, Fellner M, Gasser B, Kinsey K, Oppel S, Scheiblauer S, Couto A, Marra V, Keleman K, Dickson BJ (2007) A genome-wide transgenic RNAi library for conditional gene inactivation in Drosophila. *Nature* **448:** 151-156.

Duarte NC, Becker SA, Jamshidi N, Thiele I, Mo ML, Vo TD, Srivas R, Palsson BO (2007) Global reconstruction of the human metabolic network based on genomic and bibliomic data. *Proc Natl Acad Sci U S A* **104:** 1777-1782.

Feala J, Coquin L, McCulloch A, Paternostro G (2007) Flexibility in energy metabolism supports hypoxia tolerance in Drosophila flight muscle: metabolomic and computational systems analysis. *Mol Syst Biol - accepted*.

Ferrarini L, Bertelli L, Feala J, McCulloch AD, Paternostro G (2005) A more efficient search strategy for aging genes based on connectivity. *Bioinformatics* **21:** 338-348.

Haddad GG, Sun Y, Wyman RJ, Xu T (1997a) Genetic basis of tolerance to O2 deprivation in Drosophila melanogaster. *Proc Natl Acad Sci U S A* **94:** 10809-10812.

Haddad GG, Wyman RJ, Mohsenin A, Sun Y, Krishnan SN (1997b) Behavioral and Electrophysiologic Responses of Drosophila melanogaster to Prolonged Periods of Anoxia. *J Insect Physiol* **43:** 203-210.

Hardie DG, Scott JW, Pan DA, Hudson ER (2003) Management of cellular energy by the AMP-activated protein kinase system. *FEBS Lett* **546:** 113-120.

Hochachka PW (1980) *Living without oxygen : closed and open systems in hypoxia tolerance*. Harvard Univ. Press, Cambridge.

Hochachka PW, Somero GN (2002) *Biochemical adaptation : mechanism and process in physiological evolution*. Oxford University Press, New York.

Ideker T, Galitski T, Hood L (2001) A new approach to decoding life: systems biology. *Annu Rev Genomics Hum Genet* **2:** 343-372.

Jamshidi N, Edwards JS, Fahland T, Church GM, Palsson BO (2001) Dynamic simulation of the human red blood cell metabolic network. *Bioinformatics* **17:** 286-287.

Johnson E, Ringo J, Bray N, Dowse H (1998) Genetic and pharmacological identification of ion channels central to the Drosophila cardiac pacemaker. *J Neurogenet* **12:** 1-24.

Jones SP, Bolli R (2006) The ubiquitous role of nitric oxide in cardioprotection. *J Mol Cell Cardiol* **40:** 16-23.

Kauffman KJ, Prakash P, Edwards JS (2003) Advances in flux balance analysis. *Curr Opin Biotechnol* **14:** 491-496.

Lavista-Llanos S, Centanin L, Irisarri M, Russo DM, Gleadle JM, Bocca SN, Muzzopappa M, Ratcliffe PJ, Wappner P (2002) Control of the hypoxic response in Drosophila melanogaster by the basic helix-loop-helix PAS protein similar. *Mol Cell Biol* **22:** 6842-6853.

Ma E, Gu XQ, Wu X, Xu T, Haddad GG (2001) Mutation in pre-mRNA adenosine deaminase markedly attenuates neuronal tolerance to O2 deprivation in Drosophila melanogaster. *J Clin Invest* **107:** 685-693.

O'Farrell PH (2001) Conserved responses to oxygen deprivation. *J Clin Invest* **107:** 671-674.

Ocorr K, Reeves NL, Wessells RJ, Fink M, Chen HS, Akasaka T, Yasuda S, Metzger JM, Giles W, Posakony JW, Bodmer R (2007) KCNQ potassium channel mutations cause cardiac arrhythmias in Drosophila that mimic the effects of aging. *Proc Natl Acad Sci U S A* **104:** 3943-3948.

Opie LH (1991) *The heart : physiology and metabolism*. Raven Press, New York.

Palsson B (2006) *Systems biology : properties of reconstructed networks*. Cambridge University Press, Cambridge ; New York.

Pan DA, Hardie DG (2002) A homologue of AMP-activated protein kinase in Drosophila melanogaster is sensitive to AMP and is activated by ATP depletion. *Biochem J* **367:** 179-186.

Paternostro G, Vignola C, Bartsch DU, Omens JH, McCulloch AD, Reed JC (2001) Age-associated cardiac dysfunction in Drosophila melanogaster. *Circ Res* **88:** 1053-1058.

Price ND, Reed JL, Palsson BO (2004) Genome-scale models of microbial cells: evaluating the consequences of constraints. *Nat Rev Microbiol* **2:** 886-897.

Schulz R, Kelm M, Heusch G (2004) Nitric oxide in myocardial ischemia/reperfusion injury. *Cardiovasc Res* **61:** 402-413.

Semenza GL (2001) Hypoxia-inducible factor 1: oxygen homeostasis and disease pathophysiology. *Trends Mol Med* **7:** 345-350.

Sheikh K, Forster J, Nielsen LK (2005) Modeling hybridoma cell metabolism using a generic genome-scale metabolic model of Mus musculus. *Biotechnol Prog* **21:** 112-121.

Spradling AC, Stern D, Beaton A, Rhem EJ, Laverty T, Mozden N, Misra S, Rubin GM (1999) The Berkeley Drosophila Genome Project gene disruption project: Single P-element insertions mutating 25% of vital Drosophila genes. *Genetics* **153:** 135-177.

Stephanopoulos G (1999) Metabolic fluxes and metabolic engineering. *Metab Eng* **1:** 1-11.

Wingrove JA, O'Farrell PH (1999) Nitric oxide contributes to behavioral, cellular, and developmental responses to low oxygen in Drosophila. *Cell* **98:** 105-114.

Wolf MJ, Amrein H, Izatt JA, Choma MA, Reedy MC, Rockman HA (2006) Drosophila as a model for the identification of genes causing adult human heart disease. *Proc Natl Acad Sci U S A* **103:** 1394-1399.

Yellon DM, Downey JM (2003) Preconditioning the myocardium: from cellular physiology to clinical cardiology. *Physiol Rev* **83:** 1113-1151.

Chapter III –

Flexibility in energy metabolism supports hypoxia tolerance in *Drosophila* flight muscle: metabolomic and computational systems analysis

Abstract

The fruit fly *Drosophila melanogaster* offers promise as a genetically tractable model for studying adaptation to hypoxia at the cellular level, but the metabolic basis for extreme hypoxia tolerance in flies is not well known. Using ^{1}H NMR spectroscopy, metabolomic profiles were collected under hypoxia. Accumulation of lactate, alanine, and acetate suggested that these are the major end products of anaerobic metabolism in the fly. A constraint-based model of ATP-producing pathways was built using the annotated genome, existing models, and the literature. Multiple redundant pathways for producing acetate and alanine were added and simulations were run in order to find a single optimal strategy for producing each end product. System-wide adaptation to hypoxia was then investigated *in-silico* using the refined model. Simulations supported the hypothesis that the ability to flexibly convert pyruvate to these three byproducts might convey hypoxia tolerance by improving the ATP/H^{+} ratio and the efficiency of glucose utilization.

III.1 Introduction

Understanding cellular adaptation to hypoxia is central to the design of treatments for injury caused by ischemia-reperfusion, stroke, and myocardial infarction. Cell damage during acute hypoxia is thought to be caused by imbalances such as decreased pH, altered calcium homeostasis, increased intracellular osmotic pressure, and mitochondrial damage, resulting directly and indirectly from decreased ATP (Corbucci et al., 2005; Hochachka & Somero, 2002). Humans have complex physiological systems for regulating oxygen homeostasis that involve multiple spatial scales and cell types and have been delicately tuned during evolution. However, at the cellular level, hypoxia resistance mechanisms most likely evolved very early and appear to be highly conserved among species (O'Farrell, 2001).

Lending support to this hypothesis, several genes have been discovered in the fruit fly *Drosophila melanogaster* that are similar in sequence and function to human genes for regulation of metabolism, signaling, and transcription during hypoxia (Lavista-Llanos et al., 2002; Pan & Hardie, 2002; Piacentini & Karliner, 1999; Wingrove & O'Farrell, 1999). Although hypoxia defenses in flies and humans seem to be quite similar at the level of individual genes, stark contrasts exist at the phenotype level. *Drosophila* have a remarkable tolerance to hypoxia that is the subject of an increasing amount of investigation (Haddad, 2006; O'Farrell, 2001). In contrast with humans, who can only survive a few minutes without oxygen, flies can fully recover from up to 4 hours in complete anoxia (Haddad et al., 1997). Differences in anaerobic generation of ATP are likely to be part of the reason for the disparity in hypoxia tolerance between humans and flies; however, *Drosophila* anaerobic metabolism is not well known.

Aerobic energy metabolism in insect flight muscle is similar to that of humans in most respects; however, there are some major differences that distinguish the species, such as the use of proline as an energy source, heavy reliance on the α-glycerol-3-phosphate shuttle, and the use of arginine as an alternative to creatine for ATP buffering (Gilmour, 1961). Anaerobic energy pathways in *Drosophila* are likely to deviate from those of humans as well. In human muscle, glycolysis is the major anaerobic energy pathway and lactate is the only end product of anaerobic metabolism (Nelson, 2000; Wadley et al., 2006). Many terrestrial insects yield lactate and alanine as anaerobic end products, but other species have been known to produce a wide array of other products during hypoxia including sorbitol, succinate, glycerol, α-glycerol-3-phosphate, pyruvic acid, and fatty acids (Hoback & Stanley, 2001). The specific end products for *Drosophila* are not known, however, the wide diversity of insect biochemistry suggests that exotic pathways for anaerobic energy production may also exist in flies (Gilmour, 1961; Hoback & Stanley, 2001).

Regardless of the pathways used, anaerobic metabolism must be regulated over the long term to balance pH, ATP production, redox potential (most importantly $NADH/NAD^+$), and coupling metabolites. Although strategies for maintaining these balances are known for many organisms (Hochachka, 1980), quantitative systems models can increase mechanistic understanding. A major advantage of a mathematical model is that conservation of mass is enforced; therefore all elements and charges are balanced within the system, including electron transport, cofactor concentration, and protons (pH). The constraint-based method uncovers the space of all possible steady-state solutions under a set of physiochemical limitations imposed on the system (Palsson, 2004). These network models are useful both for

performing detailed *in-silico* experiments and for discovering more general systems level properties (Almaas et al., 2004; Reed & Palsson, 2004).

To determine whether flies do use alternative hypoxic pathways, we applied NMR metabolomic analysis to flight muscle to discover end products for anaerobic energy metabolism. We then added all pathways that might produce these compounds, linked them to existing *Drosophila* genes, and built them into a constraint-based model of fly energy metabolism. Simulations were used to select specific anaerobic pathways from a number of alternatives by optimizing for ATP production. Metabolite fluxes measured by NMR were integrated into the model and simulations were conducted to investigate production of ATP, H^+, and glucose during hypoxia. Simulations were compared with those of classical anaerobic energy pathways in mammals to generate hypotheses for mechanisms of hypoxia tolerance in flies.

III.2 Materials and Methods

III.2.1 Fly preparation

Oregon-R wild-type flies were reared in constant darkness at 25° C. At 3-5 days old, flies were brought into the light approximately 4 hours before experiment.

III.2.2 Hypoxia experiments

The hypoxia experiments included five samples each of 5 conditions: control, 10 minutes hypoxia, 1 hour hypoxia, 4 hours hypoxia, and 4 hours control. Since the vials used for experiment did not contain food, the 4-hour control was included to offset the effects of starvation and dehydration over the same time period. Holes

were drilled the screw caps of Sarstedt 15 mL vials, and rubber tubing was inserted into each cap and sealed airtight with silicone adhesive. At the time of experiment, filter paper was soaked in distilled water and placed in each vial to prevent drying. Approximately 50 flies were transferred and the caps were screwed loosely onto each vial to allow gas to flow out. A mixture of nitrogen and 0.5% oxygen was then bubbled through distilled water and passed through the tubing into the vials. After 5 minutes of application of hypoxia, the caps were sealed airtight, the gas pressure was cut off at the source, and tubing clamps were used to seal the rubber tube, in that order. Control flies were sealed in vials with wet filter paper, but without the application of gas. Vials were lightly shaken to increase spacing among immobile flies and stored on their side at 25º C. At the end of each time point, vials were snap frozen in liquid nitrogen and frozen flies were transferred for storage at -80° C.

Females were separated from males on dry ice under a dissecting microscope, then, using forceps and miniature spring scissors (Fine Science Tools, Inc., 15003-08), 20 thoraces were separated from head and abdomen and placed into Eppendorf vials in liquid nitrogen. Thoraces were homogenized in an ice bath for 10 minutes in 300 µL of cold 1:1 acetonitrile:water buffer, homogenates were centrifuged in a cold room (4º C) for 10 minutes at 13,000 RPM, and the supernatant was ultracentrifugated for 30 minutes at 8,500 RPM using Nanosep centrifugal devices (Pall Life Sciences, Ann Arbor, MI) with a 3 kDa molecular weight cutoff. To reduce the contamination of glycerol, a membrane preservative, to below 80 µM, all Nanosep devices were washed 4 times (by 5 minutes centrifugation at 13,000 RPM) with 500 µL deionized water. Filtrate was lyophilized using a vacuum centrifuge for 2 hours at 45° C. Dried samples were then dissolved in 500 µL D_2O buffered at pH 7.4 with monobasic/dibasic sodium phosphate. The NMR standard TSP (3-trimethylsilyl-$^2H_4$-

propionic acid) was added to the samples at a ratio of 1:100 by volume, resulting in a concentration of 0.488 mM. Samples were stored at 4° C until measured.

III.2.3 NMR spectroscopy and data analysis

Analyses of samples were carried out by ^{1}H NMR spectroscopy on a Bruker Avance 500 operating at 500.13 MHz ^{1}H resonance frequency. The NMR probe used was the 5 mm TXI ^{1}H/^{2}H-^{13}C/^{15}N Z GRD. All NMR spectra were recorded at 30° C. Typically ^{1}H were measured with 512 scans into 32768 data points, resulting in an acquisition time of 1.36 seconds. A relaxation delay of 2 seconds additionally ensured T1 relaxation between successive scans. Solvent suppression was achieved via the Noesypresat pulse sequence (Bruker Spectrospin Ltd.) in which the residual water peak is irradiated during the relaxation and mixing time of 80 μs. All ^{1}H spectra were manually corrected for phase and baseline distortions within XWINNMR^{TM} (version 2.6, Bruker Spectrospin, Ltd.). Two-dimensional NMR methods including homonuclear correlation spectroscopy (TOCSY) and heteronuclear single quantum correlation spectroscopy (HSQC) were carried out in order to identify and subsequently confirm the assessment of metabolites.

Peaks in the 1D spectra were identified, aligned, and quantified by “targeted profiling” algorithms (Weljie et al., 2006) within the software Chenomix NMR Suite 4.5 (Chenomix, Inc.). The list of metabolites discovered in the 2D spectra was used to guide quantification in one dimension. Metabolite concentrations were imported into Matlab (Mathworks, Cambridge, MA) and Excel (Microsoft, Redmond, CA) for plotting and curve fitting.

III.2.4 Global metabolite profiles under hypoxia

Metabolite concentrations were measured at 10 minutes, 1 hour, and 4 hours to study the time course of adaptation and breakdown of the metabolic network under hypoxic stress. A comparison of Figure III.1 with a previous study of hypoxic isolated mouse cells (Troy, 2005) reveals obvious differences between insect and mammalian metabolic makeup and response to hypoxia. Changes in lactate, alanine, and acetate peaks can be seen clearly (boxed in red), compared with the relative stability of the size and shape of the background spectra. Water suppression techniques were successful for 22 of the 25 spectra, and in the remaining three the water signal masked some peak clusters of trehalose and glucose.

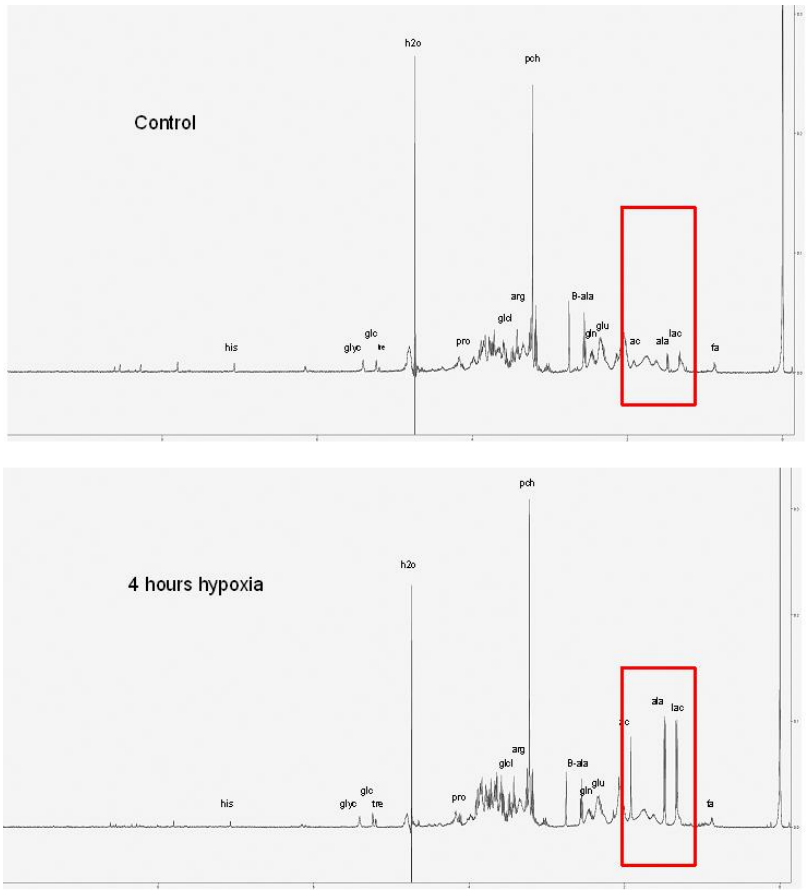

Figure III.1: Representative NMR spectra with emphasis on accumulating end products.

The spectra of some metabolites overlap considerably, which decreases confidence when assigning concentrations to those compounds. As a result, relative changes are measured more precisely than absolute concentrations, and certain metabolites were quantified with more certainty than others. The results of metabolite quantification show that many compounds remained at a constant level for all time points. Notably, of the metabolites quantified, none are seen to decrease. However, this is not necessarily an artifact. An increase in total NMR spectrum does not betray conservation of mass, since these additional small molecules may be the breakdown products of the proteins, membranes, and other macromolecules that are normally discarded during sample preparation. Also, trehalose and glycogen, the predominant sources of anaerobic energy, were not measured. Although glycogen peaks can be seen in the spectra, the absolute concentration cannot be quantified from the NMR spectra due to the fact that there are a variable number of hydrogen atoms in each glycogen polysaccharide. Trehalose has a high binding affinity to proteins, which are filtered from the sample before measurement. Additional enzymatic assays will be necessary to quantify the true time course of trehalose and glycogen concentrations. Variability in glycerol concentrations may be a result of residual glycerol on the filters used in sample preparation. Additional assays must also be done to determine true changes in glycerol during hypoxia.

In the absence of oxygen it can be assumed that only accumulation occurs for certain end products and only depletion occurs for certain substrates. For example, lactate is a product of the single enzyme lactate dehydrogenase (LDH), and under extreme hypoxic conditions this reaction is irreversible. Therefore, the time course of lactate concentrations can be assumed to closely follow LDH flux. *Drosophila* heart rate slows drastically under hypoxic conditions, as described in Chapter II, and the

resulting reduced circulation would prevent these byproducts from exiting the system and escaping measurement. Similar assumptions can be made for the end products acetate and alanine, and for the depletion of the common flight muscle substrates glycogen, trehalose, and proline. Glycogen and trehalose were not measured by NMR, and will be assayed by biochemical methods in the future. Proline concentrations did not change significantly during hypoxia. Although this substrate is required for flight, proline oxidation pathways were not considered to be important for hypoxic ATP generation.

Acetate, alanine, and lactate showed a statistically significant increasing trend with a good linear fit, but the actual time course more closely represented an exponential rise to saturation. However, since flux balance analysis rests on the assumption of steady state, reaction fluxes were derived from the slope of the linear approximation.

III.2.5 Statistical analysis

For every metabolite with at least one measurement above 0.05 mM, an analysis of variance (ANOVA) was applied to the time course, with a Bonferroni correction applied to the p-value for the number of metabolites tested. Two post hoc tests were performed for metabolites in which the null hypothesis of no change across time points was rejected by ANOVA: Tukey's test for cross-comparison of each time point, and a test for a linear trend in the data. Statistical analysis was performed using the Prism software package (GraphPad Software, Inc., San Diego, CA).

III.2.6 Building the reconstruction

An *in-silico* reconstruction of ATP-generating metabolism in *Drosophila* flight muscle was created, using the Simpheny biological database software (Genomatica, San Diego). Characteristic of these models is a high level of detailed manual curation. All genes and reactions in the reconstruction were individually inspected before inclusion into the model. Element- and charge-balanced reactions were included in the model based on evidence from sequence homology in the annotated genome, online enzyme databases, and the literature. Cellular compartment information was also included. Reed et. al (2006) reviews the reconstruction process in detail.

For the initial draft, we chose to use the human cardiac mitochondrial model (Vo et al., 2004) as a template, sifting through all ATP-producing pathways and then searching various resources (Flybase, KEGG, Brenda, MetaCyc, or PubMed)(Caspi et al., 2006; Consortium, 1998; Ogata et al., 1999; Schomburg et al., 2002), to find evidence for a counterpart in Drosophila flight muscle. Reactions were entered into Simpheny and assigned a confidence level depending on whether evidence was derived from sequence, genetic, physiologic, or biochemical evidence. Gene-protein-reaction associations were made for each reaction, and, whenever necessary, changes were made to reflect subtle interspecies differences in cofactors and substrates.

The second phase of the reconstruction was a survey of Drosophila and insect biochemistry literature, with a focus on energy-producing pathways that occur in exclusively in fruit flies or other species from the parent phylogenic order Diptera, especially the closely related blowfly on which much flight muscle research has been done. Reactions were associated with genes whenever possible, but occasionally

included in the model based on physiological or biochemical evidence even if the corresponding gene was not found.

In the third phase of the reconstruction, the model scope was expanded to account for the production of the end products (acetate and alanine) discovered in the NMR results, and to account for other metabolites and cofactors produced or used in these reactions. All pathways in the KEGG database converting pyruvate to alanine or acetate were manually inspected and then added to the model if at least one enzyme in the pathway had sequence similarity to a *Drosophila* gene. Two pathways were added for the production of alanine, and four pathways for acetate production were added.

The scope of the current *Drosophila* network spans only central, ATP-generating metabolism. Upon completion, this version of the reconstruction had a total of 162 genes, forming 143 proteins and catalyzing 158 reactions. The total number of metabolites represented in the model was 184. Reactions in the model can be grouped into 4 major pathways: glycolysis, TCA cycle, oxidative phosphorylation, and amino acid (proline and glutamate) metabolism. The pentose phosphate pathway was not included in the current version due to suggestions in the literature that in insects the pathway is used for biosynthetic purposes only (Hochachka & Somero, 2002). Fatty acid metabolism is not important for flight in Diptera, and is rarely used during hypoxic conditions (Gilmour, 1961; Hochachka, 1980).

III.2.7 Constraint-based modeling

The final product of the reconstruction process is a curated set of enzymatic reactions and metabolite transporters that define the complete metabolic network of

interest. Additional constraints can be added to this stoichiometric matrix in the form of limits on uptake rates and transporter fluxes. Reactions and their associated biochemicals are represented mathematically as a matrix of stoichiometric relationships that can be manipulated with linear algebra to reveal the solution to the equation

$$d\mathbf{x}/dt = \mathbf{S}*\mathbf{v} = \mathbf{0},$$

where **x** is the vector of metabolites, **S** is the stoichiometric matrix and **v** is the vector of reaction fluxes at steady state. The null space of S is the set of possible flux vectors that satisfy this steady state condition. Linear programming methods within SimPheny were then used to maximize a desired subset of fluxes within this solution space to find a single optimum phenotype. See (Papin et al., 2003) and (Kauffman et al., 2003) for a review of the mathematics involved in flux-balance analysis.

III.2.8 Hypoxia simulation

In muscle cells, the objective of metabolism is primarily to provide ATP to the energy-consuming myosin cross-bridges and ion pumps. In all *in-silico* experiments, ATP production was chosen as the single objective function for the linear programming algorithm. An ATP demand reaction was created in the cytosolic compartment, in which ATP and water are converted into ADP plus one phosphate ion plus one proton. The flux through this reaction was maximized subject to constraints given by the stoichiometry of the network, substrate uptake, and end product secretion. Flux information was exported into Matlab for plotting.

The *Drosophila* literature mentions three major energy substrates for flight muscle: glycogen, trehalose, and proline. Glycerol is also mentioned as a possible fuel (Martinez Agosto & McCabe, 2006), but since both the literature and our

metabolomic data are inconclusive regarding this compound, it has been excluded as a substrate. For the purposes of this model, trehalose and glycogen are functionally equivalent as the predominant sources of glucose. The depletion of glycogen and trehalose are currently unknown; therefore the amount of glucose entering glycolysis remains unknown as well. Initial simulations of hypoxia showed that proline uptake decreases as oxygen is constrained, reaching zero at oxygen levels higher than those at which lactate and acetate accumulation occur. Therefore, it is reasonable to assume for our simulations that glucose is the only substrate during hypoxia, which reduces the degrees of freedom for substrates to two: glucose and oxygen.

In order to study changes in the model output using oxygen uptake as the independent variable, the system was saturated with glucose by setting the maximum uptake to a value much higher than the threshold required to produce the measured fluxes of end products under restricted oxygen. Constraints on O_2 influx in the model were then used to simulate low extracellular oxygen concentration in hypoxic experimental conditions. We reduced O_2 uptake, leaving all other fluxes free to vary up to their constrained maxima.

III.2.9 Model Validation

The core energy-producing pathways in the model, consisting of glycolysis, TCA (tricarboxylic acid) cycle, electron transport chain, and oxidative phosphorylation, were validated using experimentally measured ratios of ATP produced per molecule of glucose and ATP per oxygen atom (P/O or ADP/O ratio).

Representative oxygen electrode recordings from a study of isolated *Drosophila* mitochondria (Ferguson et al., 2005) were used to approximate the P/O ratio in flight muscle using pyruvate/proline and glycerol-3-phosphate as NAD- and

FAD- linked substrates, respectively. These conditions were simulated in the model by constraining cytosolic pathways to zero while adding a flux of ADP in the presence of an infinite amount of substrate. The rate of oxygen consumption was compared directly to the linear portion of state 3 respiration in the experimental oxygen traces. The stoichiometry of electron transport within the model was refined to better approximate experimental results.

Whole cell simulations were performed to calculate the amount of ATP produced per glucose, with no other carbon source added. Since measurements of ATP:glucose ratio were not found in the literature, the results were compared with ATP/glucose ratios in human mitochondria.

The ADP/O ratio produced by simulation was compared to that of experiment by constraining the ADP flux to experimental value (≈ 8.9 nmol/min*μg protein) in a saturated solution of pyruvate and proline substrate as described in Ferguson, et. al (2005). Oxygen uptake in the linear region of state 3 respiration was then approximated from the oxygen electrode trace and the ADP/O ratio was calculated using the formula: $[ADP]/2[O_2]$. These conditions were simulated in the model and the resulting oxygen uptake rate was compared to experiment. After noting a large discrepancy, the stoichiometry of proton transfer was adjusted for NADH dehydrogenase and cytochrome reductase, two reactions in the electron transport chain. These refinements increased the ADP/O ratio from 2.12 to 2.76 in the model, the latter value comparing more favorably with the experimental value of 3.34 (a percent error of 17% vs 36%). The FAD^+-linked substrate α-glycerol-3-phosphate produced a poorly defined oxygen trace; however, a rough approximation of oxygen uptake provided an ADP/O ratio of 1.33. Simulation of the isolated mitochondria in

the presence of α-GP produced a ratio of 1.75. The refined model produced an ATP/glucose ratio of 33.0, which is similar to the reported value in humans of 31.5 (Nelson, 2000).

III.3 Results and Discussion

III.3.1 Global metabolite profiles under hypoxia

Of the 21 compounds with at least one sample measurement greater than 0.05 mM, 6 were found to change significantly according to one-way ANOVA: acetate, alanine, arginine, glucose, lactate, and threonine. All 6 compounds had a statistically significant linearly increasing trend. Three compounds (acetate, alanine, lactate) had high R^2 goodness-of-fit values and significant changes among several time points. In the remaining three (arginine, glucose, threonine), only the 4-hour hypoxia group was significantly different than the rest. Figure III.2 displays the statistically significant subset.

Table III.1: Approximation of end-product accumulation from NMR data. Accumulation of substrate was calculated using the sample volume (500 µL) and the flies per sample (20).

Product	Goodness-of-fit (R^2)	Slope of trendline (µM/min*sample)	Accumulation (nmol/(min·fly))
Lactate	0.81	495	12.4
Alanine	0.82	798	20.0
Acetate	0.86	485	12.1

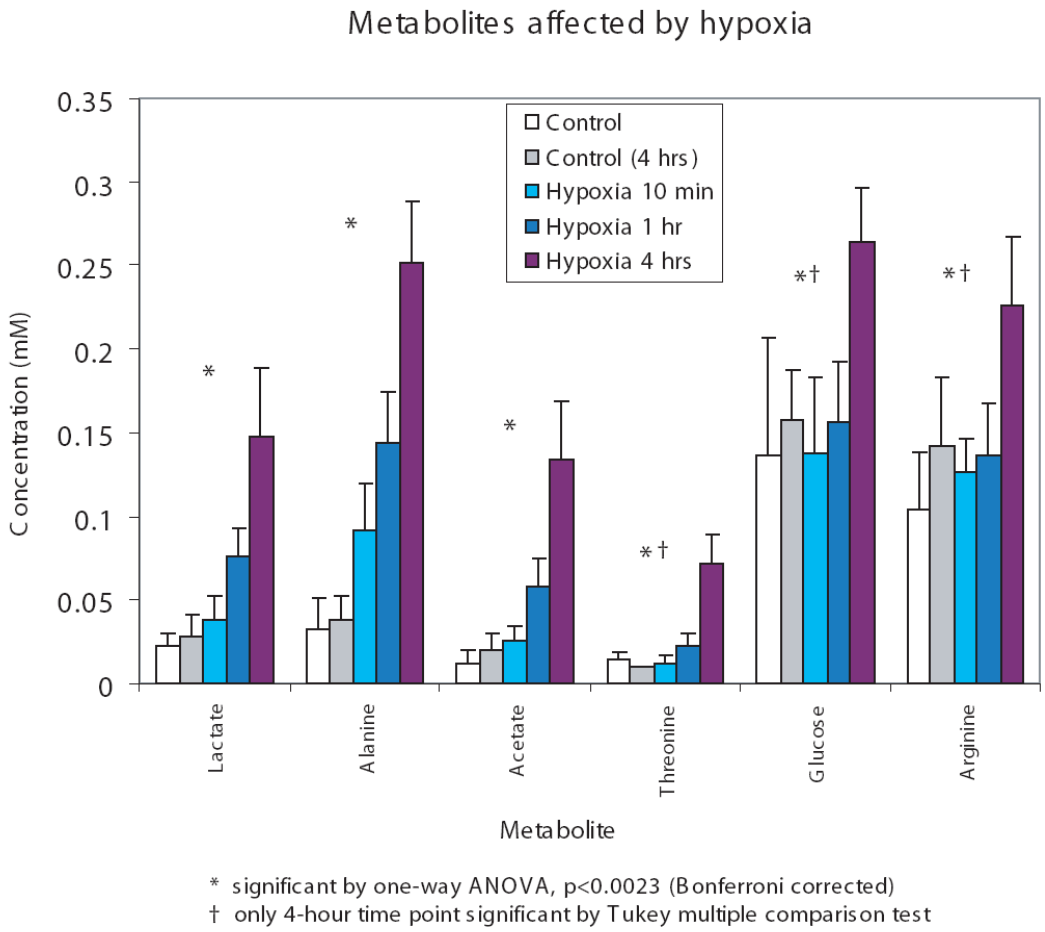

Figure III.2: Metabolites significantly altered during hypoxia, measured by ^{1}H NMR spectroscopy. Lactate, alanine, and acetate accumulate over the time course of the experiment and are byproducts of anaerobic metabolism, whereas glucose, threonine, and arginine concentrations only spike at 4 hours and are possible indications of a loss in homeostasis.

One common behavior was for the concentration of a metabolite to remain stable for the first hour of hypoxia, but to show a large increase at 4 hours. Glucose, threonine, and arginine show a statistically significant difference from early time points to the 4 hour concentration. Since the survival rate for anoxic flies at 25º C is very high for the first few hours and then starts to decline at 6 hours (Haddad et al.,

1997), it is reasonable to suggest that these metabolites are an early indication of the loss of homeostasis, i.e. the breakdown of the system under stress. Mechanisms for protecting the cell and balancing metabolic requirements may begin to lose effectiveness at some threshold period of time. For example, a likely explanation for the time course of glucose is that this substrate is replenished by a steady depletion of trehalose and glycogen supplies during the manageable first hour of hypoxia. At 4 hours, the glucose supply undergoes a large increase, which suggests that the system has experienced a drastic reduction in its ability to utilize carbohydrate substrates.

Steady accumulation of lactate, alanine, and acetate is the second phenomenon that can be seen in the NMR spectra. The end products of anaerobic metabolism in *Drosophila* were not previously known. However, the discovery of lactate and alanine accumulation is consistent with the fact that these compounds, which do not accumulate under normal conditions, are known to be byproducts of anaerobic metabolism in other terrestrial insects (Hoback & Stanley, 2001). During hypoxia, lactate fermentation regenerates NAD^+ for glycolysis, with the tradeoff of decreasing pH (Nelson, 2000), and certain other organisms have alanine and acetate fermentation pathways that perform a similar function (Gade, 1984; Hochachka & Somero, 2002). Table I contains calculated results of accumulation during the hypoxia experiment.

III.3.2 Reconstruction and expansion of Drosophila *metabolic network*

We built and validated a constraint-based model of known ATP-producing pathways in *Drosophila*. Results from the NMR metabolomics experiment were then used to refine and expand the model, as well as incorporate quantitative flux data.

These results suggest that the major metabolites that accumulate under hypoxic conditions are lactate, alanine, and acetate. We expanded the scope of the model to include several alternative pathways for generating alanine and acetate from pyruvate, and then integrated NMR measurements by placing constraints on the steady-state flux out of the system.

In other organisms, alanine is produced during hypoxia by transamination to pyruvate from another amino acid. In mammals this pathway involves the cycling of α-oxoglutarate (also known as α-ketoglutarate) and glutamate (Nelson, 2000) through enzymes that are also present in flies. We added two transaminations to the model based on genetic evidence in the KEGG pathway database (Ogata et al., 1999): alanine-α-oxoglutarate transaminase (using glutamate as in mammals) and alanine-glyoxylate transaminase (using glycine and pyruvate as substrates).

Acetate production has been previously hypothesized as a possible mechanism for dealing with mitochondrial acetyl-CoA that cannot be catabolized further in the absence of oxygen (Hochachka, 1980). The benefits of this pathway are two-fold. Acetate is a weaker acid than lactate (pK is 4.8 vs 3.7); also hydrolysis of acetyl-CoA to acetate by acetate-CoA ligase is ADP-linked, offering the additional benefit of ATP production. Genetic evidence in flies (from KEGG) also suggests alternative pathways for acetate production from pyruvate via acetyl-phosphate or acetaldehyde. These reactions were added along with the acyl-carnitine shuttle for transport of mitochondrial acetyl-CoA to the cytosol.

III.3.3 Hypoxia simulation

There are several benefits to using a quantitative model to test and generate hypotheses about hypoxic energy metabolism. First, although much is known about

the individual pathways, it becomes very hard to manually calculate and predict behavior when pathways are combined into an integrated network. With a few reasonable assumptions, steady state in this study for example, some of the vast knowledge contained in the literature and public databases can be compiled into a comprehensive, predictive model into which individual experiments, such as our metabolomic data, can be integrated. In this mathematical model, the complicated problems of balancing redox potential and accounting for proton production are solved intrinsically during flux-balance analysis.

Every simulation of hypoxia produced a flux distribution that utilized only one pathway each for production of alanine and acetate, among multiple alternatives. Alanine formation used the glutamate-dependent alanine transaminase, since *Drosophila* lack the capability to further metabolize glyoxylate produced by the alternative transaminase reaction. To produce acetate, the model utilized the acetyl-CoA synthetase reaction in every simulation. Fluxes through these reactions were constrained to a maximum determined by the NMR data, but were not set explicitly; rather, the model utilized these pathways to optimize ATP production under hypoxic conditions (Figure III.3).

Figure III.3 (facing page): Pathways of ATP generation during hypoxia. The network includes glycolysis, TCA cycle and oxidative phosphorylation, as well as reactions for generating lactate, alanine, and acetate (in red) during hypoxia. Of the two pathways for creating alanine (purple box) and four options for creating acetate (blue box) from pyruvate, optimization of the model selected one optimal route for generating each end product (nonzero fluxes in color).

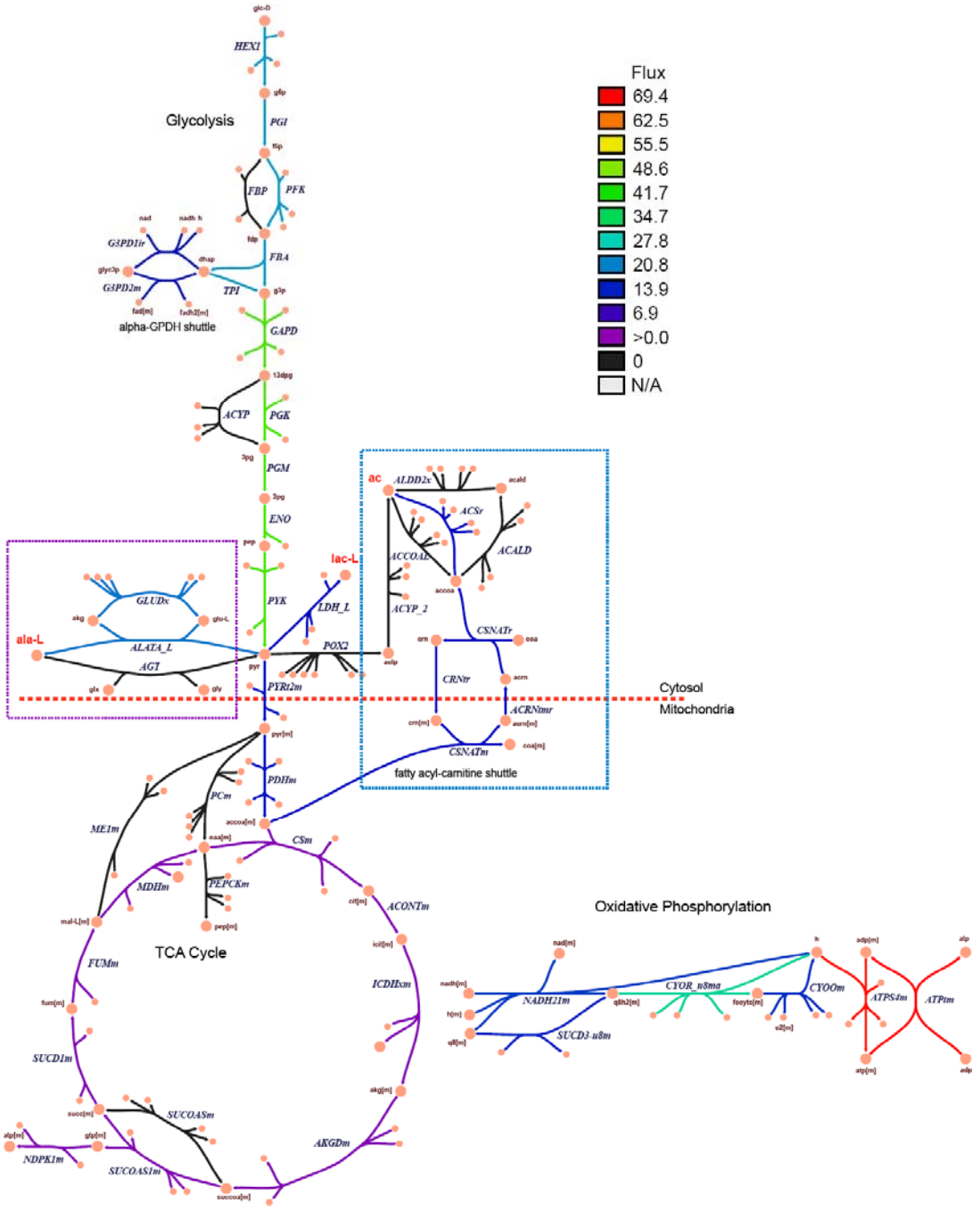
Flux
69.4
62.5
55.5
48.6
41.7
34.7
27.8
20.8
13.9
6.9
>0.0
0
N/A
Glycolysis
HEX1
PGI
FBP
PFK
FBA
TPI
GAPD
PGK
PGM
ENO
PYK
G3PD1ir
G3PD2m
alpha-GPDH shuttle
ACYP
LDH_L
lac-L
POX2
ala-L
GLUDx
ALATA_L
AGT
ac
ALDD2x
ACSr
ACCOAL
ACALD
ACYP_2
CSNATr
CRNTr
ACRNTmr
CSNATm
fatty acyl-carnitine shuttle
Cytosol
Mitochondria
PYRt2m
PDHm
PCm
ME1m
CSm
MDHm
PEPCKm
ACONTm
ICDHxm
SUCD1m
SUCOASm
SUCOAS1m
NDPK1m
AKGDm
FUMm
TCA Cycle
Oxidative Phosphorylation
NADH21m
SUCD3-u8m
CYOR_u8ma
CYOOm
ATPS4m
ATPtm

Our model was used to simulate *Drosophila* ATP production ranging from normoxia to anoxia, using two different systems: the first allowing lactate, alanine, and acetate to accumulate through known and hypothesized pathways, and the second allowing only lactate to accumulate through the fermentation pathway also used by mammals (which we call the “pseudo-mammalian” model). Figure III.4 shows a clear advantage in converting pyruvate to acetate and alanine during all low oxygen conditions. Figure III.4A plots important fluxes under varying oxygen. Figure III.4B compares these fluxes when alanine and acetate production are constrained to zero and the constraint on lactate accumulation is removed. Using pathways that generate alanine and acetate decreases proton production, increases ATP generation (Figure III.4C), and decreases glucose uptake under all hypoxic and anoxic conditions simulated.

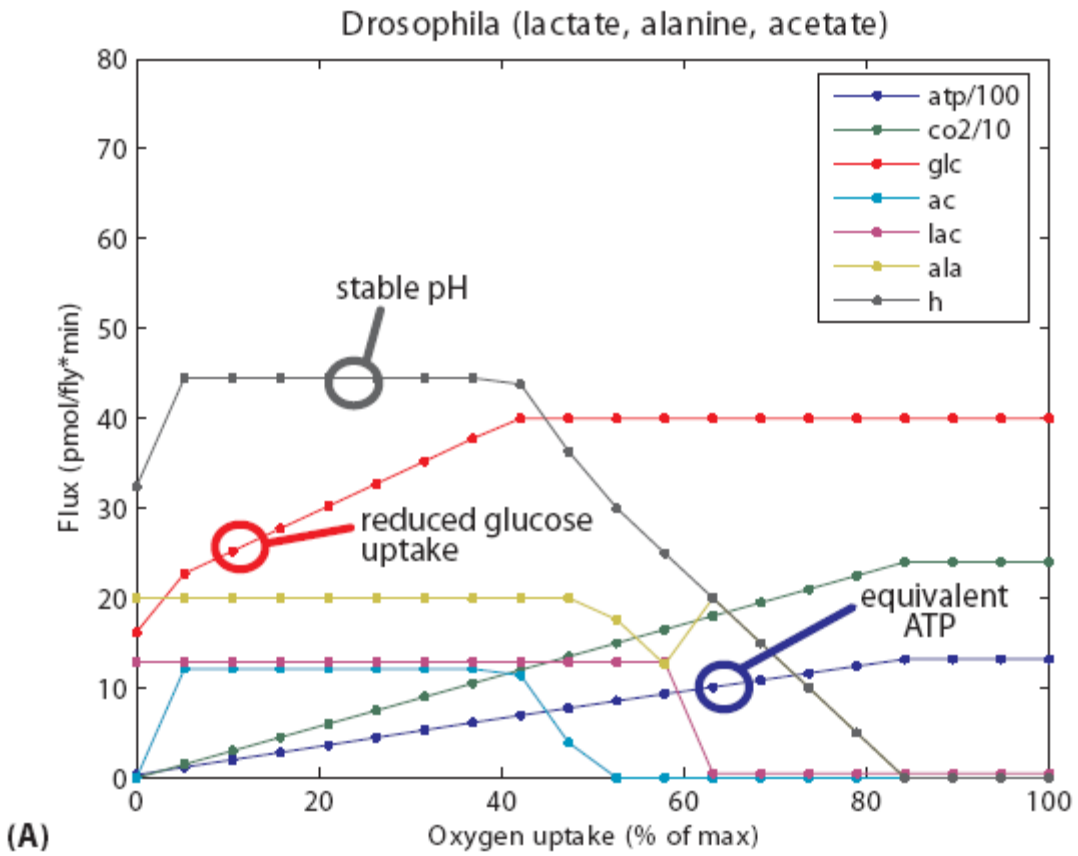

Figure III.4 (B and C on following page): Results of flux-balance analysis on the model of *Drosophila* ATP-generating metabolism.

(A) Proton production increases but then levels off at low oxygen levels as pyruvate begins to be fermented to alanine, acetate, and lactate. Glucose uptake is decreased during restricted oxygen.

(B) When pyruvate is only allowed to be converted to lactate (Pseudo-mammalian), proton production is much higher and glucose uptake remains constant during hypoxia, while

(C) ATP production remains the same or better.

Abbreviations: atp: ATP production, co2: CO_2 production; glc: glucose uptake; h: proton production; ac: acetate accumulation, lac: lactate accumulation, ala: alanine accumulation.

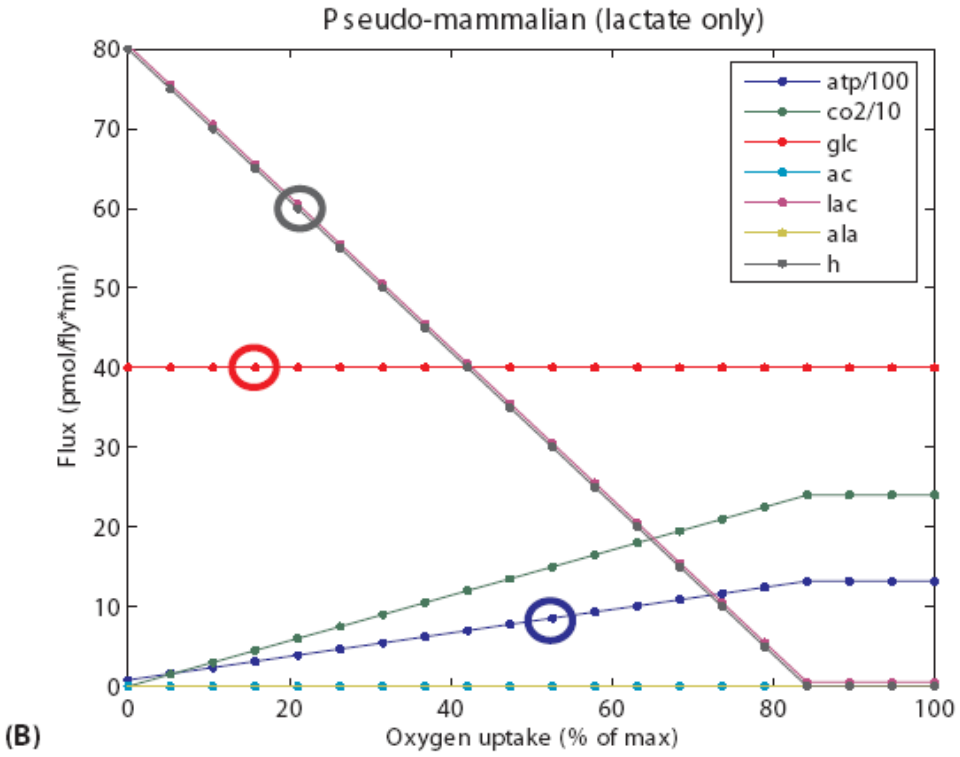

(B)

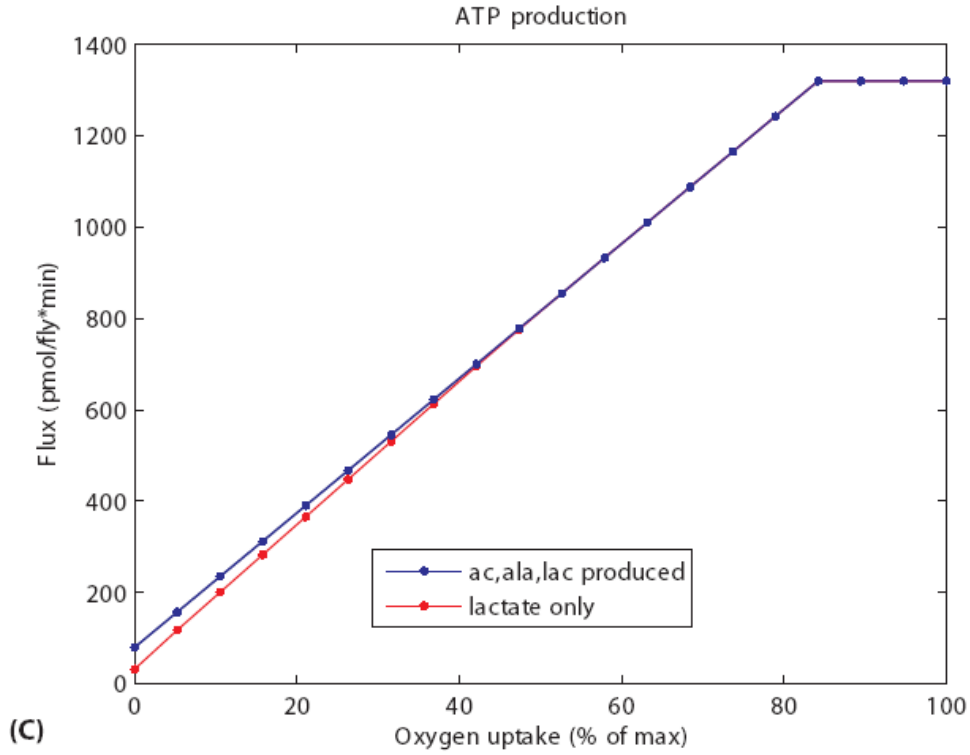

(C)

Figure III.4 (continued)

2002), since it directly quantifies the physiological tradeoff between generating energy for the system and maintaining pH levels required for homeostasis. Another suggested indicator, ATP/substrate ratio, is an obvious way of quantifying the decreased efficiency of fuel utilization as respiration, the most efficient pathway, is restricted. Since all simulations of restricted oxygen produce more ATP, use less glucose, and accumulate fewer protons in the acetate and alanine-producing system, the model suggests that these mechanisms contribute to hypoxia tolerance in flies.

III.3.4 Simplified simulations of hypoxia metabolism

We used a simple version of the constraint-based model to further examine the individual activity of anaerobic pathways and their interactions. A set of *in-silico* experiments activated various combinations of the pathways, each time using one glucose as the system input and restricting oxygen availability in steps from the aerobic domain to total anoxia. Above 6 oxygen molecules per glucose, aerobic metabolism dominated and ATP production was maximized at 33 ATP per glucose as expected. Below oxygen levels of 6 per glucose, behavior varied depending on which of the three anaerobic pathways was used.

If the lactate, alanine, and acetate pathways were all restricted, aerobic pathways and ATP production decreased linearly to zero as oxygen was restricted (Figure III.5A). When the lactate pathway was added alone, as in mammalian systems, it behaved as expected: below 6 O_2 per glucose, lactate production increased linearly with decreasing oxygen and produced an equivalent amount of protons, as glycolysis decoupled from oxidative phosphorylation with each pyruvate diverted from the mitochondria (Figure III.5B).

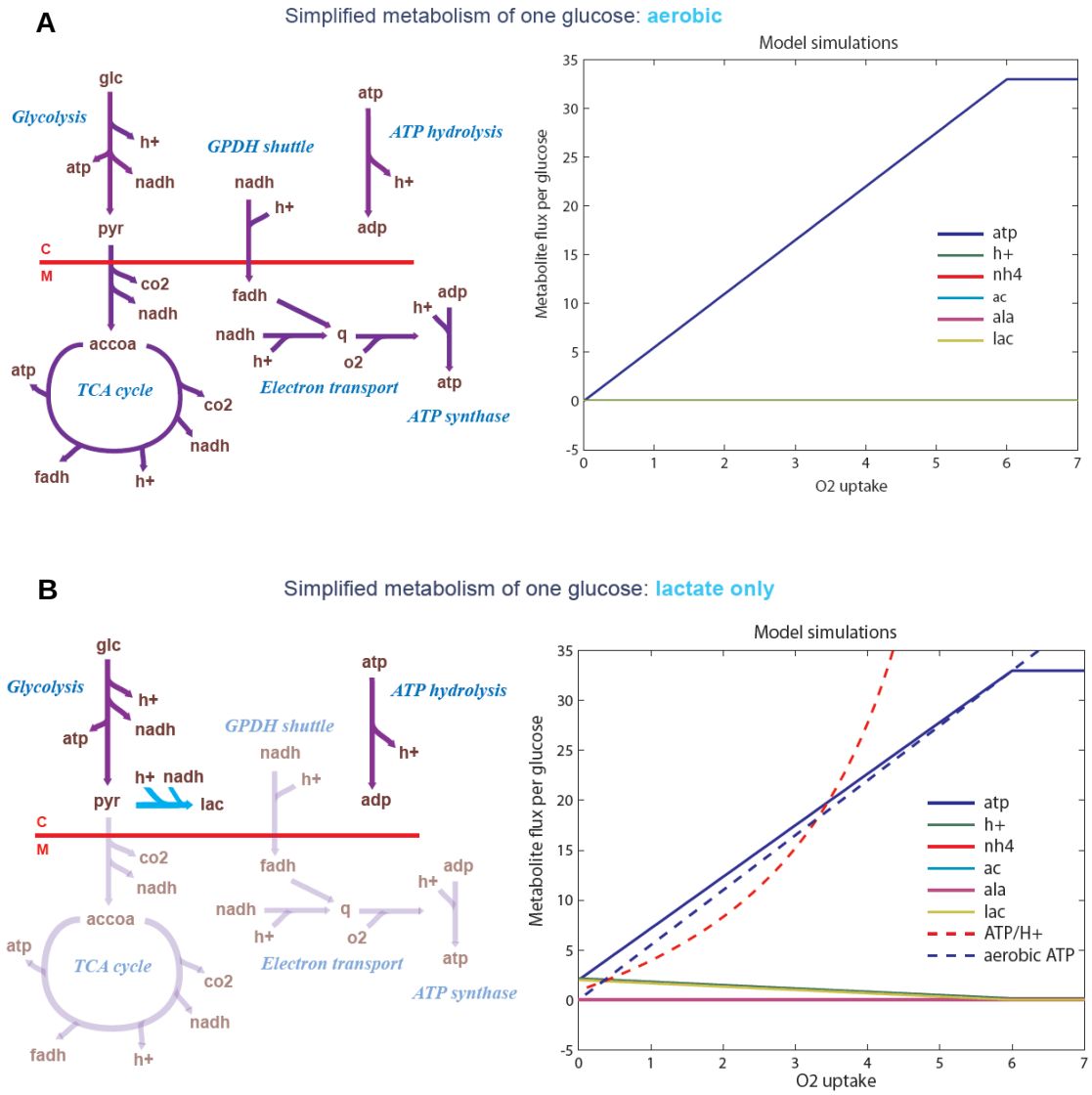

Figure III.5: Simulating classical anaerobic metabolism

A) Anaerobic pathways restricted (aerobic metabolism only)

B) Classical mammalian pathway using fermentation of lactate

In *Drosophila*, alanine transaminase can be found both in the cytosol and the mitochondria in a tissue-specific manner, with the cytosolic version suggested to be expressed in fat body and the mitochondrial version expected in muscle tissue (Gilmour, 1961). However, we found that the benefit of the alanine pathway under

hypoxia was highly dependent on which compartment the enzyme was expressed Figure III.6. In simulation of the alanine pathway individually, the mitochondrial version of the enzyme had no improvement over aerobic pathways and was not activated. The cytosolic version was similar to the lactate pathway, since it replenishes NAD for glycolysis, and displayed oxygen-dependent activity. Also as in the lactate pathway, alanine production caused creation of H+ as glycolysis and oxidative phosphorylation were decoupled. One additional feature of this pathway is that the production of each alanine also required a consumption of NH4 from the cytosol. This consequence of alanine fermentation is well known, and in hypoxic mammalian muscle amino groups are also expected to come from glutamate (Taegtmeyer et al., 1977). If scavenging free ammonium ions from the cytosol is an added benefit to the cell, the model suggests that the alanine pathway has equal or better utility than lactate fermentation during hypoxic conditions.

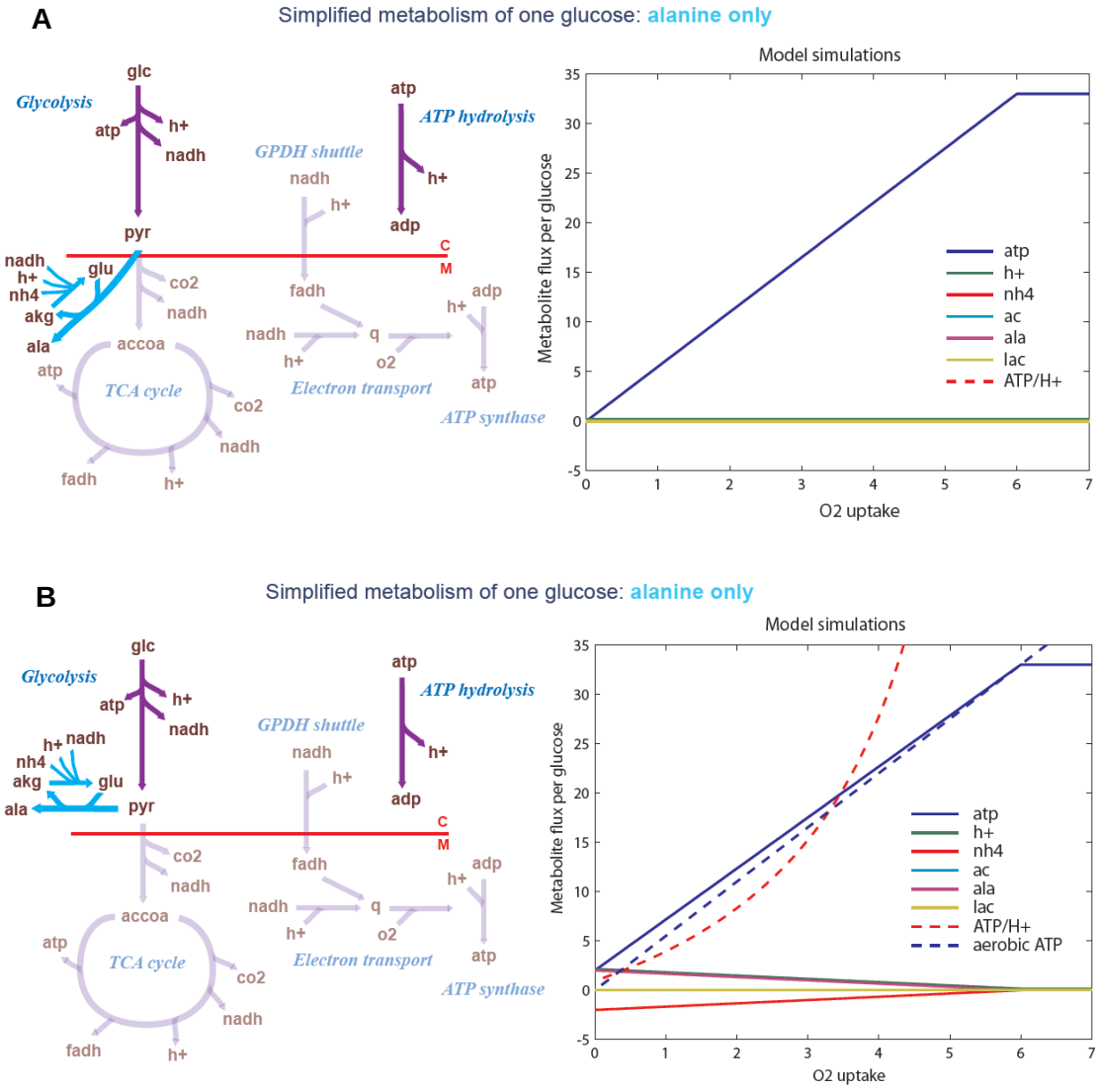

Figure III.6: Only cytosolic alanine is beneficial as an aerobic end product.

A) Mitochondrial alanine transaminase does not balance NADH/NAD+ or contribute to the ATP objective and is not used by the model.

B) Cytosolic alanine production replenishes NAD+, as in lactate fermentation, but also consumes free ammonium.

Acetate production required some oxygen, since it does not replenish NAD+ and in fact produces more NADH than the other pathways due to the reliance of pyruvate dehydrogenase to form acetyl-CoA. However, two additional ATP are produced from each glucose without requiring the TCA cycle or electron transport chain, so the benefit of this pathway in hypoxic conditions manifested as a higher ATP/H+ ratio under mild hypoxia. Specifically, maximal benefit of the acetate pathway was at 1/3 the oxygen uptake of the fully aerobic system. In total anoxia, however, metabolism was completely shut down without a supply of NAD+. Production of each acetate accumulates a proton by the same mechanism as in the other pathways.

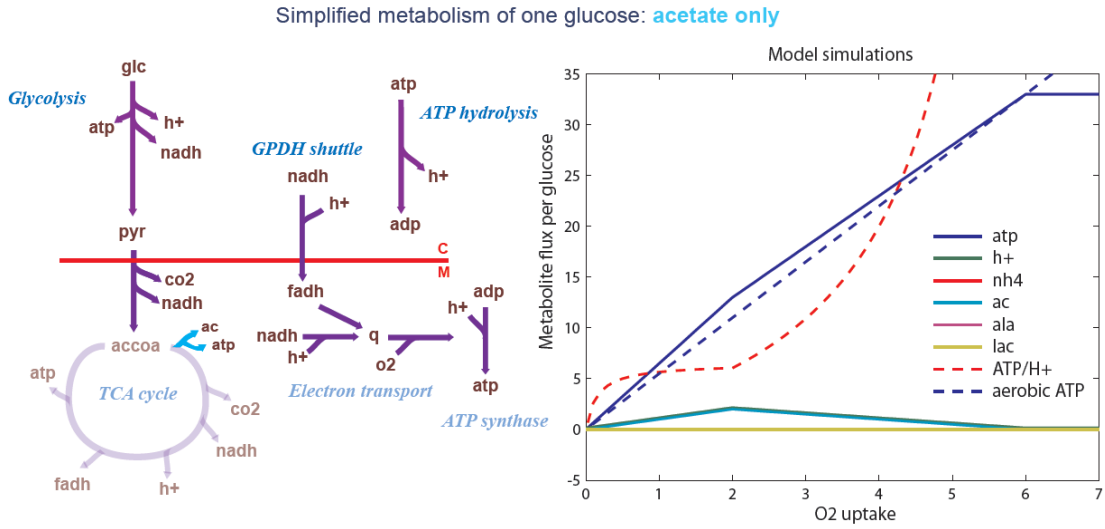

Figure III.7: Acetate improves ATP/H+ ratio but requires a small amount of oxygen (optimally 1/3 of aerobic O2 uptake).

Combining all anaerobic pathways maximized the benefit over the entire range of available oxygen. In mild hypoxia (2 to 6 O_2 per glucose), the TCA cycle and its numerous oxidation steps were shut down as acetyl-CoA was diverted to acetate. Below 2 O_2 per glucose, lactate and alanine activity saw a linear increase in activity

as acetate production decreased proportionally. The ATP-proton ratio saw a boost due to acetate production, but because of lactate and alanine this figure did not drop to zero as O_2 levels approached total anoxia. At very low O_2, free ammonium was consumed for each alanine produced.

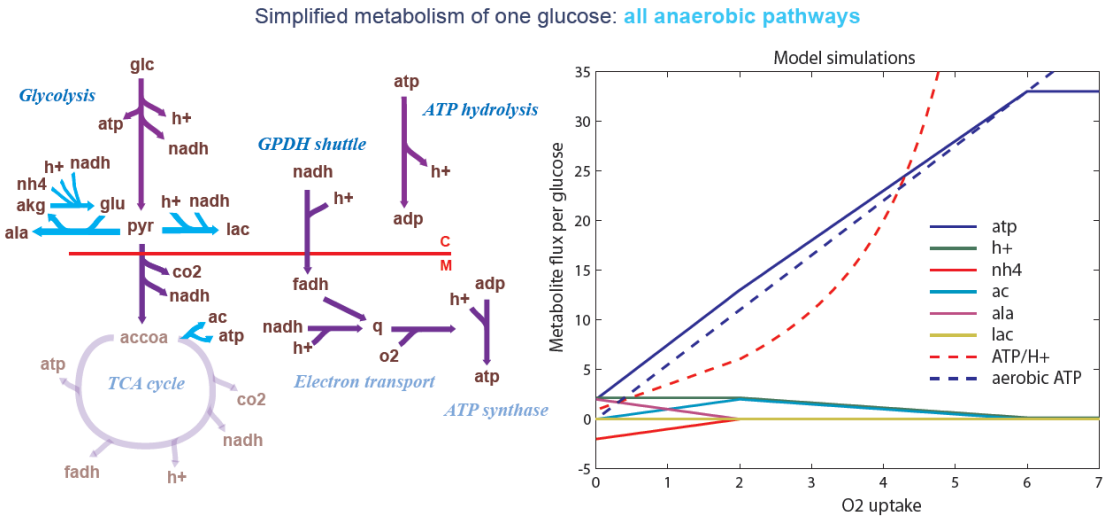

Figure III.8: When all three anaerobic pathways are used, ATP/O2 and ATP/H+ curves are highest and free NH4 is consumed in the cytosol.

III.3.5 Lactate dehydrogenase mutant

The model was next used to simulate a lactate dehydrogenase (LDH) loss-of-function mutant. As hypothesized, the lactate pathway produced a neutral effect on the system as a whole in the computer model, since alanine production equivalently resupplied NAD+ to glycolysis. The NH_4 scavenging of the alanine pathway suggested by the model may even cause an LDH knock-out to have a beneficial effect on hypoxia survival, since the source of pyruvate normally shared by the two pathways would instead be completely converted to alanine with the uptake of an additional ammonium ion.

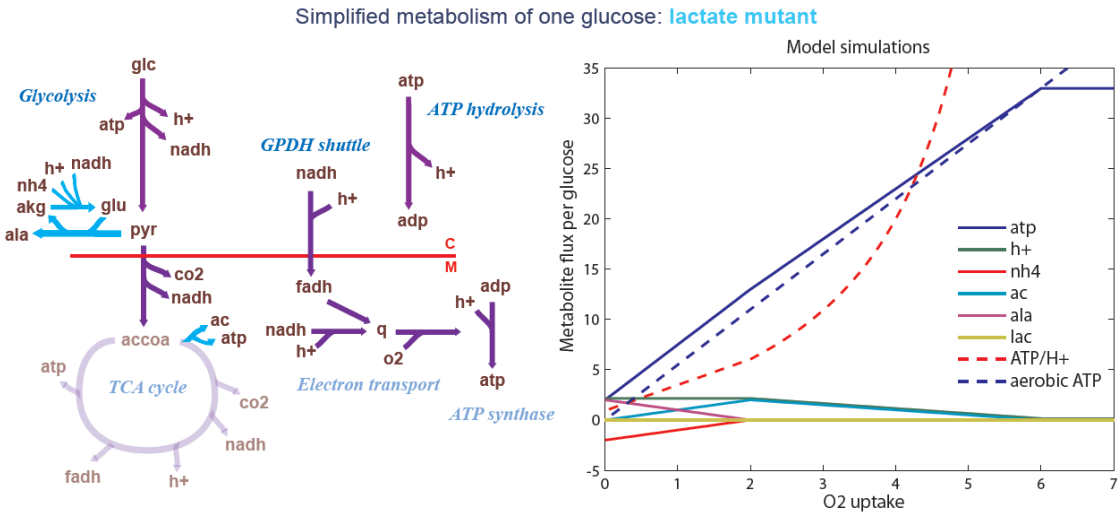

Figure III.9: Inhibiting lactate dehydrogenase activity has a neutral effect on ATP/H+ ratio, and may be beneficial due to increased NH4 uptake in the cytosol.

We used ^{1}H NMR to obtain the metabolic profile of an LDH deletion (Bloomington stock number 8063). The heterozygous deletion strain was out-crossed with Oregon-R wild type flies for one generation. Lactate production in the LDH deletion was inhibited compared to controls, while alanine and acetate accumulation was greater. Although the model does not specifically predict an increase in acetate production, the rise in alanine supports the hypothesis that the alanine pathway is a redundant alternative to lactate production.

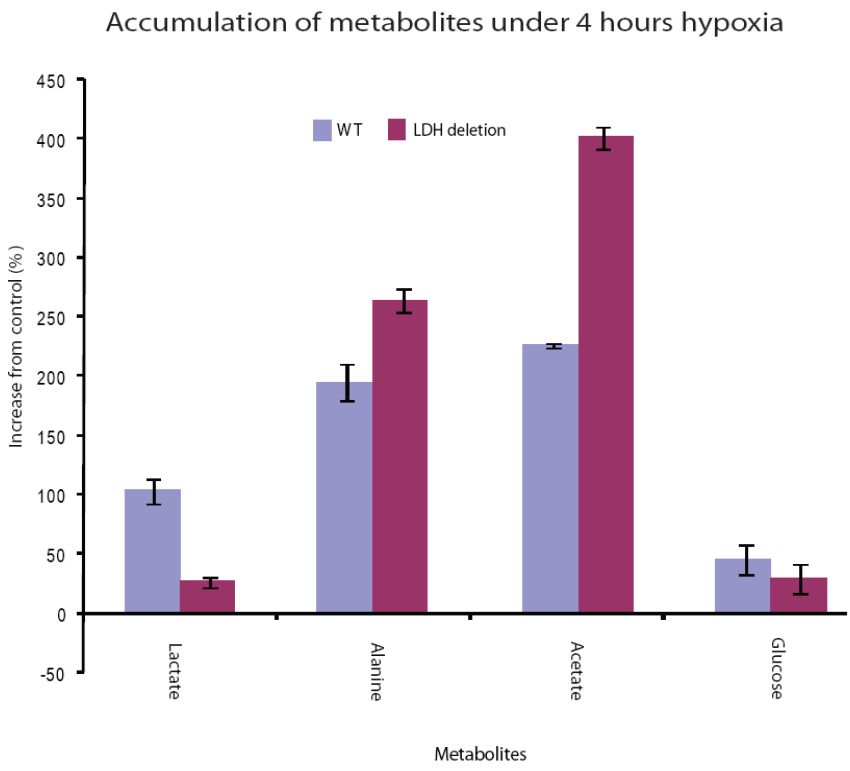

Figure III.10: Metabolic effects of the lactate dehydrogenase deletion

A) Computer simulations suggest neutral effects on ATP metabolism and proton production. Ammonium consumption in the cytosol would be greater as the alanine pathway activity increases to handle surplus NADH.

B) Metabolic profiles show inhibited lactate production in the deletion strain, with increased activity in the other pathways.

Cardiac phenotypes were acquired by the techniques in Chapter II, and whole-body recovery was measured using the protocol in Chapter IV. Both assays saw improvements in function, supporting the predictions of the model.

Figure III.11 (facing page): Physiological assays of the LDH deletion.

A) Heart rate in LDH deletions recovered faster than wild type

B) LDH deletion strains also recovered whole-body activity faster than the wild type

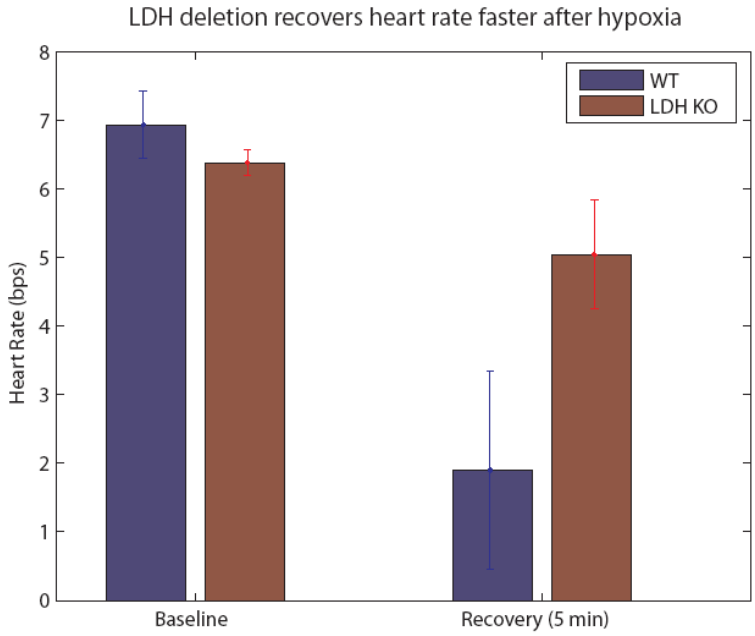
LDH deletion recovers heart rate faster after hypoxia
Heart Rate (bps)
WT
LDH KO
Baseline
Recovery (5 min)

A

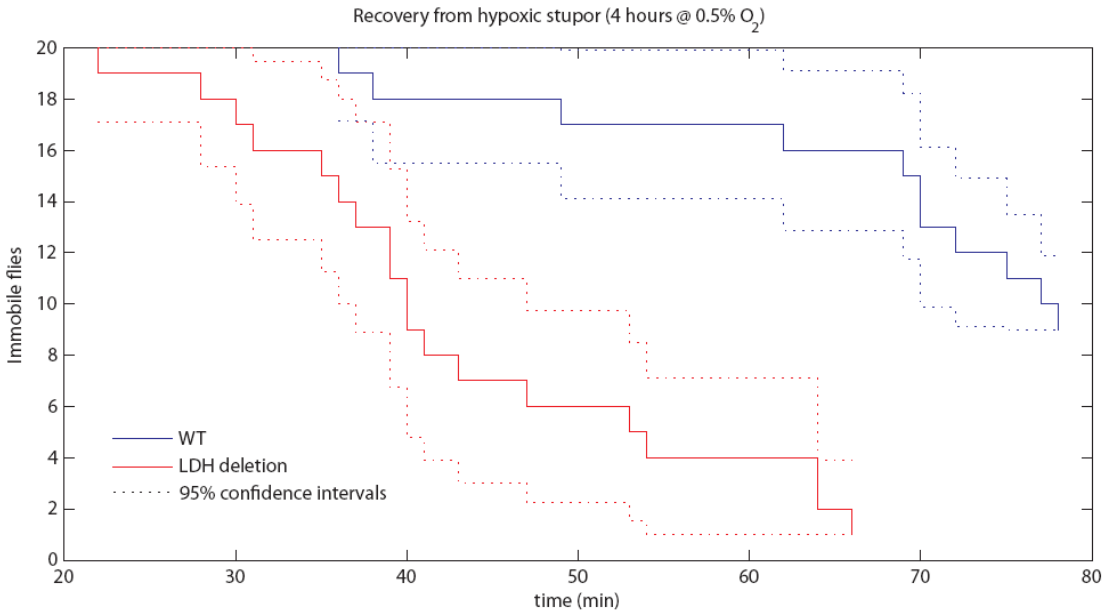
Recovery from hypoxic stupor (4 hours @ 0.5% O2)
Immobile flies
time (min)
WT
LDH deletion
95% confidence intervals

B

III.4 Summary

Our approach can be used to generate and test new hypotheses about the metabolic basis for hypoxia tolerance. Both NMR metabolomic profiling and quantitative systems modeling suggest that having several pathways for the fermentation products of pyruvate may contribute to hypoxia tolerance in fruit flies. Specifically, we used metabolomics with the flux-balance model to generate several experimentally testable hypotheses:

- Alanine and acetate production pathways improve hypoxia tolerance in flies by more efficient use of glucose (ATP/substrate ratio) and lower proton production (ATP/H+ ratio) when produce the same ATP under a given oxygen availability.
- Only the cytosolic version of alanine transaminase is active during anaerobic alanine production in flight muscle.
- Acetate production uses reversible mitochondrial acetyl-CoA synthetase, and is beneficial to metabolism under mild hypoxia but its use tapers off in complete anoxia.
- Hypoxic use of lactate dehydrogenase is redundant and possibly detrimental when alanine pathways are available, and an LDH deletion should have neutral to beneficial phenotypic effect.

All of these hypotheses represent interesting and novel directions of research into the Drosophila hypoxia response, and the last hypothesis (regarding the LDH deletion) was tested and supported by our own experiments. Future work will verify these modeling results, and will take advantage of the vast *Drosophila* gene deletion

library (Spradling et al., 1999) by applying further NMR, phenotypic, and biochemical experiments on mutants suggested by the model.

Acknowledgements

Chapter 3, in part, is adapted from an article that originally appeared in Molecular Systems Biology , volume 3, article number 99, published April 2007. The dissertation author was the primary investigator and author of this paper, which was co-authored by Drs. Laurence Coquin, Andrew D. McCulloch, and Giovanni Paternostro.

We would like to thank Polly Huang for helping with the preparation of NMR samples and Khoi Pham for adding various genes and reactions to the model. We would also like to thank the lab of Dr. Bernhard Palsson, especially Adam Feist and Thuy Vo, for offering their expertise on mitochondrial biochemistry, flux-balance analysis, and the SimPheny software platform.

References

Almaas E, Kovacs B, Vicsek T, Oltvai ZN, Barabasi AL (2004) Global organization of metabolic fluxes in the bacterium Escherichia coli. *Nature* **427:** 839-843.

Caspi R, Foerster H, Fulcher CA, Hopkinson R, Ingraham J, Kaipa P, Krummenacker M, Paley S, Pick J, Rhee SY, Tissier C, Zhang P, Karp PD (2006) MetaCyc: a

multiorganism database of metabolic pathways and enzymes. *Nucleic Acids Res* **34:** D511-516.

Consortium (1998) FlyBase: a Drosophila database. Flybase Consortium. *Nucleic Acids Res* **26:** 85-88.

Corbucci GG, Marchi A, Lettieri B, Luongo C (2005) Mechanisms of cell protection by adaptation to chronic and acute hypoxia: molecular biology and clinical practice. *Minerva Anestesiol* **71:** 727-740.

Ferguson M, Mockett RJ, Shen Y, Orr WC, Sohal RS (2005) Age-associated decline in mitochondrial respiration and electron transport in Drosophila melanogaster. *Biochem J* **390:** 501-511.

Gade G (1984) Anaerobic Energy Metabolism. In *Environmental Physiology and Biochemistry of Insects*, Hoffmann KH (ed) pp 119-136. Springer-Verlag, Berlin.

Gilmour D (1961) *The biochemistry of insects*. Academic Press, New York,.

Haddad GG (2006) Tolerance to low 02 : Lessons from invertebrate genetic models. *Exp Physiol*.

Haddad GG, Wyman RJ, Mohsenin A, Sun Y, Krishnan SN (1997) Behavioral and Electrophysiologic Responses of Drosophila melanogaster to Prolonged Periods of Anoxia. *J Insect Physiol* **43:** 203-210.

Hoback WW, Stanley DW (2001) Insects in hypoxia. *J Insect Physiol* **47:** 533-542.

Hochachka PW (1980) *Living without oxygen : closed and open systems in hypoxia tolerance*. Harvard Univ. Press, Cambridge.

Hochachka PW, Somero GN (2002) *Biochemical adaptation : mechanism and process in physiological evolution*. Oxford University Press, New York.

Kauffman KJ, Prakash P, Edwards JS (2003) Advances in flux balance analysis. *Curr Opin Biotechnol* **14:** 491-496.

Lavista-Llanos S, Centanin L, Irisarri M, Russo DM, Gleadle JM, Bocca SN, Muzzopappa M, Ratcliffe PJ, Wappner P (2002) Control of the hypoxic response in Drosophila melanogaster by the basic helix-loop-helix PAS protein similar. *Mol Cell Biol* **22:** 6842-6853.

Martinez Agosto JA, McCabe ER (2006) Conserved family of glycerol kinase loci in Drosophila melanogaster. *Mol Genet Metab* **88:** 334-345.

Nelson DaC, M (2000) *Lehninger Principles of Biochemistry*. Worth Publishersd, New York.

O'Farrell PH (2001) Conserved responses to oxygen deprivation. *J Clin Invest* **107:** 671-674.

Ogata H, Goto S, Sato K, Fujibuchi W, Bono H, Kanehisa M (1999) KEGG: Kyoto Encyclopedia of Genes and Genomes. *Nucleic Acids Res* **27:** 29-34.

Palsson B (2004) Two-dimensional annotation of genomes. *Nat Biotechnol* **22:** 1218-1219.

Pan DA, Hardie DG (2002) A homologue of AMP-activated protein kinase in Drosophila melanogaster is sensitive to AMP and is activated by ATP depletion. *Biochem J* **367:** 179-186.

Papin JA, Price ND, Wiback SJ, Fell DA, Palsson BO (2003) Metabolic pathways in the post-genome era. *Trends Biochem Sci* **28:** 250-258.

Piacentini L, Karliner JS (1999) Altered gene expression during hypoxia and reoxygenation of the heart. *Pharmacol Ther* **83:** 21-37.

Reed JL, Famili I, Thiele I, Palsson BO (2006) Towards multidimensional genome annotation. *Nat Rev Genet* **7:** 130-141.

Reed JL, Palsson BO (2004) Genome-scale in silico models of E. coli have multiple equivalent phenotypic states: assessment of correlated reaction subsets that comprise network states. *Genome Res* **14:** 1797-1805.

Sauer U (2006) Metabolic networks in motion: 13C-based flux analysis. *Mol Syst Biol* **2:** 62.

Schomburg I, Chang A, Hofmann O, Ebeling C, Ehrentreich F, Schomburg D (2002) BRENDA: a resource for enzyme data and metabolic information. *Trends Biochem Sci* **27:** 54-56.

Spradling AC, Stern D, Beaton A, Rhem EJ, Laverty T, Mozden N, Misra S, Rubin GM (1999) The Berkeley Drosophila Genome Project gene disruption project: Single P-element insertions mutating 25% of vital Drosophila genes. *Genetics* **153:** 135-177.

Taegtmeyer H, Peterson MB, Ragavan VV, Ferguson AG, Lesch M (1977) De novo alanine synthesis in isolated oxygen-deprived rabbit myocardium. *J Biol Chem* **252:** 5010-5018.

Troy H, Chung, Y.L., et. al. (2005) Metabolic profiling of hypoxia-inducible factor-1-B-deficient and wild type Hepa-1 cells: effects of hypoxia measured by 1H magnetic resonance spectroscopy. *Metabolomics* **1:** 293-303.

Vo TD, Greenberg HJ, Palsson BO (2004) Reconstruction and functional characterization of the human mitochondrial metabolic network based on proteomic and biochemical data. *J Biol Chem* **279:** 39532-39540.

Wadley GD, Lee-Young RS, Canny BJ, Wasuntarawat C, Chen ZP, Hargreaves M, Kemp BE, McConell GK (2006) Effect of exercise intensity and hypoxia on skeletal muscle AMPK signaling and substrate metabolism in humans. *Am J Physiol Endocrinol Metab* **290:** E694-702.

Weljie AM, Newton J, Mercier P, Carlson E, Slupsky CM (2006) Targeted profiling: quantitative analysis of 1H NMR metabolomics data. *Anal Chem* **78:** 4430-4442.

Wingrove JA, O'Farrell PH (1999) Nitric oxide contributes to behavioral, cellular, and developmental responses to low oxygen in Drosophila. *Cell* **98:** 105-114.

Chapter IV –

Metabolomic and flux-balance analysis of aging and hypoxia tolerance in *Drosophila* muscle tissue

Abstract

The fruit fly *D. melanogaster* is increasingly used as a model organism for studying acute hypoxia tolerance and for aging, but the interactions between these two factors are not well known. Here we show that hypoxia tolerance degrades with age in post-hypoxic recovery of whole-body movement, heart rate and ATP content. We previously used ^{1}H NMR metabolomics and a constraint-based model of ATP-generating metabolism to discover the end products of hypoxic metabolism in flies and generate hypotheses for the biological mechanisms. We expand the reactions in the model using tissue- and age-specific microarray data from the literature, and then examine metabolomic profiles of thoraxes after 4 hours at 0.5% O_2 and after 5 minutes of recovery in 40- versus 3-day-old flies. Model simulations were constrained to fluxes calculated from these data. Simulations suggest that the decreased ATP production during reoxygenation seen in aging flies can be attributed to reduced recovery of mitochondrial respiration pathways and concomitant over-dependence on the acetate production pathway as an energy source.

IV.1 Introduction

Aging is universal to eukaryotic organisms, and at the cellular level its effects are global, reaching virtually all cellular processes. Normal function deteriorates with age, but more dangerous is the loss of ability to respond to external stresses, contributing to a higher risk of death from external causes (Rose, 1991). Of particular interest is the age-related decline of cellular hypoxia tolerance, since hypoxic damage to heart and brain tissue is the source of pathology in heart attacks and strokes. In the heart, both the incidence and mortality of ischemic events worsen with age (Bonow et al., 1996). Currently there is a need for preventative measures to improve tolerance to ischemia-reperfusion injury in high-risk patients. The fruitfly *Drosophila* presents a possible source of new discoveries, since it shares fundamental oxygen regulation pathways with humans but is highly tolerant to hypoxia stimuli (and accompanying reoxygenation as well) (Krishnan et al., 1997). *Drosophila* is also a common model for aging research, and relationships have begun to be explored between aging and chronic hypoxia tolerance (Vigne & Frelin, 2007), and between aging and oxidative stress (Zou *et al.*, 2000). However, the interaction between aging and acute hypoxia tolerance in flies has not yet been investigated.

The exact mechanism whereby reversible hypoxic tissue damage finally evolves into irreversible damage is still controversial (Opie, 1998a)**,** but is likely to involve both necrotic and apoptotic mechanisms, stemming from metabolic stresses introduced during reperfusion as well as the ischemic event itself. Reduced O_2 causes reduction in oxidative metabolism and increased dependence on glycolysis.

Under normal conditions of mild hypoxia and steady ATP demand, such as in highly active muscle tissue, consumption of protons by oxidative pathways cannot keep up with protons produced by ATP hydrolysis and a reversible state of acidosis results (Robergs et al., 2004). Contractile machinery and metabolic enzymes are negatively regulated by acidosis (Opie, 1998a). In severe hypoxia, ion pumps are inhibited by depletion of ATP. Ion pump inhibition causes decreased uptake of calcium by the sarcoplasmic reticulum and reduced extrusion from the cell (Steenbergen et al., 1987), and this calcium accumulation can damage mitochondria. Upon reperfusion, the cell experiences sudden oxygen influxes that its inactive oxidative pathways and damaged mitochondria cannot immediately metabolize, resulting in the creation of reactive oxygen species (Ambrosio et al., 1987). It has been suggested that one way that hypoxia tolerant organisms prevent these dangerous imbalances by rapid and global regulation of metabolism (Hochachka, 1980; Hochachka, 2003).

All animals have complex, multiscale systems for regulating oxygen homeostasis (Hochachka & Somero, 2002). At the cellular level, hypoxia resistance mechanisms most likely evolved very early and appear to be highly conserved among species (O'Farrell, 2001). Supporting this hypothesis, several fly genes have been discovered that are similar in sequence and function to human genes for regulation of metabolism, signaling, and transcription during hypoxia (Lavista-Llanos et al., 2002; Pan & Hardie, 2002; Wingrove & O'Farrell, 1999). Although the hypoxia response in flies and humans seems to share similarities at the level of individual genes, stark contrasts exist at the phenotype level. Flies have a remarkable tolerance to hypoxia that is the subject of an increasing amount of investigation. In contrast with humans, who can only survive a few minutes without oxygen, flies can fully recover from up to 4 hours in complete anoxia (Krishnan et al., 1997). Genetic determinants of fly

hypoxia tolerance have been discovered by genetic screens (Haddad et al., 1997), and one enzyme unique to *Drosophila* increased hypoxia tolerance when transferred to human cells (Chen et al., 2003). Flies' innate hypoxia tolerance can be further improved by directed evolution, and gene deletions mimicking these evolutionary changes in gene expression improve tolerance in wild-type flies (Zhou et al., 2007).

The fruitfly is also one of the principal model organisms used for studying the genetics of aging, for a number of reasons. Flies develop to adulthood quickly, have a short life span, and share a number of characteristics of functional senescence with humans (Grotewiel et al., 2005). Little is known about how aging degrades hypoxia defenses. However, aging is well known to profoundly affect metabolism, and metabolism plays a central role in genetic interventions on the aging process. In fact, many of the best characterized genes that can accelerate or retard aging in model organisms act on the insulin pathway and on mitochondria and are studied in flies (Giannakou & Partridge, 2007). Heart and muscle tissue are good indicators of functional senescence since they have a single functional purpose (contraction) which is highly dependent on metabolic regulation, and they have easily quantifiable phenotypes in flies (heart rate and physical activity). Another advantage of using fruitflies to study muscle tissue biochemistry is that the fly thorax is composed primarily of flight muscle by mass, which allows for easy dissection of relatively large numbers of flies with fairly high specificity for muscle tissue. (However, it must be noted that an unavoidable limitation of using whole thoraxes is that there will be some contamination with hemolymph and other tissue.)

The physiological effects and responses to extreme oxygen conditions can manifest on many biological levels. Because metabolites are downstream of gene

transcripts and proteins, changes in metabolite levels can provide an indication of the overall integrated response of an organism. To obtain a better understanding of the system-wide effects of hypoxia on fly muscle tissue, we use NMR spectroscopy to simultaneously measure many metabolites present in the tissue and their changes in response to hypoxic stress, as described previously (Feala et al., 2007). This approach, termed metabolomics, is complementary to genomics and proteomics in studying the complex biological system response to chemical, physical, and genetic factors (Goodacre et al., 2004; Griffin, 2003; Griffin & Bollard, 2004; Nicholson & Wilson, 2003). The simultaneous measurement of a large number of metabolites, in combination with the use of a constraint-based computational model, allows us to quantify global changes in metabolite fluxes.

The present study investigates how aging affects the metabolic response to hypoxia in *Drosophila melanogaster*. First, we exposed young and old flies to severe hypoxia and compared the age-related degradation in physiological recovery at the levels of the organism (whole-body activity), organ (heart rate), and cell (ATP content). Then, for both age groups, we gathered metabolite profiles during hypoxia and recovery and compared these to an untreated control. Metabolite fluxes were calculated for hypoxia and recovery and integrated into the model, then simulations of network function were inspected for differences in key fluxes such as ATP, H^+, and glucose. This analysis generated hypotheses for mechanisms of the loss of hypoxia tolerance with age, and these hypotheses were checked for consistency against existing transcription profiles of young and old flies (Girardot et al., 2006). The results show the utility of NMR metabolomic profiling for characterization of the instantaneous physiological condition, enabling direct visualization of the perturbation of, and return to, homeostasis.

IV.2 Materials and Methods

IV.2.1 Fly preparation

Oregon-R wild-type flies were reared in constant light at 25° C and food was changed twice a week. Young flies (referred to as “3 day” or “3d” elsewhere in the text) were harvested for experiment at 3-5 days of age, and old flies (“40 day” or “40d” in the text) were collected at 38-42 days old. Because of the relatively small number of females surviving to 40 days of age, only males were used for experiment.

IV.2.2 Hypoxia experiments

The hypoxia experiments included five samples each of 3 conditions: control, 4-hour hypoxia, and 4 hours of hypoxia plus 5 minutes of recovery. A hypoxia chamber was created using four Sarstedt 50 mL plastic tubes. Two holes were drilled into the screw caps of the tubes and rubber hosing was inserted into each hole and sealed airtight with silicone adhesive. The hosing from the four tubes was then connected in parallel to a single inflow and a single outflow hose. At the time of experiment, filter paper was soaked in distilled water and placed in each tube to prevent drying. Approximately 50 flies were transferred into each tube, with two of the tubes containing young and two containing old flies. A mixture of nitrogen and 0.5% oxygen was then bubbled through distilled water and passed through the tubing into the vials. After circulating gas through the tubes for 15 minutes, the inflow and outflow hoses were sealed airtight with clamps, with the inflow sealed an instant before outflow in order to equalize the chamber pressure to the atmosphere. Control flies were similarly transferred from food vials and sealed in tubes with room air over the same time period in order to control for the effects of starvation and dehydration. Vials were lightly shaken to increase spacing among the immobile flies and stored on

their side at 25º C. For the 5-minute recovery group, tubes were opened and exposed to room air after the 4-hour hypoxia duration.

For NMR and biochemical assays, vials were snap frozen in liquid nitrogen at the end of each time point and shaken to remove heads, legs, and wings. For each sample, 20 male thoraxes were separated from abdomen with microforceps on dry ice under a dissecting miscrosope and stored at -80° C until measurement.

IV.2.3 Heart rate measurement

Baseline heart rate was measured as described previously (Broderick et al., 2006; Paternostro et al., 2001). Briefly, 10 flies were anesthetized with triethylamine (Carolina Biological), and mounted on their backs on microscope slides using double-sided tape. Custom software and a motorized stage were used to locate and record the position of the heart, then draw a virtual line of pixels across the heart walls. Microscope recordings of the pixel values along this line were concatenated to create time-space (M-mode) image representations of heart wall motion, from which heart rate was extracted by custom image analysis algorithms.

The slide was placed in the custom hypoxia chamber for 4 hours as described above, then removed and M-mode images of the fly hearts were again recorded over the first 20 minutes of recovery. Since flies were exposed to room air simultaneously and therefore had to be measured in parallel, the software automatically multiplexed measurements by rotating through the 10 saved heart positions, recording four-second M-mode images each time. The time from exposure to room air was recorded alongside each image, then image data were binned into four 5-minute periods. Heart rate for each fly was calculated as the inverse of the average beat-to-beat interval

over the first 5 minutes, normalized to baseline values, and this statistic was compared for the two age groups by the t-test.

IV.2.4 Whole body recovery

In whole-body recovery experiments, flies were exposed to hypoxia as described above, except that at the 4-hour timepoint flies were transferred to a lit surface where 10 males from each age group were chosen at random and separated with a paintbrush from the population. Recovery period, or the time from exposure to room air until the fly was standing upright on all legs, was recorded for each fly. Kaplan-Meier estimates and 95% confidence intervals for the cumulative distribution function were calculated using Matlab (MathWorks, Cambridge MA).

IV.2.5 NMR preparation

Thoraxes were homogenized in an ice bath for 3 minutes in 300μL of cold 1:1 acetonitrile:water buffer, using an OMNI TH homogenizer. Homogenates were centrifuged in a ice bath (4º C) for 10 minutes at 12,000 RPM. 10μL of the supernatant was used to determine the total protein concentration by the Bradford methods. For the Bradford assays, samples were diluted 10 times with extraction buffer. The supernatant was ultracentrifugated for 30 minutes at 8,500 RPM using Nanosep centrifugal devices (Pall Life Sciences, Ann Arbor, MI) with a 3 kDa molecular weight cutoff. To reduce the contamination by glycerol, a membrane wetting agent, to below 80μM, all Nanosep devices were washed 4 times (by 5 minutes centrifugation at 13,000 RPM) with 500μL deionized water. Filtrate was lyophilized using a vacuum centrifuge for 2 hours at 45° C. Samples were stored at -80° C until measured.

IV.2.6 NMR spectroscopy and data analysis

Dried samples were dissolved in 500µL D_2O buffered at pH 7.4 with monobasic/dibasic sodium phosphate. The NMR standard TSP (3-trimethylsilyl-$^2H_4$-propionic acid) was added to the samples at a ratio of 1:100 by volume, resulting in a concentration of 0.488 mM. Analyses of samples were carried out by ^1H NMR spectroscopy on a Bruker Avance 500 operating at 500.13 MHz 1H resonance frequency. The NMR probe used was the 5 mm TXI 1H/2H-13C/15N Z GRD. All NMR spectra were recorded at 25° C. Typically ^1H were measured with 512 scans into 16384 data points, resulting in an acquisition time of 1.36 seconds. A relaxation delay of 2 seconds additionally ensured T1 relaxation between successive scans. Solvent suppression was achieved via the Noesypresat pulse sequence (Bruker Spectrospin Ltd.) in which the residual water peak is irradiated during the relaxation and mixing time of 80 µs. All ^1H spectra were manually corrected for phase and baseline distortions within XWINNMR™ (version 2.6, Bruker Spectrospin, Ltd.). Two-dimensional NMR methods including homonuclear correlation spectroscopy (TOCSY) and heteronuclear single quantum correlation spectroscopy (HSQC) were carried out in order to identify and subsequently confirm the assessment of metabolites. Peaks in the 1D spectra were identified, aligned, and quantified by “targeted profiling” algorithms (Weljie et al., 2006) within the software Chenomix NMR Suite 4.5 (Chenomix, Inc.). The list of metabolites discovered in the 2D spectra was used to guide quantification in one dimension.

IV.2.7 Standards and scaling factors for metabolite concentrations

In NMR spectra, the peak integrals relate directly to the number of protons giving rise to the peak, and hence to the relative concentrations of the substances in the sample. Absolute concentrations can be obtained if the sample contains an added

internal standard of known concentration, or if the concentration of a substance is known by independent means (e.g., glucose determination by biochemical assay)

To determine absolute concentration of the 10 metabolites included in the model (alanine, lactate, glutamine, glutamate, glucose, pyruvate, proline, oxaloacetate and 4-aminobutyrate), a known concentration standard was acquired under the same experimental conditions and scaling factors were calculated for each metabolite.

50μL of 10mM freshly made solution of each standard was added to 450uL of D_2O buffered at pH 7.4 with monobasic/dibasic sodium phosphate containing 0.488mM of TSP (3-trimethylsilyl-$^2H_4$-propionic acid). Acquisition of the standards were carried out as described in the previous paragraph in duplicate, and quantified using the software Chenomix NMR suite 4.5 (Chenomix, Inc). The ratio $[Std]_{Chenomix}/[Std]_{solution}$ is defined as the scaling factor and is reported as the average the 2 experiments.

IV.2.8 ATP assay

Twenty thoraxes from 3 days old flies or 40 days old males flies were homogenized in 300μL of 6M-guanidine-HCl in extraction buffer (100mM Tris-Acetate and 2mM EDTA, pH 7.75) to inhibit ATPase (Schwarze et al., 1998) and placed at 95°C for 5 minutes. The samples were then centrifugated in a cold room for 10 minutes at 12,000 RPM and the supernatant was diluted 500 times with the extraction buffer and mixed with luminescent solution (ATPLite, Perkin Elmer). The luminescence was measured by a luminometer (BT) and results were compared to the standards. The relative ATP level was calculating by dividing the luminescence by the total protein concentration.

IV.2.9 Glycogen and Trehalose assay

Glycogen and trehalose concentrations are difficult to quantify by our NMR assay. Trehalose, although visible in the spectra, binds proteins with high affinity and thus a highly variable proportion is filtered from the supernatant along with the soluble proteins. Glycogen can also be seen in the spectra, but cannot be quantified due to the variable lengths of each polymer chain. Therefore, these important substrates were measured biochemically.

Twenty thoraxes from 3 days old flies or 40 days old males flies were homogenized in an ice bath for 3 minutes in 300μL of 0.25M Na_2CO_3 using an OMNI TH homogenizer and incubated at 95°C for 2 hours to denature proteins. Aqueous solutions of 1M of acetic acid (150μL) and 0.2M of sodium acetate (600μL) were mixed with the homogenates and the suspensions were centrifugated for 10 minutes at 12,000 RPM. 100μl of the supernatant were placed in eppendorf to determine the glucose background. 200μL of supernatant were incubated overnight at 37°C with trehalase solution (0.05U/mL in 0.2M sodium acetate pH: 5.2).(Schulze et al., 1995) Glycogen was assayed using the method developed by Keppler and Decker (Keppler & Decker, 1974) with some modifications. 50μL aliquots were incubated with 500μL of an *A. niger* glucoamylase solution (8.7U/mL in 200mM of Acetate buffer pH: 4.8) for 2 hours at 40°C under constant agitation. The suspensions were centrifugated for 5 minute at 4000 RPM and glucose was determined on 20μL of supernatant by addition of 170μL of a G6-DPH (0.9U/mL)/ATP (1.6mM)/NADP (1.25mM) mixture in triethanolamine hydrochloride buffer (380mM TEA.HCl and 5.5mM of $MgSO_4$, pH: 7.5) and 10μL of Hexokinase solution (32.5U/μL in 3.2M ammonium sulphate buffer pH:6) and read at 340nm in a SpectraMax 190 (Molecular Device).

IV.2.10 Statistical analysis

Student's t-test were performed to compare means between 2 samples. $P<0.05$ were considered statistically significant. For analysis of the NMR data, Bonferroni t-tests were performed. Furthermore, for every metabolite with at least one measurement above 0.01 mM, an analysis of variance (ANOVA) was performed, with a Bonferroni correction applied to the p-value for the number of metabolites tested. Tukey's post-hoc tests were performed for metabolites, in which the null hypothesis of no change with treatment was rejected by ANOVA, for cross-comparison of each treatment. All statistical analysis were performed using GraphPad Prism software.

For the Principal Component Analysis, all metabolites with at least one measurement above 0.01 mM were included in the dataset. Each sample was normalized by protein content measured by the Bradford assay, and selected metabolites were scaled using standards as described above. Data from all samples (young and old; control, hypoxia and recovery) were combined into one matrix and principal components were computed using the princomp function in Matlab (Mathworks, Inc., Cambridge, MA). Principal component scores for the samples were plotted and visualized within Matlab.

IV.2.11 Expanding the metabolic network reconstruction

Our reconstruction of the central, ATP-generating metabolic network of Drosophila flight muscle, (described in Feala et al., 2007), was expanded and refined using the absolute gene expression profile derived from an Affymetrix microarray of whole thorax in 3-day old flies (Girardot et al., 2006). Raw microarray data were combined with Affymetrix Drosophila Genome 2.0 annotation files to obtain gene identifiers, which were then linked to reactions and pathways of the KEGG database

(Kanehisa et al., 2008; Kanehisa & Goto, 2000) using the dme_pathway.list and dme_enzyme.list batch files downloaded from the KEGG FTP server[1]. Genes from the microarray dataset were grouped by whether they had a KEGG identifier, and those existing in the KEGG database were further grouped by pathway. Mean expression levels in 3-day thorax were calculated for each KEGG pathway containing more than one Drosophila gene. Pathway expression levels were also visualized on KEGG pathway diagrams using the G-language Microarray System[2] (Arakawa et al., 2005) on log-transformed expression data, which were re-scaled to range from 0 to 100 in order to fit the input format of the web service. The list of pathways with mean expression level greater 500 were visualized with this system and also investigated by a literature survey in order to determine whether to include the pathway in the model. The list of all Drosophila genes in KEGG was also sorted by thorax expression level and genes with expression levels greater than 500 were manually examined by literature and database search to determine inclusion in the model. Genes and reactions were entered into the model using the SimPheny biological database software (Genomatica, San Diego).

IV.2.12 Flux-balance analysis

Metabolite concentrations for the three experimental conditions (control, 4-hour hypoxia, 5-minute recovery) were converted into two sets of fluxes by dividing the differences in mean concentrations by the time period, resulting in units of nmol*mg $prot^{-1}$*min^{-1}. Standard errors (SE) of the metabolite fluxes were calculated from SE of the concentrations (using the formula $SE_{C2-C1} = \sqrt{[SE_{C1}^2 + SE_{C2}^2]}$ for

[1] ftp://ftp.genome.jp/pub/kegg/genes/organisms/dme
[2] http://www.g-language.org/data/marray

subtracting random variables for concentration C_1 and C_2) and converted to the same units. Eleven compounds with measured hypoxia fluxes above .05 nmol*mg prot-1*min-1 were included in the model except for glycerol, which was contaminated by glycerol coating on the membrane filter, and β-alanine, a structural amino acid which saw a reverse flux during recovery that was unfeasible to incorporate in the current version of the model. Fluxes of glycogen and free glucose were similarly estimated from the biochemical assays. Metabolite pools were then simulated in the model by creating a sink for each compound and forcing fluxes into/out of the system to the values calculated from the data.

Flux-balance analysis was performed to simulate system flux distributions during hypoxia and recovery for both young and old flies. The objective function in all simulations was the reaction representing utilization of ATP via hydrolysis. The SimPheny software was used for initial flux-balance calculations and for visualizing superimposed fluxes on the metabolic network.

We used Matlab (Mathworks, Inc., Cambridge MA) to analyze the sensitivity of flux distributions to variance in the data. The COBRA toolbox for constraint-based analysis (Becker et al., 2007) was used to import the SimPheny simulations and run flux-balance analysis within Matlab. Then, pseudo-random sets of fluxes were created by sampling normal distributions with mean and standard errors equal to those calculated for each metabolite flux. A group of 10,000 random flux sets was created for each of the four experimental conditions (old and young, recovery and hypoxia). Virtual “sinks” with unlimited capacity were created for each compound in order to represent metabolite pools, allowing intracellular accumulation and depletion in case substrates and end products did not perfectly balance. For each sampled set,

fluxes into and out of the metabolite pools were constrained to the randomly selected fluxes and flux-balance analysis was performed.

IV.3 Results

IV.3.1 Post-hypoxic recovery of physiological function

The advantages of using Drosophila to study mechanisms of aging are further enhanced by the many similarities in age-related degradation of function between flies and humans. For example, we previously found that flies experience a decline in maximum heart rate with age that is similar to humans (Paternostro et al., 2001). Grotewiel et. al. (2005) review other age-related declines in flies, including motor activity, stress response (including oxidative stress), and ATP production. We examined the senescence of the physiological response to hypoxia in three different experiments on young (3-day-old or “3-day”) and old (40-day-old or “40-day”) flies.

Flies respond to acute hypoxic stress by falling into a motionless, prostrate stupor, from which they can fully recover after several minutes (Haddad et al., 1997b). Aging significantly delayed the recovery of whole-body activity after extreme hypoxic stress (4 hours at 0.5% O2, N = 16 males each group) according to Student’s t-Test. Figure IV.1A depicts the cumulative recovery to standing position for each group, with Kaplan-Meier estimates of 95% confidence intervals. Young flies began to return to standing position after an interval of 32 minutes post-hypoxia, with approximately 2/3 arousing within the first 2 hours. Old flies remained motionless for the first 4 hours post-hypoxia, with 2/3 arousing within 8 hours. After 24 hours, the percent of fully recovered flies was equivalent between the two age groups.

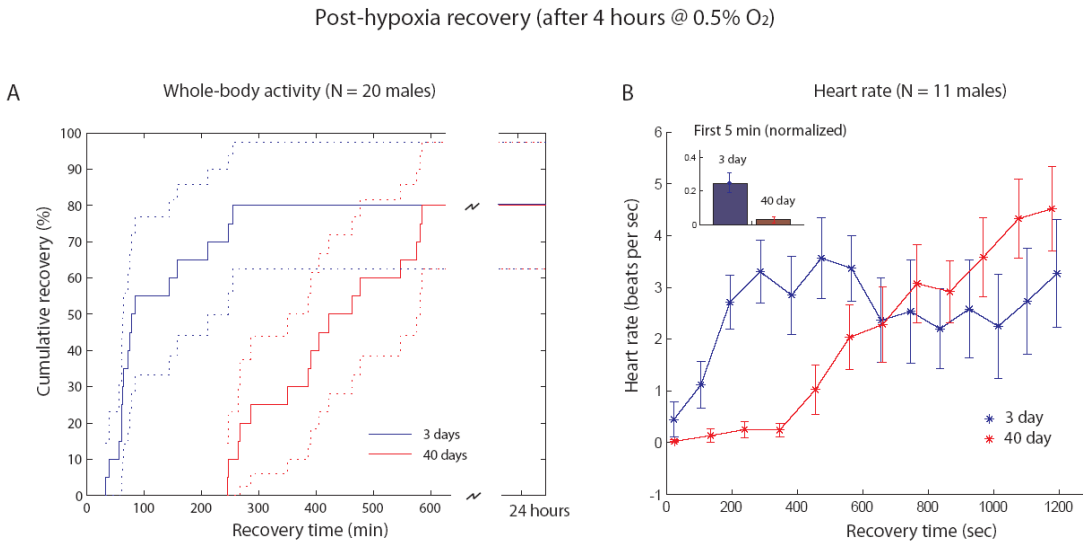

Figure IV.1: Recovery of physiological function in flies after severe hypoxic stress.

A) Whole body recovery was defined as time taken to recover from hypoxic stupor to a standing position. Old flies took 2 to 3 times longer to recover than young after 4 hours of 0.5% oxygen.

B) The hearts of young flies began beating again immediately on reoxygenation, while older fly hearts remained inactive for nearly 5 minutes. (inset) When heartbeats during the first 5 minutes were binned, 3-day-old heart rates were significantly higher ($p<0.05$). In both age groups, hearts had stopped by the end of the hypoxic period.

Recovery of heart activity after the same treatment followed a similar trend, though on a different timescale (shown in Figure IV.1B, N = 11 males for each group). The fly has a tube-like heart that normally contracts at 6 to 8 beats per second (bps). At the end of the hypoxic period, the hearts of both young and old flies were completely stopped. In young flies, the heart began slowly beating within the first minute, increasing quickly to approximately 3 bps in the third minute, then maintaining a range between 2 and 4 bps for the remainder of the 20 minute measurement

duration. In contrast, older hearts remained mostly motionless for the first 6-7 minutes, and then steadily recovered over the remaining interval. Heart rates for both groups eventually recovered to baseline levels, but this happened over a longer timescale than presented here (the measurement duration was limited for technical reasons). Inverse beat-to-beat intervals binned over the first 5 minutes of measurement and normalized to baseline were significantly different ($p < 0.05$) by Student's t-test (Figure IV.1A).

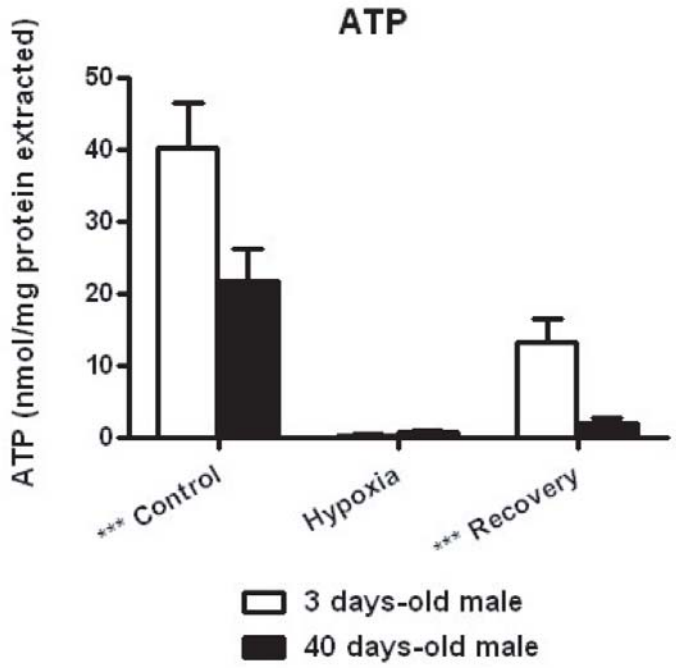

Figure IV.2: ATP concentrations in young and old fly thoraxes after a control period, at the end of hypoxia (4 hours at 0.5% O_2) and after 5 minutes of recovery. Concentrations are normalized to protein content. Differences are statistically significant ($p<0.01$) for control and recovery measurements, but not for hypoxia.

Similarly, we measured ATP concentrations in flies at baseline, at the end of a 4-hour hypoxia stimulus and after a 5-minute recovery period – reflecting the time period seen in the heart recovery data (Figure IV.2). Under normal oxygen, ATP concentrations are 1.8-fold higher in 3-day than 40-day flies (P=0.006). However, at end of the hypoxia treatment, ATP levels are very low and equivalent in the two age groups. When the flies are allowed to recover, ATP concentration is 6.6-fold higher in 3-day flies than 40-day ones (P<0.001).

IV.3.2 Metabolite Assays

IV.3.2.1 Glycogen, glucose and trehalose

Glycogen, free cellular glucose, and trehalose are the major sources of carbohydrate fuel in flight muscle in many Diptera such as bees and blowflies (Childress et al., 1970; Suarez et al., 2005), and are likely to be for *Drosophila melanogaster* as well. The large deposits of glycogen in flight muscle of flies, the depletion of these reserves after prolonged flights, and the rapid catabolism of the polysaccharide by flight muscle *in vitro*, indicate that glycogen provides a major vehicle for storage of sources of potential energy which can be mobilized to meet the metabolic requirements of active muscle (Sacktor & Wormser-Shavit, 1966). The disaccharide trehalose can also support flight activity; it was identified as the principal blood sugar in many species of insects, was found in muscle, was found to be reduced in concentration within these loci after flight, and was metabolized in vitro by flight muscle.(Sacktor & Wormser-Shavit, 1966)

Glycogen and trehalose concentrations are difficult to quantify by our NMR assay. Trehalose, although visible in the spectra, binds proteins with high affinity and thus a highly variable proportion is filtered from the supernatant along with the soluble

proteins. Glycogen can also be seen in the spectra, but cannot be quantified due to the variable lengths of each polymer chain. Therefore, these important substrates were measured biochemically, following enzymatic assays developed by Parrou (Parrou & Francois, 1997).

As for ATP, we measured glycogen concentrations in flies at baseline, at the end of a 4-hour hypoxia stimulus, and after a 5-minute recovery period (Figure IV.3). Glycogen was found to be the major source of fuel used by young and old flies to produce glucose under hypoxic conditions, with concentrations decreasing greatly as the substrate was consumed over the hypoxia duration. In both age groups, hypoxic trehalose levels were not statistically different from the ones measured under normoxia, and further there were no significant differences across age groups for the two treatment conditions. Old flies showed consumption of glycogen and trehalose during the recovery period (p = 0.004 for glycogen and p = 0.005 for trehalose.)

IV.3.2.2 ^{1}H NMR metabolomics

NMR spectra were used to quantify free metabolite concentrations in samples of 20 fly thoraxes, homogenized, filtered of protein, and buffered in 500µL of D_2O (see Materials and Methods). Of 37 metabolites identified, 26 had at least one measurement higher than our measurement threshold of 10µM (in the D_2O homogenate). Free glucose was measured by both NMR and biochemical assays, allowing us to check for consistency in the data. Glucose concentrations had similar qualitative behavior in both datasets, increasing in young flies during hypoxia and then returning toward baseline levels during recovery, while in old flies remaining steady during hypoxia but decreasing during recovery.

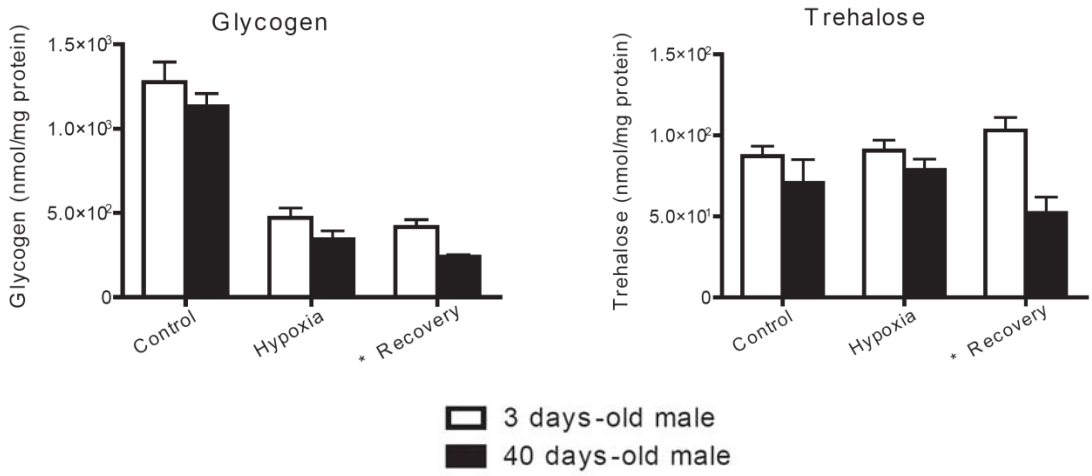

Figure IV.3: Glycogen and trehalose concentrations in young and old fly thoraxes after a control period, at the end of hypoxia (4 hours at 0.5% O_2) and after 5 minutes of recovery. Concentrations are normalized to protein content. Differences between the ages are statistically significant ($p<0.05$) for recovery measurements, but not for hypoxia or control periods.

Metabolomics experiments generate multivariate data, which complicate statistical analysis by typically having a larger number of variables than experimental samples. Principal component analysis (PCA) is a vector transformation that can reduce this high dimensionality by projecting the data "cloud" (each point in the cloud representing a data sample) onto new axes in the multivariate space. The new axes are an orthogonal set of basis vectors that are a weighted composite of the variables (in this case, metabolites).

We applied PCA to the metabolomic profiles of young and old flies. When plotted on their principal components (Figure IV.4A), young and old flies had very similar profiles in control and hypoxic conditions, with large shifts on PC 2 during 4 hours hypoxia and smaller movements in the direction of PC 1. After 5 minutes in room air, both groups returned toward controls along the direction of PC 2, whereas

young flies continued to drift slightly along PC 1. Older flies had a pronounced movement along PC1 during recovery, corresponding to the large increase in acetate seen in NMR data.

Decomposition of the data by PCA captured nearly 80% of the variability of the concentration data with the first principal component (PC), with the second PC contributing another 15% to the total variability. Acetate production dominated PC 1, while alanine and lactate production were responsible for most of the changes on PC 2. Oxalacetate, glutamate, glucose, and glutamine had minor contributions to the two PCs (Figure IV.4B). Although similar conclusions can be drawn from direct inspection of the NMR profiles, PCA confirmed that these changes were the main sources of variability across the 6 datasets. In addition, the data show that acetate production is orthogonal to alanine and lactate, and may therefore be attributed to separate regulatory mechanisms.

Figure IV.4: (facing page) Principal component analysis of the metabolomics data.

(A) Data samples plotted along the first two principal components (PCs) showed a large separation between young and old flies during recovery but not for the control or hypoxic conditions. The differences between young and old flies are most prominent on PC 1, while the different experimental oxygen conditions are best separated along PC 2.

(B) The principal components are a composite of metabolite concentrations. PC 1 is dominated by acetate concentrations, while PC 2 has highest contributions from lactate and alanine. Other metabolites contribute small amounts to the vector weighting. (inset) The first two principal components represent over 95% of the variation in the data.

A

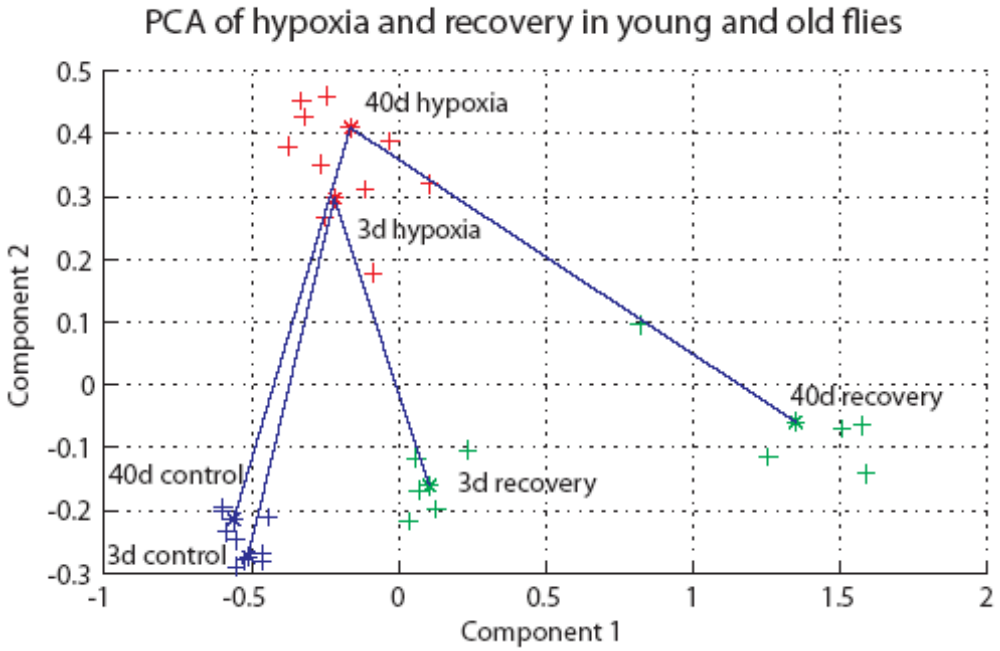
PCA of hypoxia and recovery in young and old flies
40d hypoxia
3d hypoxia
40d recovery
3d recovery
40d control
3d control
Component 2
Component 1
0.5
0.4
0.3
0.2
0.1
0
-0.1
-0.2
-0.3
-1
-0.5
0
0.5
1
1.5
2

B

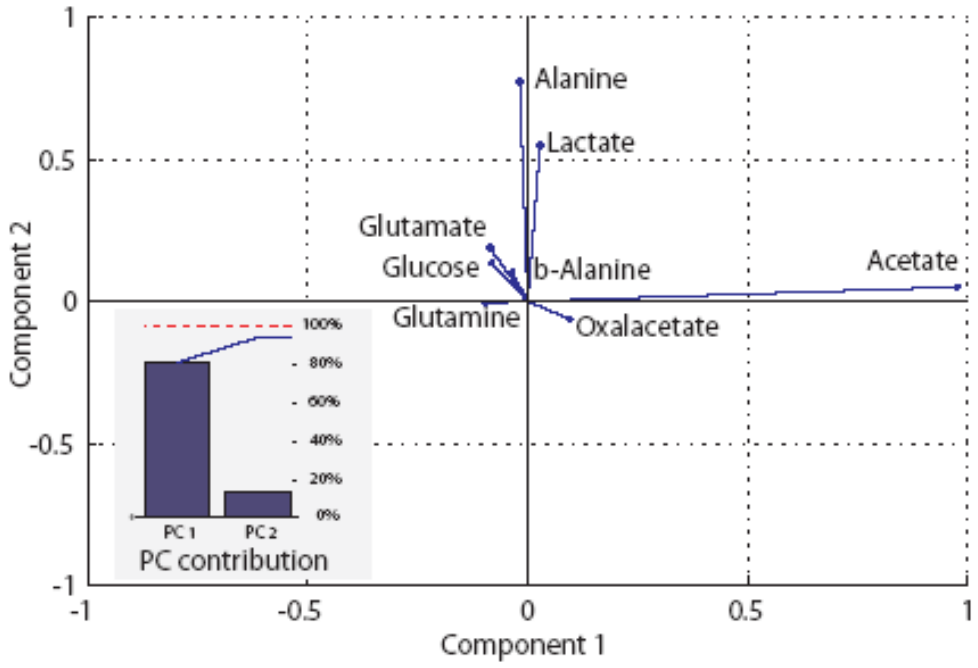
Composition of principal components
Alanine
Lactate
Glutamate
Glucose
b-Alanine
Acetate
Glutamine
Oxalacetate
100%
80%
60%
40%
20%
0%
PC 1
PC 2
PC contribution
Component 2
Component 1
1
0.5
0
-0.5
-1
-1
-0.5
0
0.5
1

One-way analysis of variance evaluated the effect of hypoxia treatment and recovery, independent of the age groups. Out of the 26 metabolites with concentrations above the 10μM threshold, only 10 were affected by the treatment ($p < 0.047$ with Bonferroni correction). As we reported previously, lactate, alanine and acetate are the major end products of hypoxic metabolism in Drosophila, and again were the only metabolites with large increases over the hypoxic duration in both young and old flies. On reoxygenation, fluxes reverse quickly and increase several hundred-fold, and we observed that most of the metabolites returned to control levels within the 5-minute measurement duration. However, as suggested by the PCA analysis, the acetate level continued to increase during recovery in both young and old flies.

We also employed the Student t-test to individually identify metabolites that significantly vary between old and young flies for each treatment. We noticed that during normoxia and hypoxia few metabolites vary significantly between age groups, even before Bonferroni correction for the number of metabolites. The highest confidence differences between the ages appear during the recovery period. After 5 minutes recovery under normal oxygen conditions, the lactate level returns to its normal value in young flies whereas in old flies it is still increased by 80% compared to control ($p = 0.005$). Both young and old flies continue to produce acetate during recovery, though old flies produce much more (young: +534% compared to control; old: +1800% compared to control, $p = 0.005$). It is also interesting to note that during recovery in old flies, oxalacetate concentration increased by 230% compared with control.

During hypoxia, the production of alanine is not matched by consumption of proline, as it is during aerobic exercise in insect flight muscle. In fact, amino groups do not balance in hypoxia or recovery for either age group, therefore protein degradation and formation may be a factor, respectively, under these conditions. Production or consumption of free amino groups was calculated during flux-balance analysis, described below.

IV.3.3 Metabolic reconstruction

In order to further refine our existing genome-scale metabolic reconstruction (Feala et al., 2007) for muscle tissue, we created a filtered gene list based on global gene expression measured in 3-day-old thoraxes by Girardot (2006). Since thorax tissue is composed mostly of flight muscle, highly expressed enzyme genes in this dataset could be added with confidence to our metabolic network. These data were measured on Affymetrix microarrays, which provide absolute measurements of mRNA levels.

Table IV.1: Comparison of Drosophila models

	Version 0.5 (Feala *et. al.*, 2007)	Version 1 (current)
Genes	169	211
Reactions	171	196
Metabolites	76	83
Pathways	Glycolysis TCA cycle Oxidative phosphorylation Fatty acid oxidation Proline degradation Alanine/glutamate met ROS detoxification	Glycolysis Gluconeogenesis Pentose phosphate shunt TCA cycle Oxidative phosphorylation Fatty acid oxidation Proline degradation Alanine/glutamate metabolism Glutamine metabolism Tyrosine/phenylalanine metabolism Aminosugar metabolism ROS detoxification Starch and sucrose metabolism
Average confidence 0-4 scale (non-transport rxns)	1.83	2.4

The histograms in Figure IV.5 display the distribution of the microarray data after filtering and integration with the KEGG Pathway Database. The distribution of thorax genes linked to at least one KEGG enzyme (Figure IV.5B) has an interesting bimodal distribution which is much less prominent in the histogram of all genes (Figure IV.5A). This “long tail” roughly corresponds to the threshold of expression (500) for inclusion into the model, which was determined empirically from a literature and database search of samples of genes at all levels of expression. The distribution of mean expression level for all KEGG pathways is shown in Figure IV.5C. The right tail of this distribution also seems to correspond to pathways known to be active in flight muscle tissue, as exemplified by the pathways labeled in the figure. Table IV.1 notes new pathways that were included in the model based on mean expression level. In all, 49 new genes and 38 new reactions were added to the model from the previous version, resulting in totals of 211 genes and 196 reactions. In addition, the new version contains many minor improvements to existing reactions, such as cellular compartment assignments and gene-protein-reaction associations, as well as the removal of enzymes and pathways with low expression levels. A complete map of the network is shown in Appendix C, along with a list of reactions.

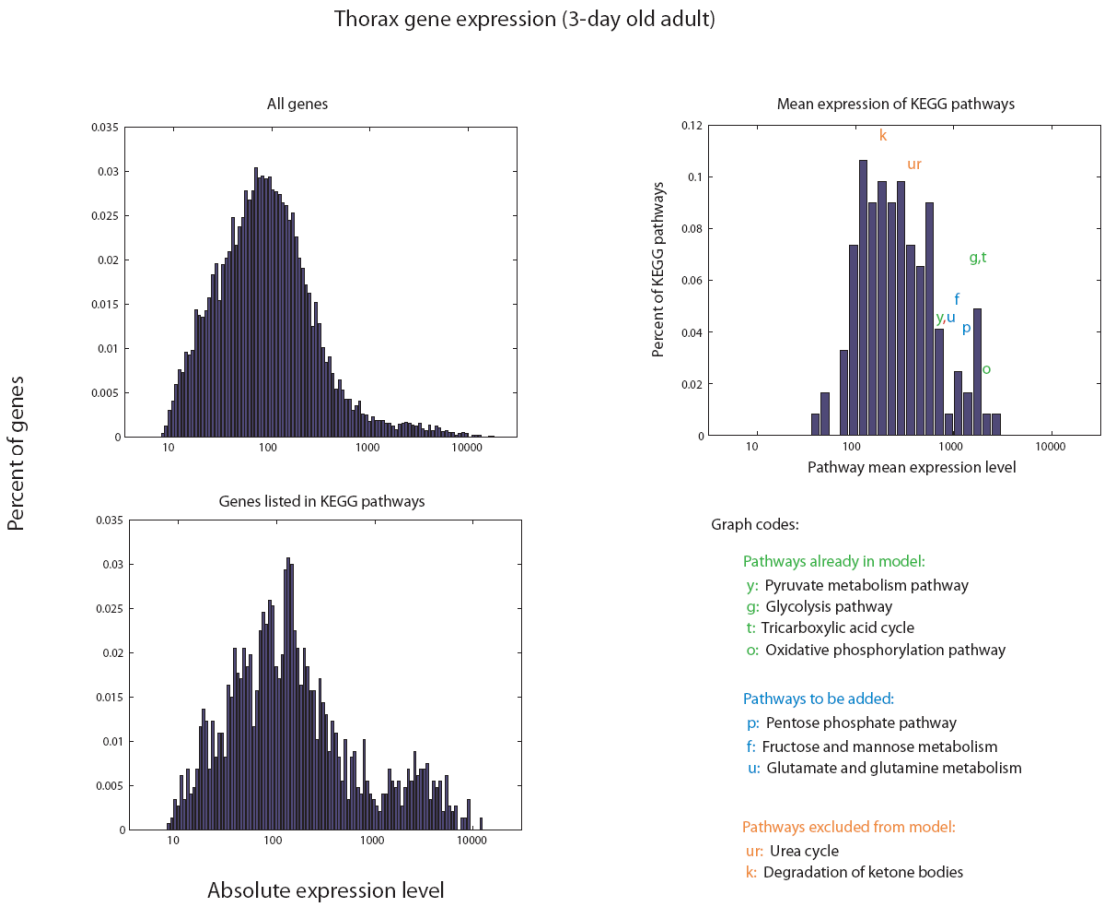

Figure IV.5: Histograms of absolute thorax expression data, filtered through the KEGG pathway database.

(Top left) Histogram of raw absolute expression data from 3-day-old thorax Affymetrix microarrays, after preprocessing and normalization described in (Girardot et. al., 2006) (Bottom left) Gene expression histogram for the subset of genes listed in at least one KEGG pathway. Note the accentuated "fat tail" of the filtered data, resulting in a slightly bimodal distribution.

(Top right) Mean expression levels of thorax genes for the 122 KEGG pathways. Selected pathways are color-coded according to inclusion in the model (based on literature data) and positioned above the bin that contains the corresponding average gene expression.

IV.3.4 Flux-balance analysis

Though a few *Drosophila* enzymes have been extensively studied, most of the reaction kinetics in fly central metabolism are unknown. To capture as wide a scope of pathways as possible, while avoiding the necessity of kinetic parameters, we instead applied flux-balance analysis to our network reconstruction. The major assumption in flux-balance analysis is that the system is at steady state, therefore intra-system metabolite concentrations do not change.

In addition to the steady state requirement, our analysis assumes that accumulation and depletion of metabolites are linear and unidirectional, i.e. fluxes are constant over the measurement period and there is no consumption of accumulating metabolites or synthesis of depleted metabolites. The fact that the heart stops beating during hypoxia supports the assumption that the cells use only the carbohydrate stores that we measure, and nutrients are not supplied by the fat body via recirculated hemolymph.

The model was constrained using data from eleven metabolites which were chosen based on the magnitude of the changes during hypoxia and recovery and the existence of each metabolite within the network. To increase accuracy of the simulations, absolute concentrations were estimated from the NMR spectra using correction factors as described in the Methods. For each metabolite selected, we approximated a flux by dividing the concentration differences by the experimental time period (4 hours for hypoxia, 5 minutes for recovery). Figure IV.6 (top row) shows estimated fluxes of these metabolites for each condition, derived from concentration data in the NMR and biochemical assays. Exchange reactions were added to the model and for each simulation their fluxes into or out of the system were constrained to approximate rates of accumulation or depletion.

Using the mean and standard error calculated for each flux, Gaussian distributions were constructed and sampled to create 10,000 sets of the eleven metabolite fluxes, which were then applied to the model to analyze the sensitivity of simulations to variation in the NMR data. All populations of fluxes for each reaction had approximately normal distributions. Figure IV.6 (bottom row) shows intrasystem fluxes calculated in flux-balance simulations. The variance of calculated fluxes is probably conservative in that each measured flux is treated as an independent random variable during sampling even though in the biological system there are likely many correlations among metabolites that are disregarded here. Intrasystem fluxes in the model follow the same pattern as the NMR data, with wide variances during hypoxia but much tighter distributions during recovery.

Except for glutamate degradation and the resultant production of ammonium, hypoxic fluxes were not significantly different between old and young flies (Figure IV.6 – left). The opposite signs of measured oxaloacetate fluxes drive a small set of anaplerotic reactions, involving glutamate, in different directions; however, the fluxes are small in both age groups. Young flies consume more free ammonium, driven by surplus production of alanine shown in the NMR data. However, some protein degradation, which was not included in this model, may partially account for the appearance of NH_4 not provided by free amino acids. Glycolysis and TCA cycle pathways are used at the same rate in young and old, although production of lactate is slightly higher in the old flies. Proton production and accumulation of anaerobic end products is high for both age groups. Surprisingly, calculations of ATP production during the hypoxic period were the same in old and young flies.

Figure IV.6 (facing page): Fluxes calculated from NMR data and by flux-balance analysis.

(Left) Fluxes during 4-hour hypoxia period.

(Right) Fluxes during 5-minute post-hypoxic recovery.

(Top) Fluxes calculated from NMR concentration profiles. These fluxes were applied to the model as constraints. Error bars mark standard errors derived from concentration measurements.

(Bottom) Fluxes calculated in flux-balance simulations. Error bars mark standard errors of simulations in sensitivity analysis.

Compound abbreviations: glcgn: glycogen, ac: acetate, ala: alanine, lac: lactate, abut: 4-aminobutyrate, glc: free glucose, glu: glutamate, gln: glutamine, oaa: oxaloacetate, pro: proline, pyr: pyruvate, o2: oxygen, co2: carbon dioxide, h2o: water, h: protons, nh4: ammonia. Reaction abbreviations: atps: ATP synthase, atp: total ATP production, nadh: NADH dehydrogenase, sucd: succinate dehydrogenase (Complex II), cyoo: cytochrome oxidase, pfk: phosphofructokinase, gpdh: glycerol-3-phosphate dehydrogenase, pyk: pyruvate kinase, pdh: pyruvate dehydrogenase, cs: citrate synthase, sucd: succinate dehydrogenase (TCA cycle), mdh: malate dehydrogenase.

Model flux summary

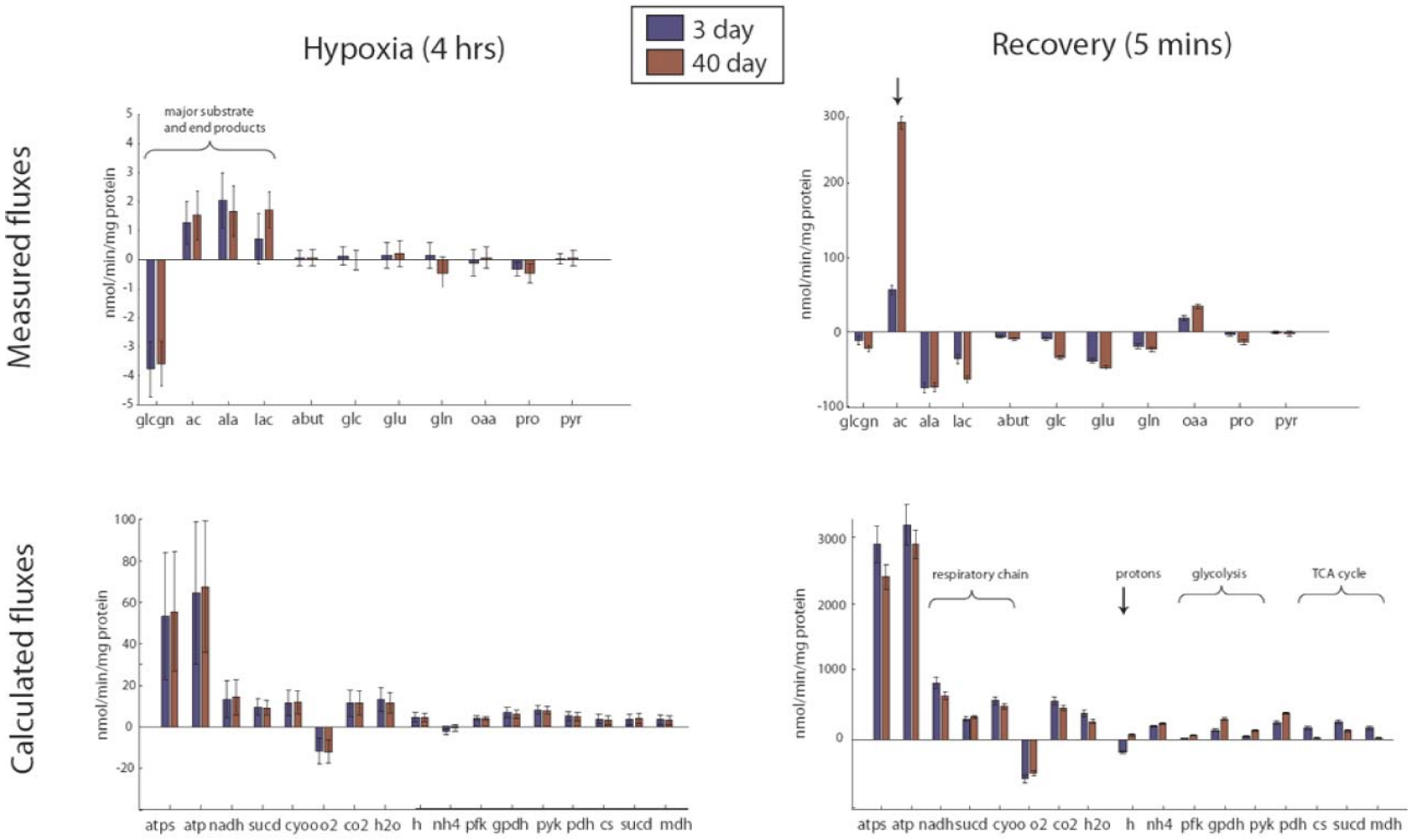

During recovery, intrasystem fluxes in the model show more drastic differences between the ages, especially in the recovery of oxidative pathways. Old flies show much higher acetate production during recovery, which causes the model to calculate slightly higher glycolytic fluxes and much lower TCA cycle fluxes due to the difference in acetyl-CoA conversion to acetate *versus* oxidation via the TCA cycle. As the flux map of Figure IV.7 shows, reduced activity of the TCA cycle diverts acetyl-CoA through the acetate pathway. Differences in ATP production during recovery are significant; however, the additional ATP from the cleavage of CoA makes up for some of the resulting loss of efficiency in carbon utilization. Due to the slow recovery of oxidative metabolism, proton fluxes are negligible in old flies, a marked difference from the proton consumption that occurs during recovery in 3-day flies. Table IV.II shows key fluxes and ratios from the simulations.

Table IV.2: Averages of key fluxes in the simulations

	3d hypoxia	**40d hypoxia**		**3d recovery**	**40d recovery**
Glucose	- 3.6	- 3.6		- 19.4	- 53.3
Oxygen	- 11.5	- 11.8		- 576	- 492
ATP	64.5	67.6		$3.17*10^3$	$2.89*10^3$
H+	4.1	4.1		-135	55.3

(-) = consumption; (+) = production.
glucose = free glucose + glycogen
units: nmol/min/mg prot

Figure IV.7 (facing page): Flux map comparing recovery fluxes in young versus old flies. Fluxes of young and old are represented by the red-green color scale, while color coding from black to yellow indicates a ratio of 1 over a large range of absolute flux values. Numerical flux values are printed next to reaction abbreviations. Major anaerobic end products are shown in blue.

Flux balance analysis of recovery from hypoxia: Young versus old flies

(simulations based on NMR fluxes at 5 minutes reoxygenation after 4 hours at 0.5% oxygen)

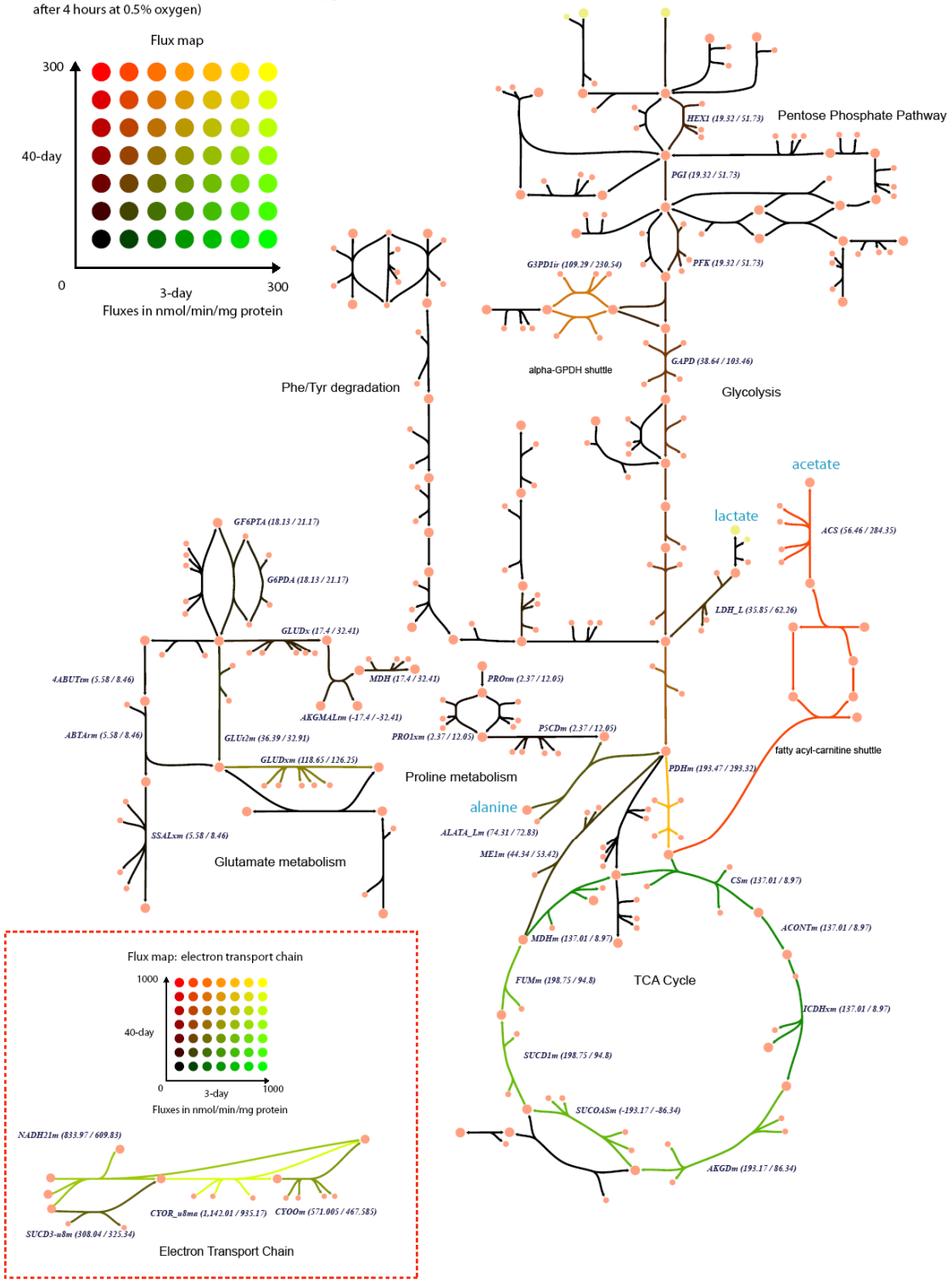

IV.4 Discussion

Aging causes deterioration of a variety of physiological functions at the organism level, which originate from global degradation and dysregulation at the cellular and molecular scale. The nature of aging as a genome-wide, multiscale phenomenon invites a systems-level approach to understanding the cellular mechanisms by which phenotypes degrade. In this study we have focused on hypoxia tolerance in Drosophila, which is notably higher than that of mammals but degrades similarly with age, as we show using three different physiological measurements at three different scales. Though our physiological phenotype measurements were not significantly different between young and old flies during hypoxia, upon reoxygenation the age groups had major differences. At the organism level, old flies have slower whole-body recovery of activity following hypoxic stress; at the organ level, post-hypoxic heart rate takes longer to recover in older flies; and at the cellular level, ATP levels are slower to recover after hypoxia in old flies.

We used metabolomic and computational analysis of muscle metabolism to search for clues as to the molecular basis for this delayed recovery. Global metabolite profiles were gathered during baseline, after a long hypoxic period, and then after a short recovery as in the physiological measurements, and the data were entered into our microarray-supported stoichiometric model of Drosophila central metabolism. Flux-balance analysis within this model, driven by flux estimates from the metabolic profiles, reiterated that the major differences in metabolic function between young and old flies occur on reoxygenation rather than during hypoxic stress. Further, the model also predicts that differences in recovery of mitochondrial respiration, and the

resulting effects on proton production and glucose utilization in old flies, may contribute to the differences in physiological recovery.

Aging is often described as a generalized deterioration of function but our results show that not all metabolic pathways are equally affected. The impairment in metabolic recovery after hypoxia seems to be mainly in pathways downstream of pyruvate (Krebs cycle and respiration) rather than in the anaerobic portion of glycolysis. In our model, the decline in respiratory function seems to account for most of the difference in hypoxia tolerance with age, which is widely supported by evidence that mitochondrial function plays a major role in the overall functional decline seen with age in *Drosophila* (Dubessay et al., 2007; Ferguson et al., 2005) similar to its role mammals (Kujoth et al., 2005; Martin, 2001; Martin et al., 2003; Trifunovic et al., 2004). Activity of electron transport chain enzyme complexes I, III, and IV decrease with age in flies although the expression of certain protein subunits of these complexes remains unchanged (Dubessay et al., 2007; Ferguson et al., 2005). Microarray (Girardot et al., 2006; Zou et al., 2000) and Northern blot (Dubessay et al., 2007) measurements of RNA expression suggest that transcript levels of TCA cycle and respiratory enzymes are highly downregulated with age. Glucose and glycogen consumption is necessarily higher, since all other catabolic pathways are less efficient in terms of ATP production. The decreased ADP/O ratios seen in mitochondrial assays of old flies (Dubessay et al., 2007) were not included in our model simulations, but would most likely only accentuate these results.

The specific cause of this decline in respiratory metabolism is still under investigation. Multiple intermittent reperfusions during anoxia causes injury in young flies, marked by lower rates of respiration on reoxygenation (Lighton & Schilman,

2007), which supports the hypothesis that fly mitochondria can be damaged by reactive oxygen species (ROS) created by oxygen reperfusion. In older flies, reduced respiration has been attributed to both a lifetime of accumulated damage from (Dubessay et al., 2007; Ferguson et al., 2005), and a chronically active response to (Zou et al., 2000), the generation of ROS in the mitochondria.

Another possible contributor to the physiological response to hypoxia in heart and muscle tissue is acidosis. The production of lactate, alanine, or acetate end products from pyruvate partially uncouples glycolysis from oxidative metabolism, causing an imbalance in proton production (by ATP hydrolysis) and consumption (by ATP synthase) (Robergs et al., 2004). Since acidosis negatively regulates contractility both at the sarcoplasmic reticulum and actin-myosin interaction (Opie, 1998b), heart rate and muscular activity would be expected to recover faster in the system that is quicker to reverse proton accumulation. Young and old flies produce an equivalent amount of protons during hypoxia, suggesting that acidosis is unavoidable even in hypoxia-tolerant organisms. However, after 5 minutes of reoxygenation, protons in 3-day flies are being consumed at a high rate by ATP synthase, while the model calculates nearly zero proton flux in 40-day flies. This, in combination with the lower rate of ATP production in old flies according to the model, can help to explain our observations of age-related differences in recovery of physiological functions. Our ATP assay also confirms slower restoration of ATP levels in older flies.

In anaerobic pathways, the major difference between old and young flies is in the production of acetate. Out of the three end products lactate, alanine, and acetate, acetate is the only compound still being produced during recovery, and the reason might be that the additional ATP and NADH per glucose created by this pathway

result in a better ATP/H^+ ratio than that of the other two pathways. Therefore, acetate production, in both young and old flies, may represent the most efficient utilization of any surplus pyruvate that exceeds the oxidative capacity of the recovering mitochondria at 5 minutes post-reperfusion. The model, which solves for the optimal flux distribution for ATP production, supports this hypothesis by converting all pyruvate to acetate when oxygen is restricted, and given a choice of anaerobic pathways with unlimited flux capacity.

Although the long-term, steady-state physiological responses to hypoxic stimulus were the same for both age groups, the stress of hypoxia-reoxygenation treatment showed short-term dysfunction in aging flies, across molecular to functional scales. Therefore, in addition to static differences in mitochondrial enzyme levels and activity, as others have measured, our results suggest that aging also affects the dynamic regulation of these enzyme fluxes in response to stress. One question that is opened by these data is whether the higher oxidative stress is creating new mitochondrial damage or merely making evident the effects of damage that has already accumulated with age. Also, are these results caused by the damage to the mitochondrial enzymes directly or to the ROS defenses that protect them?

Our approach compiled genome-scale data from several sources (the annotated fly genome, microarrays, and NMR metabolomics), along with detailed data from specific assays and the biochemical literature, and integrated them into a quantitative computer model that can be validated against future experiments. The model helped us to understand systems-level mechanisms for differences in the hypoxia response in young and old flies that both support and contribute to existing data regarding aging and mitochondrial dysfunction. In the future, specific molecular

mechanisms can be further analyzed by comparing to similar models in other species and by perturbation analysis using selected enzyme mutations.

Acknowledgements

Chapter 4, in full, has been submitted for publication of the material as it may appear in Molecular Systems Biology. The dissertation author and the first author (Laurence Coquin) were the primary investigators and contributed equally to this paper. Co-authors were Drs. Andrew D. McCulloch and Giovanni Paternostro

We would like to thank Matthew Owen for managing the fly stocks used for experiment, Rachel Nguyen for collecting survival data, and Francis Le for constructing the hypoxia chambers. This work was supported by the NIH grants BES-0506252 (McCulloch), P41-RR08605 (McCulloch), and R21-AG026729 (Paternostro).

References

Ambrosio G, Weisfeldt ML, Jacobus WE, Flaherty JT (1987) Evidence for a reversible oxygen radical-mediated component of reperfusion injury: reduction by recombinant human superoxide dismutase administered at the time of reflow. *Circulation* **75:** 282-291.

Arakawa K, Kono N, Yamada Y, Mori H, Tomita M (2005) KEGG-based pathway visualization tool for complex omics data. *In Silico Biol* **5:** 419-423.

Becker SA, Feist AM, Mo ML, Hannum G, Palsson BO, Herrgard MJ (2007) Quantitative prediction of cellular metabolism with constraint-based models: the COBRA Toolbox. *Nat Protoc* **2:** 727-738.

Beckonert O, Keun HC, Ebbels TM, Bundy J, Holmes E, Lindon JC, Nicholson JK (2007) Metabolic profiling, metabolomic and metabonomic procedures for NMR spectroscopy of urine, plasma, serum and tissue extracts. *Nat Protoc* **2:** 2692-2703.

Bonow RO, Bohannon N, Hazzard W (1996) Risk stratification in coronary artery disease and special populations. *Am J Med* **101:** 4A17S-22S; discussion 22S-24S.

Broderick KE, Feala J, McCulloch A, Paternostro G, Sharma VS, Pilz RB, Boss GR (2006) The nitric oxide scavenger cobinamide profoundly improves survival in a Drosophila melanogaster model of bacterial sepsis. *Faseb J* **20:** 1865-1873.

Chen Q, Behar KL, Xu T, Fan C, Haddad GG (2003) Expression of Drosophila trehalose-phosphate synthase in HEK-293 cells increases hypoxia tolerance. *J Biol Chem* **278:** 49113-49118.

Childress CC, Sacktor B, Grossman IW, Bueding E (1970) Isolation, ultrastructure, and biochemal characterization of glycogen in insect flight muscle. *J Cell Biol* **45:** 83-90.

Dubessay P, Garreau-Balandier I, Jarrousse AS, Fleuriet A, Sion B, Debise R, Alziari S (2007) Aging impact on biochemical activities and gene expression of Drosophila melanogaster mitochondria. *Biochimie* **89:** 988-1001.

Feala JD, Coquin L, McCulloch AD, Paternostro G (2007) Flexibility in energy metabolism supports hypoxia tolerance in Drosophila flight muscle: metabolomic and computational systems analysis. *Mol Syst Biol* **3:** 99.

Ferguson M, Mockett RJ, Shen Y, Orr WC, Sohal RS (2005) Age-associated decline in mitochondrial respiration and electron transport in Drosophila melanogaster. *Biochem J* **390:** 501-511.

Giannakou ME, Partridge L (2007) Role of insulin-like signalling in Drosophila lifespan. *Trends Biochem Sci* **32:** 180-188.

Girardot F, Lasbleiz C, Monnier V, Tricoire H (2006) Specific age-related signatures in Drosophila body parts transcriptome. *BMC Genomics* **7:** 69.

Goodacre R, Vaidyanathan S, Dunn WB, Harrigan GG, Kell DB (2004) Metabolomics by numbers: acquiring and understanding global metabolite data. *Trends Biotechnol* **22:** 245-252.

Griffin JL (2003) Metabonomics: NMR spectroscopy and pattern recognition analysis of body fluids and tissues for characterisation of xenobiotic toxicity and disease diagnosis. *Curr Opin Chem Biol* **7:** 648-654.

Griffin JL, Bollard ME (2004) Metabonomics: its potential as a tool in toxicology for safety assessment and data integration. *Curr Drug Metab* **5:** 389-398.

Grotewiel MS, Martin I, Bhandari P, Cook-Wiens E (2005) Functional senescence in Drosophila melanogaster. *Ageing Res Rev* **4:** 372-397.

Haddad GG, Sun Y, Wyman RJ, Xu T (1997) Genetic basis of tolerance to O2 deprivation in Drosophila melanogaster. *Proc Natl Acad Sci U S A* **94:** 10809-10812.

Hochachka PW (1980) Living without oxygen : closed and open systems in hypoxia tolerance. Harvard Univ. Press, Cambridge.

Hochachka PW (2003) Intracellular convection, homeostasis and metabolic regulation. *J Exp Biol* **206:** 2001-2009.

Hochachka PW, Somero GN (2002) Biochemical adaptation : mechanism and process in physiological evolution. Oxford University Press, New York.

Kanehisa M, Araki M, Goto S, Hattori M, Hirakawa M, Itoh M, Katayama T, Kawashima S, Okuda S, Tokimatsu T, Yamanishi Y (2008) KEGG for linking genomes to life and the environment. *Nucleic Acids Res* **36:** D480-484.

Kanehisa M, Goto S (2000) KEGG: Kyoto Encyclopedia of Genes and Genomes. *Nucleic Acids Research* **28:** 27-30.

Keppler D, Decker K (1974) *Methods of Enzymatic Analysis*. Academic Press, New York.

Krishnan SN, Sun YA, Mohsenin A, Wyman RJ, Haddad GG (1997) Behavioral and electrophysiologic responses of Drosophila melanogaster to prolonged periods of anoxia. *Journal of Insect Physiology* **43:** 203-210.

Kujoth GC, Hiona A, Pugh TD, Someya S, Panzer K, Wohlgemuth SE, Hofer T, Seo AY, Sullivan R, Jobling WA, Morrow JD, Van Remmen H, Sedivy JM, Yamasoba T, Tanokura M, Weindruch R, Leeuwenburgh C, Prolla TA (2005) Mitochondrial DNA

mutations, oxidative stress, and apoptosis in mammalian aging. *Science* **309:** 481-484.

Lavista-Llanos S, Centanin L, Irisarri M, Russo DM, Gleadle JM, Bocca SN, Muzzopappa M, Ratcliffe PJ, Wappner P (2002) Control of the hypoxic response in Drosophila melanogaster by the basic helix-loop-helix PAS protein similar. *Mol Cell Biol* **22:** 6842-6853.

Lighton JR, Schilman PE (2007) Oxygen reperfusion damage in an insect. *PLoS ONE* **2:** e1267.

Martin GM (2001) Frontiers of aging. *Science* **294:** 13.

Martin GM, LaMarco K, Strauss E, K LK (2003) Research on aging: the end of the beginning. *Science* **299:** 1339-1341.

Nicholson JK, Wilson ID (2003) Opinion: understanding 'global' systems biology: metabonomics and the continuum of metabolism. *Nat Rev Drug Discov* **2:** 668-676.

O'Farrell PH (2001) Conserved responses to oxygen deprivation. *J Clin Invest* **107:** 671-674.

Opie LH (1998a) *The heart : physiology, from cell to circulation*. Lippincott-Raven, Philadelphia.

Opie LH (1998b) The regulation of the heartbeat. In *Cardiovascular Physiology*, Berne R, Levy M (eds). Mosby Medical Books, St. Louis.

Pan DA, Hardie DG (2002) A homologue of AMP-activated protein kinase in Drosophila melanogaster is sensitive to AMP and is activated by ATP depletion. *Biochem J* **367:** 179-186.

Parrou JL, Francois J (1997) A simplified procedure for a rapid and reliable assay of both glycogen and trehalose in whole yeast cells. *Anal Biochem* **248:** 186-188.

Paternostro G, Vignola C, Bartsch DU, Omens JH, McCulloch AD, Reed JC (2001) Age-associated cardiac dysfunction in Drosophila melanogaster. *Circ Res* **88:** 1053-1058.

Robergs RA, Ghiasvand F, Parker D (2004) Biochemistry of exercise-induced metabolic acidosis. *Am J Physiol Regul Integr Comp Physiol* **287:** R502-516.

Rose MR, ebrary Inc (1991) *Evolutionary biology of aging*. Oxford University Press, New York.

Sacktor B, Wormser-Shavit E (1966) Regulation of metabolism in working muscle in vivo. I. Concentrations of some glycolytic, tricarboxylic acid cycle, and amino acid intermediates in insect flight muscle during flight. *J Biol Chem* **241:** 624-631.

Schulze U, Larsen ME, Villadsen J (1995) Determination of intracellular trehalose and glycogen in Saccharomyces cerevisiae. *Anal Biochem* **228:** 143-149.

Schwarze S, Weindruch R, Aiken JM (1998) Oxidative stress and aging reduce COX 1 RNA and cytochrome oxidase activity in *Drosophila*. *Free Radical Biology and Medicine* **25:** 740-747.

Steenbergen C, Murphy E, Levy L, London RE (1987) Elevation in cytosolic free calcium concentration early in myocardial ischemia in perfused rat heart. *Circ Res* **60:** 700-707.

Suarez RK, Darveau CA, Welch KC, Jr., O'Brien DM, Roubik DW, Hochachka PW (2005) Energy metabolism in orchid bee flight muscles: carbohydrate fuels all. *J Exp Biol* **208:** 3573-3579.

Trifunovic A, Wredenberg A, Falkenberg M, Spelbrink JN, Rovio AT, Bruder CE, Bohlooly YM, Gidlof S, Oldfors A, Wibom R, Tornell J, Jacobs HT, Larsson NG (2004) Premature ageing in mice expressing defective mitochondrial DNA polymerase. *Nature* **429:** 417-423.

Vigne P, Frelin C (2007) Plasticity of the responses to chronic hypoxia and dietary restriction in an aged organism: evidence from the Drosophila model. *Exp Gerontol* **42:** 1162-1166.

Wingrove JA, O'Farrell PH (1999) Nitric oxide contributes to behavioral, cellular, and developmental responses to low oxygen in Drosophila. *Cell* **98:** 105-114.

Zhou D, Xue J, Chen J, Morcillo P, Lambert JD, White KP, Haddad GG (2007) Experimental selection for Drosophila survival in extremely low O2 environment. *PLoS ONE* **2:** e490.

Zou S, Meadows S, Sharp L, Jan LY, Jan YN (2000) Genome-wide study of aging and oxidative stress response in Drosophila melanogaster. *Proc Natl Acad Sci U S A* **97:** 13726-13731.

Chapter V –

Metabolic profiling and computational modeling of Drosophila metabolism following adaptation to chronic hypoxia

Abstract

We explored global metabolic effects of hypoxic adaptation, using a population of *Drosophila* flies experimentally selected to survive chronic hypoxic environment over several generations. NMR-based metabolic profiles were gathered for thoraxes of adapted and control flies for chronic and acute exposure to room air (20% oxygen), mild hypoxia (4% O_2), and severe acute hypoxia (4 hours at 0.5% oxygen). When compared qualitatively by Principal Component Analysis, the hypoxia-adapted flies showed similar metabolomic profiles when in their adapted oxygen level as the control flies showed in room air; by contrast, adapted flies in room air qualitatively resembled the stressed profiles of either group under severe acute hypoxia. Adapted flies are better able to tolerate severe acute hypoxia as well, and we explored the mechanisms of this tolerance using data-driven flux-balance analysis of the two groups. A network model of fly metabolism was constrained to flux estimates for 10 metabolites from the different NMR profiles, and optimized for ATP

production with flux-balance analysis. In the model, adapted flies produced more ATP per glucose consumed, and created fewer protons per ATP. In simulations, the source of this efficiency was traced to differential usage of Complex I over Complex II in the electron transport chain, driven by upregulation of pyruvate into mitochondrial respiration rather than through anaplerotic pyruvate carboxylase. Previous microarray data support this direction of pyruvate regulation, and greater use of Complex I in adapted flies was experimentally confirmed in a separate study. The model generated other specific pathway-based hypotheses for hypoxia tolerance that can be followed up experimentally in the future.

V.1 Introduction

Drosophila are remarkably tolerant to hypoxic stress and reoxygenation injury but, as we (previous chapters) and others (Akasaka et al., 2006; Ma et al., 2001; Wingrove & O'Farrell, 1999) have shown, this tolerance can be reduced by specific genetic mutations and by global degradation due to aging. The converse question, and more important from a translational standpoint, is whether hypoxia defenses can be improved as well. Our preliminary results with lactate dehydrogenase deletions in Chapter III suggest that targeted metabolic interventions may improve recovery from hypoxic stress. Zhou et. al. (2007) demonstrated that global adaptation via directed evolution can also improve hypoxic function, and that genetic interventions mimicking specific adaptations in gene expression can enhance tolerance in unadapted flies as well.

Briefly, over many generations Zhou et. al experimentally selected flies for their survival in oxygen levels, which were decreased incrementally at each generation. A control population (called “naïve” flies from here on) was cultured in

parallel in room air (20% O_2). Once the selected population was able to withstand chronic levels of 4% oxygen, lethal to naïve flies, the populations were compared at the genotype and phenotype level. Adapted flies had better recovery from anoxic stress, higher oxygen consumption in chronic hypoxia, and decreased body size. Gene expression profiles of adapted versus naïve flies showed 4% percent of the genome differed in mRNA transcript levels, with half of the differences from downregulation, and genetic perturbation of some downregulated candidates conferred enhanced hypoxia tolerance in normal strains.

Microarray analysis provided a useful snapshot of the genetic origin of enhanced function, but metabolic profiles are a complementary indicator of the cellular phenotype. In collaboration with Dan Zhou and Gabriel Haddad we used ^{1}H NMR spectroscopy (methods detailed in Chapters III and IV) to measure metabolic profiles for adapted and naïve flies, then examined these profiles by multivariate analysis to find the main sources of metabolite variation and observe how the groups clustered and shifted within multidimensional space under hypoxic stress.

Next, we approximated fluxes from hypoxia and control groups, fitted the model to these fluxes as constraints, and compared ATP efficiency and proton accumulation between adapted and naïve flies. Enzyme-controlled fluxes were compared across groups, and similarly to Chapters III and IV we found trends in the regulation of pyruvate metabolism, though the specific mechanisms were different. Finally, we compared regulation of fluxes in the model to regulation of genes in the microarray data and saw parallels in the regulation of enzymes involved in pyruvate metabolism.

V.2 Materials and Methods

Flies were cultured in chronic and acute hypoxia conditions as described in Zhou et. al. (2007). Hypoxia experiments and NMR spectra were gathered for each group as described in Chapters III and IV.

For the Principal Component Analysis, all metabolites with at least one measurement above 0.01 mM were included in the dataset. Each sample was normalized by protein content measured by the Bradford assay, and selected metabolites were scaled using standards as described above. Data from all samples (young and old; control, hypoxia and recovery) were combined into one matrix and principal components were computed using the princomp function in Matlab (Mathworks, Inc., Cambridge, MA). Principal component scores for the samples were plotted and visualized within Matlab.

Flux-balance simulations were performed as in Chapter IV, and mapping the network to gene expression data was performed within the SimPheny software as in Chapter IV as well.

V.3 Results and Discussion

We gathered metabolic profiles for each population under their respective steady state (chronic) culture conditions (4% and 20% oxygen, respectively) and under acute hypoxia (4 hours at 0.5% oxygen). We then compared adapted and naïve flies in equivalent oxygen by measuring naïve flies at 4% (after 4 hours). Finally, adapted flies were measured after culturing for one generation in room air and then subjected to acute hypoxia (4 hours at 0.5%), in order to compare acute stress over a similar step size (20% to 0.5%). For simplicity and to differentiate the perceived hypoxic stress, we labeled the experimental conditions as “steady state” for

chronic culture conditions, “mild hypoxia” for smaller steps in oxygen (4% to 0.5% and 20% to 4% O_2), and “severe hypoxia” for the large step size (20% to 0.5% O_2). Males and females were measured separately for each experiment. The experimental groups are summarized in Figure V.1.

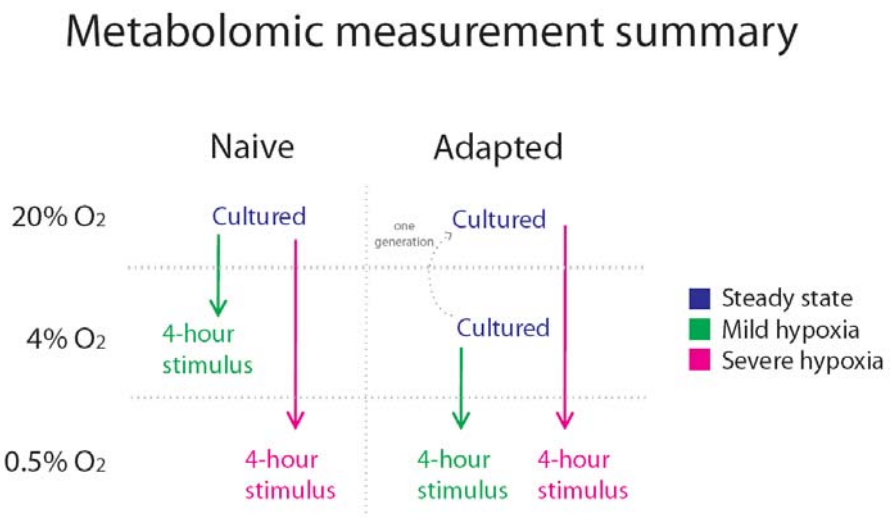

Figure V.1: Summary of the experimental conditions for the 7 metabolic profiles. Measurements were gathered for both males and females in all conditions illustrated, for a total of 14.

V.3.1 Normalization

Individual samples within groups were normalized by the sum of all metabolite concentrations in the sample, and then re-scaled by the group average of these concentration totals. Normalization among groups was performed using Bradford assays of the soluble protein content, as in Chapter I.V. To minimize the effect of high variability in the Bradford assays, metabolite concentrations for each group were divided by their mean protein content, discarding the highest and lowest protein measurements. Selected metabolites were scaled empirically using standards

(described in detail in Chapter 4), in order to account for small variations in the scaling relationships between peak size and metabolite concentration.

V.3.2 Raw concentration profiles

Thirty-five metabolites appeared in all 14 individual metabolic profiles, making the data difficult to examine by direct inspection. One trend, however, is readily apparent in the raw data. All hypoxic stresses (except for severe hypoxia in adapted females) tended to increase the levels of most metabolites, including free glucose. This is consistent with previous experiments and implies that, since not every metabolite can be an anaerobic end product, substrates such as starches and proteins are broken down into monomers for fuel faster than they can be consumed by catabolic pathways. Figure V.2 displays raw concentration profiles.

V.3.3 Principal component analysis

Principal component analysis (PCA) can reduce the dimensionality of the data and provide an unbiased determination of which metabolites vary across groups, and by how much. Furthermore, this technique can be used to visualize the different groups and their hypoxic responses in multidimensional space, and then trace movements within this space back to specific metabolites.

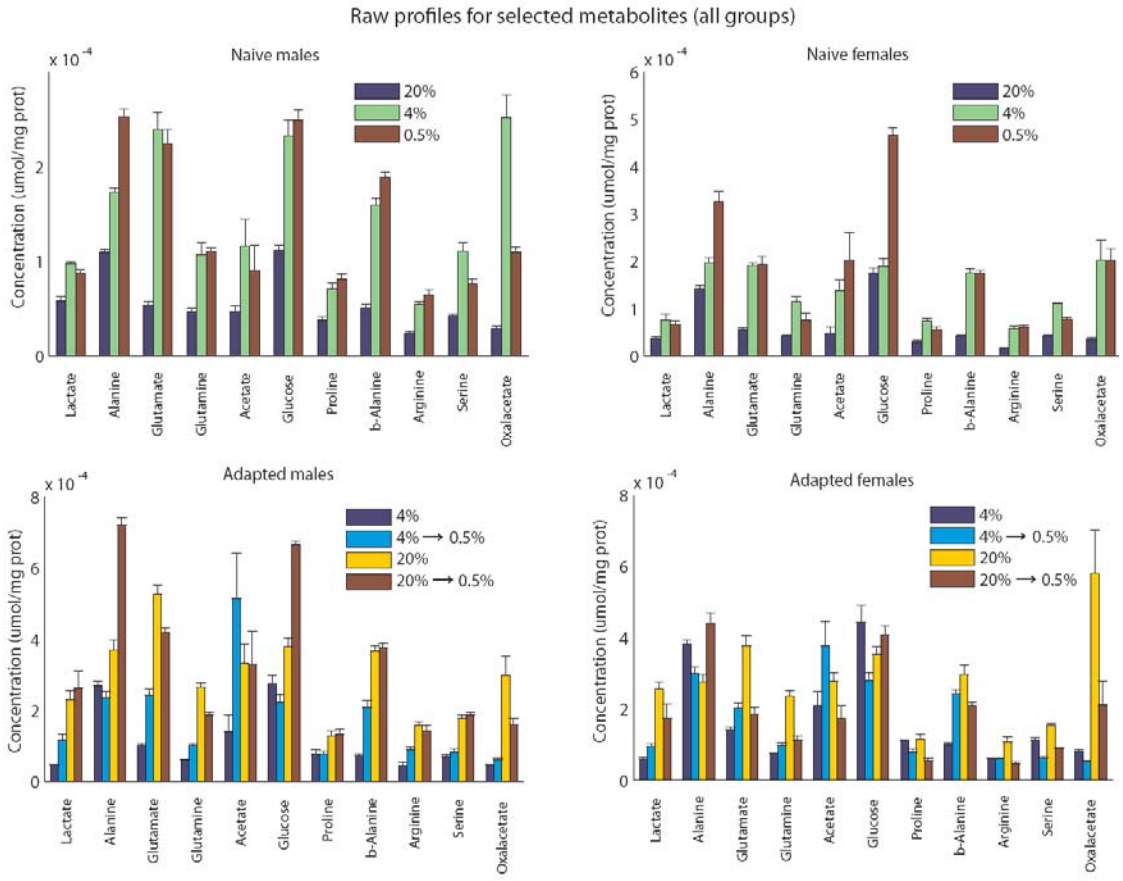

Figure V.2: Raw metabolite profiles, for selected metabolites over all experimental groups.

When the 14 metabolic profiles were decomposed by PCA, the first three principal components (PCs) accounted for approximately 90% of the variation in the data (Figure V.3A). Each PC was composed of a vector of metabolite contributions (Figure V.3B): PC 1 has large contributions from many metabolites and represents the trend of global increases in metabolites during hypoxic stress, especially for the compounds (in order) glucose, alanine, oxalacetate, β-alanine, glutamate, and lactate. The PC 2 axis is representative of increased oxalacetate and decreases in glucose and alanine. Separation of groups along PC 3 can mostly be attributed to different acetate concentrations. Figure V.3C plots average PCA scores for all 14

groups. The top axes display the average scores along PC 1 and PC 2, and the bottom axes plot PC 1 versus PC. Lines are drawn to connect steady state profiles for each group with profiles under acute hypoxia conditions. The direction of these lines can be interpreted as changes in specific metabolites by mapping onto Figure V.3B.

Males and females in the same experimental group tend to cluster together, and their hypoxic shifts (represented by lines) are often parallel, with some exceptions to both trends - most notably in the case of severe hypoxia. Steady state profiles cluster in the same region with the exception of adapted flies at 20% O_2, which are in the same region of the multidimensional space as stressed profiles. Adapted flies travel shorter distances along PC 1 during hypoxia than naïve flies, meaning the global increase in metabolites is smaller. Severe and mild stresses in both populations can be differentiated by the direction of their shifts along PC 2, which represents oxalacetate (accumulating in mild hypoxia), alanine and glucose (accumulating in severe hypoxia). Variation along PC 3, representing acetate levels, is dominated by mild hypoxia in adapted flies.

Although multivariate analysis has little to say about detailed molecular mechanisms of hypoxia tolerance, the results from PCA suggest that these mechanisms may be linked to a small handful of metabolites. They also hint that the genetic differences in adapted flies are tailored to their specific level of oxygen, since steady state profiles of adapted flies in normoxia are much closer to stressed profiles than to the cluster of other steady state groups. Correlations between specific metabolites and experimental groups (such as acetate in adapted flies under mild hypoxia) are interesting but cannot be interpreted as adaptations in themselves, since activity in one pathway can simply be an indirect effect of regulating another.

Figure V.3 (facing page): Principal component analysis of all metabolite profiles.

A) Contribution of principal components (PCs). PC 1 causes approximately 60% of the variation, and PCs 1 through 3 account for approximately 90% of the differences among groups.

B) Mapping metabolites to PCs. PC 1 represents global increases, PC 2 represents oxalacetate, alanine, and glucose, and PC 3 represents acetate.

C) Average group scores along the first three principal components. Lines represent shifts from 4-hour hypoxia stimulus. Fluxes are divided into "steady state", "mild hypoxia", and "severe hypoxia" as in Figure 1.

A

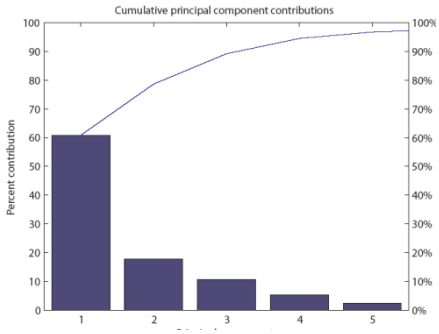
Cumulative principal component contributions
Percent contribution

B

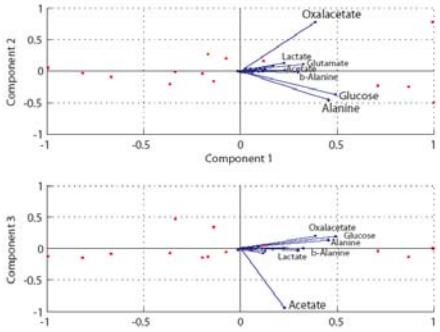
Component 2
Component 1
Component 3
Oxalacetate
Lactate
Glutamate
b-Alanine
Glucose
Alanine
Acetate

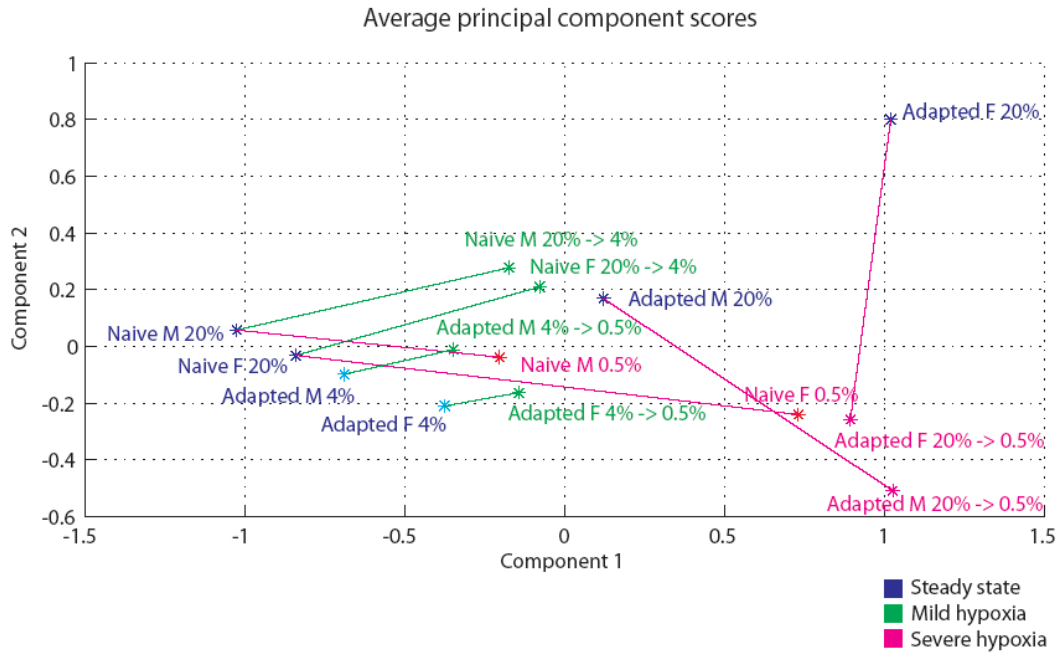
Average principal component scores
Component 2
Component 1
Naive M 20%
Naive F 20%
Adapted M 4%
Adapted F 4%
Naive M 20% -> 4%
Naive F 20% -> 4%
Adapted M 4% -> 0.5%
Adapted F 4% -> 0.5%
Adapted M 20%
Naive M 0.5%
Naive F 0.5%
Adapted F 20%
Adapted F 20% -> 0.5%
Adapted M 20% -> 0.5%
Steady state
Mild hypoxia
Severe hypoxia

C

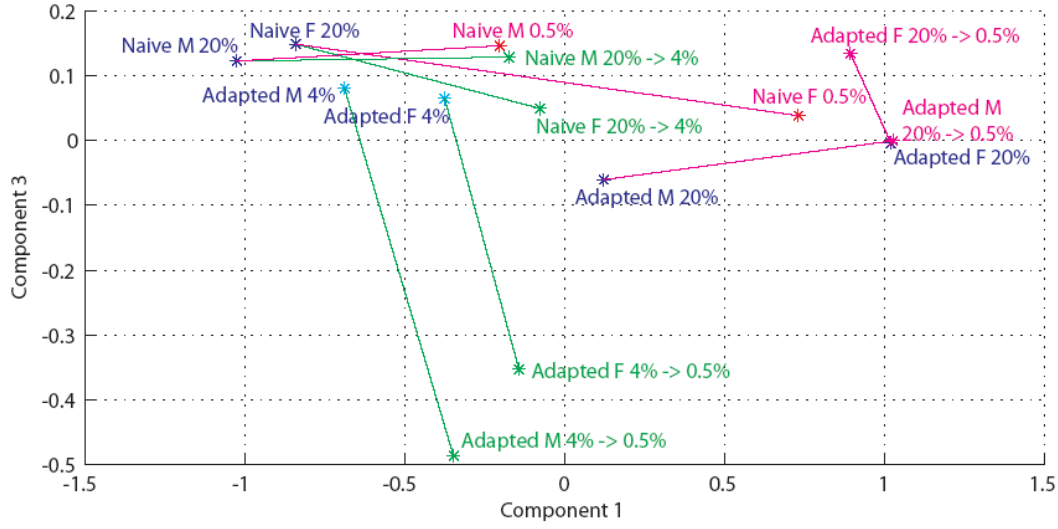
Component 3
Component 1
Naive M 20%
Naive F 20%
Naive M 0.5%
Naive M 20% -> 4%
Adapted M 4%
Adapted F 4%
Naive F 20% -> 4%
Naive F 0.5%
Adapted F 20% -> 0.5%
Adapted M 20% -> 0.5%
Adapted F 20%
Adapted M 20%
Adapted F 4% -> 0.5%
Adapted M 4% -> 0.5%

To investigate differences at the level of pathway activity, we fitted our computer model of fly metabolism to fluxes estimated from the time course of metabolite profiles. The fact that these shifts had consistent patterns across gender and conditions lends confidence to the idea that metabolites fluxes within the model may elucidate general properties.

V.3.4 Flux-balance analysis

We used flux-balance analysis to examine pathway activity during 8 acute hypoxic stimuli (all combinations of adapted *versus* naïve, severe *versus* mild stress, and male *versus* female). Ten metabolites were chosen for fitting the model, based on the requirements that they (1) were present in the NMR spectra in sufficient concentrations for all experimental conditions, (2) were represented in our metabolic reconstruction, and (3) changed concentration (accumulated or dissipated) in a direction that correctly coincided with any irreversible pathways. Fluxes were approximated by dividing differences in two concentrations by the experiment time (4 hours), and standard errors for fluxes were derived by adding the variances of the two concentration measurements.

Glycogen availability was unconstrained for all simulations. This assumption was supported by the large increase in free glucose for most hypoxic measurements, indicating that glycogen and trehalose breakdown supplied glucose monomers faster than the system could use them. We did not have measurements of oxygen consumption, which presented a modeling challenge. Since our flux-balance model optimizes for ATP production, the combination of unconstrained glycogen and unconstrained oxygen would simply produce infinite fluxes of both. Instead, for each

experiment we swept the oxygen consumption constraint over ranges that encompassed the qualitative features of the model.

All simulations required some minimum level of oxygen to produce the fluxes observed in the NMR spectra. Below this level, the model was infeasible and above this oxygen uptake, aerobic activity converted any additional substrates to CO_2. This minimum oxygen consumption was lower in the adapted than the naïve flies, suggesting that the pathways that remain active during hypoxia in adapted flies are more efficient in their use of oxygen. The plot of ATP production versus O_2 uptake in Figure V.4 demonstrates this graphically: in adapted flies the ATP/O_2 curves are shifted up, therefore ATP production is higher at a given O_2 while O_2 consumption is lower for a given ATP output. Therefore, although we did not measure oxygen consumption for each group, simulations suggest that the adapted metabolism is more efficient regardless of where the O_2 operating point may lie. Similar patterns were seen in substrate efficiency: adapted flies produced more ATP per substrate than naïve flies.

Next we examined the simulated flux distributions across the 8 groups at the level of enzyme fluxes. Each experimental group likely operated at a different O_2 uptake, but for the sake of direct comparison of pathway activity we compared the simulations at an oxygen flux of 10 nmol/min/mg protein, which gives feasible solutions for all groups (refer to Figure V.4). At this simulated O_2 flux, adapted flies generate more ATP, produce fewer protons, and consume less glycogen (Figure V.5). The differences are more pronounced at lower oxygen uptake, but hold true at all O_2 fluxes.

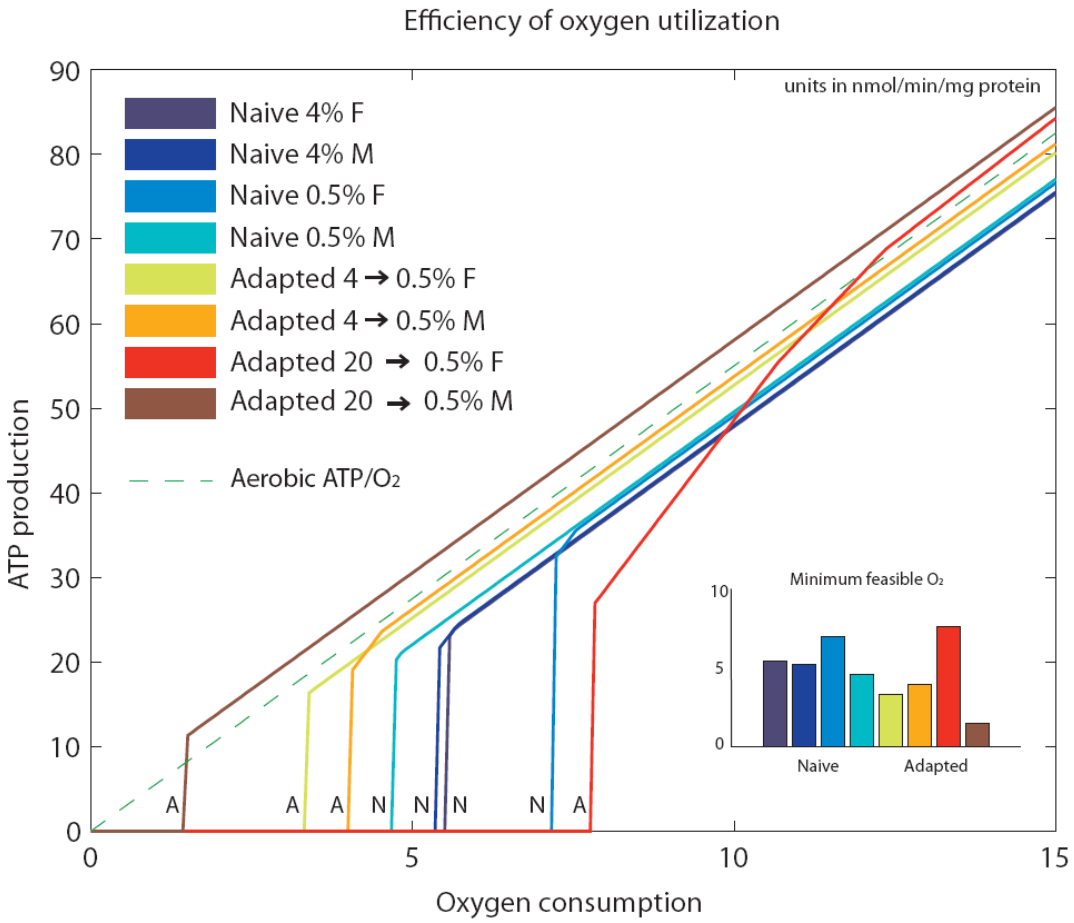

Figure V.4: Efficiency of oxygen utilization in terms of ATP production. In adapted flies, ATP-O_2 curves were shifted in the direction of more ATP produced for each unit of oxygen. (Inset) Except for females under severe hypoxia, adapted flies had lower minimum levels of oxygen required to fuel their anaerobic pathways.

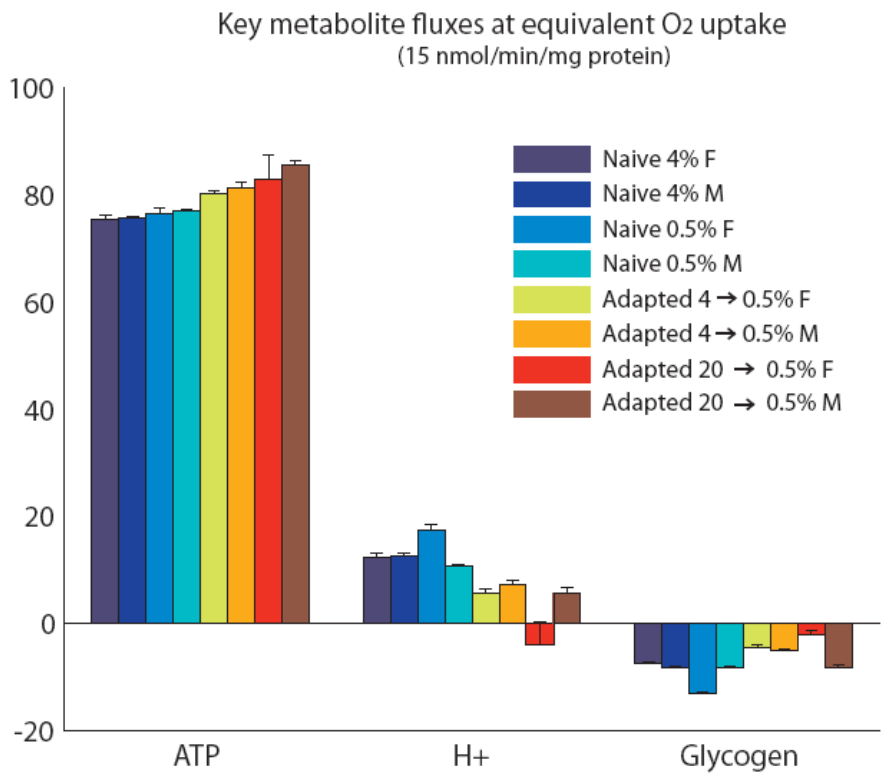

Figure V.5: Production of key metabolites at a common O_2 uptake rate (15 nmol/min/mg protein). Naïve flies have lower ATP/proton and ATP/substrate ratios than adapted flies at any given oxygen supply. Error bars indicate standard deviation of 100 simulations incorporating the variances of NMR measurements. H+ stands for proton accumulation.

We also inspected important reactions in the model at this simulated oxygen uptake. All reactions with nonzero fluxes that were not transport or exchange reactions (i.e. enzyme-linked transformation reactions) were clustered by their flux values for unbiased extraction of pathways. Figure V.6 shows reactions representative of the largest clusters in the clustergram (not shown). Most of the reactions have some variability across groups, especially for the naïve and adapted females in severe hypoxia, but a few reactions differ between naïve and adapted flies for both sexes and hypoxic stimuli. Pyruvate kinase, the last step in glycolytic

formation of pyruvate, is representative of the reduced glycolytic flux in adapted flies. Pyruvate carboxylase, an anaplerotic reaction producing oxalacetate from pyruvate, has its activity reduced by more than half in adapted flies. The TCA cycle shows few consistent trends among the groups, but the electron transport chain shows large differences among the groups. Adapted flies utilize Complex I, NADH dehydrogenase, at a higher rate, while naïve flies rely more on Complex II (succinate dehydrogenase) activity, driven by GPDH transport of reducing equivalents from the cytosol. A reducing equivalent entering the electron transport chain via Complex I generates more ATP and consumes an additional proton, than one entering via Complex II. Experiments in isolated mitochondria have demonstrated that activation of Complex II produced a lower P/O ratio than Complex I (Ferguson et al., 2005).

Two linked mechanisms seem to account for the worse performance of naïve flies under hypoxia. First, the excess glycolytic activity in naïve flies is diverted through pyruvate carboxylase and into oxalacetate, at a cost of one additional ATP for the conversion plus a pyruvate that would be used more efficiently in another pathway. Second, the glycolytic flux produces excess NADH which, without a corresponding increase in alanine or lactate to balance it, must be shuttled to the mitochondria through GPDH and Complex II (with its disadvantage in substrate efficiency relative to Complex I, as mentioned above).

Figure V.6 (facing page): Fluxes through key reactions at a common oxygen uptake. Compared with naïve flies, simulations of adapted flies showed lower glycolysis, pyruvate carboxylase, GPDH, and Complex II activity, and higher fluxes through Complex I.

Abbreviations: PYK – pyruvate kinase, ACS – acetyl-CoA synthase, ALAT – alanine transaminase (cytosolic), LDH – lactate dehydrogenase, PC – pyruvate carboxylase, PDH – pyruvate dehydrogenase, CS – citrate synthase, SuccDH – succinyl CoA dehydrogenase (TCA cycle), MDH – malate dehydrogenase (mitochondrial), GPDH – glycerol-3-phosphate dehydrogenase shuttle, Complex II – succinyl CoA dehydrogenase (electron transport chain), Complex I – NADH dehydrogenase.

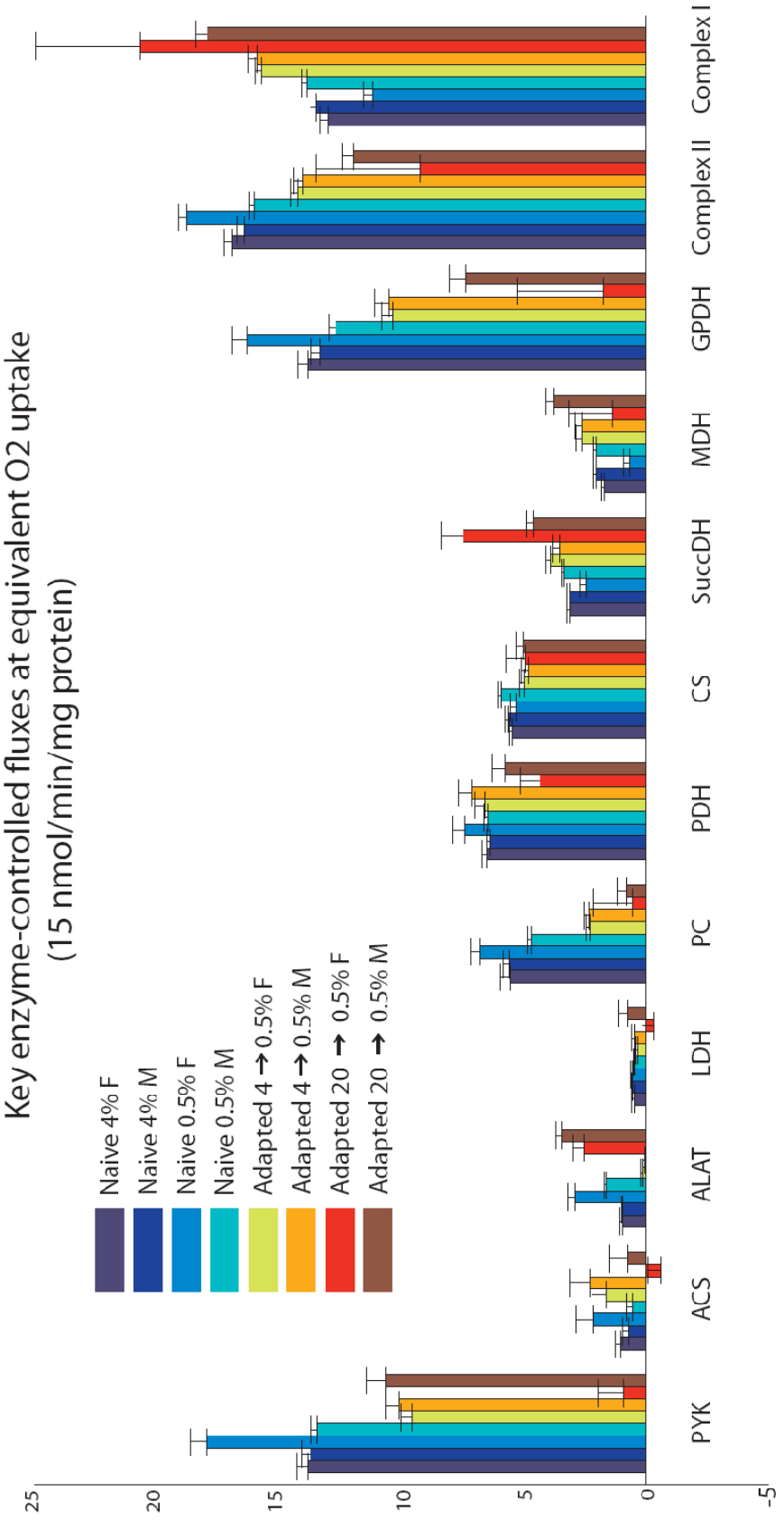
Key enzyme-controlled fluxes at equivalent O2 uptake
(15 nmol/min/mg protein)
Naive 4% F
Naive 4% M
Naive 0.5% F
Naive 0.5% M
Adapted 4 → 0.5% F
Adapted 4 → 0.5% M
Adapted 20 → 0.5% F
Adapted 20 → 0.5% M
25
20
15
10
5
0
-5
PYK
ACS
ALAT
LDH
PC
PDH
CS
SuccDH
MDH
GPDH
Complex II
Complex I

These conclusions are robust with respect to the choice of oxygen uptake at which we run the model. Regardless of whether the groups are compared at a common level of ATP production, at a common O_2 consumption, or whether each group is simulated at its own minimum feasible oxygen uptake, there are clear differences in glycolytic flux and pyruvate carboxylase activity, resulting in heavier use of Complex I and an increased ATP generating efficiency in the adapted flies. A cartoon depiction of these pathways is illustrated in Figure V.7.

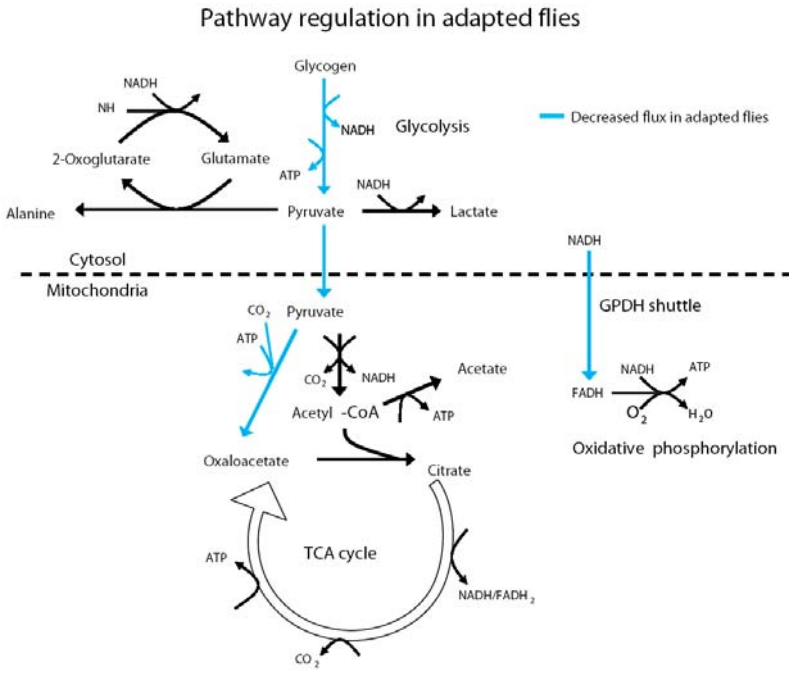

Figure V.7: Cartoon of downregulated fluxes in simulations of adapted flies. In naïve flies, oxalacetate production in the NMR profiles drives increased activity of glycolysis, pyruvate carboxylase, and Complex II of the electron transport chain.

V.3.5 Incorporating gene expression profiles

The microarray data obtained by Zhou et. al. (2007) showed many changes in gene expression after adaptation to chronic hypoxia, but no individual genes coding

for enzymes in our model exceeded the significance threshold. However, connected modules of regulated genes are less likely than individual genes to be significant by chance and thus the same significance threshold is not applicable. Therefore, we mapped the gene expression measurements to our data and explored the effect of a slightly reduced significance threshold. After adjusting the threshold to 10% fold changes in expression, a cluster of enzymes near the pyruvate branchpoint reaches the threshold. Pyruvate carboxylase is downregulated and pyruvate dehydrogenase is upregulated, the net effect of which might cause large changes of pyruvate flux. In addition, malate dehydrogenase expression is upregulated, which could cause additional inhibition of pyruvate carboxylase by dominating the production of oxalacetate, their shared product. Unlike pyruvate carboxylase, however, increased flux through malate dehydrogenase would be balanced by TCA cycle activity and oxalacetate would not accumulate. Metabolic Control Theory (Fell, 1997) has demonstrated that tighter control of pathway fluxes can be maintained by regulation of demand than supply, i.e. near the end of a pathway. Therefore, this differential control of the fate of pyruvate may be enough to drive the increase in glycolysis, and may also be a target for enhancing hypoxia tolerance.

V.4 Summary

Previously, Zhou et. al. used experimental selection over several generations to adapt a *Drosophila* population to be able survive chronic hypoxia. Adaptation to chronic hypoxia is a remarkable feat for directed evolution over a relatively small number of generations, considering the complexity and scale of cellular mechanisms involved in oxygen regulation. We studied metabolic aspects of this adaptation, first measuring metabolic concentration profiles using ^{1}H NMR spectroscopy. Principle

Component Analysis of concentration profiles suggested that these genetic adaptations are optimized for a single oxygen concentration, since steady state profiles of adapted flies cultured in normoxia more closely resemble the metabolic signatures of acute hypoxic stress than those of adapted flies in chronic hypoxia or control flies in normoxia.

When we fitted a flux-balance model to metabolic profiles gathered after 4 hours of acute hypoxia, a common regulatory mechanism surfaced regardless of the degree of hypoxic stress or gender. Surprisingly, the differences between adapted and naïve flies in various measures of efficiency could be traced to one source: the fate of pyruvate in the mitochondria, either carboxylation to oxalacetate or dehydrogenation to acetyl-CoA, had multiple consequences for the system. When overlaid with gene expression data from adapted flies, this branchpoint connected to three differentially regulated enzymes.

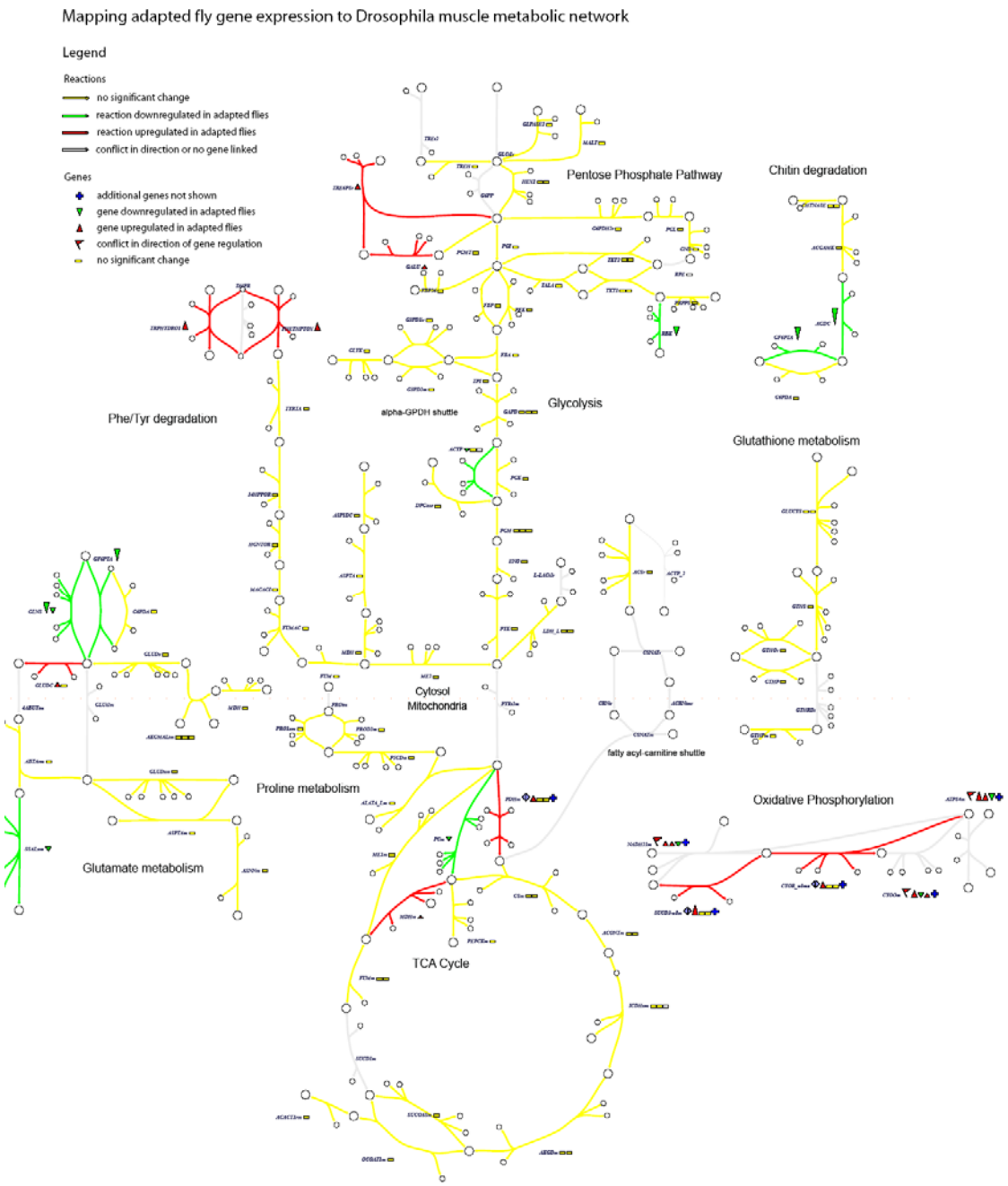

Figure V.8: Gene expression mapped to the metabolic reconstruction. At the pyruvate branchpoint, pyruvate carboxylate is downregulated and pyruvate dehydrogenase upregulated in adapted flies, which matches the regulation of fluxes seen in simulation.

References

Akasaka T, Klinedinst S, Ocorr K, Bustamante EL, Kim SK, Bodmer R (2006) The ATP-sensitive potassium (KATP) channel-encoded dSUR gene is required for Drosophila heart function and is regulated by tinman. *Proc Natl Acad Sci U S A* 103: 11999-12004.

Fell D (1997) *Understanding the control of metabolism*. Portland Press ; Distributed by Ashgate Pub. Co. in North America, London ; Miami Brookfield, VT.

Ferguson M, Mockett RJ, Shen Y, Orr WC, Sohal RS (2005) Age-associated decline in mitochondrial respiration and electron transport in Drosophila melanogaster. *Biochem J* 390: 501-511.

Ma E, Gu XQ, Wu X, Xu T, Haddad GG (2001) Mutation in pre-mRNA adenosine deaminase markedly attenuates neuronal tolerance to O2 deprivation in Drosophila melanogaster. *J Clin Invest* 107: 685-693.

Wingrove JA, O'Farrell PH (1999) Nitric oxide contributes to behavioral, cellular, and 6developmental responses to low oxygen in Drosophila. *Cell* 98: 105-114.

Zhou D, Xue J, Chen J, Morcillo P, Lambert JD, White KP, Haddad GG (2007) Experimental selection for Drosophila survival in extremely low O2 environment. *PLoS ONE* 2: e490.

Chapter VI –

Conclusions and future directions

VI.1 Summary of results

The work presented in this thesis represents a first step towards establishing a network-based analysis of cardiac hypoxia, using the fruit fly Drosophila as a model organism. We introduced new automation technology for rapid measurement of fly heart function, reconstructed the fly metabolic network using with genome-scale datasets, measured metabolic concentration profiles with NMR spectroscopy, and combined these techniques to measure and simulate the effects of hypoxia in cardiac and flight muscle. Our findings repeatedly pointed to the metabolism of pyruvate at the end of the glycolytic pathway as the most crucial set of pathways for cellular hypoxia tolerance in fly muscle tissue. The following details specific findings from each chapter of the dissertation.

Chapter I

Chapter I provided a background on cardiac hypoxia in humans, establishing known pathways and defense mechanisms as well as some strategies for improving cardiac hypoxia tolerance that are currently being explored. We pointed out gaps in understanding that have hindered this research. Then we introduced *Drosophila* as a hypoxia tolerant organism with many genetic similarities to humans, and established

the fruit fly as an excellent model for applying systems biology to the study of cardiac hypoxia to discover novel defense systems.

Chapter II

In Chapter II we introduced the concept of genome-wide phenotype screening of the cardiac hypoxia response, and the unique features of the fruit fly that make this type of screen feasible. The design and implementation of automation technology was presented, with preliminary validation results using known hypoxia-sensitive mutants. Design considerations for a large-scale screen are discussed, along with potential applications of the dataset within our systems biology approach.

Chapter III

Chapter III describes the results of metabolic profiles derived from ^{1}H NMR spectroscopy over the course of 4 hours of hypoxia in wild-type flies. We introduce the metabolic reconstruction and the first iteration of refinement, adding pathways for alanine and acetate production as suggested by the NMR data. Then we constrain the model to flux estimates from the NMR concentration data and use flux-balance simulations to point out improvements in metabolic function (ATP/H+ and ATP/substrate ratios) as compared to a mammalian system producing lactate only. All three anaerobic pathways were examined individually in simulation to understand their specific functional benefit. An enzyme mutation for lactate dehydrogenase (LDH) was simulated with neutral to positive effect according to the above metrics. Heart function was measured *in vivo* for an LDH deletion strain using the technology of Chapter II, with improved recovery to hypoxia compared to wild-type. Recovery of whole-body activity showed similar improvement.

Chapter IV

In Chapter IV we extended our reconstruction of metabolic pathways in *Drosophila* flight muscle using microarray data, then used flux-balance modeling and our physiological measurements of heart rate and physical activity to study the degradation of the hypoxia response in aging flies. We found that aging degraded physiological recovery to hypoxia in a whole-body activity assay, *in vivo* measurement of heart rate, and ATP production. Metabolomic profiles and flux-balance modeling suggested that the root of the physiological differences was a delay in the recovery of mitochondrial fluxes, with excess pyruvate converted to acetate rather than oxidized via the TCA cycle. These conclusions were consistent with aging research in flies and microarray data from the literature.

Chapter V

Chapter V introduced a strain of flies adapted to chronic hypoxia (Zhou et al., 2007) and applies a similar analysis to Chapter IV in order to find differences in metabolic regulation. Principal Component Analysis was used to calculate major sources in metabolite variation over 14 different metabolic profiles for adapted and control flies under various conditions. Differences between groups could be attributed to concentrations of oxalacetate, acetate, alanine, and glucose. PCA also confirmed global increases in free metabolite concentrations under hypoxic stress for all groups. Modeling suggested that adapted flies have more efficient utilization of oxygen and substrates, with lower proton accumulation, due to downregulation of pyruvate carboxylase and heavier use of Complex I over Complex II in the electron transport chain.

VI.2 Limitations

VI.2.1 Genetic background

The measurements described here range in scale from the molecular to the phenotype level. The higher a measurand lay on this scale and the more global the effects of the stimulus, the more factors that can affect its value. To use this project as an example, a molecular measurement of thoracic lactate after hypoxia depends mainly on regulation of enzymes, substrates, products in muscle tissue. Measurement of whole-body recovery from hypoxia, however, depends on metabolic homeostasis in all tissue types, neural commands to muscle fibers in response to restoration of oxygen, moisture levels, and many others. Hypoxia in itself is a wide-ranging stimulus, affecting practically all tissue types and cellular subsystems.

Measurements of complex phenotypes in response to global stimuli therefore require very stringent controls. The experiments in this thesis controlled for age, temperature, feeding and culture conditions, circadian influences, and humidity, but one major limitation in the use of genetic manipulations was that genetic backgrounds were not well controlled. In fact, the confounding of different background strains is seen in the characterization of hypoxia responses in the heart (Appendix B). Genetic differences are similarly expected to affect whole-body recovery from hypoxia as well as metabolomic profiles of the cellular response. We compared our mutant stocks against their corresponding wild-type strains, but did not out-cross multiple times or excise P-elements as additional controls for genetic differences.

Therefore, isogenetic backgrounds are needed for future experiments. When studying small numbers of mutants it is generally acceptable to out-cross several times with the wild-type control strain to approximate an isogenetic background.

Since a major goal of this research was to develop a scalable framework for large-scale iterative screens of many mutants, out-crossing was not a feasible methodology. One possible solution to this problem is to use transgenic RNAi libraries, described in Future Directions. Also, biochemical validation of protein levels for selected mutants would increase confidence in our results, though this is not feasible for all stocks within a larger screen.

VI.2.2 Hypoxia stimuli

At the beginning of this project, little was known about how the fly heart would respond to different oxygen levels and exposure times, therefore the experimental setup was designed for flexibility of the O_2 stimulus. However, the custom design required a tradeoff in quality, since the equipment was built in our lab, and no doubt added some variability to the results. Though we derived statistically significant conclusions in spite of the variations, future experiments may require additional precision. Now that we have found a protocol that brings out differences between wild type and hypoxia-sensitive mutants as well as young and old flies, parts of this customized setup can be exchanged for more commercially available hypoxia research equipment.

VI.2.3 Heart measurements

Measurements of fly heart rate were hampered by the above limitations as well as artifacts created by reflexive body movement in response to hypoxia. Although the invention of a restrictive slide “chamber” reduce this movement, the heart images often drift slightly across the microscope view and confound analysis algorithms. Also, the very slow heart rate in the first few minutes of recovery causes high numbers of false positives in the beat detection, as the algorithm adapts its

threshold and finds false beats within the noise. We manually inspected all of the data in this thesis for accuracy, but if large screens are to be performed more work must be done to improve the automated analysis.

Additionally, heart rate is only one of many possible measurements of cardiac function. At the least, the effectiveness of the heart as a fluid pump should be quantified with two measurements: rate of contraction and amount of fluid moved per contraction. In mammalian hearts, this concept is described in the terms *cardiac output* equals *heart rate* times *stroke volume*. To approximate the cardiac output of the fly, we need some estimator of stroke volume in addition to heart rate in order to make the case that the hearts of a certain strain of flies function "better" than another. Our manual inspection confirmed that fractional shortening was not drastically different between groups, but automated analysis would have failed to detect differences. Feature-based detection of wall movement (described later) could estimate fractional shortening of the tube diameter, which would be a useful indirect measurement of stroke volume.

VI.2.4 Metabolomics

The ^{1}H NMR spectrum provides a global perspective of metabolites present in high concentrations in a tissue sample. However, concentration measurements only provide a snapshot in time of the integral of all fluxes into and out of a metabolite pool. Another problem with these data is that the relatively low sensitivity of NMR spectroscopy prevents intermediate metabolites from being quantified, which would better identify specific pathways. There are other technical limitations to NMR-based metabolomics that I will not mention here, since they are generally not intrinsic to the technique and may be overcome as the technology is improved.

VI.2.5 Metabolic reconstruction and modeling

Though this was a systems biology project, the sparse metabolic literature for flies (relative to humans, yeast, or *E. coli*, the organisms more commonly used for this approach) made it necessary to narrow the scope of our model to ATP-generating central metabolism. NMR metabolomics allowed us to find heavily used pathways during hypoxia, and genome-wide expression data let us add highly expressed enzymes.

The problem with a model that incorporates only highly active pathways, however, is that metabolic fluxes are distributed according to a power-law (Almaas et al., 2004). This means that although a handful of fluxes indeed dominate, the number of enzymes with low but non-negligible activity is larger than would be expected in a normal distribution. Therefore, the aggregate impact of all low-activity pathways is likely to be a very important factor in the hypoxia response. In contrast with the pathways that supply them, pathways that demand ATP and metabolic cofactors are much more widely distributed across different pathways. Therefore, though the model incorporated most of the important fluxes in central metabolism, to have a truly global model of the hypoxia response the network must be complete. The next section briefly touches on automated methods for metabolic network reconstruction, which may be useful toward this goal.

The other major limitation in the analysis is that we have studied acute hypoxia with a steady-state model. The choice of a sufficiently long time point at 4 hours helps support the steady-state assumption, but the beginning of the hypoxic

response includes some kinetic element that our linear flux approximations must necessarily ignore.

VI.3 Future directions

Although some of the above limitations are intrinsic, many are technical difficulties that can be overcome with the addition of resources such as equipment, labor, and time. Others may require new approaches but should be theoretically possible. The following are some possible future directions for this research that can address many of these limitations.

VI.3.1 Transgenic UAS-RNAi libraries

The problem of genetic noise in mutant strains is directly addressed by a major new advance in the *Drosophila* community. A genome-wide, transgenic RNAi library was recently developed, using the *white* (*w*) strain as a background for all stocks (Dietzl et al., 2007). The group designed DNA sequences that code for dsRNA transcripts to bind and deactivate specific mRNA transcripts for each gene in the genome. They then inserted each sequence into a *w* background, tied to the yeast Upstream Activating Sequence (UAS). Attaching the UAS promoter allows researchers to implement RNAi knockdown with the commonly used GAL4/UAS system, a tool the Drosophila community has long used to express genes with spatiotemporal precision. Briefly, a GAL4 driver is chosen that expresses the yeast GAL4 protein (inert in flies) at a specific time and in a specific cell type. The gene of interest (or RNAi sequence in this case) is tied to the GAL4-responsive UAS promoter in another fly line. The lines are crossed, and in the progeny GAL4 from the driver chromosome - expressed at the desired space and time – activates UAS from the responder chromosome and expresses the gene of interest (Figure VI.1).

The UAS-RNAi lines can be ordered from the stock center directly and crossed with any GAL4 driver line (also publicly available). An additional advantage for our purposes is that, with the appropriate GAL4 driver, gene knock-downs that would be lethal at the embryonic or larval stage can be delayed until adulthood, or until the application of estrogen or heat in an inducible GAL4 line. Many metabolic enzymes are lethal when disrupted in the genome, but more are likely to be viable when disrupted only in adulthood or for a brief period using this system. Also, muscle specificity of a GAL4 driver will control for influences from other tissues, for example muscle coordination by neural commands during whole-body recovery. A GAL4 driver specifically for the heart organ has been designed and tested as well (Akasaka et al., 2006).

In preparation for large-scale screens, several GAL4 lines were tested with UAS-GFP responders, and with a lactate dehydrogenase UAS-RNAi line. Expression of GAL4 in adult thorax was verified with the GFP responder (Figure VI.1), but future work will be needed to validate the efficiency of enzyme knockdown.

VI.3.2 Biochemical validation

Mutant and RNAi stocks are commonly used in Drosophila research, but gene expression levels are often measured by Northern or Western blot for validation. As mentioned in the Limitations, it would be difficult to do this for each stock in a large-scale mutant screen; however, we have begun to analyze protein expression in the LDH deletions used in Chapter III, as well as an RNAi knockdown of the same gene. Preliminary data from our lab (LoPresti P., unpublished data) show decreased levels of the LDH enzyme in Western blots of the GAL4/UAS-RNAi knockdown, and even further reduction in enzyme levels in the heterozygous LDH deletion, when compared

with the wild type. These results show promise for the use of heterozygous enzyme knockouts and the GAL4/UAS-RNAi method in large-scale screen, although further experiments are needed to control for protein content (using a standard such as actin or GAPDH).

VI.3.3 Precision oxygen control

In the Limitations it was mentioned that a standard commercial hypoxia chamber, available from multiple vendors, would be desirable for future experiments. Sable Systems, Inc. (Las Vegas, NV) has recently developed a precision hypoxia chamber and CO_2 sensor specifically for measuring individual flies. This is an example of technology that would greatly increase reliability and add very important data to the models.

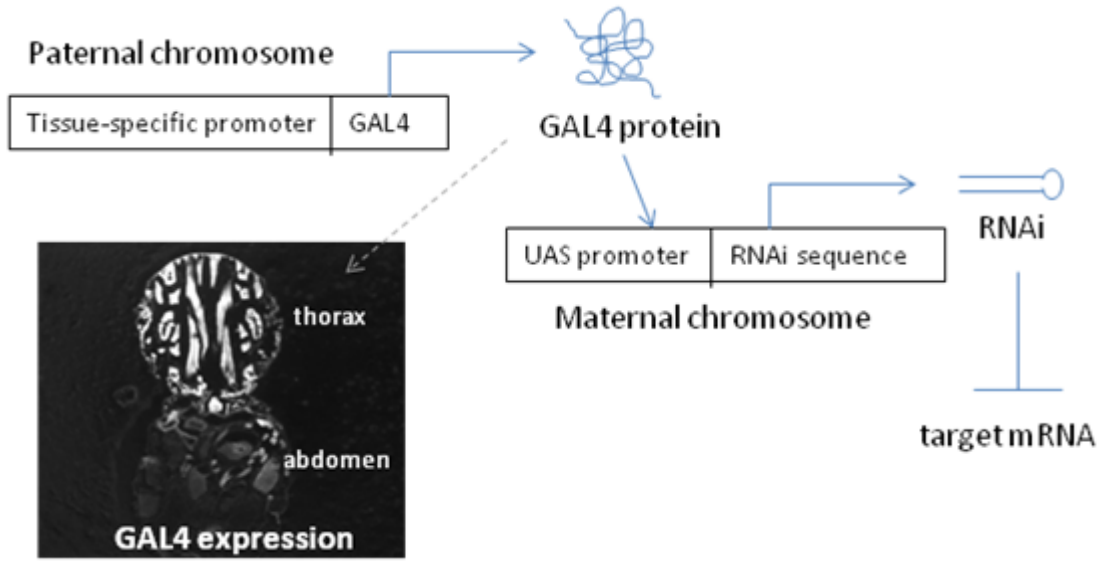

Figure VI.1: The GAL4/UAS system for tissue and temporal specificity of RNAi knockdowns. Example data shows tissue expression of our adult thorax GAL4 driver line.

VI.3.4 Automated fly mounting

After the anesthesia has taken effect, bursts of pressurized air deposit the flies on the microscope slide. After each burst, a small number of flies is expelled and the robotic stage shifts the slide slightly in order to evenly space the flies. A ‘guide’ tube positioned above the slide adds precision to this process.

The advantage of using plastic slides stems from the discovery that the wings of the fruit fly are strongly attracted to static electric charge. The wings are similarly responsive to strong electric fields generated by a high-voltage power source, which presents an opportunity for the future development of more sophisticated techniques for manipulating their body position. When flies are expelled onto the charged slides, the static electric force causes a large fraction of the flies to land properly on their backs with their wings spread.

VI.3.5 Feature-based image analysis

M-mode data are rich two-dimensional images and the measurement software records multiple images from several M-mode lines at once, yet the analysis software still uses the average brightness over each line to construct a one-dimensional signal to pass to the beat detection algorithm. Clearly, this is inadequate use of the available data, and future efforts should place high priority on improving them.

First, the image analysis should make full use of the stack of multiple (current default = 5) M-modes available. Heart detection is not 100% accurate and, even with the restrictive chamber there is often some drift from physical motion of the flies, therefore this redundancy is needed to counteract positioning errors. Future image processing should combine these images to reduce noise or at least add more sophistication to the choice of which of the images is to be analyzed.

Second, the practice of condensing the image to a one-dimensional signal throws away information and should be redesigned. Feature detection techniques might have potential for recognizing beat “structures” in the time-space images. Neural networks and Bayesian methods have been attempted in the past, and perhaps should be revisited. Template matching is another possibility, although the image patterns that must be recognized vary widely from fly to fly. We also explored cross-correlation methods for wall detection, with minor success, although the results are not presented here.

Designing a successful image analysis algorithm will be challenging since it must be robust to the noisy, highly variable M-mode data, however, the ability to measure wall diameters, RR intervals, and other features at once will be essential to the future of this project.

VI.3.6 ^{13}C isotopomer-based fluxomics

One possible technique to improve on these limitations is to use isotopomer-based fluxomics. Labeled isotopomers provide the possibility of tracing individual pathways and accurately calculating enzyme fluxes. Carbon-13 is an isotope that can be measured by NMR spectroscopy, and is naturally present at a rate of only about 1%. Enzymes do not distinguish molecules containing ^{13}C from those with the natural ^{12}C isotope, allowing substrate molecules such as glucose to be substituted with ^{13}C at various carbon positions and fed into the system., the distribution of labeled metabolites and the positions of ^{13}C within those molecules can then be measured using NMR spectroscopy. The network distribution of flux can be calculated from the data (Sauer, 2006). Calculating reaction fluxes from steady-state isotopomer distributions is a challenge in higher organisms, however, atom-mapping

matrices (AMMs) (Zupke & Stephanopoulos, 1994) and isotopomer-mapping matrices (IMMs) (Schmidt et al., 1997) provide a scalable mathematical framework that has been successful in integrating these data with metabolic networks (Vo & Palsson, 2006).

Carbon-13 isotopomer analysis can be used with mass spectrometry (MS) as well. Besides NMR spectroscopy, MS is the other commonly used technology for metabolomics, often combined with separation techniques such as gas or liquid chromatography. The metabolomics field is not yet at a consensus as to which method is better, and in fact they may provide complementary information (MS being more sensitive to smaller concentrations and NMR often preferred for precise quantification).

VI.3.7 Automated reconstruction

Down-regulation of ATP consumption is likely to be extremely important in hypoxia tolerant organisms, and so anabolic (biosynthetic) pathways must eventually be included in the model to account for this. Automated network reconstruction methods can be used to expand the model to include the entire genome. Recently, computer tools have appeared that use the complete set of open reading frames (ORFs) in an annotated genome, sometimes combined with information from existing, manually curated models, to predict reaction networks and gene-reaction associations (Karp et al., 2002; Notebaart et al., 2006). Though automated methods may accelerate the process of building genome-scale reconstructions, the resulting network must itself be curated. Details such as substrate specificity, exact reaction stoichiometry, cofactor usage, and compartmentalization are extremely important for

flux-balance analysis (Reed et al., 2006) but are unlikely to be produced correctly by any computer algorithm.

VI.3.8 Advanced constraint-based analysis

In this work we primarily used flux-balance analysis to examine the model, but other techniques can be used to study network properties in a metabolic reconstruction. The constraint-based approach includes a number of analytical tools, such as decomposition of the network into basis vectors or Monte Carlo sampling to estimate the shape of the solution space, variability and correlations between fluxes throughout this space, or deletion analysis (Palsson, 2006; Price et al., 2004). Metabolic control analysis, which examines the sensitivity of certain target fluxes or flux groups to perturbations, could be used to identify control points and important enzymatic mediators of adaptation to hypoxia (Stephanopoulos, 1999; Stephanopoulos et al., 1998).

Although the model is parameter-free, meaning that enzyme kinetics are ignored, it would also be possible to incorporate some kinetic elements in the simulations using finer time resolution of measurements, combined with a method such as dynamic flux balance analysis (DFBA).

VI.3.9 Integrating signaling networks

Beyond analyzing metabolic mechanisms of the hypoxia response, another goal of this research program is to leverage *Drosophila*'s genetic tools to screen for novel regulators of metabolism. During acute hypoxia, there are many changes in metabolic energy production and utilization pathways as the system adapts to the anaerobic state. These changes happen quickly, on the order of minutes in *Drosophila* flight muscle as shown in Chapter III. It is not possible for new genes to be

expressed and translated into proteins on these short timescales; therefore, the networks involved in metabolic regulation are strictly composed of enzymes, their covalent modification by signaling proteins, and their allosteric interactions with small molecules. Protein signaling interactions are more likely candidates for novel metabolic regulators than allosteric interactors. Allosteric interactions are usually weak, so binding of a small molecule to an enzyme is unlikely to produce large enough conformational changes in the protein to effect the extreme changes in enzyme fluxes that we have seen during hypoxia (Fell, 1997). The literature contains a few important examples of covalent modulators of enzymes during hypoxia, such as glycogen phosphorylase and AMP-activated kinase, but in general we have limited knowledge of the global signaling cascades that mediate the acute shift to anaerobic metabolism.

The yeast-two-hybrid and other methods have been successful at cataloguing immense numbers of protein-protein interactions for the construction of global networks. Online databases such as GRID, DIP, and BIND (Bader et al., 2003; Breitkreutz et al., 2003; Xenarios et al., 2002) store protein interactions, which can be overlaid onto the metabolic network as a rough sketch of signaling networks lying adjacent to metabolism. A map of interacting metabolic and signaling proteins can serve as a backbone onto which new data can be incorporated. Under the (somewhat limited, see (Hakes et al., 2008)) assumption that these networks have good coverage of the true ‘interactome,’ most proteins responsible for mediating the metabolic adaptation to hypoxia would appear as the first or second neighbors of the regulated enzymes. Therefore, a cardiac phenotype screening could begin with genes coding for proteins one link from hypoxia-responsive enzymes in the metabolic model, as in Figure VI.2.

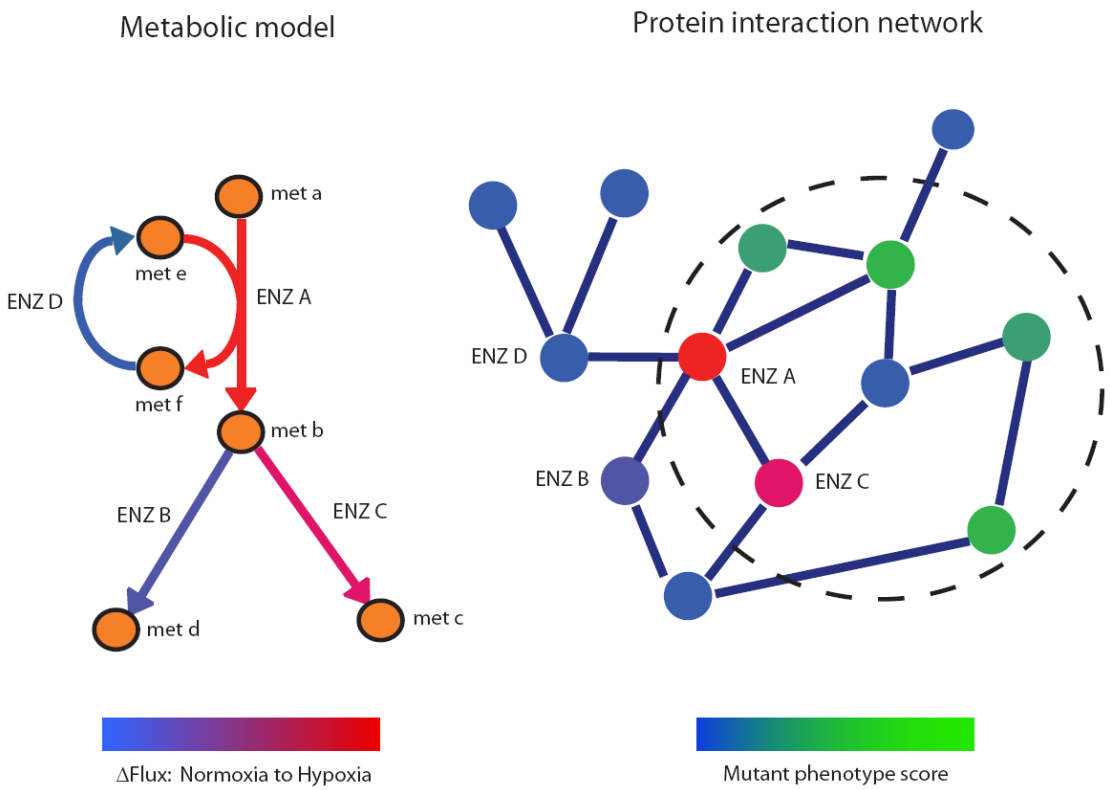

Figure VI.2: Integrating the metabolic model with a protein interaction network. Fluxes simulated by flux-balance analysis can be linked to enzymes in the protein interaction map. Phenotype values from the genetic screen can be included as node values as well. Statistical algorithms can extract well-connected modules enriched with high-scoring nodes, which can be further validated with experiment.

As a very simple demonstration, we merged the *Drosophila* protein interaction network from GRID with the list of enzyme proteins in our metabolic model, and then extracted the 'first neighbors' – all proteins in the global network that have at least one interaction with an enzyme in the model (Figure VI.3). The resulting subnetwork of enzyme interactors contains 606 proteins and 2,214 interactions, and includes proteins, such as actin, calmodulin, and several protein kinases. This first step

toward a list of screen candidates has the advantage of unbiased sampling from the global network, while at the same time being targeted toward likely metabolic regulators. Results from the cardiac phenotype screen can be examined within this network (as node values) and interpreted in contexts, such as vicinity to crucial enzymes in model simulations, clustering with other 'first neighbors' of enzymes, and extraction of small modules of highly-connected hypoxia-responsive proteins.

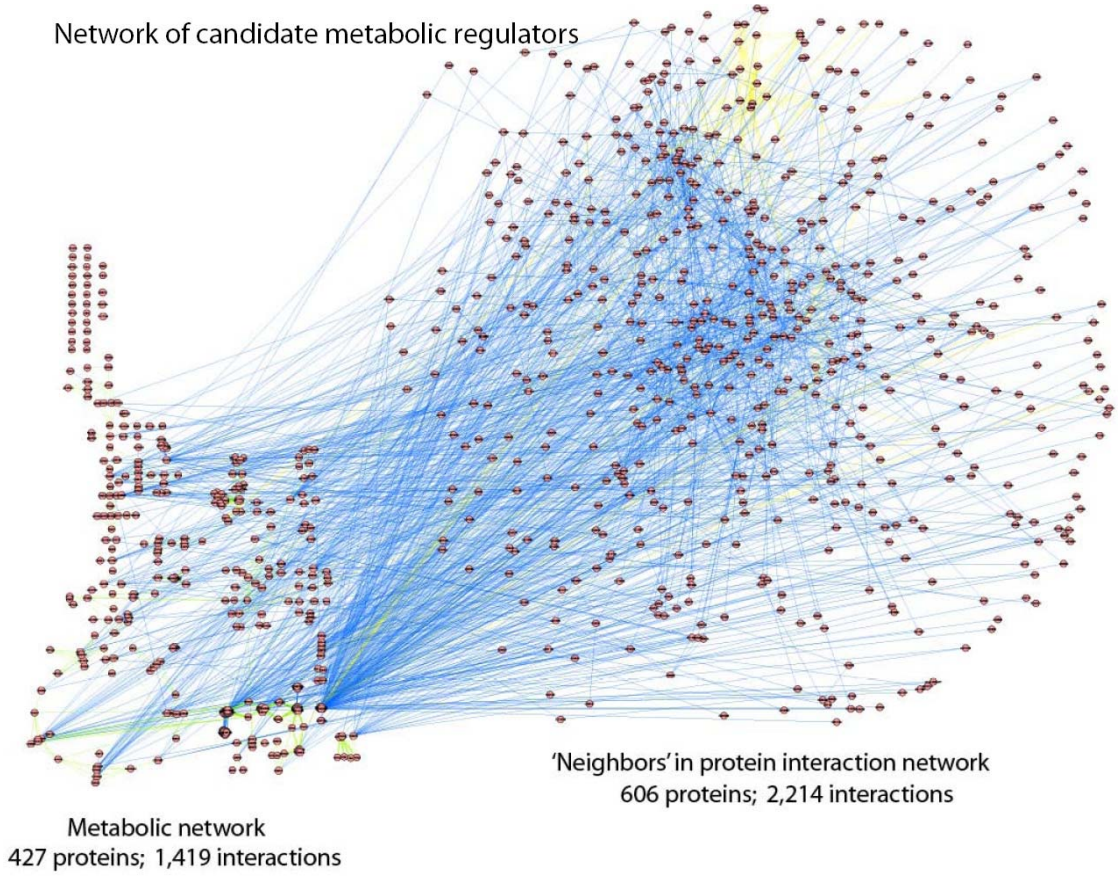

Figure VI.3: A strategy for generating a candidate gene list for a phenotype screen. Rather than screening the entire genome, which is still not feasible, the enzymes in the model and their 'first neighbors' in protein interaction networks might be enriched for important hypoxia-responsive metabolic regulators.

Conclusion

This thesis outlined a new approach to studying cardiac hypoxia in *Drosophila*, integrating rapid *in-vivo* phenotyping, metabolomics, several existing genome-wide datasets, and a constraint-based metabolic model to gain a network perspective of metabolic regulation. In the process we built a novel automated measurement system and a metabolic reconstruction of *Drosophila* flight muscle, two engineering accomplishments that in themselves may be useful to the research community. We then used these tools to gain new scientific understanding of hypoxia tolerance mechanisms in flies, under normal conditions and following genetic perturbations, aging, and adaptation to chronic hypoxia. Most new insights into metabolic hypoxia tolerance revolved around the flexible regulation of pyruvate through various anaerobic pathways, all of which exist in humans but most of which remain unused during hypoxia. Advances in the system-level understanding of hypoxia tolerance are necessary if future researchers are to redesign hypoxia defenses in humans.

References

Akasaka T, Klinedinst S, Ocorr K, Bustamante EL, Kim SK, Bodmer R (2006) The ATP-sensitive potassium (KATP) channel-encoded dSUR gene is required for Drosophila heart function and is regulated by tinman. *Proc Natl Acad Sci U S A* **103:** 11999-12004.

Almaas E, Kovacs B, Vicsek T, Oltvai ZN, Barabasi AL (2004) Global organization of metabolic fluxes in the bacterium Escherichia coli. *Nature* **427:** 839-843.

Bader GD, Betel D, Hogue CW (2003) BIND: the Biomolecular Interaction Network Database. *Nucleic Acids Res* **31:** 248-250.

Breitkreutz BJ, Stark C, Tyers M (2003) The GRID: the General Repository for Interaction Datasets. *Genome Biol* **4:** R23.

Dietzl G, Chen D, Schnorrer F, Su KC, Barinova Y, Fellner M, Gasser B, Kinsey K, Oppel S, Scheiblauer S, Couto A, Marra V, Keleman K, Dickson BJ (2007) A genome-wide transgenic RNAi library for conditional gene inactivation in Drosophila. *Nature* **448:** 151-156.

Fell D (1997) *Understanding the control of metabolism*. Portland Press ;
Distributed by Ashgate Pub. Co. in North America, London ; Miami
Brookfield, VT.

Hakes L, Pinney JW, Robertson DL, Lovell SC (2008) Protein-protein interaction networks and biology--what's the connection? *Nat Biotechnol* **26:** 69-72.

Karp PD, Paley S, Romero P (2002) The Pathway Tools software. *Bioinformatics* **18 Suppl 1:** S225-232.

Notebaart RA, van Enckevort FH, Francke C, Siezen RJ, Teusink B (2006) Accelerating the reconstruction of genome-scale metabolic networks. *BMC Bioinformatics* **7:** 296.

Palsson B (2006) *Systems biology : properties of reconstructed networks*. Cambridge University Press, Cambridge ; New York.

Price ND, Reed JL, Palsson BO (2004) Genome-scale models of microbial cells: evaluating the consequences of constraints. *Nat Rev Microbiol* **2:** 886-897.

Reed JL, Famili I, Thiele I, Palsson BO (2006) Towards multidimensional genome annotation. *Nat Rev Genet* **7:** 130-141.

Sauer U (2006) Metabolic networks in motion: 13C-based flux analysis. *Mol Syst Biol* **2:** 62.

Schmidt K, Carlsen M, Nielsen JH, Villadsen J (1997) Modeling isotopomer distributions in biochemical networks using isotopomer mapping matrices. *Biotechnol Bioeng* **55:** 831-840.

Stephanopoulos G (1999) Metabolic fluxes and metabolic engineering. *Metab Eng* **1:** 1-11.

Stephanopoulos G, Aristidou AA, Nielsen JH (1998) *Metabolic engineering : principles and methodologies*. Academic Press, San Diego.

Vo TD, Palsson BO (2006) Isotopomer analysis of myocardial substrate metabolism: a systems biology approach. *Biotechnol Bioeng* **95:** 972-983.

Xenarios I, Salwinski L, Duan XJ, Higney P, Kim SM, Eisenberg D (2002) DIP, the Database of Interacting Proteins: a research tool for studying cellular networks of protein interactions. *Nucleic Acids Res* **30:** 303-305.

Zhou D, Xue J, Chen J, Morcillo P, Lambert JD, White KP, Haddad GG (2007) Experimental selection for Drosophila survival in extremely low O2 environment. *PLoS ONE* **2:** e490.

Zupke C, Stephanopoulos G (1994) Modeling of Isotope Distribution and Intracellular Fluxes in Metabolic Networks Using Atom Mapping Matrices. *Biotechnol Prog* **10:** 489-498.

Appendix A –

Automated heart measurement technical details

A.1 Overview

This appendix contains computer code (written in the Python language), circuit diagrams, and operating instructions for the automated *Drosophila* heart measurement system described in Chapter II. The system consists of:

- An inverted microscope, set to 20x objective
- A CCD camera mounted on the microscope, connected to a Pentium IV computer running Windows XP
- An automated stage, responding to commands from the computer via a serial port.
- A custom-made network of tubing and pinch valves connected to vacuum, pressurized air, the nitrogen mixture for the hypoxia stimulus, and a small vial of FlyNap (Carolina Biological) anesthetic.
- A data acquisition board with at least two analog inputs and at least 5 digital outputs, communicating with the computer via a separate serial port, and

- A driver circuit to supply power to the pinch valves and provide protection buffers to the DAQ board.

Software interfaces for the DAQ board, automated stage, and video cameras will not be described in detail, since these aspects could change in a separate implementation. Instead, the code presented here assumes that all external functions are either controllable with the Python Serial module or else some custom code wrapped in Python that provides the basic functions used here.

A.2 Measurement protocol

A.2.1 Baseline measurement and hypoxia stimulus

- Plug in power strip
- Turn on oxygen and nitrogen gas tanks (25 psi, 1/4 rotation on large valve)
- Wait for incubator to heat up, check that temperature is at 26º C (adjust if needed)
- Initialize camera using initcam.bat
- Make sure stage position places microscope light at top left corner of slide, at start point
- Start Python 2.3 and run program “run.py”
- [*if manually mixing hypoxic gas]* Adjust O_2 mixture to desired level, using feedback (very slow) from O_2 reading in GUI

- Anesthetize flies, either manually with chambers from Caroline Biological or by placing the glass vial into the automated chamber and clicking “Anesthetize”
- Mount flies onto plastic slide, place glass cover on top and add clamps
- Place slide assembly onto stage, with the marked corner toward the top left.
- Click “Measure”
- When asked “New slide?”, click Yes.
- When prompted, enter name of stock, oxygen level, and measurement duration
- After slide is scanned (during heart detection) begin anesthetizing a new batch
- Once flies are detected click OK to begin measurements
- Adjust position only on first two M-modes at each stage (initial measurement, during gassing, recovery) leave completely still thereafter.
- If heart is not visible, click “Skip Fly”
- When prompted, remove slide and place in hypoxia chamber and begin hypoxia stimulus. After flushing 15 minutes with gas, seal and place in incubator for stimulus duration.
- Repeat, once the next batch is anesthetized

A.2.2 Recovery measurement

- Click “Measure”
- When asked “New slide?” click No.

- Locate the data folder for the current stock, and the slide.pik file within the folder. Do not double-click the file yet.
- Quickly pull the slide assembly out of the hypoxia chamber and mount on the stage.
- Double click to open the slide.pik file.
- Manually adjust position if the heart is not perfectly centered and in focus, Skip Fly if not possible.

A.2.3 End of experiments

- Take any vials out of the anesthetic chamber
- Close Python
- Turn off gas at tanks
- Unplug the system and cover the microscope

A.3 Hardware

Some specialized hardware was assembled to aid the anesthetizing and mounting process, control temperature, and mix the hypoxic gas for the stimulus. Figure A.1 displays an overview of the tubing and valve network used for anesthetizing and depositing flies onto the slide.

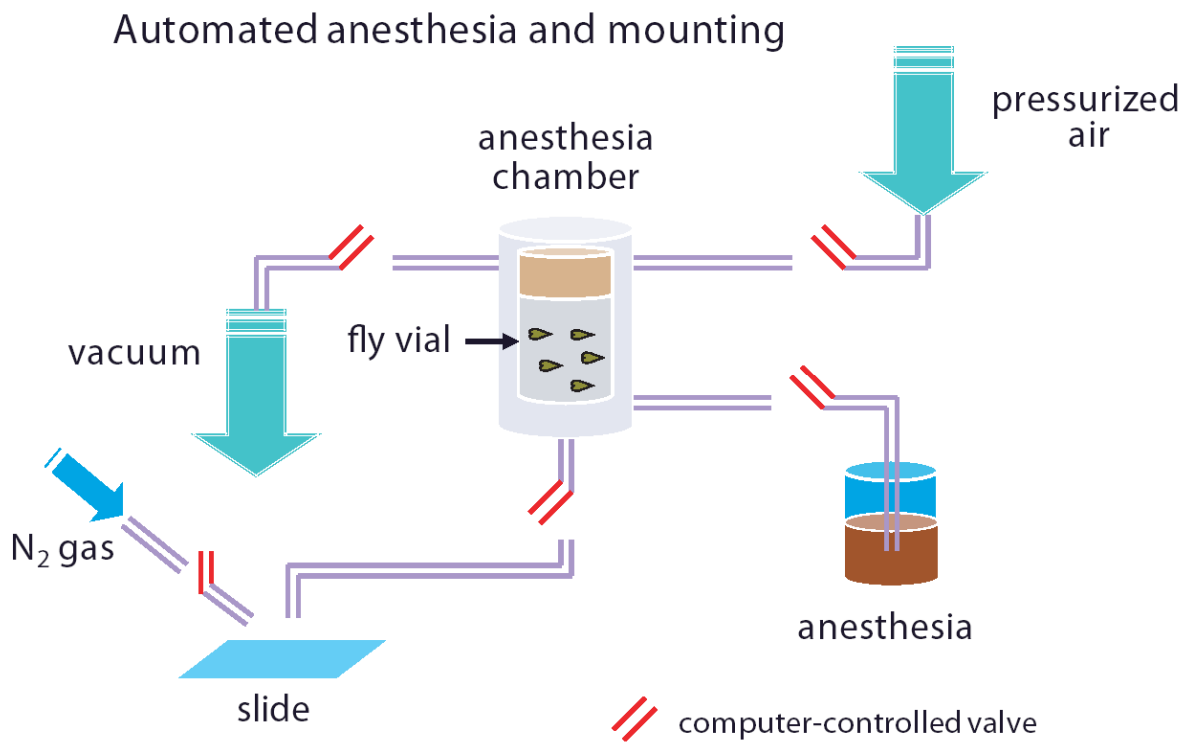

Figure A.1: Automated anesthesia and mounting overview

Figure A.2 shows the electronic schematic used to control the hardware and communicate with the computer. Gas composition and flow rate are controlled manually using a gas proportioner (GMR2-010001, Cole-Parmer, Inc.) with an oxygen sensor (KE-25) providing [O_2] feedback to the user. In the latest version of the hardware, some small changes to this configuration have been made. First, the thermostat circuit was replaced by a dedicated temperature controller unit for more stable temperatures. Also, the use of pre-mixed gas in the N_2 gas obviates the need for the gas mixer, and so the mixer is set to 100% for the N_2 line (pre-mixed gas) and 0% from the oxygen line. Also, the addition of the slide assembly for long-term

hypoxia stimuli has made it unnecessary to pass the nitrogen mixture directly onto the fly on the stage, and the hardware originally used function has been removed.

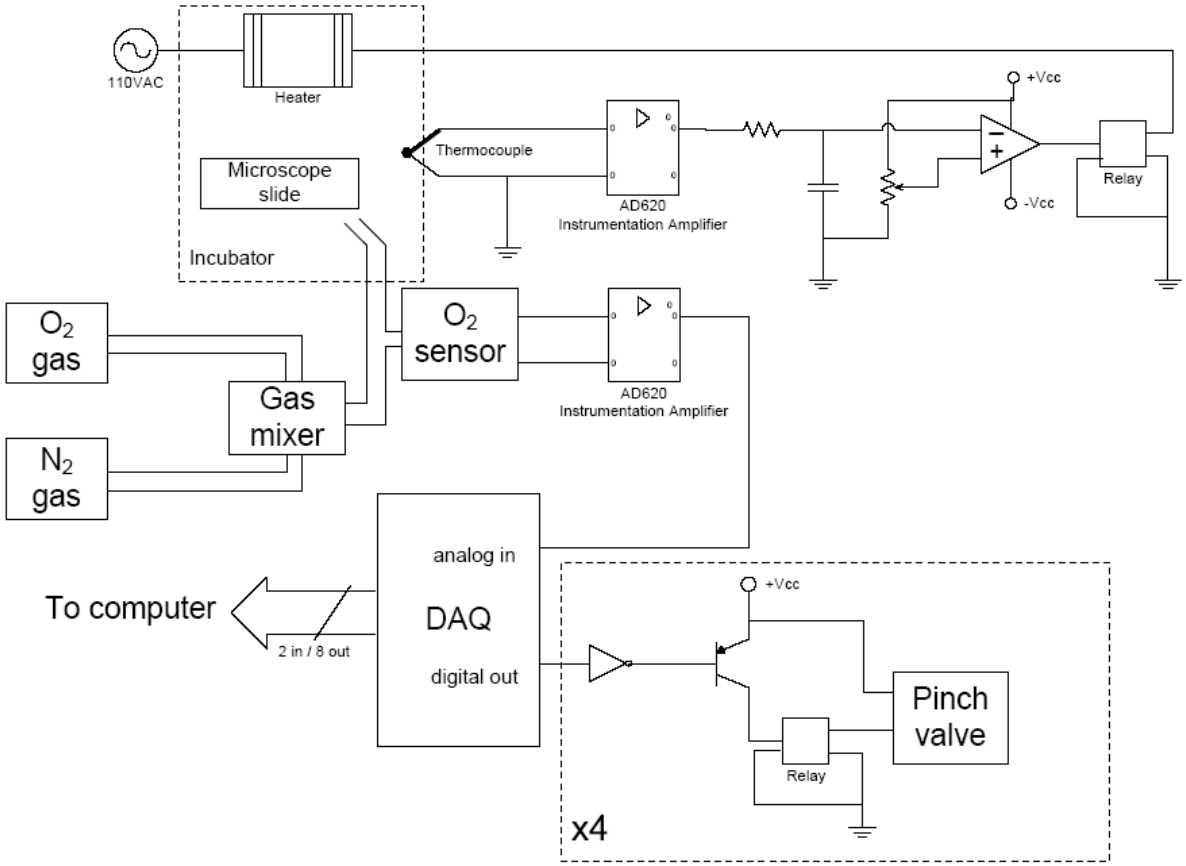

Figure A.2: Circuit and hardware schematic for all custom external hardware used in the system.

A.4 Automation code

A.4.1 Overview

The algorithms and user interface for mounting, detecting, and measuring *Drosophila* hearts were written entirely in the Python programming language. The

main script, which initializes the devices and starts the graphical user interface (GUI), is *run.py.* This script initializes the GUI and threaded operation. Within the *threads.py* script, three separate objects control the camera, mounting hardware, and detection/measurement engine. The engine contains the main sequence of operation during automation, takes input from the user, and implements most of the high-level control logic.

A.4.2 Script "run.py"

This script initializes Slide, Camera, and Mount objects, which in turn rely on Python or Python-wrapped drivers for their respective Stage, Camera, and DAQ interfaces, reproduced below. The top-level *run.py* script then initializes three thread objects (CameraThread, MountThread, and EngineThread) to allow parallel usage of the hardware. Two helper objects, FrameBuffer and Flags, are passed back and forth among the different threads. Last, the *run.py* script starts the threads and the GUI (inherently on its own thread in the background) and passes the initialized device and helper objects.

A.4.3 Script "threads.py"

The next highest levels of abstraction are the four threads of operation: GUI, mounting apparatus, camera, and the control engine. The Camera thread passes frames into the shared object FrameBuffer, and the GUI passes information to all threads through the Flags object (both contained in *shared.py)*. Both of these shared objects have Condition locks to avoid simulataneous access to the data by two threads. Each thread also has access to all of the available device drivers.

The Mounting thread controls all hardware in the mounting apparatus, with sequences for anesthetizing and depositing flies, and for measuring experimental oxygen levels using an O_2 electrode. The Camera thread continuously grabs frames, either one at a time or a specified sequence, and inserts them into the locked FrameBuffer for use by other objects. The Engine thread provides high-level control of automated detection and measurement algorithms, and is the starting point for understanding the flow of automation.

A.4.4 Script "detect.py"

The script detect.py contains all of the image processing algorithms for locating the x, y, and z position for the heart of each fly. The functions progressively refine the position, from scanning the whole slide to refining the position of the heart to the middle of the microscope frame. Detailed information on each algorithm is provided in Chapter II.

A.4.5 Script "measure.py"

All high-level measurement functions begin in the measure.py script. The EngineThread calls the proper measurement routine depending on whether the measurements are taken during baseline or recovery, and depending whether flies are measured sequentially or in multiplex.

A.4.6 Script "mmode.py"

The Measure routines all rely on the M-mode object within this script to gather the lines of pixels from the video, compile them into an M-mode image, and save the data to disk. After the orientation angle of the fly is calculated (in *detect.py*), a routine

within this object calculates the coordinates of the M-mode lines in the microscope frame and draws them in gray on the GUI.

A.4.7 Script "fly.py"

Each fly on the slide is represented by a Fly object which wraps data and position information and contains routines for saving and loading data to/from the corresponding folder.

Appendix B –

Characterization of the *Drosophila* heart to mild acute hypoxia

In characterizing the wild-type cardiac hypoxia response, we gathered additional data beyond what is presented in Chapter II. This appendix details the heart rate and regularity in response to different hypoxic conditions and temperatures.

As with other physiological functions in ectotherms such as *Drosophila*, heart rate is dependent on temperature. Similar to previous results, warmer ambient temperature sped up the HR at baseline, as well as during the hypoxia stimulus. The stress of hypoxia was expected to be compounded at high temperatures due to increased metabolic activity, however the increase in heart rate appeared to be independent of the hypoxia stimulus, as shown in Figure B.1. Higher temperature resulted in more regular heart rhythm for baseline, hypoxia, and recovery, although this effect was only statistically significant during hypoxia and between the extremes of the temperature range tested (26 C and 35 C).

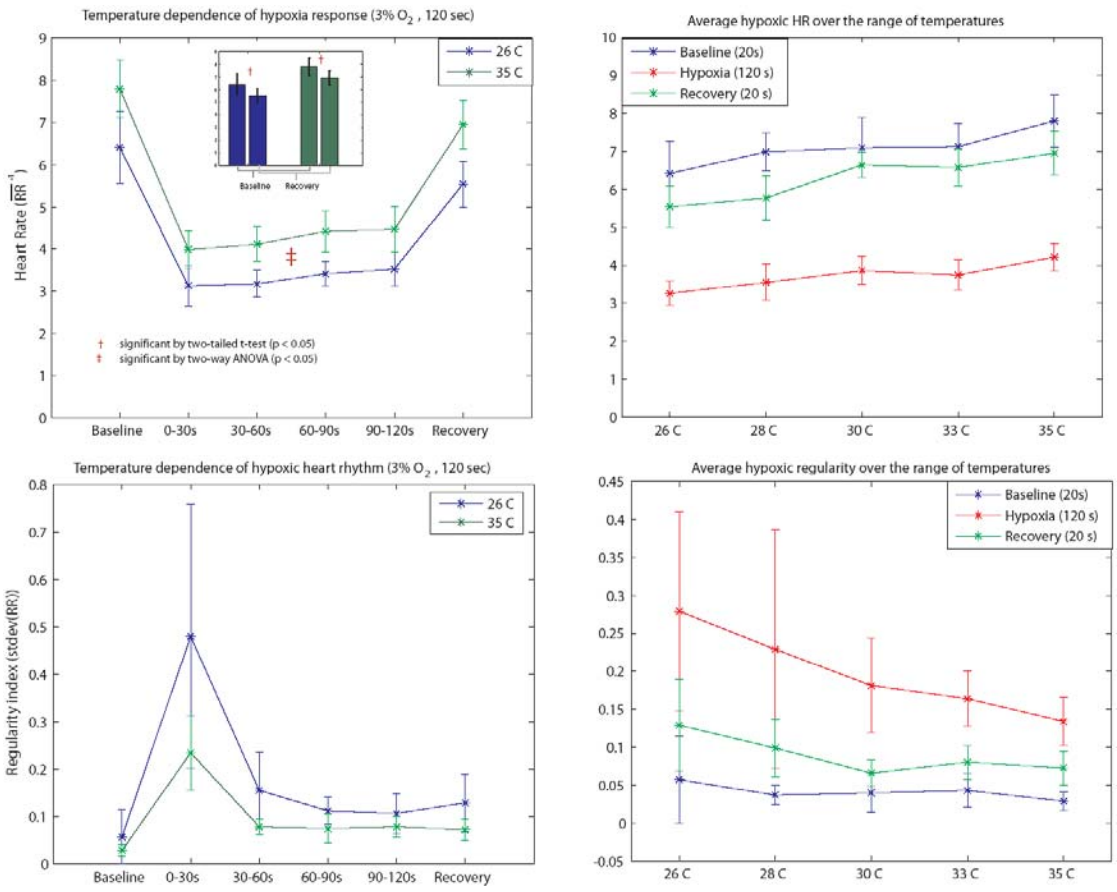

Figure B.1: Acute hypoxia response over temperatures.

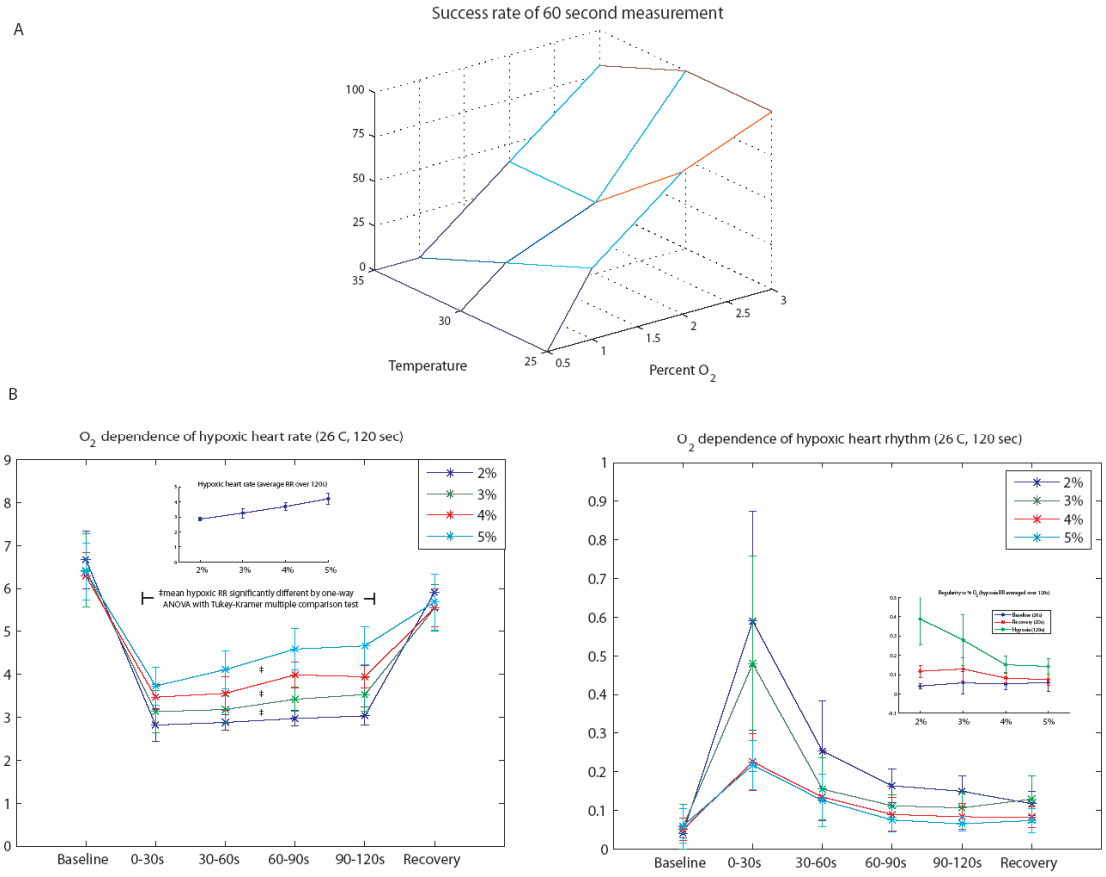

Figure B.2: Acute hypoxia response over oxygen concentrations

At oxygen concentrations below 3%, flies were seen to experience reflexive changes in body position, characterized by curling of the body and flaring of the wings in the dorsal direction. These contortions often cause the fly to shift, roll over, or lift off of the slide, making further measurement impossible. At very low oxygen, usable data are rare, and even attempts to tape the wings to the slide failed due to the curling body. The oxygen and temperature dependence of this behavior is shown in Figure B.2A. Because of this behavior, measurements were not taken below 2% O_2. The strength of hypoxia stimulus (percentage oxygen) changed hypoxic HR and also changed the shape of the response in Figure B.2B. At 2% O_2, the strongest stimulus

measured, rate was slowest and remained steady over the hypoxic time period. At oxygen percentages above 2%, HR dropped similarly for the early phase but then recovered by an amount approximately proportional to the percent O_2 and remained steady for the remainder of the hypoxic period. Recovery HR was significantly lower than baseline for all oxygen percentages. The heart was significantly more irregular for all hypoxia timepoints at 2% oxygen than at higher percentages, and for the first 30 seconds at 3% O_2 (Figure B.2B).

All further experiments were performed at 26 degrees C and 3% oxygen in order to minimize the errors from body movement described above. Males and females did not differ statistically in their HR response, though the trend was for males to have higher baseline and recovery HR than females but lower HR during hypoxia. Males had more irregular HR during hypoxia than females.

Different wild-type strains and their crosses were tested to study the effect of differences in genetic background on the cardiac hypoxia response. We used the y^1w^{67c23} strain (*yw*) since it occurs frequently as a background for P-element gene disruptions in the Bloomington *Drosophila* library. We also crossed *yw* with Oregon-R to examine the effect on hypoxic HR after outcrossing these heavily inbred strains. Oregon-R flies had significantly higher HR than *yw* for baseline and recovery, but similar hypoxic HR. The F1 cross of Oregon-R and *yw* had similar baseline and recovery HR as the Oregon-R, but during hypoxia the HR was faster than both. The *yw* strain had an irregular heartbeat as compared to both Oregon-R and the F1 cross of the two strains (Figure B.3).

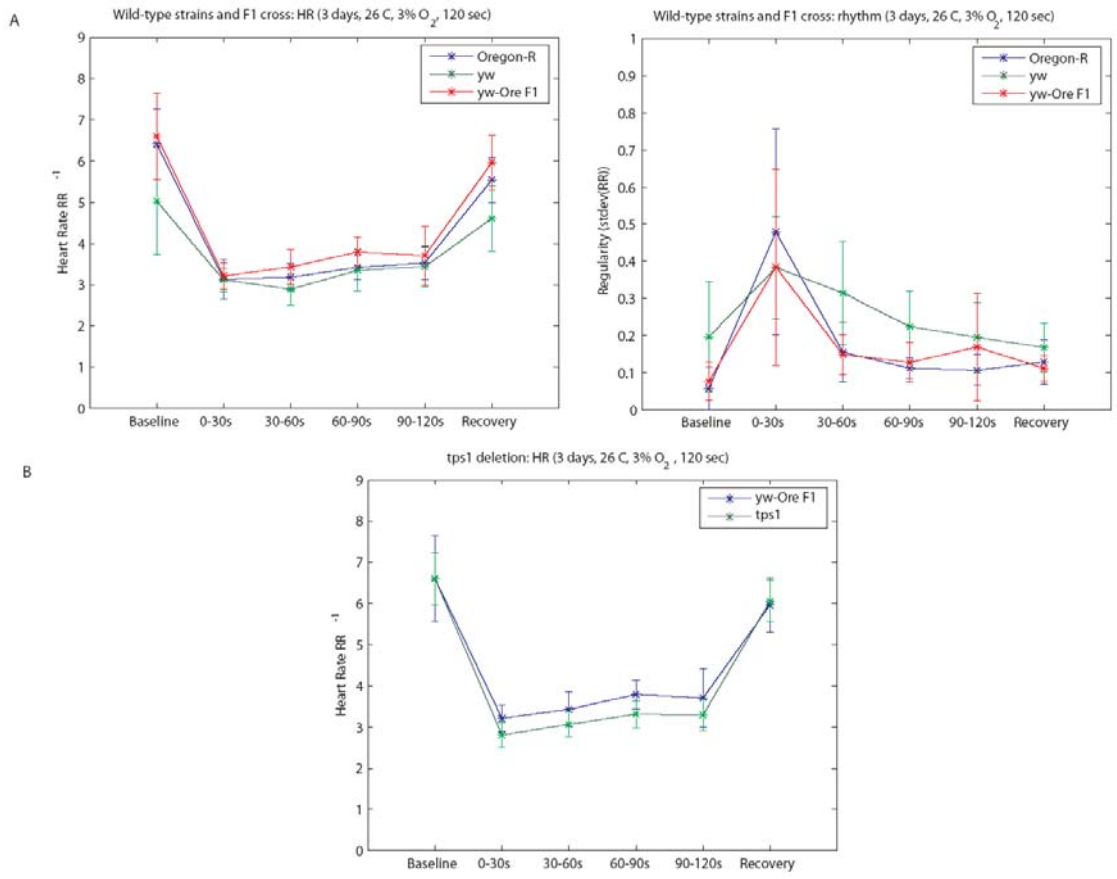

Figure B.3: Heart rate and regularity for different wild-type strains and a hypoxia-sensitive mutant

The literature describes some known hypoxia-sensitive *Drosophila* genes (described in Chapter II). We used one of these genes, *tps1*, as a positive control for detecting hypoxia sensitivity with our system. The *tps1* locus codes for the trehalose-phosphate synthase enzyme, which creates the disaccharide trehalose from glucose monomers and causes hypoxia sensitivity when disrupted in flies. Trehalose is important not only as a carbohydrate energy source for anaerobic glycolysis but also due to protective properties when bound to proteins. In one study the *Drosophila tps1* gene was transfected into human cells, which do not have a copy of the gene, and the cells became more tolerant to hypoxia.

We acquired a heterozygous P-element insertion of *tps1* and outcrossed with a wild-type strain. The *tps1* disrupted flies had similar HR in baseline and recovery but slightly, though significantly, reduced HR during hypoxia when compared with an equivalently outcrossed wild-type strain (Figure B.3).

Appendix C –

Reactions in the Drosophila metabolic reconstruction

Name	Equation
L-alanine transaminase, mitochondrial	[m] : akg + ala-L <==> glu-L + pyr
ornithine transaminase reversible (m)	[m] : akg + orn <==> glu-L + glu5sa
L-asparaginase (mitochondrial)	[m] : asn-L + h2o --> asp-L + nh4
glutamate dehydrogenase (NADP), mitochondrial	[m] : glu-L + h2o + nadp <==> akg + h + nadph + nh4
aspartate transaminase	[m] : akg + asp-L <==> glu-L + oaa
Glutamate Decarboxylase	[c] : glu-L + h --> 4abut + co2
glutamate dehydrogenase (NAD) (mitochondrial)	[m] : glu-L + h2o + nad <==> akg + h + nadh + nh4
glutamine phosphoribosyldiphosphate amidotransferase	[c] : gln-L + h2o + prpp --> glu-L + ppi + pram
succinate-semialdehyde dehydrogenase (NAD) reversible (mitochondrial)	[m] : h2o + nad + sucsal --> (2) h + nadh + succ
4-aminobutyrate transaminase, reversible (mitochondrial)	[m] : 4abut + akg <==> glu-L + sucsal
glutamine synthetase	[c] : atp + glu-L + nh4 --> adp + gln-L + h + pi
glutamine-fructose-6-phosphate transaminase	[c] : f6p + gln-L --> gam6p + glu-L
glycine N-methyltransferase	[c] : amet + gly --> ahcys + h + sarcs
L-Phenylalanine,tetrahydrobiopterin:oxygen oxidoreductase (4-hydroxylating)	[c] : o2 + phe-L + thbpt --> dhbpt + h2o + tyr-L
6,7-dihydropteridine reductase	[c] : dhbpt + h + nadh --> nad + thbpt
1-pyrroline-5-carboxylate dehydrogenase, mitochondrial	[m] : 1pyr5c + (2) h2o + nad --> glu-L + h + nadh
proline oxidase (NAD), mitochondrial	[m] : nad + pro-L --> 1pyr5c + (2) h + nadh
Proline dehydrogenase (m)	[m] : fad + pro-L --> 1pyr5c + fadh2 + h
L-Tryptophan,tetrahydrobiopterin:oxygen oxidoreductase (5-hydroxylating)	[c] : o2 + thbpt + trp-L --> 5htrp + dhbpt + h2o
4-Hydroxyphenylpyruvate:oxygen	[c] : 34hpp + o2 --> co2 + hgentis

oxidoreductase	
Homogentisate:oxygen 1,2-oxidoreductase (decyclizing)	[c] : hgentis + o2 --> 4mlacac + h
tyrosine transaminase	[c] : akg + tyr-L <==> 34hpp + glu-L
fumarylacetoacetase	[c] : 4fumacac + h2o --> acac + fum + h
maleylacetoacetate isomerase	[c] : 4mlacac --> 4fumacac
N-acetylglucosamine-6-phosphate deacetylase	[c] : acgam6p + h2o --> ac + gam6p
glucosamine-6-phosphate deaminase	[c] : gam6p + h2o --> f6p + nh4
chitinase	[c] : chtn + (2) h2o --> (3) acgam
N-acetylglucosamine kinase	[c] : acgam + atp --> acgam6p + adp + h
L-lactate dehydrogenase	[c] : lac-L + nad <==> h + nadh + pyr
aldehyde dehydrogenase (acetylaldehyde, NAD), mitochondrial	[m] : acald + h2o + nad --> ac + (2) h + nadh
alcohol dehydrogenase (ethanol)	[c] : etoh + nad <==> acald + h + nadh
aldehyde dehydrogenase (acetaldehyde, NAD)	[c] : acald + h2o + nad --> ac + (2) h + nadh
malic enzyme (NAD), mitochondrial	[m] : mal-L + nad --> co2 + nadh + pyr
Phosphoenolpyruvate carboxykinase (GTP)	[m] : gtp + oaa --> co2 + gdp + pep
malic enzyme (NADP)	[c] : mal-L + nadp --> co2 + nadph + pyr
fumarase	[c] : fum + h2o <==> mal-L
acetyl-CoA C-acetyltransferase, mitochondrial	[m] : (2) accoa <==> aacoa + coa
Beta oxidation of long chain fatty acid	[m] : (7) coa + (7) fad + (7) h2o + (7) nad + pmtcoa --> (8) accoa + (7) fadh2 + (7) h + (7) nadh
Beta oxidation fatty acid	[m] : (5) coa + (4) fad + (5) h2o + (5) nad + odecoa --> (5) accoa + (4) fadh2 + (5) h + (5) nadh + occoa
Beta oxidation fatty acid	[m] : (4) coa + (3) fad + (4) h2o + hdcoa + (4) nad --> (4) accoa + (3) fadh2 + (4) h + (4) nadh + occoa
Beta oxidation of long chain fatty acid	[m] : arachcoa + coa + fad + h2o + nad --> accoa + fadh2 + h + nadh + stcoa
Beta oxidation of med/long chain fatty acid	[m] : (3) coa + (3) fad + (3) h2o + (3) nad + occoa --> (4) accoa + (3) fadh2 + (3) h + (3) nadh
L-carnitine transport out of mitochondria via diffusion	crn[m] --> crn[c]
carnitine transport, mitochondrial, reversible	crn[c] <==> crn[m]

fatty-acid--CoA ligase (hexadecanoate)	[c] : atp + coa + hdca <==> amp + pmtcoa + ppi
carnitine O-palmitoyltransferase	[c] : crn + pmtcoa --> coa + pmtcrn
C160 transport into the mitochondria	pmtcrn[c] --> pmtcrn[m]
C160 transport into the mitochondria	[m] : coa + pmtcrn --> crn + pmtcoa
fatty-acid--CoA ligase (hexadecenoate)	[c] : atp + coa + hdcea <==> amp + hdcoa + ppi
carnitine O-palmitoyltransferase	[c] : crn + hdcoa --> coa + hdcecrn
C161 transport into the mitochondria	hdcecrn[c] --> hdcecrn[m]
C161 transport into the mitochondria	[m] : coa + hdcecrn --> crn + hdcoa
fatty-acid--CoA ligase (octadecenoate)	[c] : atp + coa + ocdcea <==> amp + odecoa + ppi
carnitine octadecenoyl transferase	[c] : crn + odecoa --> coa + odecrn
C181 transport into the mitochondria	odecrn[c] --> odecrn[m]
carnitine octadecenoyl transferase	[m] : coa + odecrn --> crn + odecoa
carnitine O-acetyltransferase	[c] : accoa + crn <==> acrn + coa
acetylcarnitine transport, mitochondrial, reversible	acrn[m] <==> acrn[c]
fatty-acid--CoA ligase	[c] : arach + atp + coa <==> amp + arachcoa + ppi
carnitine transferase	[c] : arachcoa + crn --> arachcrn + coa
transport into the mitochondria (carnitine)	arachcrn[c] --> arachcrn[m]
carnitine transferase	[m] : arachcrn + coa --> arachcoa + crn
fatty-acid--CoA ligase	[c] : atp + coa + crvnc <==> amp + c226coa + ppi
fatty-acid--CoA ligase	[c] : atp + coa + lgnc <==> amp + lgnccoa + ppi
fatty-acid--CoA ligase (n-C26:0)	[c] : atp + coa + hexc <==> amp + hexccoa + ppi
Fructose-2,6-bisphosphate 2-phosphatase	[c] : f26bp + h2o --> f6p + pi
D-sorbitol dehydrogenase (D-fructose producing)	[c] : nad + sbt-D --> fru + h + nadh
pyruvate carboxylase	[m] : atp + hco3 + pyr --> adp + h + oaa + pi
glucose-6-phosphate phosphatase	[c] : g6p + h2o --> glc-D + pi
glycerol-3-phosphate dehydrogenase (FAD), mitochondrial	fad[m] + glyc3p[c] --> dhap[c] + fadh2[m]
Glucose-6-phosphate isomerase	[c] : g6p-B <==> f6p-B
phosphoglucomutase	[c] : g1p <==> g6p

glycerol-3-phosphate dehydrogenase (NAD)	[c] : dhap + h + nadh --> glyc3p + nad
acylphosphatase	[c] : 13dpg + h2o --> 3pg + h + pi
glycerol kinase	[c] : atp + glyc --> adp + glyc3p + h
fructose-bisphosphatase	[c] : fdp + h2o --> f6p + pi
aldose 1-epimerase (glucose)	[c] : glc-bD --> glc-D
hexokinase (D-glucose:ATP)	[c] : atp + glc-D --> adp + g6p + h
pyruvate kinase	[c] : adp + h + pep --> atp + pyr
glucose-6-phosphate isomerase	[c] : g6p <==> f6p
phosphofructokinase	[c] : atp + f6p --> adp + fdp + h
fructose-bisphosphate aldolase	[c] : fdp <==> dhap + g3p
triose-phosphate isomerase	[c] : dhap <==> g3p
glyceraldehyde-3-phosphate dehydrogenase	[c] : g3p + nad + pi <==> 13dpg + h + nadh
phosphoglycerate kinase	[c] : 3pg + atp <==> 13dpg + adp
Diphosphoglycerate phosphatase	[c] : 23dpg + h2o --> 3pg + pi
phosphoglycerate mutase	[c] : 2pg <==> 3pg
enolase	[c] : 2pg <==> h2o + pep
3-oxoacid CoA-transferase	[m] : acac + succoa <==> aacoa + succ
nucleoside-diphosphate kinase (ATP:GDP)	[c] : atp + gdp <==> adp + gtp
polyphosphate kinase	[c] : atp + pi <==> adp + ppi
adenylate kinase	[c] : amp + atp <==> (2) adp
nucleoside-diphosphate kinase (ATP:GDP), mitochondrial	[m] : atp + gdp <==> adp + gtp
arginine kinase	[c] : arg-L + atp <==> adp + argp + h
adenylate kinase, mitochondrial	[m] : amp + atp <==> (2) adp
NADH dehydrogenase 2, ubiquinone-8, mitochondrial	(5) h[m] + nadh[m] + q8[m] --> (4) h[c] + nad[m] + q8h2[m]
ubiquinol-8 cytochrome c reductase	(2) ficytc[m] + (4) h[m] + q8h2[m] --> (2) focytc[m] + (4) h[c] + q8[m]
cytochrome c oxidase, mitochondrial	(4) focytc[m] + (6) h[m] + o2[m] --> (4) ficytc[m] + (6) h[c] + (2) h2o[m]
succinate dehydrogenase (ubiquinone-8), mitochondrial	[m] : fadh2 + q8 <==> fad + q8h2
ATP synthase (four protons for one ATP)	adp[m] + (4) h[c] + pi[m] --> atp[m] + (3) h[m] + h2o[m]
phosphoribosylpyrophosphate synthetase	[c] : atp + r5p <==> amp + h + prpp
Glucose-6-phosphate isomerase	[c] : g6p <==> g6p-B
ribokinase	[c] : atp + rib-D --> adp + h + r5p

ribulose 5-phosphate 3-epimerase	[c] : ru5p-D <==> xu5p-D
transketolase	[c] : r5p + xu5p-D <==> g3p + s7p
transaldolase	[c] : g3p + s7p <==> e4p + f6p
transketolase	[c] : e4p + xu5p-D <==> f6p + g3p
glucose 6-phosphate dehydrogenase	[c] : g6p + nadp <==> 6pgl + h + nadph
6-phosphogluconolactonase	[c] : 6pgl + h2o --> 6pgc + h
phosphogluconate dehydrogenase	[c] : 6pgc + nadp --> co2 + nadph + ru5p-D
acetyl-CoA synthetase reversible	[c] : ac + atp + coa <==> accoa + amp + ppi
glutathione oxidoreductase	[c] : gthox + h + nadph <==> (2) gthrd + nadp
catalase	[m] : (2) h2o2 --> (2) h2o + o2
glutathione peroxidase, mitochondria	[m] : (2) gthrd + h2o2 <==> gthox + (2) h2o
glutathione peridoxase	[c] : (2) gthrd + h2o2 <==> gthox + (2) h2o
gamma-glutamylcysteine synthetase	[c] : atp + cys-L + glu-L --> adp + glucys + h + pi
glutathione synthetase	[c] : atp + glucys + gly --> adp + gthrd + h + pi
Glutathione transport into mitochondria	atp[c] + gthrd[c] + h2o[c] <==> adp[c] + gthrd[m] + h[c] + pi[c]
superoxide dismutase	[m] : (2) h + (2) o2s --> h2o2 + o2
catalase	[c] : (2) h2o2 --> (2) h2o + o2
UTP-glucose-1-phosphate uridylyltransferase	[c] : g1p + h + utp <==> ppi + udpg
1,4-alpha-glucan branching enzyme (glygn1 -> glygn2)	[c] : glygn1 --> glygn2
alpha,alpha-trehalose-phosphate synthase (UDP-forming)	[c] : g6p + udpg <==> h + tre6p + udp
alpha,alpha-trehalase	[c] : h2o + tre --> (2) glc-D
glycogen phosphorylase (amyls -> glc-D)	[c] : glygn3 + (7) h2o --> Tyr-ggn + (7) glc-D
alpha-amylase (glygn2 -> glygn4)	[c] : glygn2 + (8) h2o --> (8) glc-D + glygn4
alpha-glucosidase	[c] : h2o + malt --> (2) glc-D
pyruvate dehydrogenase	[m] : coa + nad + pyr --> accoa + co2 + nadh
citrate synthase	[m] : accoa + h2o + oaa --> cit + coa + h
Aconitate hydratase	[m] : cit <==> icit
Isocitrate dehydrogenase (NADP+)	[m] : icit + nadp --> akg + co2 + nadph
Isocitrate dehydrogenase (NAD+)	[m] : icit + nad --> akg + co2 + nadh
2-oxoglutarate dehydrogenase	[m] : akg + coa + nad --> co2 + nadh + succoa
2-Oxoadipate:lipoamde 2-oxidoreductase(decarboxylating and acceptor-succinylating) (mitochondria)	[m] : 2oxoadp + coa + nad --> co2 + glutcoa + nadh

Succinate--CoA ligase (ADP-forming)	[m] : atp + coa + succ <==> adp + pi + succoa
succinate dehydrogenase	[m] : fad + succ <==> fadh2 + fum
fumarase, mitochondrial	[m] : fum + h2o <==> mal-L
malate dehydrogenase	[c] : mal-L + nad <==> h + nadh + oaa
malate dehydrogenase, mitochondrial	[m] : mal-L + nad <==> h + nadh + oaa
L-alanine reversible transport via proton symport	ala-L[e] + h[e] <==> ala-L[c] + h[c]
L-phenylalanine transport via diffusion (extracellular to cytosol)	phe-L[e] <==> phe-L[c]
L-proline transport via diffusion	pro-L[e] <==> pro-L[c]
L-tyrosine transport	tyr-L[e] <==> tyr-L[c]
4-aminobutanoate mitochondrial transport via diffusion	4abut[c] <==> 4abut[m]
glucose transport (uniport)	glc-D[e] --> glc-D[c]
L-lactate reversible transport via proton symport	h[e] + lac-L[e] <==> h[c] + lac-L[c]
Citrate exchange, diffusion	cit[e] <==> cit[c]
trehalose transport in via proton symporter	h[e] + tre[e] --> h[c] + tre[c]
iron (II) transport	fe2[e] --> fe2[c]
H2O transport via diffusion	h2o[e] <==> h2o[c]
o2 transport (diffusion)	o2[e] <==> o2[c]
phosphate reversible transport via symport	h[e] + pi[e] <==> h[c] + pi[c]
phosphate transport in/out via three Na+ symporter	(3) na1[e] + pi[e] <==> (3) na1[c] + pi[c]
CO2 transporter via diffusion	co2[e] <==> co2[c]
ammonia reversible transport	nh4[e] <==> nh4[c]
Na+/K+ exchanging ATPase	atp[c] + h2o[c] + (2) k[e] + (3) na1[c] --> adp[c] + h[c] + (2) k[c] + (3) na1[e] + pi[c]
proton diffusion	h[c] <==> h[e]
fatty acid transport via diffusion	arach[e] <==> arach[c]
Octadecenoate (n-C18:1) transport in via uniport	ocdcea[e] --> ocdcea[c]
acetate transport in via proton symport	ac[e] + h[e] --> ac[c] + h[c]
Hexadecanoate (n-C16:0) transport in via uniport	hdca[e] --> hdca[c]
hexadecenoate (n-C16:1) transport in via uniport	hdcea[e] --> hdcea[c]
CoA transporter	coa[e] <==> coa[c]

glycerol transport via channel	glyc[c] <==> glyc[e]
L-glutamate reversible transport via proton symport, mitochondrial	glu-L[c] + h[c] <==> glu-L[m] + h[m]
L-proline transport, mitochondrial	pro-L[c] <==> pro-L[m]
alpha-ketoglutarate/malate transporter	akg[m] + mal-L[c] <==> akg[c] + mal-L[m]
L-lactate transport, mitochondrial	h[c] + lac-L[c] <==> h[m] + lac-L[m]
Citrate transporter, mitochondrial	cit[c] <==> cit[m]
glucose transport (uniport)	glc-D[e] <==> glc-D[c]
pyruvate mitochondrial transport via proton symport	h[c] + pyr[c] <==> h[m] + pyr[m]
NH3 mitochondrial transport	nh4[c] <==> nh4[m]
H2O transport, mitochondrial	h2o[c] <==> h2o[m]
CO2 transport (diffusion), mitochondrial	co2[c] <==> co2[m]
Uncoupling protein	h[c] --> h[m]
phosphate transporter, mitochondrial	h[c] + pi[c] <==> h[m] + pi[m]
O2 transport (diffusion)	o2[c] <==> o2[m]
Acetoacetate mitochondrial transport via H+ symport	acac[c] + h[c] <==> acac[m] + h[m]
glycerol transport	glyc[c] <==> glyc[m]
CoA transporter	coa[c] <==> coa[m]
acetate mitochondrial transport via proton symport	ac[c] + h[c] <==> ac[m] + h[m]
acetate reversible transport via proton symport	ac[e] + h[e] <==> ac[c] + h[c]
carnitine O-aceyltransferase, mitochondrial	[m] : acrn + coa <==> accoa + crn
ADP/ATP transporter, mitochondrial	adp[c] + atp[m] --> adp[m] + atp[c]
aspartate 1-decarboxylase	[c] : asp-L + h --> ala-B + co2
carboxylic acid dissociation	[c] : co2 + h2o <==> h2co3
inorganic diphosphatase	[c] : h2o + ppi --> h + (2) pi
aspartate transaminase	[c] : akg + asp-L <==> glu-L + oaa
trehalose-phosphatase	[c] : h2o + tre6p --> pi + tre
N4-Acetylaminobutanal:NAD+ oxidoreductase	[c] : h2o + n4abutn + nad --> 4aabutn + (2) h + nadh
carboxylic acid dissociation	[m] : co2 + h2o <==> h2co3
NADPH demand	[c] : nadph --> h + nadp
atp demand	[c] : atp + h2o --> adp + h + pi
HCO3 equilibration reaction	[m] : co2 + h2o <==> h + hco3

4-aminobutyrate transaminase	[c] : 4abut + akg <==> glu-L + sucsal
glutamate dehydrogenase (NAD)	[c] : glu-L + h2o + nad <==> akg + h + nadh + nh4
Peroxidase (multiple substrates)	[c] : h2o2 + meoh --> fald + (2) h2o